Application of Vibration Based Methods and Statistical Pattern Recognition Techniques to Structural Health Monitoring

Ahmed Shiblee Noman

A thesis

in

The Department of

Building, Civil and Environmental Engineering

Presented in Partial Fulfillment of the Requirements
for the Degree of Master of Applied Science (Civil Engineering) at
Concordia University
Montreal, Quebec, Canada

August 2008

Your file Votre référence
ISBN: 978-0-494-45523-4
Our file Notre référence
ISBN: 978-0-494-45523-4

Abstract

Application of Vibration Based Methods and Statistical Pattern Recognition techniques to Structural Health Monitoring

Ahmed Shiblee Noman

The primary objective of Structural Health Monitoring (SHM) is to diagnose structures for damage, take necessary measures if any damage occurs, and estimate their degradation rate.

Conventional non-destructive evaluation methods are not always practical for implementation of a continuous health monitoring system. Vibration Based Damage Identification (VBDI) methods applied to SHM can be useful in interpreting the global vibration response of a structure to identify local changes. Due to complicated features of real life structures there are some uncertainties related to input parameters such as measured frequencies and mode shape data, where output is sensitive to errors in modal parameters. As all VBDI processes rely on experimental data with their inherent uncertainties, statistical procedures are helpful if one is to interpret the vibration response mixed with other ambient affects.

The objective of this study is the detection of damage by VBDI methods and statistical pattern recognition techniques. Here, two practical structures, the Crowchild Bridge in Calgary, and a 3D-Space Frame have been tested with two VBDI algorithms. The Damage Index and Matrix Update methods have been selected to study simulated damage cases on the numerical models of the selected structures. For the application of statistical pattern recognition techniques to damage identification, another in-service structure, the Portage Creek Bridge in Victoria, Canada has been tested. The classification of the patterns has been performed using outlier analysis. Alternatively, damage detection by pattern comparison using residual errors has been applied

To the memory of my father who loved me more than anything else in this world!

Acknowledgements

First and foremost, I would like to thank Dr. Bagchi, my thesis supervisor who has helped me thoroughly in this research work. Through the academic years, he has guided me always and made all efforts to grant me access to required research facilities. His guidance has not only been limited to this thesis, but also has extended to other academic areas.

I also wish to thank the authority of ISIS (Intelligent Sensing for Innovative Structures) Canada to provide me with the data needed for the research on structural health monitoring by statistical pattern recognition.

I also sincerely express gratitude to my brother Shamim who has motivated me constantly and provided me with exceptional support I needed to continue with my graduate studies at Concordia University. I also acknowledge the love of my mother, sister and other brothers, that has inspired me a lot.

Table of Contents

List of Tables x

List of Figures xi

Nomenclature xx

Chapter 1: Introduction

1.1 General 1

1.2 Brief discussion on SHM methods 3

1.2.1 Visual Inspection 3

1.2.2 Liquid Penetration Testing (LPT) 4

1.2.3 Magnetic Particle Testing (MT) 4

1.2.4 Radiographic Testing (RT) 5

1.2.5 Ultrasonic Testing (UT) 5

1.2.6 Eddy Current Testing 6

1.2.7 Static Load Test 6

1.2.8 Vibration Based Damage Identification (VBDI) 7

1.3 The advantages of VBDI over other NDE methods 8

1.4 Overall effectiveness of VBDI and its relevant features 9

1.4.1 Earlier findings 9

1.4.2 General approach of VBDI method 10

1.4.3 Limitations of VBDI methods 16

1.5 Structural Health Monitoring by Pattern Recognition Techniques 19

1.5.1 Pattern Recognition by Statistical methods 21

1.5.2 Pattern Recognition by Neural Network 25

1.6 Objectives and Scope of Proposed Research 26

1.7 Organization of the thesis 28

Chapter 2: Literature Review

2.1 General 31

2.2 Methods of VBDI and Relevant Research work 31

2.2.1 Methods based on change in natural frequency 31
2.2.2 Methods based on mode shape change 32
2.2.3 Methods based on flexibility of a structure 40
2.2.4 Methods based on matrix (model) updating 43
2.3 Review on some researches done in vibration based damage detection methods 44
2.3.1 Research on natural frequency shifts method 44
2.3.2 Research on changes in mode shapes method 46
2.3.3 Research on method based on flexibility of structure 49
2.3.4 Research on matrix updating method 50
2.4 Method Based on Statistical Pattern Recognition 52
2.5 Methods based on Neural networking 55
2.6 Summary 56

Chapter 3: Selected VBDI methods

3.1 General 59
3.2 Eigenvalue Equation 59
3.3 Modal Reduction/ Expansion 60
3.4 Algorithms for VBDI 62
3.5 Damage Index Method 64
3.6 Matrix Update Method 67

Chapter 4: Statistical Pattern Recognition Methods in SHM

4.1 General 70
4.2 Components of statistical pattern recognition. 70
4.2.1 Operational Evaluation 71
4.2.2 Data Acquisition &Cleansing 72
4.2.3 Feature extraction 73
4.2.4 Statistical Model Development 74
4.2.5 Damage Identification Approach by Pattern Comparison 76
4.3 Time Series Analysis 77
4.3.1 Weakly stationary time series 78

4.3.2 Illustration of some useful terms related to time series 78
4.3.3 Auto-Regression Moving Average Processes 80
4.3.4 Estimation of the parameters AR(p) process 81
4.3.5 Order selection of AR(p) process 83

Chapter 5: Testing of VBDI Methods by Model Simulations

5.1 General 85
5.2 Test Articles 85
5.2.1 The Crowchild Bridge 85
5.2.2 3D-Space Frame 87
5.3 Software for implementation of FEM 88
5.4 Damage simulation in the Crowchild Bridge 89
5.4.1 Model Simulation to the Crowchild Bridge 89
5.4.2 Effects of measurement errors and incomplete mode shape vectors 93
5.4.3 Discussion on the results of case studies on Crow Child Bridge 94
5. 5 Damage simulation for the 3D-Space Frame 99
5.5.1 Finite element modeling of the structure 100
5.5.2 Damage simulation 101
5.5.3 Discussion on the results of case studies on 3D Space Frame 101

Chapter 6: Application of Statistical Pattern Recognition to Damage Detection

6.1 General 127
6.2 Description of monitored the structure 127
6.3 Data collection and preprocessing 128
6.3.1 Data block Sampling Scheme 131
6.4 Feature extraction 133
6.5 Damage Identification by Statistical Model Development 134
6.6 Damage Identification Approach by Pattern Comparison 135
6.7 Discussion on the results on damage identifications 135
6.7.1 Results of Identification by Statistical modeling 135

6.7.2 Results of Identification by pattern comparison method 136
6.8 Temperature effect on Strains 137
6.8.1 Need for relation of temperature to strain values 138
6.8.2 Temperature vs. Strain relationship and comments 138

Chapter 7: Summary and Conclusions
7.1 Summary 159
7.1.1 Vibration based damage identification by modal analysis 159
7.1.2 Structural damage detection by statistical method. 160
7.2 Conclusion 162
7.3 Recommendations on further research work 165

Reference 167

Appendix A
Graphical output of VBDI case study on the Crowchild Bridge 176

Appendix B
Graphical out of VBDI case study on 3D Space Frame 195

List of Tables

Table 5.1 Natural frequencies of the Crowchild bridge model(Bagchi, 2005)

Table 5.2 Crowchild Bridge Damage Identification:1- full identification, 2-partial and 3-no identification as defined in section 5.4.3, case type is defined section 5.4.2.

Table 5.3: Crowchild Bridge Damage Identification for measured frequencies: 1- full identification, 2-partial and 3-no identification as defined in section 5.4.3, case type defined section 5.4.2

Table 5.4 Proposed 79 DOF's by Amin (2002) for analysis of 3D Space Frame by VBDI (FEM)

Table 5.5 Simulated damage cases for 3-D Space Frame

Table-5.6 3D space frame Damage Identification for 80% damage severity cases: 1-full identification, 2-partial &3-no identification as defined in section 5.4.3, and case type is defined in section 5.5.2

Table 5.7 3D space frame Damage Identification for 50% damage severity cases: 1-full identification, 2-partial &3-no identification as defined in section 5.4.3, and case type is defined in section 5.5.2

Table 6.1 Sample collection for data of strains S_1_2_C1, S_3_1_C1, Accelometers A_1_x, A_1_y and A_1_z.

List of Figures

Fig-1.1: The basic framework for a typical Vibration-based Damage Identification system

Fig 5.1 Crowchild Bridge of Calgary, Alberta, Canada

Fig 5.2 Details of the Crowchild Bridge – (a) west elevation, (b) Cross section (All dimensions are in mm) (Bagchi 2005)

Fig 5.3: (a) Nodes and element connections of 3D Space Frame; (b) details of an element of 3D space frame.

Fig 5.4 Three dimensional beam and plate-shell elements in M-FEM – (a) 3D beam element, (b) 3D plate-shell element, (c) DKT plate bending element, (d) CST plane stress element, (e) Allman's plane stress element, and (f) quadrilateral plate shell element constructed by combining two triangular elements (Bagchi 2005)

Fig 5.5: The mode shapes for CC-97 model – (a) The Finite Element Model, (b) Mode 1, (c) Mode 2, (d) Mode 4 and (e) Mode 5

Fig 5.6 The Crowchild bridge case study. Graphs showing damage with element numbers for no error and complete modes with 10% damage severity by Damage Index Method (a) original and (b) modified.

Fig 5.7 The Crowchild bridge case study.Graphs showing damage with element numbers for no error and complete modes with 10% damage severity by Matrix Update Method (a) Pseudo Inverse (b) Optimized

Fig 5.8 The Crowchild bridge case study.Graphs showing damage with element numbers for no error and incomplete modes with 10% damage severity by Damage Index Method (a) original and (b) modified.

Fig 5.9 The Crowchild bridge case study.Graphs showing damage with element numbers for no error and incomplete modes with 10% damage severity by Matrix Update Method (a) Pseudo Inverse (b) Optimized

Fig 5.10 The Crowchild bridge case study. Graphs showing damage with element numbers for random error up to 1% and incomplete modes with 10% damage severity by Damage Index Method (a) original and (b) modified.

Fig 5.11 Graphs showing damage with element numbers for random error up to 1% and incomplete modes with 10% damage severity by Matrix Update Method (a) Pseudo Inverse (b) Optimized

Fig-5.12 Mode shapes of 3D Space Frame: (a) Mode-1, (b) Mode-2 and (c) Mode-3

Fig 5.13 3D Space Frame case study. Graphs showing damage with no error in frequencies and complete modes assumed for Damage Index Method (a) original and (b) modified. (for element-29, 80% damage severity)

Fig 5.14 3D Space Frame case study. Graphs showing damage with no error in frequencies and complete modes assumed. Matrix Update (a) pseudo-inverse (b) optimized. (For element-29, 80% damage severity)

Fig 5.15 3D Space Frame case study. Graphs showing damage with no error in frequencies and complete modes assumed. Damage Index Method (a) original and (b) modified. (for element-29, 50% damage severity)

Fig 5.16 3D Space Frame case study. Graphs showing damage with no error in frequencies and complete modes assumed. Matrix Update (a) pseudo-inverse (b) optimized. (Elemenent-29, 50% damage severity)

Fig 5.17 3D Space Frame case study. Graphs showing damage with element numbers for random error up to 2% on frequencies and 10% on modes and assuming incomplete mode shapes. Damage Index Method (a) original and (b) modified. (element-29, 50% damage severity)

Fig 5.18 3D Space Frame case study. Graphs showing damage with element numbers for random error up to 2% on frequencies and 10% on modes and assuming incomplete mode shapes. Matrix Update Method (a) pseudo inverse and (b) optimized. (element-29, 50% damage severity)

Fig 6.1 Portage Creek Bridge, Victoria, British Columbia, Canada

Fig-6.2 Portage Creek Bridge Elevation of pier-2 (short columns) with sensor locations. (Huffman et al, 2006)

Fig-6.3 Time series of strain S_1_1_C1: (a) starting at 07:48:57 on 2006-4-14, No. of observations =30,000 at 1 second interval; (b): starting at 00:02:42 on 2006-4-15, No. of observations =256 at 1 second interval; (c): starting at 00:02:42 on 2006-4-15, No. of observations =256 at 1/32 second interval; (d): a steady state time series of strain S_1_1_C1

Fig 6.4 An accelometer time series at live loaded condition

Fig 6.5 Example of plotting of PACF by ITSM. The figure corresponds to a series of S_1_1_C1, live loaded condition after differencing by 1

Fig 6.6 Outlier analysis of the first AR Coefficients of Strain readings of S_1_1_C1. Pool size=132, Subgroup size = 4

Fig 6.7 Outlier analysis of the second AR Coefficients of Strain readings of S_1_1_C1. Pool size=132, Subgroup size = 4.

Fig 6.8 Outlier analysis of the third AR Coefficients of Strain readings of S_1_1_C1. Pool size=132, Subgroup size = 4.

Fig 6.9 Outlier analysis of the Fourth AR Coefficients of Strain readings of S_1_1_C1. Pool size=132, Subgroup size = 4

Fig 6.10 Outlier analysis of the First AR Coefficients of Accelometer readings of A_1_x. Pool size=124, Subgroup size = 4.

Fig 6.11 Outlier analysis of the Second AR Coefficients of Accelometer readings of A_1_x. Pool size=124, Subgroup size = 4.

Fig 6.12 Outlier analysis of the third AR Coefficients of Accelometer readings of A_1_x. Pool size=124, Subgroup size = 4

Fig 6.13 Outlier analysis of the Fourth AR Coefficients of Accelometer readings of A_1_x. Pool size=124, Subgroup size = 4.

Fig 6.14 Outlier analysis of the First AR Coefficients of Accelometer readings of A_1_y. Pool size=124, Subgroup size = 4

Fig 6.15 Outlier analysis of the Second AR Coefficients of Accelometer readings of A_1_y. Pool size=124, Subgroup size = 4

Fig 6.16 Outlier analysis of the third AR Coefficients of Accelometer readings of A_1_y. Pool size=124, Subgroup size = 4

Fig 6.17 Outlier analysis of the Fourth AR Coefficients of Accelometer readings of A_1_y. Pool size=124, Subgroup size = 4

Fig 6.18 Outlier analysis of the First AR Coefficients of Accelometer readings of A_1_z. Pool size=108, Subgroup size = 4

Fig 6.19 Outlier analysis of the Second AR Coefficients of Accelometer readings of A_1_z. Pool size=108, Subgroup size = 4

Fig 6.20 Outlier analysis of the third AR Coefficients of Accelometer readings of A_1_z. Pool size=108, Subgroup size = 4

Fig 6.21 Outlier analysis of the fourth AR Coefficients of Accelometer readings of A_1_z. Pool size=108, Subgroup size = 4

Fig 6.22 *R*-values of 27 data blocks of Strain S_1_1_C1 at Steady State Condition

Fig 6.23 Plotting of *R*-values of Strain S_1_1_C1 for 55 live loaded occurrences on continuous scanning.

Fig 6.24 Plotting of *R*-values of 31 daily live loaded condition of Strain S_1_1_C1 at 1 data block per day

Fig 6.25 Plotting of *R*-values of 39 live loaded condition of Strain S_1_1_C1 on 5 days interval

Fig 6.26 Plotting of *R*-values of 23 live loaded conditions of Strain S_1_1_C1 by monthly basis.

Fig 6.27 Plotting of *R*-values 7 selected strains of C1 at 9 live loaded conditions taken over the monitoring of the bridge

Fig 6.28 Plotting of *R*-values 8 selected strains of C2 at 9 live loaded conditions taken over the monitoring of the bridge

Fig 6.29 Plotting of *R*-values of 37 live loaded conditions of accelometer A_1_x, A_1_y and A_1_z (1 data block per 5days)

Fig 6.30 Plotting of *R*-values of 24 live loaded conditions of accelometer A_1_x, A_1_y and A_1_z (1 data block per month)

Fig 6.31 Graph of strain values of Strain S_1_1_C1 at 1second interval for 8 hours and 20 minutes at 0:0:0 time on 2006-03-01

Fig 6.32 Overall Strain vs. Temperature relationship of Strain S_1_1_C1 taking 27 monthly readings

Fig 6.33 Strain vs. Temperature relationship of S_1_1_C1 taking first 10 monthly

Fig 6.34 Strain vs. Temperature relationship of Strain S_1_1_C1, taking 11th to 20th monthly readings.

Fig 6.35 Strain vs Temperature relationship of S_1_1_C1 taking last 7 monthly readings

Fig A.1 Graphs showing damage with element numbers for no error and complete modes with 10% damage severity by Damage Index Method (a) original and (b) modified; by Matrix Update Method (c) Pseudo Inverse (d) Optimized

Fig A.2 Graphs showing damage with element numbers for no error and incomplete modes with 10% damage severity by Damage Index Method (a) original and (b) modified; by Matrix Update Method (c) Pseudo Inverse (d) Optimized

Fig A.3 Graphs showing damage with element numbers for random error up to 1% and incomplete modes with 10% damage severity by Damage Index Method (a) original and (b) modified.; by Matrix Update Method (a) Pseudo Inverse (b) Optimized

Fig A.4 Graphs showing damage with element numbers for no error and complete modes with 20% damage severity by Damage Index Method (a) original and (b) modified; by Matrix Update Method (c) Pseudo Inverse (d) Optimized

Fig A.5 Graphs showing damage with element numbers for no error and incomplete modes with 20% damage severity by Damage Index Method (a) original and (b) modified; by Matrix Update Method (c) Pseudo Inverse (d) Optimized

Fig A.6 Graphs showing damage with element numbers for random error up to 1% and incomplete modes with 20% damage severity by Damage Index Method (a) original and (b) modified; by Matrix Update Method (c) Pseudo Inverse (d) Optimized

Fig A.7 Graphs showing damage with element numbers for no error and complete modes with 30% damage severity by Damage Index Method (a) original and (b) modified; by Matrix Update Method (c) Pseudo Inverse (d) Optimized

Fig A.8 Graphs showing damage with element numbers for no error and incomplete modes with 30% damage severity by Damage Index Method (a) original and (b) modified; by Matrix Update Method (c) Pseudo Inverse (d) Optimized

Fig A.9 Graphs showing damage with element numbers for random error up to 1% and incomplete modes with 30% damage severity by Damage Index Method (a) original and (b) modified; by Matrix Update Method (c) Pseudo Inverse (d) Optimized

Fig A.10 Graphs showing damage with element numbers for no error using measured frequencies and complete modes with 10% damage severity by Damage Index Method (a) original and (b) modified; Matrix Update Method (c) Pseudo Inverse (d) Optimized

Fig A.11 Graphs showing damage with element numbers for no error using measured frequencies and incomplete modes with 10% damage severity by Damage Index Method (a) original and (b) modified; by Matrix Update Method (c) Pseudo Inverse (d) Optimized.

Fig A.12 Graphs showing damage with element numbers for random error up to 1% using measured frequencies and incomplete modes with 10% damage severity by Damage Index Method (a) original and (b) modified; by Matrix Update Method (c) Pseudo Inverse (d) Optimized

Fig A.13 Graphs showing damage with element numbers for no error using measured frequencies and complete modes with 20% damage severity by Damage Index Method (a) original and (b) modified; by Matrix Update Method (c) Pseudo Inverse (d) Optimized

Fig A.14 Graphs showing damage with element numbers for no error using measured frequencies and incomplete modes with 20% damage severity by Damage Index Method (a) original and (b) modified; by Matrix Update Method (c) Pseudo Inverse (d) Optimized

Fig A.15 Graphs showing damage with element numbers for random error up to 1% using measured frequencies and incomplete modes with 20% damage severity by Damage Index Method (a) original and (b) modified; by Matrix Update Method (c) Pseudo Inverse (d) Optimized

Fig A.16 Graphs showing damage with element numbers for no error using measured frequencies and complete modes with 30% damage severity by Damage Index Method (a) original and (b) modified; by Matrix Update Method (c) Pseudo Inverse (d) Optimized

Fig A.17 Graphs showing damage with element numbers for no error using measured frequencies and incomplete modes with 30% damage severity by Damage Index Method (a) original and (b) modified; by Matrix Update Method (c) Pseudo Inverse (d) Optimized

Fig A.18 Graphs showing damage with element numbers for random error up to 1% using measured frequencies and incomplete modes with 30% damage severity by Damage Index Method (a) original and (b) modified; by Matrix Update Method (c) Pseudo Inverse (d) Optimized

Fig B.1 Graphs showing damage with no error in frequencies and complete modes assumed for case-D1 by Damage Index Method (a) original and (b) modified; by Matrix Update (c) pseudo-inverse (d) optimized.

Fig B.2 Graphs showing damage with no error in frequencies and complete modes assumed for case-D2 by Damage Index Method (a) original and (b) modified; by Matrix Update (c) pseudo-inverse (d) optimized.

Fig B.3 Graphs showing damage with no error in frequencies and complete modes assumed for case-D3S by Damage Index Method (a) original and (b) modified; by Matrix Update (c) pseudo-inverse (d) optimized

Fig-B.4 Graphs showing damage with no error in frequencies and complete modes assumed for case-D3L by Damage Index Method (a) original and (b) modified; by Matrix Update (c) pseudo-inverse (d) optimized.

Fig B.5 Graphs showing damage with no error in frequencies and complete modes assumed for case-D4S by Damage Index Method (a) original and (b) modified; by Matrix Update (c) pseudo-inverse (d) optimized.

Fig B.6 Graphs showing damage with no error in frequencies and complete modes assumed for case-D4L by Damage Index Method (a) original and (b) modified; by Matrix Update (c) pseudo-inverse (d) optimized

Fig B.7 Graphs showing damage with no error in frequencies and complete modes assumed for case-D5S by Damage Index Method (a) original and (b) modified; by Matrix Update (c) pseudo-inverse (d) optimized.

Fig B.8 Graphs showing damage with no error in frequencies and complete modes assumed for case-D5L by Damage Index Method (a) original and (b) modified; by Matrix Update (c) pseudo-inverse (d) optimized

Fig B.9 Graphs showing damage with no error in frequencies and complete modes assumed for case-D6S by Damage Index Method (a) original and (b) modified; by Matrix Update (c) pseudo-inverse (d) optimized.

Fig B.10 Graphs showing damage with no error in frequencies and complete modes assumed for case-D6L by Damage Index Method (a) original and (b) modified; D6Lby Matrix Update (c) pseudo-inverse (d) optimized

Fig B.11 Graphs showing damage with no error in frequencies and complete modes assumed for case-D7S by Damage Index Method (a) original and (b) modified; by Matrix Update (c) pseudo-inverse (d) optimized

Fig B.12 Graphs showing damage with no error in frequencies and complete modes assumed for case-D7L by Damage Index Method (a) original and (b) modified; by Matrix Update (c) pseudo-inverse (d) optimized

Fig B.13 Graphs showing damage with no error in frequencies and complete modes assumed for case-D8S by Damage Index Method (a) original and (b) modified; by Matrix Update (c) pseudo-inverse (d) optimized

Fig B.14 Graphs showing damage with no error in frequencies and complete modes assumed for case-D8L by Damage Index Method (a) original and (b) modified; by Matrix Update (c) pseudo-inverse (d) optimized

Fig B.15 Graphs showing damage with element numbers for random error up to 2% on frequencies and 10% on modes and assuming incomplete mode shapes for case-D1 by Damage Index Method (a) original and (b) modified; by Matrix Update Method **(c)** pseudo inverse and **(d)** optimized

Fig B.16 Graphs showing damage with element numbers for random error up to 2% on frequencies and 10% on modes and assuming incomplete mode shapes for case-D2 by Damage Index Method (a) original and (b) modified; by Matrix Update Method (c) pseudo inverse and (d) optimized.

Fig B.17 Graphs showing damage with element numbers for random error up to 2% on frequencies and 10% on modes and assuming incomplete mode shapes for case-D3S by Damage Index Method (a) original and (b) modified; by Matrix Update Method (c) pseudo inverse and (d) optimized.

Fig B.18 Graphs showing damage with element numbers for random error up to 2% on frequencies and 10% on modes and assuming incomplete mode shapes for case-D3L by Damage Index Method (a) original and (b) modified; by Matrix Update Method (c) pseudo inverse and (d) optimized

Fig B.19 Graphs showing damage with element numbers for random error up to 2% on frequencies and 10% on modes and assuming incomplete mode shapes for case-D4S by Damage Index Method (a) original and (b) modified; by Matrix Update Method (c) pseudo inverse and (d) optimized

Fig B.20 Graphs showing damage with element numbers for random error up to 2% on frequencies and 10% on modes and assuming incomplete mode shapes for case-D4L by Damage Index Method (a) original and (b) modified; by Matrix Update Method (c) pseudo inverse and (d) optimized

Fig B.21 Graphs showing damage with element numbers for random error up to 2% on frequencies and 10% on modes and assuming incomplete mode shapes for case-D5S by Damage Index Method (a) original and (b) modified; Matrix Update Method (c) pseudo inverse and (d) optimized

Fig B.22 Graphs showing damage with element numbers for random error up to 2% on frequencies and 10% on modes and assuming incomplete mode shapes for case-D5L by Damage Index Method (a) original and (b) modified; by Matrix Update Method (c) pseudo inverse and (d) optimized

Fig B.23 Graphs showing damage with element numbers for random error up to 2% on frequencies and 10% on modes and assuming incomplete mode shapes for case-D6S by Damage Index Method (a) original and (b) modified; by Matrix Update Method (a) pseudo inverse and (b) optimized

Fig B.24 Graphs showing damage with element numbers for random error up to 2% on frequencies and 10% on modes and assuming incomplete mode shapes for case-D6L by Damage Index Method (a) original and (b) modified; by Matrix Update Method (c) pseudo inverse and (d) optimized

Fig B.25 Graphs showing damage with element numbers for random error up to 2% on frequencies and 10% on modes and assuming incomplete mode shapes for case-D7S by Damage Index Method (a) original and (b) modified; by Matrix Update Method (c) pseudo inverse and (d) optimized

Fig B.26 Graphs showing damage with element numbers for random error up to 2% on frequencies and 10% on modes and assuming incomplete mode shapes for case-D7L by Damage Index Method (a) original and (b) modified; by Matrix Update Method (c) pseudo inverse and (d) optimized

Fig B.27 Graphs showing damage with element numbers for random error up to 2% on frequencies and 10% on modes and assuming incomplete mode shapes for case-D8S by Matrix Update Method (a) pseudo inverse and (b) optimized; by Matrix Update Method (c) pseudo inverse and (d) optimized

Fig B.28 Graphs showing damage with element numbers for random error up to 2% on frequencies and 10% on modes and assuming incomplete mode shapes for case-D8L by Damage Index Method (a) original and (b) modified; by Matrix Update Method (c) pseudo inverse and (d) optimized

Nomenclature

$\boldsymbol{\beta}$	Perturbation factor indicating the change in matrix due the damage
τ_{ij}	jth feature from the ith subgroup of pool of feature
S_t	Standard deviation of the means of subgroups
γ_{ij}	Damage index γ_{ij} for the jth element in ith mode
$\boldsymbol{\varphi}_{\mathbf{a}}^{\mathbf{g}}$	Generalized inverse of mode shape matrix corresponding to degrees freedom **a**
S_i	Modal strain energy in the ith mode
S_i^d	Modal strain energy in the ith mode at damaged state
$\mathbf{R_i}$	Residual vector for ith mode
S_{ij}	Strain energy contributed by the jth element to the structure in ith mode
S_{ij}^d	Strain energy contributed by the jth element to the structure in ith mode at damage state
EI_j	Flexural rigidity of jth element of structure
$\overline{X}_i$	Mean of ith subgroup of features
$\psi_i^{d''}$	Modal curvature of a beam at damaged state
$\boldsymbol{\varphi}_{\mathbf{a}}^{\mathbf{T}}$	Transpose of mode shape matrix corresponding to degrees of freedom **a**
EI^d	Flexural rigidity of a beam at damaged state
EI_j^d	Flexural rigidity of jth element of structure at damaged state
$\boldsymbol{\varphi}_{\mathbf{di}}$	*ith* mode shape of the damaged structure
$\boldsymbol{\varphi}_{\mathbf{i}}^{\mathbf{T}}$	Transpose of ith mass-ortho-normal mode shape matrix
$\boldsymbol{\beta}_{\mathbf{k}}\mathbf{K}_{\mathbf{j}}$	Change in stiffness of element j
$Z_{\alpha/2}$	Percentage point of the normal distribution zero mean and unit variance such that $p[z \geq Z_{\alpha/s}] = \alpha/2$
$\{X_t\}$	Time series of X variable

$\mathbf{I}_a$	Identity matrix of size (a by a), and
$\boldsymbol{\varphi}_i$	*i*th mass-ortho-normal mode shape
$\psi_i''(x)$	Modal curvature of a beam
$\boldsymbol{\varphi}_a$	Mode shapes corresponding to degrees of freedom **a**
$\boldsymbol{\varphi}_r$	Mode shapes corresponding to degrees of freedom **r**
$\mathbf{u}_r$	Unmeasured displacements along degrees freedom **r**
$\rho_x(h)$	Autocorrelation function (ACF) of a stationary time at lag h
$\gamma(h)$	Auto-covariance function (ACVF) of a time stationary time series at lag h
θ	Coefficient vector of moving average process (MA)
$\gamma_x(r,s)$	Covariance function of a time series for all integers *r* and *s*
$E(\cdot)$	Denotes expectation function
$\mu(t)$	Mean of a time series
$\mathbf{u}_a$	Measured displacements along degrees freedom **a**
σ^2	Variation of a time series
$\{Z_t\}$	White noise of auto regressive moving average (ARMA) process
F_{ij}^d, F_{ij}	Total strain energy contributed by damaged element *j* in *i*th mode
$\mathbf{B}$	Modal residuals matrix
ϕ	Coefficient vector of auto regressive process (AR)
EI	Flexural rigidity of a beam
$\mathbf{K}$	Stiffness matrix of the structure
$\mathbf{k}_j$	Stiffness matrix of member *j*
$\mathbf{M}$	Mass matrix
R	Residual error index of a test block to the reference
$\mathbf{T}$	Transformation matrix transform incomplete mode shapes matrix $\boldsymbol{\varphi}_a$ to full size that corresponds to complete mode shapes.
$\mathbf{u}$	Displacement vector of the system
$\mathbf{y}$	Modal coordinates of structure
$\delta\boldsymbol{\varphi}_i$	Change in *i*th mass-ortho-normal mode shape

$\delta\mathbf{K}$	Change in stiffness matrix of the structure
$\delta\lambda_i$	Change in eigenvalue (squared frequency)
λ_i	Eigenvalue (squared frequency) of the structure

Chapter 1

Introduction

1.1 General

Structural Health Monitoring (SHM) is relatively a new field in engineering, mostly studied in aerospace engineering. In the last two decades it has created research interests in other disciplines of engineering including civil engineering. In general, SHM is concerned with performance monitoring of structures to ascertain the strength and performance states of critical members of the structures and determine the presence of any anomaly such as damage, or evaluate its degradation and remaining service life. A structural health monitoring system usually consists of sensors, data acquisition system, data transfer mechanism, data manipulation, and diagnosis.

In a general context, damage assessment can be defined at four levels (Rytter, 1993). In increasing order of difficulty, the four levels are:

(1) To detect whether there is damage,

(2) To determine the location of damage,

(3) To quantify the extent of damage, and finally

(4) To carry out prognosis such as safety evaluation and remaining life prediction.

There are various forms of structural degradation, such as cracking, corrosion, reduction in material properties that indicate the strength, reinforcement rupture, fractured welds, or loosened bolts.

Apart from detecting flaws in structures, the scope of SHM also includes the assessment of degradation rate of the structure.

SHM can reduce the chance of catastrophic failure, maintenance cost, and down time for rehabilitation. According to Mufti (2001), more than 40% of the bridges in service in Canada are over 30 years old. Therefore many of these bridges really need proper diagnosis, rehabilitation or even partial re-construction in order to make them safe enough for traffic and also prevent long down-time if sudden collapse occurs in the extreme cases. Chase and Washer (1997) conducted a similar survey for the bridges in United States of America, and found that about 33% of the total bridges were deficient. Most of these bridges were built before 1970, and their health condition is yet to be determined by any instrumental and scientific approach. Therefore in the context of structural safety, the need for the application of SHM has become highly important. Moreover for maintenance and rehabilitation purposes, the need for SHM has increased recently.

During the last two decades of advances in SHM technology, many new sensing methods with various systems for data collection to data management have been developed. With the advent of new technologies, innovative algorithms have been developed for monitoring civil infrastructures.

1.2 Brief discussion on SHM methods

Almost all damage detection methods for in-service stuctural components are non destructive. *Candian Institute of NDE* describes non-destructive Examination (NDE), also referred to as NDT (nondestructive testing) and NDI (nondestructive inspection), is a family of specialized technical inspection methods which provide information about the condition of materials and components without destroying them (CINDE 2008). Though conventional NDE methods are tools for performance assessment, their scope can extend to almost all types of engineering, especially structural, aerospace and marine engineering

Relevant conventional NDE methods are briefly described below along with Vibration Based Damage Identification (VBDI) techniques which is also a type of NDE method. The purpose of discussing these conventional NDE techniques is to draw some comparison between them and VBDI methods.

1.2.1. Visual Inspection

Visual inspection is the predominant nondestructive evaluation (NDE) technique used in bridge inspections. However, since implementation of the National Bridge Inspection Standards in the US in 1971, a comprehensive study of the reliability of visual inspection has cast some doubt on this method as it relates to highway bridge inspections. Factors that appeared to affect the accuracy of visual inspection results include visual acuity and color vision; light intensity, inspector qualification and experience; and perceptions of maintenance, complexity, and accessibility. The damage might be the spalling of

concrete, steel corrosion and cracking in reinforced concrete structures, loosening of bolts, and crack in weld. The part of the structure to be inspected must be accessible. This sometimes becomes impossible for large and complex structures. For underwater and space structures, the inspectors need to be geared and equipped properly. To reach the ordinarily inaccessible structural elements to examine, sometimes it may be necessary to use robotics technology and special transportation means.

1.2.2 Liquid Penetration Testing (LPT)

LPT is an advanced type of visual inspection. It is relatively simple and it can detect flaws in all type of materials. The flaw should be open to the surface and this requirement is a drawback to this method. Some fluid materials such as petroleum or watery substances dyed with color are inserted into the surface and they seep deep into the material. A white developer material is placed on the surface. The penetrated liquid strains the developer if there is any flaw. It is clearly not applicable for the determination of the strength of the material. This method is highly sensitive and needs prior knowledge of the location of the damage.

1.2.3 Magnetic Particle Testing (MT)

MT is applicable to metal substances only. A magnetic field is propagated by electrical equipment. Unlike Penetration Testing, the flaws do not have to be open to the surface,

but it must be close to it. So, prior knowledge of the damage is still required. MT works best for flaws which are elongated rather than round. Magnetic field is generated inside the specimen or structural component to be tested. Distribution of magnetic particles such as iron over the magnetized area indicates flaw patterns. This method is not suitable for concrete and wood, two other major building materials of conventional structures. Circular type damage is not suitable for MT, adding to its disadvantages further. Assessment of strength is not possible by the analyzing the formation of the magnetic particles.

1.2.4 Radiographic Testing (RT)

Usefulness of RT depends on the density and thickness of the testing component. The denser and thicker materials will absorb more radiation. Therefore if a component such as column has some crack inside it, cracked area will absorb less radiation than the rest of the column from the radiator. The pattern on film capturing the radiation will indicate the location and extent of the flaws. However two dimensional views sometimes hide additional defects in a structural component.

1.2.5 Ultrasonic Testing (UT)

Ultrasonic testing uses transmission of mechanical vibration created by sophisticated equipment to identify both linear and non-linear damage. Any material that can act as a medium of transmission of mechanical vibration can be tested with this method. The propagated wave is reflected by a damaged area because of its different acoustic nature. Reflected waves are converted to electric energy and being received by a cathode ray

tube (CRT) as signals. The pattern of the signals shows the location and extent of the damage. Again, prior knowledge of the damage is needed in this method. This method is expensive too.

1.2.6 Eddy Current Testing

The Eddy Current Method is usable only on electrically conductive materials. A magnetic field is created by electrified coil around the component. Fluctuating magnetic field induces an eddy current. The damaged portion resists the flow of eddy current. This can be identified by voltmeter reading. The equipment is small, but only a small area can be tested at a time. Prior knowledge of damage is required in this method, too.

1.2.7 Static Load Test

In static load test method, some loads of significant magnitude are placed at some critical locations of the segment to be tested. The displacements and deformations at some relevant locations are measured by sensors attached to those places. If structure is weakened, obvious deviation from the normal state can be observed from the test.

Usually this test is done after some possible occurrence of damage in part of the structure. This test is useful in determining the reduced strength of whole structure due to the presence of damage. However, like visual inspection this test cannot be used for the prior warning of occurrence of damage or the reduction of strength. Another drawback of this

method is that the structure may have to be evacuated for the test. The cost of instrumentation and time involvement are other disadvantages of the test.

1.2.8 Vibration Based Damage Identification (VBDI)

There has been substantial work on Vibration Based Damage Identification in recent years. VBDI depends on the change of dynamic characteristics of the structures. These characteristics are natural frequencies, mode shapes and damping properties. These characteristics directly depend on material properties, geometry and support condition which contribute to the stiffness and also the distribution of mass. Both stiffness and mass matrices together determine frequencies and mode shapes of a structure. Damage can cause change to any of these dynamic characteristics. Therefore, the VBDI method uses any change to dynamic or modal parameters of structures to identify, locate and detect the severity of the damage. The damage identification process also includes precise modeling of structure and calculation of damage detection algorithm, which necessitates computer programming. In addition, very accurate determination of modal parameters is a prerequisite to good diagnosis of the structure. This thesis consists of application of VBDI on two real structures. Therefore its advantages will be discussed compared to other NDE methods more thoroughly in the following section. Its disadvantages are discussed later in section 1.4.3.

1.3 The advantages of VBDI over other NDE methods

Among various methods discussed above, static load test and VBDI are global damage detection methods and the rest are direct local damage detection methods. Among the direct methods, most commonly used is visual inspection. Yet its reliability has been under question based on the study by Federal Highway Administration (FHWA, 2001). Other local NDE methods are found more reliable and definitive than visual inspection. The main advantage of local NDE methods over global methods is that they capable of detecting and locating damage quite precisely. However, NDE methods are generally capable of inspecting small areas at a time. The evaluation of a large and complex structure can be costly and time consuming and sometimes impossible by local NDE methods. The portion of the structure has to be accessible to apply any of local NDE methods. Moreover frequent inspection of structures is also impractical by these methods.

VBDI and Static load test, though less accurate in local detection of damage, are solutions to the problems encounter by other NDE methods. Static load test has some drawbacks; the structure has to be evacuated during test, instrumentation is usually more costly than that required for VBDI and subterranean and space structures are very hard to be evaluated by this test. Once proper installment for measuring vibration and also displacement along various degrees of freedom is done, the system can be monitored almost seamlessly using integrated VBDI system.

1.4 Overall effectiveness of VBDI and its relevant features

For the last a few years, there has been some noticeable research work done in the VBDI technique, or some times referred as vibration based damage detection (VBDD) technique. From those research studies some strengths and weaknesses of this global damage detection method have been worked out, and it has given the scope for further research in the future.

1.4.1 Earlier findings

A number of researchers have explored the use of VBDI for assessing the condition of bridges and other types of structures (Doebling et al., 1996, 1998). VBDI techniques have been particularly successful when applied to rotating machinery (Shives and Mertaugh 1986, Farrar and Duffey 1999), but have also been successfully applied to well-defined aerospace or mechanical systems (West 1982, Hunt et al. 1990; Chang, 1997 &1999), and to simple structures such as beams or trusses (Pandey and Biswas, 1994).

A number of efforts have been made to apply VBDI techniques to real bridge structures over the last decade Toksoyand Aktan (1994), Farrar et al. (1994), Jauregui and Farrar (1996), Zhang and Aktan (1998), Peeters (2000), Catbas and Aktan (2002), Ventura et al. (2002), Kim and Stubbs (2003), Zhou (2006). These research studies have convincingly shown that VBDI can be a tool for damage detection in practical structures. However, most of them also have mentioned that this method is good for identifying typically severe damage scenarios and some totally ignored the moderately damaged components in identification.

1.4.2 General approach of VBDI method

Dynamic properties, such as natural frequencies, mode shapes and modal damping of a structure depends on some physical parameters of the structures such as mass, stiffness and damping. The damage can change any of the physical properties of the structure and this in turn will change the dynamic, also referred as vibration characteristics of the structures. Hence, there should be relation between the change in dynamic characteristics and the occurrence of damage. Therefore in most VBDI techniques it is needed to know the dynamic characteristics of the test structure before and after the damaged state

VBDI method is an integrated approach of experimental and analytical processes. In most cases, the major components of this process are: 1) Measurement of dynamic characteristics, 2) Computer modeling of the real structure, and 3) Detecting damage by identification algorithm. A high degree of accuracy of the process of all components is required for reliable VBDI system. As VBDI is highly sensitive to degree of accuracy, therefore, total understanding of these components is a prerequisite for the successful application of the method whose components are briefly described below. The framework of the VBDI system is shown in Fig-1.1

1) Measurement of dynamic characteristics:

Accuracy of the measurement of frequencies, mode shapes and modal damping of structures depends on some factors like the vibration methods, sensing technology, and arrangement of sensors on the structures and signal processing of the data obtained from sensors.

There are two types of vibration methods used in practice. First, controlled excitation, which is applicable on small structures and laboratory specimens. The second method is ambient excitation, which is the only available method for many real life structures that are too large to be vibrated adequately by the first method.

Sensor Technology:

In recent years, there has been significant advancement in sensing technology by electrical and communication engineering. Optical fiber sensors, piezoelectric sensors and dielectric sensors are some of the most popular in this category, but the first two are most used in the monitoring of bridge structures.

The sensors should be robust enough to stay in good condition under various loading and environmental conditions. Long-term behavior of sensors can be assessed by some in-field methods. However, there is a technique recently developed know as pattern recognition which is effective in identifying the accuracy of sensor readings. This method which is also useful in SHM, too, is a major field of research in this thesis and it will be discussed thoroughly later.

Since a signal is the primary input of the VBDI system, its accuracy should be high enough, otherwise the system will give a wrong output even if other components of the system are perfect. Calibration of the sensors should be done with respect to their host structures.

An optimum distribution and proper orientation of sensors on large complex structures with many degrees of freedom is needed to ensure adequate measurement for modal parameters, and also the low cost of the sensing system (Amin, 2002).

Data Processing

Not all portions of the data gathered from the sensors are needed for identification of dynamic characteristics of the structures. Some of the responses may not represent those of the actual structure. Some data contain an environmental component which needs to be separated to get the structural component. Even those signals that may be related to vibration characteristics of the structure are not collected in readily usable form. Therefore they must undergo some processing technique to extract modal features such as frequencies, mode shapes and damping. For example, Fourier transformation converts accelerometer readings to frequencies.

2) Computer modeling of physical properties of real structure

To apply the damage detecting algorithm, in most cases an appropriate simulated computer model is needed. Usually the model developing software utilizes the concept of Finite Elements and therefore is called finite element modeling (FEM). This FEM is then combined with damage detection algorithm. The model should very closely represent the real structure. However this is not so easily obtained. In real life, structures are relatively large in size with the inherently greater uncertainties in material properties, support conditions, and connectivity of components. Therefore a meticulous approach is needed to create a proper model that shows the values of modal parameters close to that

measured by sensing and signal processing. As well, development of FEM of large structures can be sometimes labor intensive and time consuming.

3) Detecting damage by VBDI algorithms

In the past two decades a good amount of research on VBDI has given emergence to various methods and algorithms for identification of damage, its location, severity and nature. Studying substantial amount of literature, Doebling et al (1996) and Farrar et al (1994) have provided some extensive and resourceful review on damage detection by VBDI. Chang(1999), Aktan at al (1999), Zhang and Aktan (1998), Peeters (2000), Catbas and Aktan (2002), Ventura et al. (2002), Kim and Stubbs (2003) and Humar et al. (2006) have worked intensively on damage detection methods.

While some of the methods for damage detection are briefly described in this section, others that are more related to the present work will be explained more thoroughly later in Chapter 3.

Vibration based damaged detection method is dependent on modal frequencies and shapes. It has been observed in some of the research studies mentioned above that local response is sensitive to higher frequency modes, while global responses are sensitive to lower frequency modes. Unfortunately it is very difficult to measure higher frequency modes accurately, while higher frequency modes are more indicative of local damage. Moreover, higher frequency modes need more energy making excitation process harder.

For that reason, most vibration-based damage identification methods rely on lower modes of vibration. The members that contribute very little strain energy are not identifiable some times. The members that undergo a rigid body displacement at low modes also cannot be detected for damage.

It has been observed that the relation between modal damping and damage is not so consistent. Also, measurement of damping ratio of the practical structures with sufficient accuracy is very difficult. Therefore, modal damping is not a popular choice for VBDI approach. Usually it is also not incorporated in a VBDI system.

Sensor installation is not always possible as per the theoretical requirements. In order to make the process of damage identification reliable, it is always required to measure modal displacements at various modes accurately. To do so, it may sometime be required to place numerous sensors on the structure. However it is impractical and very expensive to implement a sensing system to give complete mode shapes. Sometimes some points are not accessible in a complex and large structure. Therefore it is required determine the optimum number and location of sensors. This objective is not so easily obtainable and it involves some approximate computer simulated approach which is very much labor and time consuming. In most cases, damage detection algorithms interpolate between sensor locations to get the intermediate values for mode shapes. This process further induces uncertainty errors to the process.

The change in mode shapes and mode shape curvatures and modification in mass, stiffness and damping matrices are used for detecting damage by these methods

Frequency Changes

At the rudimentary state of VBDI, most of damage detection was based on shift in modal frequency induced by damage. Cawley and Adams (1979) and Salawu (1997) have used of modal frequency changes in damage identification. In a complex structure, the change of modal frequencies is not very sensitive to the damage of some members. This imposes a significant limitation on this method. Practically, this method shows reliable result when the amount of damage is high.

Mode Shape Changes

This method uses mode shapes curvature or derivatives to deduce damage pattern. This method proposed by Pandey et al (1991) is based on the fact the damage in a beam will change the flexural rigidity of the beam, hence the change of curvature should differ in damaged from undamaged state and it is inversely proportional to the flexural stiffness. Apparently, damaged portions will have larger increase in mode shapes than rest of the structure. It is difficult to calculate the curvature from measured mode shaped result, indicating a limitation of this method.

Strain Energy Changes

This method is alternatively known as damage index method which was proposed by Strubbs and Kim (1994) to identify damage in a beam-type structure. They defined

damage index as the change in strain energy content of the structure when it is deformed in a particular mode shape. A statistical approach is used to examine the change in strain energy and identify damaged portion of the structures from these changes. This method requires the complete shape, but experimentally it is almost impractical and highly expensive to install sensing system that will give a complete mode shape. Therefore interpolation is usually carried out to get the complete mode shape and this incurs numerical errors.

Methods Based on Updating Properties Matrices

These methods rely on updating physical properties matrices of structures, so that the frequencies and mode shapes of the modified system are in accordance with the measured characteristics of the damaged structures. Different algorithms are used to get the update matrices. Various methods obtain updated matrices by solving equation of structural motions, equations of physical properties of the structures and modal characteristics. Optimal Matrix Update Method, Sensitivity Based Update Method and Hybrid Matrix Update Method are some of the commonly used damage detection algorithms under this category.

1.4.3 Limitations of VBDI methods

Though it was previously discussed in section 1.3, the various advantages the VBDI method has over other NDE methods, it does have some significant limitations. Therefore it should be combined with one or more of other NDE methods to assess a structure completely.

VBDI method depends on the change of stiffness for damage identification. However not all types of damage reduce stiffness. For example, excessive reduction of pre-stressing forces in the strands or their failure will not reduce stiffness of the concrete element of a pre-stressed structural component.

Many VBDI methods rely on Finite element models of a structure. The real challenge of this modeling is to make it closely represent the real structure in the context of dynamic responses to excitation in various modes. There are some uncertainties associated with this type of model, such as assumption of material properties, support conditions, behavior of joints, in FEM modeling. Such uncertainties increase with the complexity of the structures.

Damage detecting algorithms themselves have their own limitations. Many widely used algorithms are based on updating of matrices such as stiffness, mass and damping. In these techniques, non-linear optimization is made to make the matrices compatible to the damaged state. For analyzing complex structures, these processes sometimes yield impractical results that may not to be acceptable.

It has been commonly observed by using various damage detection algorithms that dynamic characteristics of a structure are less sensitive to damages at lower levels, whereas early detection of damage in the structures is very important in order to reduce the rehabilitation cost significantly.

Based on the literature review on the research on vibration-based damage detection methods, Doebling et al. (1996) indicates that there are many critical issues that need to be addressed in the future in order to increase the effectiveness of these methods. It was found in the review that most of the techniques require prior analytical models and/or prior test data for the detection and location of damage. Many algorithms need a detailed and reasonably accurate FEM of the structure. Others presume that a data set from the undamaged structure is available. Often, the difficulty of availability of this type of data can make the method practically not feasible. The minimization of dependency on FEM and prior data may be a challenging task. The issue related to the optimal number and location of sensors that are needed to produce accurate mode shapes and frequencies are also required to be addressed. It is found that most techniques that appear to work well in example cases actually perform poorly when subjected to the measurement constraints imposed by actual testing. In general, the damage detection methods are found to be more sensitive to errors in case of low level of damage states.

Considering the advantages and disadvantages of VBDI in this chapter, it can be inferred that although these methods have some distinct advantages, they also have some limitations. Among these, are the limitations posed by need for sophisticated finite element modeling, and modal analysis which need considerable human interaction, which is prone to errors. Other than that, uncertainty in measurement data and lack of accuracy in detecting damage at the early stage are also notable limitations of these methods. To avoid such disadvantages, some pattern recognition approaches have been developed by researchers in recent years. These methods, though theoretically deem reasonably sound,

have not yet been widely applied on real life structures, though some experimentally demonstrated their applicability on small structures.

1.5 Structural Health Monitoring by Pattern Recognition Techniques

Most of the pattern recognition approaches of damage detection are on a global basis; although some work has been done to locate the damage and determine its severity. Since this method is arguably the newest of all global damage detection methods, much more research needed to develop methodologies to detect local damages with severity of the structures.

According to Sohn et al (2000), sensors measuring strains and vibration of a structure produce signals that always respond to the change of environmental and operational conditions. Each group of signals can be considered a pattern (a definable entity) that has some relation to the structural and ambient condition. They proposed that if the effect of ambient condition to the patterns is normalized, they should be nearly identical or close to one another for similar vibration effect as long as structural vibration property remains same. However, it can be assumed, the change in physical properties, mainly stiffness, should be reflected on the processed signal blocks or patterns. Based on this assumption, various methods of damage detection by pattern recognition have been developed

Pattern recognition is aimed for machine learning process, i.e., ability of a computer to identify and classify (group) them to make a decision. It is this feature that makes it very

much attractive to create automated structural health monitoring system. Once a suitable pattern recognition system implemented on a computer that is linked to a database of the sensing system, it will automatically diagnose the structure without human involvement. Recognition of patterns can be divided into two types:

1) Supervised learning: Here input patterns of the vibration of a structure are compared to a pre-defined class. Classes are designed by system designer. Supervised recognition refers to the case where data is available for both undamaged and damaged state.

2) Unsupervised learning: In this method, patterns of vibration are categorized to undefined classes. Here classes are learned based on the similarity of patterns. Unsupervised learning refers to the case when data is available only for one state, usually undamaged condition.

Learning from a training set and applying it to the test set to identify, classify or discriminate is the basic approach in most pattern recognition techniques. There are two approaches of pattern recognition in structural health monitoring.

1) Statistical approach

2) Neural Networking

1.5.1 Pattern Recognition by Statistical methods

Statistical pattern recognition in terms of structural health monitoring has gained attention recently in the civil and aerospace engineering fields. This method incorporates the techniques of signal acquisition from sensors installed on the structure, and then processing of signals, constructing models of training data for classification, then identification and discrimination of the testing data and making decision accordingly

For the past few years, several studies have been conducted for damage detection in the context of structural health monitoring. Farrar et al (1999 and 2001) have proposed a generalized integrated approach for structural health monitoring by statistical pattern recognition.

Here the general approach typically followed in statistical pattern recognition in SHM is described as outlined by Farrar et al (1999 and 2001).

Data collection

Data is usually collected through a sensing system attached to the test structure. Sensitivity and accuracy of the sensors should be high, especially in the case of real life large structures where vibration can only be obtained by ambient excitation as opposed to controlled excitation which is applicable to small structures only. However placement and orientation of sensors are less critical than in the case of conventional methods of VBDI which use dynamic characteristics to determine damage, hence the accurate

measurement of mode shapes is required, and therefore sensors are needed to be placed accordingly. Statistical pattern recognition does not need to deal with the mode shapes.

Data Preprocessing

Rarely signals obtained from sensors can be readily used for modeling. Signals are usually gathered continuously. They can be polluted by other activities of the test or nearby installation. Strain data is significantly influenced by temperature and external loading. In some model types, data needs to be corrected for all or some of these external noises on the signals.

When data are collected continuously, it is necessary to separate the signals of significant ambient oscillation from those of the idle condition. This technique is similar to classification, but it does not need the involvement of any complicated pattern recognition approach. Separation of data of accelerometers can be done by applying simple statistical techniques involving moving average method. Usually a systematic statistical algorithm is utilized to pick up the signal blocks relevant to vibration analysis of the structure.

Feature Extraction

It is the process of extracting variables that are dependent on the structural damage condition. Since all signal types are basically time dependent, typically a time series model is constructed to determine the feature vectors. The feature vectors contain the set

of damage sensitive variables of the structure. These features are compared to determine health of the structure.

Since signals are mainly time series type, model types appropriate for time series analysis are usually utilized in damage sensitive feature extraction. One such popular method is Auto-Regressive Moving Average (ARMA) modeling. It has two parts; Auto-Regressive (AR), which depends on the previous output of the time series, and Moving Average (MA) that uses only the input of the system to predict future values. When degree of MA is 0, ARMA process is reduced to AR model which is the most used methods in damage detection.

Analysis of feature distribution

This is the final step that discriminates damaged state from undamaged state. Various algorithms are applied for this classification:

1) Group classification

Group classification attempts to classify the features into either "undamaged" or "damaged" categories by some statistical quantities. It uses the experience of previous state of undamaged and damaged states to make decision on categorization of damaged conditions and their extent of severity.

This method is applicable to supervised learning. However, in reality rarely damaged conditions can be available for the current test structures. Nonetheless, it is possible to use patterns of damage conditions of previously recorded similar structures.

2) Outlier detection

This method is used when data are available only for the undamaged state therefore; it is applicable to unsupervised learning process only. This detection algorithm attempts identify damage states observing significant change in features that cannot be explained by extrapolation of previously observed features when the structure was at normal state. Multivariate Probability Density Function estimation can be used in this type of analysis. Statistical process control is another means that can be employed to identify outliers. This approach has the advantage that it can detect trends in the data that is useful to predict the time when particular features will become outliers .

3) Regression analysis

This method attempts to correlate data features with particular locations or extents of damage. The features are mapped to a continuous parameter, such as spatial location, or a remaining-useful-life temporal parameter, as opposed to group classification where the features correspond to discrete categories such as "damaged" or "undamaged".

Regression analysis for damage detection requires the availability of features from the undamaged structure and from the structure at varying damage levels. Therefore it is applied on supervised learning type.

If the structure is damaged most values of extracted features should fall outside some threshold value determine by the specific algorithm.

1.5.2 Pattern Recognition by Neural Network

A neural network (NN), sometimes called an Artificial Neural Network, is a mathematical model similar to a human brain. Many interconnecting nodes known as artificial neurons form the system of networking. The connections between their input and output are known as weighted edges. It is an adaptive system based on the input-output data transmission during the learning phase of the system.

Using a sequential training procedure, it is possible that a neural network can learn input-output relationship of processed signal obtained from sensors measuring vibration and strain data.

A Commonly used family of neural networks for pattern classification tasks (Mao and Mohiuddin, 1996) is the feed-forward network, which includes multilayer perception and Radial-Basis Function (RBF) networks. These networks are organized into layers and have unidirectional connections between the layers.

Another popular network is the Self-Organizing Map (SOM), or Kohonen-Network (Kohonen, 1995), which is mainly used for data clustering and feature mapping. The learning process involves updating network architecture and connection weights so that a network can efficiently perform a specific classification/clustering task.

Pattern recognition by neural network requires very little amount of structural engineering knowledge. Neural networks have some good nonlinear algorithms for feature extraction of the structure, (mainly the damage sensitive and its localization features), and classification of the damage (e.g., multilayer perceptions). Though principles of pattern recognition by neural network seem to differ from those of statistical approach, most neural network models are implicitly equivalent, or similar to statistical pattern recognition methods. Ripley (1993) and Anderson et al (1990) also discuss this relationship between neural networks and statistical pattern recognition. Anderson (1990) pointed out that "neural networks are statistics for amateurs. Most NN's conceal the statistics from the user."

1.6 Objectives and Scope of the Proposed Research

The objectives of present thesis are as follows:

- To develop a reasonably close computer model of the test structures, and update the structural models to correlate their response to the test data.
- To assess various vibration-based damage detection algorithms using the correlated structural models and identify the uncertainties associated with the methods.
- To develop a statistical pattern recognition scheme for assessing the structural condition and degradation rate of a bridge using the monitoring data.
- To develop a statistical pattern recognition scheme for isolating the contribution of thermal strain in the measured strain data.

The first part of the research is on the application of vibration-based damage identification techniques to practical structures, to evaluate their feasibility in practice, and to assess their performance. One of the structures considered here is a three span bridge and the other one is a space frame. The second part of the research is the study of a realistic approach of statistical pattern recognition using the vibration and strain data collected from a bridge. The different structure has been used for second part because the vibration and strain data are not available for the structures tested in the first part of the research work. The following steps have been followed to achieve the above goals:

Step-1: Development of finite element models of structures considered using the as-built physical and mechanical properties and refinement of respective models by realistically adjusting the physical properties to bring the dynamic characteristics of the model to the measured values, as close as possible.

Step-2: Application of various damage detection algorithms on the FE model considering various simulated damage cases which include various practical factors such as measurement noise and incomplete spatial measurements of mode shape vectors.

Step-3: Classification of the sensor data to identify the idle and live loaded condition of a bridge by inspecting its monitoring data.

Step-4: Development of time series models of training and testing data to extract the damage sensitive features; and calculation of other relevant parameter such as residual errors.

Step-5: Development of a scheme for discriminating or classifying the statistical features and parameters obtained in Step-4 for damage detection.

1.7 Organization of the thesis

Chapter-1: Introduces vibration based damage identification techniques and statistical pattern recognition methods for structural health monitoring. It also briefly reviews these two methods.

Chapter-2: Discusses the reviewed literature on damage detection techniques related to the proposed research fields and also proposed research areas are identified.

Chapter-3: Describes the theoretical background of VBDI techniques and mathematical principles of various damage detection algorithms that are used for proposed damage detection.

Chapter-4: Discusses the literature and theories involving an integrated statistical pattern recognition approach for structural health monitoring. It also describes the mathematical background for modeling of time series data from sensors.

Chapter-5: Describes the physical properties of the test structures and presents the detailed results of various simulated damage conditions using a software system capable of creating finite element models and applying various damage detection algorithms.

Chapter-6: Demonstrates the statistical pattern recognition scheme on a three span concrete bridge, and discusses the results.

Chapter-7: Discusses the findings of the proposed project, interpreting the relevant features of the research work and based on them, and discusses the scope for further research.

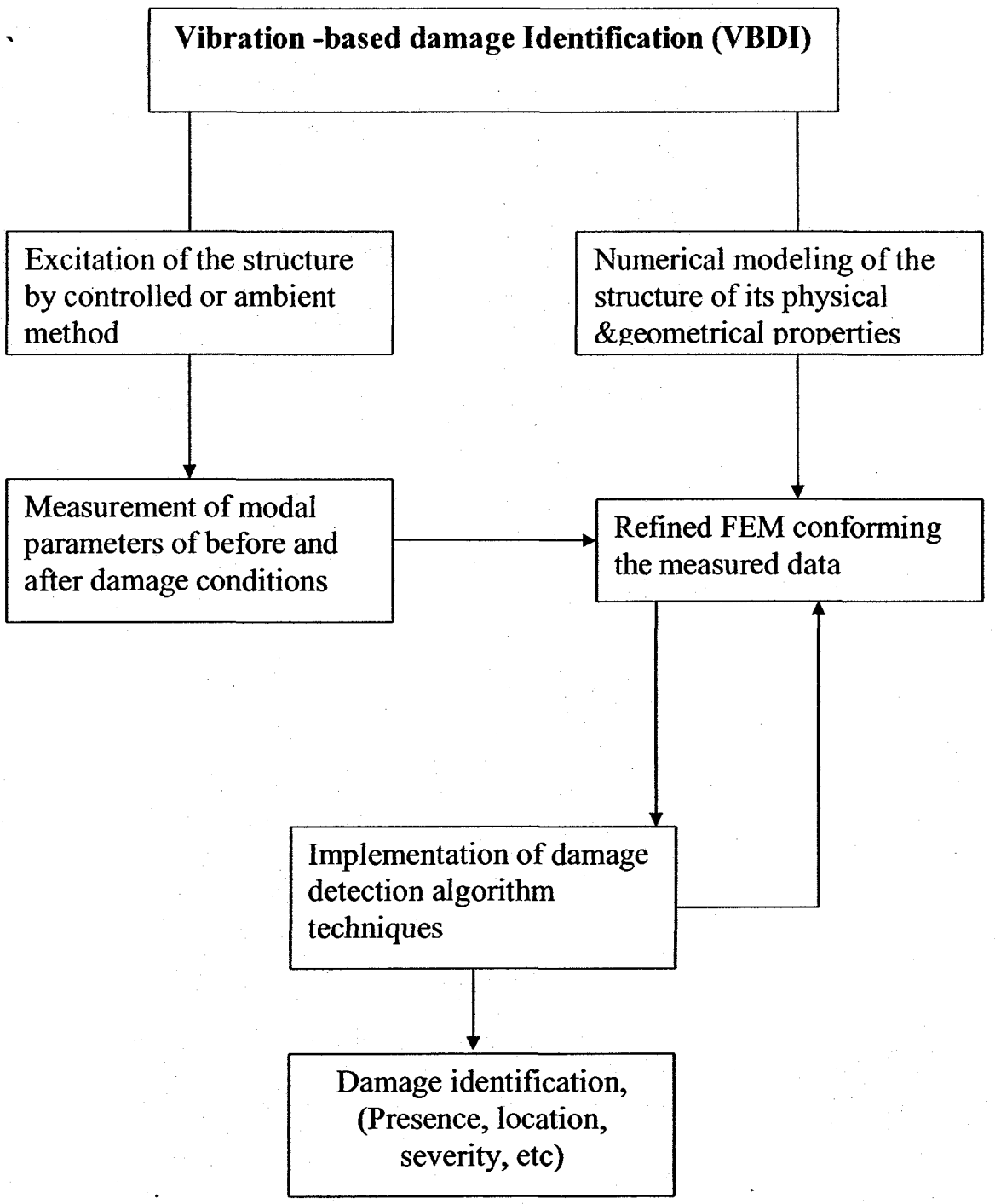

Fig-1.1: The basic framework for a typical Vibration Based Damage Identification system

Chapter 2

Literature Review

2.1 General

In this chapter, relevant literature has been reviewed for the purpose of understanding the field of thesis and identifying the scope of work. The review covers materials on primarily vibration based damage detection methods and statistical analysis. In addition, other relevant areas are briefly explored.

2.2 Methods of VBDI and Relevant Research work

Over the last four decades, many damage indices, derived from damage induced changes to modal parameters, have been proposed. Detailed review of these techniques has been provided by Doebling et al. (1996, 1998). Here, VBDI techniques are classified based on specific measured and implemented dynamic properties. Work on various VBDI techniques are described in the following subsections.

2.2.1 Methods based on change in natural frequency

There is substantial technical work available on the method of damage detection using shifts or changes in natural frequency. The changes in structural properties such as

stiffness, mass and damping are reflected on the change in frequencies induced by excitation. This is the basic assumption of this method for damage identification by frequency shifts.

However, there are some limitations to this method. By different research studies, changes in frequency have been observed to be quite insensitive to damage; and additionally natural frequencies are highly sensitive to changes in temperature and other environmental conditions. Consequently the detection of damage can be difficult even in relatively simple cases because measured frequencies may include the effect of ambient conditions.

There are two categories to the method of damage detection by change in frequencies.

Category-1 methods are limited to Level 1 damage identification, and

Category-2 is typically used for Level 2 and Level 3 damage identification.

The definitions of the levels of damage identification are provided in section-1.1.

2.2.2 Methods based on mode shape change.

(a) Method of direct change in mode shape

It has been observed in various studies that changes in mode shapes may work as good indicators for the damage identification, and also determination of the location of damage. Single-number approach of mode shape changes has been suggested to detect

damage. A common single-number measure is called the Modal Assurance Criterion (MAC) (Ewins, 2000). The MAC value of two modes ϕ and ϕ^* (the mode shape in the undamaged and damaged states respectively) is expressed as:

$$MAC = \frac{\left|\sum_{j=1}^{n} \phi_j \phi_j^*\right|^2}{\sum_{j}^{n} \phi_j^2 \sum_{j}^{n} \phi_j^{*2}} \qquad (2.1)$$

with n is the degrees of freedom defining the mode shape.

The MAC value thus indicates the degree of correlation between two modes. It ranges between 0 to 1, here, 0 indicates no correlation between two mode shapes and 1 means the exact correlation between the two. It is the deviation from 1 of MAC value obtained by relative comparison between two mode shape measurements is considered as a damage indicator for the structure in consideration.

Allemang (2002) gave an overview on the application of MAC values and some related criteria for the correlation between two modes. Srinivasan and Kot (1992) applied this method on a shell structure and claimed that changes in mode shapes were better indicators of damage than resonant frequency shifts. These changes were determined quantitatively using changes in the MAC values drawing comparison between the damaged and undamaged mode shapes.

The Co-ordinate Modal Assurance Criterion (COMAC) is differentiated from the MAC definition. It gives both local and combining information from different modes. The COMAC at modal co-ordinate j with m modes is defined as (West, 1984):

$$COMAC_j = \frac{\left|\sum_{i=1}^{m} \phi_{j,i}\phi_{j,i}^{*}\right|^2}{\sum_{j}^{m}\phi_{j,i}^2 \sum_{i}^{m}\phi_{j,i}^{*\,2}} \qquad (2.2)$$

If the modal displacements at co-ordinate j from two sets of measurements are identical, the COMAC value equals to 1 for this co-ordinate. The smallest COMAC value at any point indicates a possible location of damage.

Any structural damage should reduce stiffness locally. Therefore the biggest change in mode shape displacement is expected to occur at the damaged locations. The definition of unit-norm normalized mode shape is used for interpretation of the change of mode shape method. For a free vibrating system, the dynamic equilibrium equations can be written as:

$$[m]\{\ddot{y}\}+[k]\{y\}=\{0\} \qquad (2.3)$$

where $[m]$ and $[k]$ are the system mass and stiffness matrices respectively, and

$\{y\}$ and $\{\ddot{y}\}$ are the displacement and acceleration vectors of the system respectively.

The displacement vector $\{y\}$ associated with a particular mode of vibration can be expressed as follows:

$$\{y\}=\{\phi\}\sin(\omega t) \qquad (2.4)$$

where $\{\phi\}$ is a mode shape of the system,

ω is the angular natural frequency associated with that mode shape and t is time. Hence,

$$\{\ddot{y}\} = \omega^2 \{y\} \sin(\omega t) \qquad (2.5)$$

Substituting Eq. 2.4 and Eq. 2.5 into Eq. 2.3, a set of simultaneous homogeneous algebraic equations are obtained as follows:

$$([k] - \omega^2 [m])\{\phi\} = \{0\} \qquad (2.6)$$

Solution of this equation yields its i_{th} eigen-value, ω_{io}^2, and its i_{th} eigenvector, $\{\phi_{io}\}$.

The total number of eigen-values and eigen-vectors equals to the rank of the stiffness and mass matrices. This number is equal to the number of the degrees of freedom of the system. The amplitude of mode shape $\{\phi_{io}\}$ is always indeterminate. Practically in a dynamic test, the amplitude of mode shapes is also indeterminate, but the shape of the mode defined by the ratio between different measurement points is determinate. For the graphical comparisons of the relative shift in mode shapes, they are normalized so that comparison between the shapes before and after occurrence of damage can be possible. Various techniques are available to normalize mode shapes. For example, one of the elements in the eigen-vector is considered as a benchmark point, and the values of the remaining elements can be computed. A disadvantage of this normalization method is that if the benchmark point is chosen at the damaged location, the shift in mode shape at the location of damage will have zero value. Another method uses the mass matrix to normalize mode shapes using the equation below:

$$\phi_i^T [m] \phi_i = 1, \ \phi_i = \alpha \phi_{io} \qquad (2.7)$$

where, ϕ_i is the i_{th} normalized mode shape, and

α is a constant scalar.

For the application of this method, the mass matrix has to be known. It can be a time consuming and arduous process. However, most bridge structures consist of simply supported beams or continuous beams of uniform cross-section. In this case, the mass matrix can be written in simplified diagonal form of $[m] = m_u I$, where m_u is a constant scalar, and I is a diagonal identity matrix. Assuming that m_u=1, then $[m] = I$, the normalization procedure then can be expressed as:

$$\phi_i^T \phi_i = 1, \text{ or } (\alpha\phi_{io})^T (\alpha\phi_{io}) = 1 \qquad \textbf{(2.8)}$$

Then

$$\alpha = \frac{1}{\sqrt{\phi_{io}^T \phi_{io}}} \qquad \textbf{(2.9)}$$

The unit-norm normalized mode shape is calculated as follows:

$$\phi_i = \frac{\phi_{io}}{\sqrt{\phi_{io}^T \phi_{io}}} \qquad \textbf{(2.10)}$$

When the mode shapes are normalized, the change in mode shape can be written as:

$$\Delta\phi_i = |\phi_i^*| - |\phi_i| \qquad \textbf{(2.11)}$$

where, ϕ_i and ϕ_i^* represent the ith unit-norm normalized mode shapes before and after damage respectively.

(b)Method based on change in mode shape curvature

Instead of using direct measurements of mode shapes, the use of mode shape curvature, i.e., derivatives are used in this method. Here the second derivative of the mode shape with respect to position is taken. For a beam, with the curvature κ, and bending strain can be expressed as,

$$\varepsilon = \frac{y}{R} = \kappa . y \qquad (2.12)$$

where R is the radius of curvature, and

y is the perpendicular distance from the point in consideration to the neutral axis.

Problems with the measurement of strain and the computation of strain from displacements or accelerations have been addressed by some researchers (Pandey et al., 1991, Chance et al., 1994, Salawu and Williams, 1994).

The method of mode shape curvatures for damage detection was introduced by Pandey et al. (1991). Let's assume that the i_{th} unit-norm normalized mode shapes for a structure in its undamaged and damaged states are denoted by the vectors ϕ_i and ϕ_i^*, respectively. The curvature vectors associated with these mode shapes are therefore denoted as ϕ_i'' and $\phi^*{}_i''$, which are actually the second spatial derivative. The increase in mode shape curvature associated with damage is calculated as:

$$\Delta\phi_i'' = \left|\phi^*{}_i'' - \phi_i''\right| \qquad (2.13)$$

Large positive peaks within the $\Delta\phi_i''$ vector correspond to the possible location of damage. Eq. 2.13 can be written alternatively

$$\Delta\phi_i'' = \left|\phi''_i\right| - \left|\phi_i''\right| \qquad \textbf{(2.13a)}$$

If multiple modes are used, the sum of differences in curvature can be used as a damage indicator as follows:

$$\Delta\phi'' = \sum_{i=1}^{n} \Delta\phi_i'' \qquad \textbf{(2.14)}$$

where n is the number of modes used.

Usually, analytical expressions for mode shapes are unknown in practice. Mode shapes are constructed by measured values at a finite number of discrete locations on the structure. In this situation, mode shape curvature vectors can be computed using the central difference approximation for the second derivative as given by the following equation,

$$\phi_{ji}'' = \frac{\phi_{(j+1)i} - 2\phi_{ji} + \phi_{(j-1)i}}{h^2} \qquad \textbf{(2.15)}$$

where ϕ_{ji}'' is the curvature at point j corresponding to the i_{th} mode

ϕ_{ji} is the displacement at point j corresponding to the i_{th} mode, and

h is the average distance between discrete points in the ϕ_i vector.

(c) Change of modal strain energy (damage index method)

Various researchers have worked on identification of damage in structure by the method of change in modal strain energy (MSE) to detect structural damage. The method was introduced by Stubbs et al. (1992). They developed it considering the decrease in modal strain energy caused by damage located between two degrees of freedom. Such diagnosis

is derived from the curvature of the measured mode shapes. This method is better known as the damage index method. It is applicable for a beam structure.

For a beam, the damage index β_{ji} based on the change in modal strain energy at location j for the i_{th} mode can be written as follows:

$$\beta_{ji} = \frac{\left(\int_a^b \left[\phi_i^{"*}(x)\right]^2 dx + \int_0^L \left[\phi_i^{"*}(x)\right]^2 dx \right)}{\left(\int_a^b \left[\phi_i^{"}(x)\right]^2 x + \int_0^L \left[\phi_i^{"}(x)\right]^2 dx \right)} x \frac{\int_0^L \left[\phi_i^{"}(x)\right]^2 dx}{\int_0^L \left[\phi_i^{"*}(x)\right]^2 dx} = \frac{NUM_{ji}}{DEN_{ji}} \qquad \textbf{(2.16)}$$

where $\phi_i^{"}(x)$ and $\phi_i^{"*}(x)$ are continuous mode shape curvature functions for the i_{th} mode in terms of distance, x, along the beam, corresponding to the undamaged and damaged structures, respectively, based on the second derivatives of continuous displacement mode shape functions, $\phi_i(x)$ and $\phi_i^{"}$. In addition, L is the length of the beam, and a and b are the limits of a segment of the beam over which the damage is being evaluated.

In discrete form, on the assumption that the distances between points in the mode shape vectors are same, calculation of the damage index is carried out by

$$\beta_{ji} = \frac{\left(\phi_{ji}^{"*}\right)^2 + \sum_{k=1}^{m}\left(\phi_{ki}^{"*}\right)^2}{\left(\phi_{ji}^{"}\right)^2 + \sum_{k=1}^{m}\left(\phi_{ki}^{"}\right)^2} x \frac{\sum_{k=1}^{m}\left(\phi_{ki}^{"}\right)^2}{\sum_{k=1}^{m}\left(\phi_{ki}^{"*}\right)^2} = \frac{NUM_{ji}}{DEN_{ji}} \qquad \textbf{(2.17)}$$

All the variables have been defined already. If more than one mode is used, a single index for each location, j, is formed by

$$\beta_j = \frac{\sum_{i=1}^{n} NUM_{ji}}{\sum_{i=1}^{n} DEN_{ji}} \qquad (2.18)$$

Assuming that the set of damage indices for the structure constitute a sample population of a normally distributed random variable, a normalized damage indicator Z_j for a given location is calculated as follows:

$$Z_j = \frac{\beta_j - \mu_\beta}{\sigma_\beta} \qquad (2.19)$$

where μ_β and σ_β are the mean and standard deviation of damage indices for all locations, respectively. Damage indices that fall two or more standard deviations from the mean value (i.e. $Z_j \geq 2$) may indicate a possible damage location (Stubbs et al., 1995).

2.2.3 Methods based on flexibility of a structure

These methods employ a dynamically measured flexibility matrix to estimate changes in the static behavior of a structure. It is based on the relationship between the applied static force and the structural displacement. Each column of the flexibility matrix represents a set of nodal displacements of the structure due to a unit force applied at one of the degrees of freedom.

(a) Change in flexibility method

If **F** is the flexibility matrix of a structure in its undamaged state and $\mathbf{F}^*$ flexibility matrix of a structure in its damaged state, from a few of the lower vibration modes as follows (Pandey and Biswas 1994):

$$\mathbf{F} \approx \sum_{i=1}^{n} \frac{1}{\omega_i^2} \phi_i \phi_i^T \qquad (2.20)$$

$$\mathbf{F}^* \approx \sum_{i=1}^{n} \frac{1}{\omega_i^{*2}} \phi_i^* \phi_i^{*T} \qquad (2.21)$$

where ω_i is the angular frequency of the i_{th} mode,

n is the number of measured modes,

ϕ_i are the unit-norm normalized mode shapes, and asterisks signify properties of the damaged structure.

The change in flexibility caused by damage is obtained from the difference between the matrices:

$$\Delta\mathbf{F} = \mathbf{F}^* - \mathbf{F} \qquad (2.22)$$

where $\Delta\mathbf{F}$ is the change in flexibility matrix.

If $\bar{\delta}_j$ represents the maximum of the absolute values of elements in that j_{th} column of the $\Delta\mathbf{F}$ matrix,

$$\bar{\delta}_j = \max\left|\Delta\mathbf{F}_{ij}\right|, i = 1 \ldots m \qquad (2.23)$$

where ΔF_{ij} are elements of $\Delta\mathbf{F}$, and

m is the number of points of definition of the mode shape.

The parameter $\bar{\delta}_j$ is taken to be a measure of the change of flexibility at point j. The largest value of $\bar{\delta}_j$ usually indicates of the possible location of damage.

(b) Change in uniform flexibility curvature method

Zhang and Aktan (1995) claimed that the change in the curvature of a surface loaded by a uniformly distributed force, calculated using the uniform load flexibilities, as described below, showed sensitivity to local damage

The j_{th} column of the flexibility matrix $\boldsymbol{F}$ calculated by Eq.(2.20) is actually the deflected shape of the structure when a unit load is applied at the j_{th} degree of freedom. If a unit load is applied at each degree of freedom simultaneously, the sum of corresponding elements of all columns of the flexibility matrix produces a vector representing a deflected shape which is referred to as the uniform load flexibility vector. It is denoted as vector $\boldsymbol{f}$. Elements of the uniform flexibility curvature vector, $\boldsymbol{f''}$, may be calculated from $\boldsymbol{f}$, using the central difference approximation,

$$f_j'' = \frac{f_{j+1} - 2f_j + f_{j-1}}{h^2} \qquad \textbf{(2.24)}$$

where h is the average distance between measurement locations.

The absolute increment value of the curvature at location j is calculated as

$$\Delta f_j'' = \left| f_j''^* - f_j'' \right| \qquad \textbf{(2.25)}$$

where the asterisk corresponds to the damaged state. The largest positive value of $\Delta \boldsymbol{f''}$ can be considered an indicator for the damage location. Again, as an alternative to Eq. 2.25, Eq. 2.25a is suggested to locate damage.

$$\Delta f_j'' = \left| f_j''^* \right| - \left| f_j'' \right| \qquad \textbf{(2.25a)}$$

2.2.4 Methods based on matrix (model) updating

This category of damage identification is based on the adjustment of structural model parameters in a numerical model, such as matrices of stiffness, mass, or damping, to match closely the measured static or dynamic response. Another updating technique is based on the choice of the objective function to be minimized, on the constraint conditions of the problem and on the numerical scheme used to solve the minimization problem.

Matrix updating techniques for damage identification require the development of a numerical model, usually a finite element model (FEM) of the structure. In FEM updating is an optimization problem in which differences between experimental data, usually of damaged state and analytical modal data have to be minimized by adjusting uncertain model parameters. The numerical model must represent closely to the real structure in order to detect, locate and quantify the damage. The main objective of solution procedure is the minimization of the residual between the matrices of experimental and analytical modal properties

In the beginning, it is necessary to select the appropriate updating parameters. The stiffness of supports, torsion and bending stiffness of individual beam elements are examples of some updating parameters. The matrix updating method of damage identification has a unique advantage of applicability without the data of the baseline state.

2.3 Review on some research done in vibration based damage detection methods

Over last a few decades, there have been substantial amount of work done in the field of vibration based damage identification methods. In this section, examples of some work done in this field will be briefly mentioned.

2.3.1 Research on natural frequency shifts method

Loland and Dodds (1976) employed changes in the resonant frequencies and response spectra to identify damage in offshore oil platforms. Changes in resonant frequencies of 3% over time were detected and attributed to changes to the mass of the decks and to change in the tide level. Frequency changes of 10% to 15% were recorded when some sort of structural modification was implemented. Such modification resembled a structural failure near the waterline.

Thus, the authors deducted that change in natural frequency and the response spectrum could be used to monitor structural health. However, Fox's numerical and experimental study (1992) of a beam produced a somewhat different conclusion. He noticed that changes in the resonant frequencies did not serve as good indicator for diagnosis of the beam. Resonant frequencies even actually were observed to increase slightly for some reason when some mode of damage was induced. Inaccuracies in the methods used to estimate the resonant frequencies were considered the reason for these unexpected observations.

Kim and Stubbs (2003) carried out an experiment on the bridge that spanned across the Rio Grand River on U.S. Interstate Highway 40 in New Mexico. It was observed that measured natural frequencies of the first three low modes slightly increased when two separate low severity damage cases were studied. The reason for the increments was thought to be changes in ambient temperature. When two high severity damage cases were studied, the natural frequencies of the first three modes decreased compared with the undamaged state. It became apparent from experimentation that the temperature effect on frequencies appeared high enough to obscure outcome of this method.

Nasser et al. (2005) proposed an expression showing the effect of temperature on modal parameters. It was argued that the temperature changes the flexural stiffness of a structure, and as all modal parameters depend on stiffness, consequently the modal parameters are influenced by temperature. They modified their damage identification tests that considered the measured temperature as a nuisance parameter. By statistical testing process, they observed the changes in the modal parameters and eliminated the temperature effect to get them rectified.

Category-2 frequency change based methods, which includes Level 2 or Level 3 damage identification, are used to estimate various damage parameters, such as crack length and/or location, from frequency shifts. Cawley and Adams (1979) proposed a damage identification method based on shifts in the natural frequency. They experimentally derived natural frequencies and numerically generated a sensitivity matrix. They used these frequencies and matrix to predict the location and magnitude of damage in plate

structures. They tested the method on an aluminum plate and a cross-ply carbon-fiber-reinforced polymer (CFRP) plate. Good agreement was shown between the predicted and actual damage sites. The method also was able to determine the severity of the damage correctly. It should be noted that the tests were carried out in a constant-temperature enclosure, which kept the structure being tested at $25 \pm 1^{\circ}$ C so that temperature did not affect on the change of frequencies.

Many other Category-2 frequency change based methods were introduced in the literature reviews of Doebling et al. (1996 and 1998). All of them were model-based, typically relying on the use of finite element models. The requirement for an accurate model is a drawback for these types of methods, especially for complicated structures mostly seen in practical field.

According to literature review performed by Salawu (1997) on structural damage identification by the shifts in eigen-frequencies, the simplicity of determination of eigen-frequencies in the damage detection of structures makes this method easy to apply. In order to get correct diagnosis, influence of the ambient conditions on frequencies should be taken into account and eliminated accordingly.

2.3.2 Research on changes in mode shapes method

(a) Direct change in mode shape

Fox (1992) tested this method on a beam damaged by a saw cut that concluded that single-number measures of mode shapes did not seem to be good at detecting damage.

If only resonant frequencies and mode shapes were considered, graphical comparisons between variations in mode shapes were found to be a better way for detecting damage location.

Salawu and Williams (1995) found the MAC values useful in indicating the mode which was benefited mostly by structural repairs. The COMAC values were shown to be effective indicators for locating the repairs. In their tests, two of the three repaired locations were correctly identified; however, two false locations were also identified. MAC and COMAC values seemed to give good identifications when the modes and measurement locations used in the analysis properly represented the damage. They concluded that this method may not identify all damage configurations properly.

(b) Method on change in mode shape curvature

Pandey et al. (1991) implemented FEM's of simply supported and cantilevered beams. From observations, they found that the modal curvature was more sensitive to damage than the MAC or COMAC values. They further pointed out that experimental mode shapes were better obtained by direct strain measurement than by measurement of accelerations.

Salawu and Williams (1994) carried out a mode shape measurement computation using a central difference approximation. They deduced comparison of the effectiveness of this method to a direct change in modes method. They illustrated that the direct curvature change method was not a good damage indicator using their experimental data. They

suggested that the selection of modes on the analytical use was important in damage detection. For the methods based on mode shape curvature and mode shape relative difference were to be successful in detecting damage of a complex real structure, it was required to define sufficiently accurate experimental mode shapes and therefore it would be required to measure the response at an accurate number of points at proper locations and orientations.

Chance et al. (1994) observed that numerical computation of curvature from mode shapes produced unacceptable errors. When they used measured strain to calculate curvature directly, their result improved perceptibly.

(c) Change of modal strain energy (damage index method)

Stubbs and Kim (1995) and Kim and Stubbs (2003) implemented damage index method to a steel bridge. In their studies using the three lowest vibration modes, damage was successfully identified with its locations.

Earlier, Kim and Stubbs (1995) tested this method to a model plate girder. They found that the damage could be identified with decent accuracy, while localization error was relatively small and number of missing detection of true damage locations was low. However, a relatively large number of occurrences of false-positive detection were observed in their study.

Chen et al. (1999) applied a two-dimensional strain energy distribution to identify damage on an aluminum plate and a composite plate subjected to different damage configurations and successfully detected damage and its locations.

2.3.3 Research on method based on flexibility of structure

(a) Change in flexibility method

Pandey and Biswas (1994) tested the change in the flexibility method by several numerical examples applied on a spliced beam. Their success of this method with the experimental data indicated that this method should be able to detect damage of real structures. From a numerical study, it was found that this method worked best when the damage occurred at sections of high bending moment. The accuracy of the flexibility matrix was found to be affected by high-frequency modes. Therefore the method would be more effective if only low frequency modes were used. The lower modes also have advantage of linearity. Higher frequencies in some cases are associated with nonlinearity and this sometimes poses difficulty.

(b) Other flexibility-based methods

There are also some other methods based on the change of flexibility of structures. The principle of these methods is same, they vary in their procedures.

Aktan et al. (1994) illustrated the use of modal flexibility as a "condition index" to show the relative integrity of a bridge. This technique was tested on two bridges. The modal

flexibility was first derived from dynamic tests. Then it was verified from correlations of the static deflections induced by a set of truck-loading. The modal flexibility was observed to be successful in condition assessment. Aktan et al (1994) also calibrated three dimensional analytical models of the bridges to experimental data. Then they utilized the calibrated models as base models for condition assessment in the absence of baseline experimental data.

Toksoy and Aktan (1994) computed the dynamic flexibility of a bridge and verified the cross-sectional deflection profiles with and without a baseline data set. Deviation normality in the deflection profile was found to be able to assess damage scenario even without a baseline data set.

2.3.4 Research on matrix updating method

Hajela and Soeiro (1990) introduced two optimization methods of matrix update to detect structural damage. They verified their proposed methods on a fifteen-bar planar truss and a two-bar planar truss and successfully identify damage using an FEM model.

Zimmerman and Smith (1992) carried out some dynamic tests on a laboratory model, and used the measured output as the input to an FEM and optimized it. Then they simulated damage in the model. They used the subspace rotation algorithm developed by Zimmerman and Kaouk (1992), and diagnosed damage in the FEM successfully.

Casas and Aparcio (1994) proposed a method for identifying the cracked portions of concrete beams. Their method utilized a least squares method to quantify the equivalent moments of inertia for beam elements in an FEM. The algorithm was based on minimization of the residuals between measured frequencies and modal amplitudes and those computed by the FEM. The method was found to be successful in identifying damage in a physical model. However the identification was found to be only effective when severe level of damage was induced on members.

Fares and Maloof (1997) constructed a probabilistic framework to identify damage in structures. The framework was purported to identify damage and its severity, level of error and detection of false identification. They applied the method to identify cracks extending part-way on a model of a plate and successfully illustrated their purpose of their proposed framework.

Hu et al. (2001) introduced a matrix update method using a special subspace rotation algorithm. They effectively identified damage, its location and severity in an aluminum beam with two fixed ends.

Amin (2002) applied model updating method on FEM of 8-bay 3D space frame. He used experimentally obtained mode shapes and frequencies of the structure as the input of FEM. He also demonstrated a way of determining minimum required sensor locations for mode shape measurement to produce sufficiently accurate input value for the algorithm.

He tested the method for various configurations of damage scenario and found it adequate for detection of damage, its location and severity.

2.4 Method Based on Statistical Pattern Recognition

Recently, statistical pattern recognition paradigm has been considered as one of the damage detection techniques based on vibration data of structures. Farrar at el (1999) have identified and discussed generally the various components of damage detection of structures by statistical pattern recognition technique.

Statistical model development deals with the methods for extracting features that are sensitive to damage to identify the damaged state and its location in the structure. The technique to be used to construct for a statistical model depends on the availability of the data at damaged state. When data are available for both undamaged and damaged states of the structure, the statistical modeling falls into the general classification referred to as *supervised learning*. If data for damaged state are not available, the process is called *unsupervised learning*. By modeling of the extracted features, classes representing undamaged and damaged states are constructed.

In general, damage assessment can be defined at four levels (Rytter, 1993) as mentioned in section 1.1. The statistical models are used to identify damage to fit any of these levels in a quantifiable manner. Experimental structural dynamic techniques can be used to address the first two levels. Analytical models are usually needed to identify damage at

level 3 and 4 unless examples of data are available from the system (or a similar system) when it exhibits varying damage levels.

Sohn et al (2000) proposed a process of structural health monitoring using a statistical pattern recognition paradigm. They applied a method called a statistical process control technique to diagnose damage in a concrete column as the test article was progressively damaged. Autoregressive (AR) model was selected for time series modeling. Coefficients of AR model were selected as the damage sensitive features for the subsequent control chart analysis. A unique aspect of this study is the combination of various projection techniques such as principal component analysis, linear and quadratic discriminant operators with the statistical process control. The process successfully diagnosed the damage stages in the column.

Sohn et al (2003) incorporated extreme value statistics in the pattern recognition method. When the structure undergoes structural degradation, it is expected that the prediction errors by time series model will increase for the damage case. Based on this premise, a damage classifier is constructed using a sequential hypothesis testing technique called the sequential probability ratio test (SPRT). The sequential test assumes a Gaussian distribution of the sample data sets is often used. This assumption, however, might impose potentially misleading behavior on the extreme values of the data, i.e., those points in the tails of the distribution. To overcome this difficulty, the performance of the SPRT was improved by integrating extreme values statistics to it. The method was

verified on a three-story laboratory test specimen and it could successfully differentiate between various damage stages,

Taha and Lucero (2005) proposed a method to improve pattern recognition and damage detection by supplementing Intelligent Structural Health Monitoring (ISHM) with fuzzy sets. They utilized Bayesian updating to demarcate levels of damage into fuzzy sets accommodating the uncertainty of ambiguous damage states. By using data simulated from finite element analysis of a prestressed concrete bridge, the proposed technique successfully detected damage.

Nair and Kiremidjian (2006) proposed two algorithms for detection of damage with its location. In their first algorithm they used AR model for feature extraction of the vibration data and metric in the AR coefficient spaces was used for damage localization. In the second model a Gaussian Mixture Model (GMM) was used to model the feature vector. For damage detection the gap statistics which determined the optimal number of mixtures, GMM was used. Damage correlation was used to damage localization. For damage extent, the Euclidean metric between the centers of the Gaussian mixtures of the damaged and undamaged data were used. The techniques were practically exemplified on a physical model of 4-story frame structure in laboratory.

Mita and Qian 2006 proposed two methods for determination of damage localization and extent of damage. The first one was based on statistical pattern recognition using the Parzen-window method. The other method one was free-forward back-propagation neural network. They performed some series of vibration test on a model of 5-story shear-frame structure. The degree and extent of damage was successfully determined.

2.5 Methods on Neural networking

Recently some studies have been performed on neural networks for damage detection of structures to identify damage and its location in complex structures.

Among various techniques, the multilayer perception (MLP) is one of the most common techniques used in the field of neural networking. This MLP technique is trained by back-propagation method. The "back-prop" neural network consisted of a group of cascaded sigmoid functions. In back-propagation network, the sum of weighted and biased outputs of one layer is used as the inputs to next layer. A sigmoid function is the solution to a first order differential equation. Once the architecture for the network is selected, the actual function represented by the neural network is encoded by the weights and biases. The back propagation learning technique adjusts the weights and biases by minimizing the error between the predicted and measured outputs.

Wu et al. (1992) applied a back-prop neural network to identify damage in a three-story building. The structure was modeled as a two-dimensional shear building vibrated by an earthquake. The damage was simulated by reducing the stiffness of a specified member. The neural network was used to identify damage and its severity in members. Acceleration data was processed by using the Fourier transform. Using the data from the top floor, only the damage on third floor was identified with acceptable accuracy. Using the data from the first and second floors, damage on the first and third floor was identified successfully.

Doebling et al. (1996) provided a literature review of neural network-based damage identification methods. In their review, it was mentioned that modeling of damage was mostly linear type (e.g. induced by reduction in cross section). However, in practice non-linear cases are expected.

Masri et al. (2000) proposed a method based on neural network for the identification of damage in nonlinear dynamic systems. They implemented it on a damped Duffing oscillator by deterministic excitation. They used neural network to predict the response of the same nonlinear oscillator under stochastic excitations. They found that neural network was able to create a fairly accurate model representing non-linear dynamic system.

As compared with other damage detection methods that use the knowledge of structural dynamics, neural network is still in its rudimentary stage in identification of damage. Though it does not employ structural analysis, like other VBDI methods do, in most studies mass, stiffness data are required. Further study in this technique is needed to make it a viable tool for diagnose practical structures.

2.6 Summary

Among research work done on VBDI, four major categories have been identified and separately discussed. These categories are:

1) methods based on shift in frequencies,

2) methods based on change in mode shape,

3) methods based on flexibility, and

4) methods on matrix updating.

Most research studies based on shift of frequencies are model-based, typically relying on the use of finite element models. The requirement for an accurate model is a drawback for these types of methods, especially for complicated structures as seen in practical field. Moreover, damage detection by this method is affected by temperature.

Methods based on change in curvature are also effective in detecting damage to some extent. However, it has a drawback of requirement of measurement of mode shapes accurately. Among the subcategories of the method based on change in curvature, modal strain energy (damage index) method seems to show successful results on model structures but there have been few applications on complex real life structures.

Another promising field of research is the method based on model or matrix updating. In the reviewed literature there are some demonstrations of this method on model structures, but still significant amount of exploration on complex structure is needed for further refinement of those methods to meet the practical requirement.

From the literature review of the studies on identification of damage by both neural network and statistical pattern recognition, it has been found that the two methods are still at their rudimentary stage. Most of research studies done so far dealt with model

frame structures. The situation demands more researches in both fields. Therefore any of these statistical methods seem a promising field of research.

Based on the review on the studies discussed so far, the application of two VBDI techniques have been selected for current project. These are: vibration based damage identification by "modal strain energy" method (damage index method) and "matrix updating method." In addition, structural health monitoring by statistical pattern recognition has been chosen for another part of the research.

Chapter 3

Selected VBDI methods

3.1 General

Among several algorithms of vibration-based damage detection, two of the methods have been used in this project. These are Damage Index Method and Matrix Update method. These methods have been selected based on the literature review presented in the previous chapter and their relative merits as determined from the study presented in Humar et al. (2006). These methods are later applied on FEM models to study two real structures for simulated damage detection based on practical input of dynamic characteristics.

3.2 Eigenvalue Equation

In general, vibration-based damage detection algorithms use the basic eigen-value equation, which for an undamaged or healthy structure is expressed as:

$$\mathbf{K}\boldsymbol{\varphi}_i = \lambda_i \mathbf{M}\boldsymbol{\varphi}_i \qquad (3.1)$$

Where,

K is the stiffness matrix of the structure,

$\boldsymbol{\varphi}_i$ is the *i*th mass-ortho-normal mode shape,

λ_i is the associated eigen-value (squared frequency), and

M is the mass matrix.

The eigen-value equation for the damaged structure is expressed as Equation 3.2 where it is assumed that the perturbation in the mass matrix due to structural damage is not significant.

$$(K + \delta K)(\varphi_i + \delta\varphi_i) = (\lambda_i + \delta\lambda_i)M(\varphi_i + \delta\varphi_i) \qquad (3.2)$$

If $\varphi_{di} = \varphi_i + \delta\varphi_i$ is the *ith* mode shape of the damaged structure, by pre-multiplying both sides of Eq (3.3) by φ_i^T, we get

$$\frac{\varphi_i^T \delta K \varphi_{di}}{\varphi_i^T M \varphi_{di}} = \delta\lambda_i \qquad (3.3)$$

If the damage severity is small, undamaged and damaged mode shapes will be very close to each other, in that case, $\varphi_{di} \approx \varphi_i$, Eq. 3.3 can be written as,

$$\varphi_i^T \delta K \varphi_{di} = \delta\lambda_i \qquad (3.4)$$

3.3 Modal Reduction/ Expansion

As mentioned in the Chapter 1, it is practically almost impossible to measure all degrees of freedom of a large and complex structure to obtain complete mode shapes. This problem produces spatial incompleteness. In order to use the incomplete modal vectors in FE model-based damage detection process, the measured degrees of freedom need to correspond to the finite element model which can be achieved by FE model reduction, or

mode vectors expansion methods. There are various methods available for the reduction of modal degrees of freedom of an FE model, such as Guyan reduction (Guyan 1965), and dynamic condensation (Leung 1978, Miller 1980, Friswell et al., 1995). The other approach is to expand the incomplete mode shapes obtained from measured degrees of freedom to match the full number of degrees of freedom of finite element model by extrapolation, or modal expansion technique. System Equivalent Reduction Expansion Process (SEREP) is one such method for modal expansion approach (O'Callahan et al., 1989). A brief description of this method which is applied in this work is as follows:

An un-damped free vibration response of a system of N degrees of freedom can be expressed as:

$$\mathbf{M\ddot{u} + Ku = 0} \qquad \textbf{(3.5)}$$

Where,

M is the mass matrix,

K is the stiffness matrix, and

u is the displacement vector of the system.

The displacements **u** can be expressed in terms of the *m* measured mode shapes and the corresponding modal coordinates as

$$\begin{bmatrix} \mathbf{u}_a \\ \mathbf{u}_r \end{bmatrix} = \begin{bmatrix} \boldsymbol{\varphi}_a \\ \boldsymbol{\varphi}_r \end{bmatrix} \mathbf{y} \qquad \textbf{(3.6)}$$

Where,

$\mathbf{u}_a$ are measured displacements along degrees freedom **a,**

$\mathbf{u}_r$ are unmeasured displacements along degrees freedom **r,**

φ_a are mode shapes corresponding to degrees of freedom **a,**

φ_r are mode shapes corresponding to degrees of freedom **r,** and

y are the modal coordinates

If mode shapes of the undamaged structures are available, from Eq. (3.6) we can write

$$\mathbf{u}_a = \varphi_a \mathbf{y} \tag{3.7}$$

The matrix is not necessarily to be a square matrix therefore it has no inverse matrix. However by taking a generalized inverse, the modal coordinates **y** can be expressed in terms of $\mathbf{u}_a$ by:

$$\mathbf{y} = (\varphi_a^T \varphi_a)^{-1} \varphi_a^T \mathbf{u}_a = \varphi_a^g \mathbf{u}_a$$

Using above expression, we can write,

$$\mathbf{u}_r = \varphi_r \mathbf{y} = \varphi_r \, \varphi_a^g \mathbf{u} \tag{3.8}$$

The complete displacement matrix now can be now expressed as

$$\begin{bmatrix} \mathbf{u}_a \\ \mathbf{u}_r \end{bmatrix} = \begin{bmatrix} \mathbf{I}_a \\ \varphi_r \varphi_a^g \end{bmatrix} \mathbf{u}_a = \mathbf{T}\mathbf{u}_a \tag{3.9}$$

Where,

$\mathbf{I}_a$ is an identity matrix of size (ax a), and

T is the transformation matrix that transforms incomplete mode shapes matrix φ_a to full size that corresponds to complete mode shapes.

3.4 Algorithms for VBDI

A number of analytical techniques of vibration-based damage detection have been developed over last two decades. Earlier, most of the work on vibration-based structural

health monitoring (SHM) was related to aerospace and mechanical engineering. Later, the application on vibration-based assessment was expanded to health monitoring of civil engineering structures. Doebling et al (1996) provided an extensive review on related to this subject.

A number of different analytical techniques have been developed for the identification of damage from the changes in dynamic properties. The following list (Humar et al, 2006) includes the most of the techniques developed:

1. Methods based on frequency changes
2. Methods based on mode shape changes
3. Mode shape curvature method
4. Methods based on change in flexibility matrix
5. Methods based on changes in uniform flexibility shape curvature
6. Damage index method
7. Method based on modal residual vector
8. Matrix update methods
9. Neural network methods

Among the above techniques, the *damage index method* and *matrix update method* are used in the present work for their relative merits.

3.5 Damage Index Method

This method was first proposed by Stubbs et al. (1995). It is applicable to beam type structures. It identifies damaged elements by comparing modal strain energy before and after damage conditions.

Let us assume a linear elastic beam of *NE* elements. Damage causes reduction in the flexural rigidity of one or more elements. Measurements of the lowest *nm* mode shapes have been made both on the undamaged and the damaged structure. Modal curvatures can then be derived by a numerical differentiation method, i.e. the central difference operation. The modal strain energy in the *i*th mode is given by,

$$S_i = \int_0^L EI(x)[\psi_i''(x)]^2 dx \qquad (3.10)$$

Where,

L is the length of the beam,

EI is the flexural rigidity, and

$\psi_i''(x)$ denotes modal curvature.

Integration in Eq.(3.10) can be carried out by numerical method with fair accuracy.

The strain energy contributed by the *j*th element lying between $x = a$ and b is

$$S_{ij} = \int_a^b EI_j(x)[\psi_i''(x)]^2 dx \qquad (3.11)$$

Total strain energy contributed by element j is given by the ratio $F_{ij} = S_{ij} / S_i$.

For damage structure the above two equations can be modified as

$$S_i^d = \int_0^L EI^d(x)[\psi_i^{d''}(x)]^2 dx \tag{3.12}$$

$$S_{ij}^d = \int_a^b EI_j^d(x)[\psi_i^{d''}(x)]^2 dx \tag{3.13}$$

Total strain energy contributed by damaged element j is given by the ratio $F_{ij}^d = S_{ij}^d / S_i^d$. Unless the structural damage is catastrophic, it can be assumed that damaged is confined to a few elements, in that case, total flexural rigidity of the damaged structure will be close to that of undamaged structure and we can assume $EI_j^d \approx EI_j$. It can be further assumed

$$F_{ij}^d \approx F_{ij}. \tag{3.14}$$

Substituting Eq. (3.10) through (3.13) in equation (3.14), we get,

$$\gamma_{ij} = \frac{EI_j}{EI_j^d} = \frac{\int_a^b [\psi_i^{d''}(x)]^2 dx}{\int_0^L EI(x)[\psi_i^{d''}(x)]^2 dx} x \frac{\int_0^L EI(x)[\psi_i''(x)]^2 dx}{\int_a^b [\psi_i''(x)]^2 dx} \tag{3.15}$$

Equation (3.15) provides the damage index γ_{ij} for the jth element in mode No. i. To use the information available from the nm measured modes the definition of damage index is modified as follows

$$\gamma_j = \frac{\sum_{i=1}^{nm} f_{ij}^d}{\sum_{i=1}^{nm} f_{ij}} \tag{3.16}$$

Where

$$f_{ij} = \frac{\int_a^b [\psi_i''(x)]^2 dx}{\int_0^L EI(x)[\psi_i''(x)]^2 dx} \qquad (3.17)$$

A similar expression can be developed for f_{ij}^d . Elements having noticeably large value of γ_j are likely to be considered damaged.

When the strain energy contributed by the *jth* member in the modes being considered is very small, the denominator will be very small in magnitude This will create numerical problems in the evaluation of Eq. (3.15) or Eq.(3.16). In such a case Eq.(3.16) is modified as follows

$$\gamma_j = \frac{1 + \sum_{i=1}^{nm} f_{ij}^d}{1 + \sum_{i=1}^{nm} f_{ij}} \qquad (3.18)$$

In this research, the algorithm using equation (3.18) is named as "Modified" damage index method and the one using equation (3.16) is named as "Original" damage index method.

The method as outlined above for a beam structure can be extended to a structure of a general type. Thus for a healthy structure the strain energy of member *j* in mode *i* is given by.

$$S_{ij} = \boldsymbol{\varphi}_{ij}^T \mathbf{k}_j \boldsymbol{\varphi}_i \qquad (3.19)$$

The total strain energy of the structure deforming in its mode *i* is given by,

$$S_i = \sum_j \boldsymbol{\varphi}_{ij}^T \mathbf{k}_j \boldsymbol{\varphi}_i = \boldsymbol{\varphi}_{ij}^T \mathbf{K}_j \boldsymbol{\varphi}_i \qquad (3.20)$$

Where,

$\mathbf{k}_j$ is the stiffness matrix of member j, and

$\mathbf{K}$ is the stiffness matrix of the structure.

Similar expressions can be written for the damaged structure. It may be noted that in deriving S_i^d the global stiffness matrix of the damaged structure $\mathbf{K}_d$ is taken as being approximately equal to $\mathbf{K}$.

As before the fractional strain energy is expressed as $F_{ij} = S_{ij} / S_i$ and $F_{ij}^d = S_{ij}^d / S_i^d$. Assuming that $F_{ij}^d \approx F_{ij}$ and expressing the stiffness matrix of damaged member j as $k_j^d = k_j / \gamma$, we obtain an expression similar to Eq.(3.16) for the damage index, with,

$$f_{ij} = \frac{\boldsymbol{\varphi}_{ij}^T \mathbf{k}_j \boldsymbol{\varphi}_i}{\boldsymbol{\varphi}_{ij}^T \mathbf{K}_j \boldsymbol{\varphi}_i} \qquad (3.21)$$

$$f_{ij}^d = \frac{\boldsymbol{\varphi}_{ij}^{dT} \mathbf{k}_j \boldsymbol{\varphi}_i^d}{\boldsymbol{\varphi}_{ij}^{dT} \mathbf{K}_j \boldsymbol{\varphi}_i^d} \qquad (3.22)$$

To avoid numerical error, equation (3.18) should be applied in this case, also.

3.6 Matrix Update Method

The matrix update method was first developed by Kabe (1985). Here its basic mathematical mechanism is discussed.

$\delta\mathbf{K}$ in Eq.(3.4) also can be considered the perturbation in stiffness matrix. Let us assume that $\delta\mathbf{K}$ can be assembled from the changes in the element stiffness matrices expressed in terms of perturbation factor $\boldsymbol{\beta}$. In that case, Eq. (3.4) can be expressed as

$$\delta\lambda_i = -\sum_{j=1}^{ne} \varphi_i^T \mathbf{k}_j \varphi_{di} \beta_j \qquad (3.23)$$

Or, $$\mathbf{D}\boldsymbol{\beta} = -\delta\boldsymbol{\lambda} \qquad (3.24)$$

where

ne is the number of elements,

D is an *m* by *ne* matrix whose elements are $d_{ij} = \varphi_i^T \mathbf{k}_j \varphi_{di}$,

$\boldsymbol{\beta}$ is the *ne*-vector of the unknown changes in element stiffness matrices, and

$\delta\boldsymbol{\lambda}$ is the *m*-vector of the difference in the model and measured eigen-values.

If difference between the values in model and measured values is small, the expression d_{ij} can written as $d_{ij} = \varphi_i^T \mathbf{k}_j \varphi_i$

If $m = ne$, by solving Eq. (3.24) we can get values of $\boldsymbol{\beta}$. Usually *m* is much smaller than *ne*. In that case solution of Eq. (3.24) is under deterministic. Such problem has infinite number of solutions. One way to get a unique solution is to apply a least squares technique. Another way is minimization of an objective function subject to specified constraints. This is known as "Optimization" method which is one of the algorithms applied in this research work. The preservation of symmetry and connectivity, closeness to original model, and positive definiteness are some of the equality constraints imposed in various optimization techniques.

Another process for the solution of Eq. (3.24) is the "Pseudo-Inverse" method which is basically the equation bellow.

$$\beta = -\mathbf{D}^{T}(\mathbf{D}\mathbf{D}^{T})^{-1}\delta\lambda \qquad (3.25)$$

This solution is useful for updating the analytical model. The computed frequencies and mode shapes are thereby compared with measured modal data. The model thus becomes more accurate. Such refined model can be used as basic, or reference model in the future evaluation of the structure. This variant of matrix update method is also applied in this research.

Chapter 4

Statistical Pattern Recognition Methods in SHM

4.1 General

Application of statistical pattern recognition techniques to structural health monitoring is relatively new. Over the last a few years, some work has been done on the statistical pattern recognition paradigm as applied to SHM. Because all SHM processes rely on experimental data with its inherent uncertainties, statistical analysis procedures are necessary if one is to identify the dynamic nature of structure including effect of sudden change due to live load and also steady change of temperature over time. In this chapter general components of statistical pattern recognition techniques in determining structural damage detection will be discussed. Farrar et al (1999) has outlined typical procedures of statistical process recognition techniques on structural damage detection.

4.2 Components of statistical pattern recognition

Typical components of statistical pattern recognition mentioned by Farrar et al (1999) are as follows:

1) Operational evaluation,

2) Data acquisition & cleansing,

3) Feature extraction, and

4) Statistical model development.

There can be other parts of the basic components such as data compression before feature extraction, and data reduction before statistical modeling for statistical pattern recognition technique. These additional parts are some times needed to manage extremely large amount of data. Each of these components is briefly described below.

4.2.1 Operational Evaluation

Operational evaluation is concerned with three aspects in the implementation of a structural health monitoring system by any methods including statistical pattern recognition.

1) Definition of damage

It is to be defined for the system being investigated and, if there is a possibility of occurrence of multiple damages, it is to select the most concerning ones usually the damage in the most important locations.

2) Ambient condition:

This includes both operational and environmental, under which the system to be monitored.

3) Limitations on acquiring data:

Operational evaluation begins to set the baselines of the parameters to be monitored and how the monitoring will be accomplished. This evaluation starts to tailor the health monitoring process to features that are unique to the system being monitored and tries to take advantage of unique features of the postulated damage that is to be detected.

4.2.2 Data Acquisition &Cleansing

The data acquisition portion involves,

1) Selection of the types of sensors and location where they should be placed,

2) Determination of the number of sensors to be used, and

3) Setup of data acquisition/storage/transmittal hardware.

This process is highly dependent on the application and economic consideration usually dominates the selection. The non-structural conditions always vary with time. Therefore it is needed to normalize the data to make them compatible to analyze for damage detection. Commonly normalization is done by applying it to the measured responses by the measured inputs. In the case of varying environmental or operating condition it is done by normalizing the data in some temporal way, so that the data can be compared at similar times of an environmental or operational cycle. Sources that affect the variation of data and the structure monitored are to be identified and minimized. For those variability sources which can be eliminated, they should be made available to be statistically quantified.

Data cleansing is the process of selectively choosing data to accept for, or reject from the feature selection process. The data cleansing process is usually based on knowledge gained by individuals directly involved with the data acquisition.

The data acquisition and cleansing is not a one-way through process of the system. The knowledge gathered from feature extraction and statistical modeling can be useful to enhance the data acquisition and cleansing process.

4.2.3 Feature extraction

Feature extraction is the process of the identifying damage-sensitive properties derived from the measured vibration response that allows one to distinguish between the undamaged and damaged structures (Sohn et al., 2000). Typically, systematic differences between time series from the undamaged and damaged structures are nearly impossible to detect by human eye. Therefore, other features of the measured data must be examined for damage detection.

Since vibration data either obtained from accelometer or strain gauge is in essence a time series, typically mathematical processes for time series analysis are utilized to extract features. The basic background of time series analysis is described separately in Section 4.3.

4.2.4 Statistical Model Development

Statistical model development is a technique that implements algorithms to analyze the distribution of extracted features to determine the damage state of the structure. The appropriate algorithm to use in statistical model development will depend on availability of data of damaged states of a structure. In this study, data for known damaged state of the structures are not available. Therefore outlier analysis is performed.

In this study, control chart analysis, which is the most commonly used Statistical Process Control technique for Outlier Analysis, is used. It is also suitable for automated continuous system monitoring. It can be applied to the selected features to investigate the existence of damage in the structure. When the system experiences abnormal conditions, the mean and/or variance of the extracted features are expected to change.

Here X-bar control charts are employed to monitor the changes of the selected feature's mean and to identify samples that are inconsistent with the past data sets.

Application of the S control chart, which measures the variability of the structure over time, to the current test structure is presented in Fugate et al. (2000). Several variations of the control charts can be found in Montgomery (1997).

To monitor the mean variation of the features, they are first arranged in subgroups of size p. τ_{ij} is the jth feature from the ith subgroup. The subgroup size p is often taken to be 4 or 5 (Montgomery, 1997). If p is chosen too large, a drift present in individual subgroup

mean may be obscured, or averaged-out. An additional reason for the using subgroups, as opposed to individual observations, is that the distribution of the subgroup mean values can be reasonably approximated by a normal distribution as a result of central limit theorem.

Next, the subgroup mean $\overline{X}_i$ and standard deviation S_i of the features are computed for each subgroup ($i = 1,,,,,q$, where q is the number of subgroups):

$$\overline{X}_i = mean(\tau_{ij}), \text{ and}$$

$$S_i = std(\tau_{ij})$$

Here, the mean and standard deviation are with respect to p observations in each subgroup.

Finally, an X-bar control chart is constructed by drawing a centerline (CL) at the subgroup mean and two additional horizontal lines corresponding to the upper and lower control limits, UCL and LCL, respectively versus subgroup numbers (or with respect to time).

The centerline and two control limits are defined as follows:

$$UCL, LCL = CL \pm Z_{\alpha/2} \frac{S}{\sqrt{n}} \qquad \textbf{(4.1)}$$

and

$$CL = mean(\overline{X_i})$$

Here mean is calculated with respect to all sub groups. i.e., *i=1,2,.....,q*. $Z_{\alpha/2}$ is the percentage point of the normal distribution zero mean and unit variance such that

$$p[z \geq Z_{\alpha/s}] = \alpha/2$$

The variance S^2 = mean (S_i^2). If the system experienced damage, this would likely be indicated by an unusual number of subgroup means outside the control limits; a charted value outside the control limits is referred to as an *outlier* in this thesis. The monitoring of damage occurrence is performed by plotting $\overline{X}$ values obtained from the new data set along with the previously constructed control limits.

4.2.5 Damage Identification Approach by Pattern Comparison

The basic concept of this approach was first proposed first by Sohn et al (2001). It is logical to assume that the patterns in data in same state of condition, either steady or agitated, taken at various points of time of the structure will not vary significantly if the structure does not change significantly. Conversely if the structure has undergone a significant change, it should reflect in the patterns of both states of condition.

In order to observe the variation of structure by studying the patterns of signals or data blocks, it is necessary to nominate certain block as *reference data block* with which patterns of the other data series or blocks are compared. Usually, the reference data blocks for a particular condition are taken from the earlier time of the observation of the structure and other data blocks are called test block. The time series model (AR model in this study) particularly developed for reference block is defined as *reference model*. As structure undergoes changes, usually, degradation, so will the pattern of data series

change. Therefore the pattern of other data blocks will not match closely with that of reference block. So, if we fit reference model to the testing blocks, the "residual errors" should reflect the extent of variation of the signals. It's natural, if a structure undergoes a significant degradation, residual error by fitting reference model will be significantly high.

After calculating all coefficients of a time series model and fitting it to the data it is possible the get the residuals for all points. An average value of the residual can be defined as, ε = (Residual SS)/N, where SS is the summation of squares of residuals after fitting the model with actual values, and N is the observation number. This value ε is the key parameter that can be used to see how good a reference model fits to the pattern of testing data blocks. $R = \sqrt{\varepsilon_t / \varepsilon_r}$ is a measurement of the goodness of reference model on a testing block and called *residual error index* of a test block to the reference. Here, t and *r* suffices correspond to the testing and reference blocks, respectively. If value of the ratio shows a clear increasing trend over long time, then it can be said that the structure is degrading.

4.3 Time Series Analysis

Techniques of time series analysis are the mostly utilized to extract the damage sensitive features of the signals of vibration and strains readings. Mathematical modeling of data is thoroughly covered in statistical textbooks on time series (e.g. "Introduction to Time

Series Analysis and Forecasting" by Montgomery et al., 2008). Here only those materials that are relevant to this study will be outlined.

4.3.1 Weakly stationary time series

The processing of time series for feature extraction mostly performed on the weakly stationary type. Let $\{X_t\}$ be a time series with $E(X_t^2) < \infty$. The *mean function* of $\{X_t\}$ is given as,

$$\mu(t) = E(X_t). \tag{4.2}$$

The *covariance function* of $\{X_t\}$ is given by Eq. (4.3)

$$\gamma_x(r,s) = Cov(X_r, X_s) = E[(X_r - \mu_x))(X_s - \mu_x(s))] \tag{4.3}$$

for all integers r and s.

Then, $\{X_t\}$ is *(weakly) stationary* if (i) $\mu_x(t)$ is independent of *t,* and (ii) $\gamma_x(t = h,t)$ is independent of t for each *h.* Here $E(\cdot)$ denotes an expectation function

4.3.2 Illustration of some useful terms related to time series

Auto-covariance function:

Let $\{X_t\}$ be a stationary time series. The *auto-covariance function* (ACVF) of $\{X_t\}$ at lag *h* is

$$\gamma(h) = Cov(X_{t=h}, X_t). \tag{4.4}$$

The *autocorrelation function* (ACF) of $\{X_t\}$ at lag *h* is

$$\rho_x(h) \equiv \frac{\gamma_x(h)}{\gamma_x(0)} = Cor(X_{t+h,}X_t) \tag{4.5}$$

iid noise:

A time series with no trend or seasonal component and in which the observations are simply independent and identically distributed random variables with zero mean. We refer to such a sequence of random variables X_1, X_2, ... as *iid* noise. By definition we can write, for any positive integer *n* and real numbers $x_1,\ldots. x_n$,

$$p[X_1 \le x_1,\ldots,X_n \le x_n] = p[X_1 \le x_1]\ldots P[X_n \le x_n] = F(x_1)\ldots F(x_n), \quad \textbf{(4.6)}$$

Where $F(\cdot)$ is the cumulative distribution function of each of the identically distributed random variables $X_1, X_2,\ldots$.The observations in this model have no dependency among one another.

For all $h \ge 1$ and all $x_1,\ldots. x_n$

$$p[X_{n+h} \le x | X_1 = x_1,\ldots,X_n = x_n] = P[X_{n+h} \le x], \quad \textbf{(4.7)}$$

It is shown that the knowledge of $X_1,\ldots,X_n$ is not needed for predicting the behavior of X_{n+h}. Given the values of $X_1,\ldots,X_n$, the function *f* that minimizes the mean squared error $E[(X_{n+h} - f(X_1,\ldots,X_n))^2]$ is actually identically zero

iid noise though too simple in form to apply it for any real life time series, it is in fact a basic concept that is needed to create the model of complicated time series.

For *iid* noise $\{X_t\}$ and $E(X^2) = \sigma^2 < \infty$, the first requirement for the weakly stationary time series is satisfied, since $E(X_t) = 0$ for all *t*. For being independent,

$$\gamma_x(t+h,t) = \sigma^2, \text{ if } h = 0, \quad \text{or,} \quad = 0, \text{ if } h \neq 0 \qquad \textbf{(4.8)}$$

which is independent of t. Hence, *iid* noise with finite second moment is stationary.

White noise

If $\{X_t\}$ is a sequence of random variables, each with zero mean and variance σ^2, then obviously $\{X_t\}$ is stationary with same covariance functions as *iid* noise above. Such a sequence is known as *white noise*. All *iid* noises are white noises, too, but any white noise is not always *iid*.

4.3.3 Auto-Regression Moving Average Processes

Auto-Regression Moving Average (ARMA) process is one of the most popularly utilized methods used in extracting damage sensitive elements of time series data of vibration and displacements.

Definition

$\{X_t\}$ is an ARMA(p, q) if $\{X_t\}$ is "stationary" and if for every t,

$$X_t - \phi_1 X_{t-1} - \ldots - \phi_p X_{t-p} = Z_t + \theta_1 Z_{t-1} + \ldots + \theta_q Z_{t-q} \qquad \textbf{(4.9)}$$

Where $\{Z_t\}$ is a white noise of zero mean and σ^2 variance, i.e., $\{Z_t\}$~WN $(0,\sigma^2)$, and the polynomials, $(1 - \phi_1 z - \ldots - \phi_p z^p)$ and $(1 + \theta_1 z + \ldots + \theta_q z^q)$ have no common factors. The process $\{X_t\}$ is said to be an *ARMA (p,q) with mean* μ if $\{X_t - \mu\}$ is an ARMA(p,q) process. Eq. (4.5) can be written in alternatively in a concise form:

$$\phi(B)X_t = \theta(B)Z_t \tag{4.10}$$

Where $\phi(\cdot)$ and $\theta(\cdot)$ are pth and qth-degree polynomials $\phi(z) = 1 - \phi_1 z - \ldots - \phi_p z^p$, $\theta_z = 1 + \theta_1 z + \ldots + \theta_q z^q$, and B is the backward shift operator as given by Eq. 4.11.

$$\{B^j X_t = X_{t-j}, B^j Z_t = Z_{t-j}, j = 0, \pm 1, \ldots) \tag{4.11}$$

The time series $\{X_t\}$ is called *autoregressive process of order p* or AR(p) if $\theta(z) \equiv 1$, and A *moving-average process of order q* or MA (q) if $\phi(z) \equiv 1$. Coefficients of $\phi(\cdot)$ polynomial of AR(p) process are considered damage sensitive features (Sohn et al, 2000) for damage detection by statistical pattern recognition. An important condition of ARMA process is that it is stationary. For the purpose of feature extractions in the proposed work AR(p) is to applied.

4.3.4 Estimation of the parameters AR(p) process

For any AR(p) process $\phi = (\phi_1, \ldots, \phi_p)'$ are called parameters or AR-coefficients. There are usually two methods: the Yule-Walker estimation and Burg Estimation are applied to estimate the parameters. The first one is more common and has been used in the proposed work.

Yule-Walker Estimation

For a pure autoregressive model the moving-average polynomial $\theta(z)$ is equal to 1.

By the definition of Eq.(4.6) we can write,

$$X_t = \sum_{j=0}^{\infty} \psi_j Z_{t-j}, \tag{4.12}$$

Where, $\psi(z) = \sum_{j=0}^{\infty} \psi_j z^j = 1/\phi(z)$.

Multiplying each side of Eq.(4.10) by X_{t-j}, $j=0,1,2,....,p$, taking expectations and using Eq. (4.7), we obtain Yule-Walker equations.

$$\Gamma_p \phi = \gamma_p \qquad \textbf{(4.13)}$$

and

$$\sigma^2 = \gamma(0) - \phi' \gamma_p \qquad \textbf{(4.14)}$$

Where, Γ_p is the covariance matrix,$[\gamma(i-j)]_{i,j=1}^{p}$, and $\gamma_p = (\gamma(1),...., \gamma(p))'$. By using the above equations we can get $\gamma(0),...., \gamma(p)$ from σ^2 and ϕ. If we replace the covariances $\gamma(j)$, $j=0,....,p$, in Equations (4.13) and (4.14) by corresponding sample covariances $\hat{\gamma}(j)$, we get some equations, for Yule-Walker estimators $\hat{\phi}$ and $\hat{\sigma}^2$ of ϕ and σ^2. These are:

$$\hat{\Gamma}_p \hat{\phi} = \hat{\gamma}_p \qquad \textbf{(4.15)}$$

$$\hat{\sigma}^2 = \hat{\gamma}(0) - \hat{\phi}' \hat{\gamma}_p \qquad \textbf{(4.16)}$$

Where, $\hat{\Gamma}_p = [\hat{\gamma}(i-j)]_{i,j=1}^{p}$, and $\hat{\gamma}_p = (\hat{\gamma}(1),...., \hat{\gamma}(p))'$. If $\hat{\gamma}(0) > 0$, then $\hat{\Gamma}_m$ is non-singular for every m = 1,2, ..., then Eq.(4.15) and Eq.(4.16) take form as,

$$\hat{\phi} = \left(\hat{\phi}_1,....,\hat{\phi}_p\right)' = \hat{R}_p^{-1} \hat{\rho}_p \qquad \textbf{(4.17)}$$

and,

$$\hat{\sigma}^2 = \hat{\gamma}(0)\left[1 - \hat{\rho}_p' \hat{R}_p^{-1} \hat{\rho}_p\right], \qquad \textbf{(4.18)}$$

Eq.(4.17) and (4.18) are called *sample Yule-Walker Equations.* With $\hat{\phi}$ as per Eq.(4.16), it is possible that $1 - \hat{\phi}_1 z - \cdots - \hat{\phi}_p z^p \neq 0$ for $|z| \leq 1$.

4.3.5 Order selection of AR(p) process

Unique true order of the model data actually does not exist. By following some guidelines, one can find an optimal order for AR process. There are a few techniques usually applied to find the order *p*. Out of these, a common technique involving sample *partial auto relation functions (PACF)* of an ARMA process is being discussed here as it will be later applied in performing AR(*p*) process to the project data.

The *PACF* of an ARMA process $\{X_t\}$ is the function $\alpha(\cdot)$ defined as, $\alpha(0) = 1$, and $\alpha(h) = \phi_{hh}$, h $\geq$ 1, where ϕ_{hh} is the last component of $\phi_h = \Gamma_h^{-1}\gamma_h$, $\Gamma_h = [\gamma(i-j)]_{i,j=1}^{h}$, and $\gamma_h = [\gamma(1), \gamma(2), \ldots, \gamma(h)]'$ as already defined.

If $\{X_t\}$ is a casual AR(*p*) process defined by Eq.(4.6) with $\{Z_t\}$~iid(0, σ^2), and if we fit a model with order $m > p$ using Yule-Walker equations, with coefficient vector $\hat{\phi}_m = \hat{R}_m^{-1} \hat{\rho}_m$ such that $m > p$; then, the last component $\hat{\phi}_{mm}$ of the vector $\hat{\phi}_m$ is approximately normally distributed with mean = 0, and variance = 1/n. $\hat{\phi}_{mm}$ is the sample partial auto-correlation at lag *m*.

For an AR(p) process, partial auto-correlations $\hat{\phi}_{mm}$, m > p are zero. Then values $\hat{\phi}_{kk}$, k > p, are compatible with the observations with N(0, 1/n). k > p, $\hat{\phi}_{kk}$ should fall between the limits $\pm 1.96n^{-1/2}$ with around 0.95 probability. This suggests using a preliminary estimator of p the smallest value m such that $\left|\hat{\phi}_{kk}\right| < 1.96n^{-1/2}$ for $k < m$.

Chapter 5

Testing of VBDI Methods by Model Simulations

5.1 General

In this chapter, the application of the two approaches of VBDI methods as presented in Chapter 3 is discussed. The approaches are applied on computer model simulation of two practical structures. The effectiveness of the methods to identify damage of different levels at various elements has been tested. The ability of the algorithms in the presence of simulated random errors has also been examined. The comparison is made between error and error-free cases. The results of the studies at different steps are presented.

5.2 Test Articles

Two experimental test articles are used in this work. The first one is the Crowchild Bridge (ISIS, 2008) located in Calgary, Alberta and the second one is a 3D space frame tested at the Canadian Space Agency (Amin, 2002).

5.2.1 The Crowchild Bridge

The Crowchild Bridge is a two-lane traffic overpass with three continuous spans (Fig-5.1) and reported to be the first continuous steel free deck bridge in the world (Tadros *et*

al., 1998). The strength of a steel free deck, as explained in Bakht and Mufti (1998) is derived from the arching action in concrete deck due to external confinement of the bridge deck provided by closely spaced transverse steel straps connecting the girders. Consequently, no flexural reinforcement is necessary in the deck. Generally a nominal amount of fiber reinforced polymer (FRP) reinforcing bars or fiber reinforced concrete are provided for crack control. The cantilever portion of the deck requires flexural reinforcement which is usually provided using FRP bars. Design of such bridge decks avoids conventional steel reinforcement altogether and thus avoids the problem of steel corrosion which reduces the service life of a structure.

The details of the bridge superstructure are shown in Figure 5.2. It is composed of five 900 mm deep longitudinal steel girders, a polypropylene fiber reinforced concrete slab deck and prefabricated glass fiber reinforced concrete barriers. The five longitudinal girders are spaced at 2 m. Four evenly spaced cross-frames in each span and steel girder diaphragms at the supports connect the main girders. The main girders are also connected by evenly spaced steel straps placed across the top of the girders. The girders and straps are connected to the deck slab by stainless steel studs. The deck is 9030 mm wide and does not contain any internal steel reinforcement. The slab thickness is 275 mm along the girders and 185 mm elsewhere.

5.2.2 3D-Space Frame

The structure is an erectable aluminum space frame built from commercially available hardware (Meroform M12) produced by MERO. Fig-5.3 shows the nodes and element connectivity and the detail of a typical element of the Frame (Amin, 2002). The nodal joint design allows the frame to be assembled into numerous configurations in any of three orthogonal directions, thereby providing structures with varying complexity. The elements are aluminum tubes with screwed solid steel end connectors, which when tightened into the node also clamp the tube by means of an internal compression fitting. These features allow any frame elements to be replaced without disassembly of the whole frame, which is very useful introducing damage in any of the frame elements. The space frame consists of eight bays. Each assembled bay is a cube shaped structure with 707mm sides. This test article represents a large space structure such as the main supported structure of the International Space Station (ISS). It was tested at the Canadian Space Agency (Amin, 2002).

The frame is supported by the flexible suspension system to simulate a free-free boundary condition. This configuration allows the simulation of the expected on-orbit boundary condition of a large space structure such as the ISS. The frame is supported by a suspension system which does not restrain the structure at any point, so that the test article is freely suspended in space and exhibits rigid body motions.

In the test structure, eight lumped masses were attached to simulate a large structure with attached instrumentation. The larger three masses were 2.75 kg each are attached to the

nodes 6, 17 and 30 and the smaller five masses were 1.75 kg each are attached to the nodes 4, 9, 25, 28 and 36.

5.3 Software for implementation of FEM

Damage detection algorithms by finite element modeling (FEM) as described in Chapter 3 have been implemented by the program M-FEM developed in MATLAB (1999). Element and its formation used by M-FEM are briefly described in Bagchi et al. (2007).

The element library in M-FEM includes a three dimensional beam element (Fig. 5.4 a) and a plate-shell element (Fig. 5.4b). The plate and shell element is formed by the DKT plate bending element (Batoz, 1982) and the triangular plane stress element together. The DKT plate bending element has three degrees of freedom (DOF) per node (Fig. 5.4c), two rotational DOFs (θ_x and θ_y) about the orthogonal horizontal directions, x and y, and a translational DOF (w) along the vertical direction, z. A triangular plane stress element and the plate bending element together form in a facet shell element. The resulting shell element has six DOFs per node as shown in Fig. 5.4f. Half of these six DOFs are contributed by the DKT plate bending element and the remaining three DOF's need to come from the plane stress element. Two versions of the plane stress element have been implemented in M-FEM: - the constant strain triangle (CST) with two DOFs per node corresponding to the in-plane displacements (Zienkiewicz and Taylor, 1989) shown in Fig. 5.4d, and - the plane stress triangular element with three DOFs per node, two

corresponding to the in-plane displacements and the other corresponding to the vertex rotation or drilling DOF (Allman, 1984) shown in Fig. 5.4e.

Since the CST element has only two DOFs (u and v in x and y directions, respectively) per node, the resulting shell element has zero stiffness associated with the remaining DOF corresponding to the rotation about the z axis (θ_z). θ_z is often referred to as the drilling DOF and in the case of DKTCST combination, a small stiffness of arbitrary magnitude may need to be added to the drilling DOF to avoid numerical difficulties when some of the adjacent elements are coplanar. Unlike the CST element, the drilling DOF stiffness arises naturally in Allman's element, and no adjustment is necessary for adjacent co-planer elements. A quadrilateral plate-shell element is formed by combining two triangular elements as shown in Fig. 5.4f.

5.4 Damage simulation in the Crowchild Bridge

The first test article which is the Crowchild Bridge is used for the evaluation of the effectiveness of the FEM model and also Damage Index and Matrix Update Methods for detecting damage.

5.4.1 Model Simulation to the Crowchild Bridge

The bridge structure was originally modeled by Bagchi (2005) using the finite element program, M-FEM described earlier. He also performed some analysis to calculate its frequencies using his FEM model. The discussion of his results and also information on

the structural build of the bridge, its properties and tests of material strength and frequencies are available in his paper.

An analytical model of the Crowchild Bridge was constructed using three dimensional beam elements for the piers, girders, diaphragms and cross frames including the steel straps, and shell elements for the deck and side barriers. The deck elements were connected to the girder elements by rigid beam elements. The piers were assumed to be fixed at their base, while roller and pin supports were assumed to exist at the north and south abutments, respectively. The finite element model contained 351 elements, 247 nodes and 1399 active degrees of freedom. The densities of steel and concrete were assumed to be 76 and 24 kN/m^3, respectively. The concrete compressive strength was taken as 35 MPa. The modulus of elasticity for concrete was assumed to be 30 GPa for the deck and 27 GPa for the barrier and piers; for steel it was assumed to be 200 GPa. The FE model of Crowchild Bridge is shown in Fig 5.5a

Initially, the concrete was assumed to be un-cracked. The model based on this assumption was updated and correlated with the data obtained from the vibration test conducted in 1997 by the University of British Columbia (Ventura et al., 2000). This model was referred to as the CC-97 model.

During the process of model updating, the stiffness coefficients of individual elements were modified to fine tune the resulting modal frequencies of the system. The natural frequencies of the undamaged structure derived from model CC-97 are given in Table

5.1, while the mode shapes are shown in Figs 5.5. It was found from the observation that the maximum difference in eigen frequencies between the initial finite element model and the test was 9.1% and by limiting the degree of stiffness adjustment to 35% of the original stiffness, it was possible to achieve a correlated model in 29 iterations. Changing the stiffness of some elements by as much as 35% is necessary to bring the eigen-frequencies close to the experimental values (within 1%). Such a change in stiffness may seem to be physically unrealistic.

In model updating terms it means that the analytical model has many flaws which could not be physically corrected at the model building stage, and the adjustment to stiffness actually accounts for these flaws such as incorrect boundary conditions, inaccurate initial stiffness which arises due to situations such as, cracking in concrete and loosening or jamming of bolts, which are difficult to quantify and model.

The field tests conducted by the University of Alberta team in 1998-99 (Cheng and Afhami, 1999) revealed that the frequencies of the bridge reduced slightly perhaps due to cracking of concrete. The crack patterns have been mapped by Cheng *et al.* (1999) and it was found that the number and width of the cracks increased considerably in 1998 as compared to 1997. To consider the effect of cracking, the stiffness of the concrete elements is reduced, and the model was correlated with the 1999 test results. The stiffness of deck elements was assumed to be 90% of un-cracked stiffness in the positive moment region, and 80% in the negative moment region. The stiffness of the barrier was assumed to be 90% in the positive moment region and 70% in the negative moment region. The

pier stiffness is reduced by 10%. The correlated base model was referred to as the CC-99 model. Its mode shapes are similar to those of CC-97 (as shown in Fig 5.5). The frequencies of the updated structure are shown in Table 5.1. It was found that the maximum difference in eigen-frequencies between the initial finite element model and the test was 11.3%. Because of this high difference, the modal parameters failed to converge even after 100 iterations, when the degree of stiffness adjustment was limited to 35%.

When the limit of stiffness adjustment was relaxed to 45%, the modal parameters converged in 19 iterations. A 45% change in the stiffness of some elements may seem quite high, it is possible that the stiffness of those elements were not assessed correctly while building the model, and some of the factors affecting the stiffness such as, concrete cracking, complex boundary conditions, loosening/stiffening of a bolt connection, are hard to model correctly.

The results of the convergence study highlight the necessity of building the initial model to represent the actual structure as closely as possible by manual adjustments. However, for a large and complex model such as the one presented here, manual adjustment is difficult. The mathematical process of model updating, and the resulting stiffness adjustment factors provide some information that can be used in conjunction with manual adjustment of element parameters.

Though the accuracy of above model was tested to be not so high, nonetheless, it is very much difficult to develop a model of structure with such complexity in boundary conditions, stiffness, etc. The more detailed practical assessment of those parameters is necessary and it is labor intensive, time consuming and costly. Considering these limitations, an attempt has been taken to simulate damage scenarios and test the ability of the proposed algorithms to detect, locate, and qualify damage of the structure, using the existing model.

5.4.2 Effects of measurement errors and incomplete mode shape vectors

The bridge has been analyzed using FEM model by M-FEM software. The bridge deck has 15 slab segments (Fig 5.5a). The target area for testing is the segment in the middle along with the longitudinal girders at that location. All elements at that location are simulated for damage scenario by reducing their stiffness in the FEM by certain fractions which are also considered damage severity factors or simply damage factors. The elements in this area are elements 53 through 58, 174, 177, 180, 183 &186.

In this study, damage factor of 0.1, 0.2 and 0.3 were applied to all elements of the middle span segment. Elements 53 through 58 were modeled as plate-shell elements and the elements 174, 177, 180, 183 &186.were modeled as 3d- beam elements. In the model, displacements along three transitional of 247 nodes are assumed to be measured by sensors. Therefore total displacements along total 741 directions are assumed measured.

The effect of measurement error is considered in calculated frequencies and incomplete mode shapes are also considered for case study. The types of case undertaken for each damage factor and algorithms are as follows:

- Case-I: No errors in frequency and mode shape measurements and complete mode shapes
- Case- II: No errors in frequency and mode shape measurements and incomplete mode shapes
- Case-III: Inducing error up to 1% in both frequency and mode shape measurements and incomplete mode shapes

The cases stated above in this section use the computed frequencies by M-FEM of the FEM model of the structure. The similar case study is conducted using the measured frequencies. Using M-MEM, all these cases have been analyzed for different damage factors. While the sample figures and plots are presented here in discussing results produced by proposed algorithms, remaining figures are given in Appendix A.

5.4.3 Discussion on the results of case studies on Crowchild Bridge

Figures 5.6-5.11 present the output of the analysis for 10% severity on three cases defined in the section 5.4.2. These graphs shall be explained and discussed here to exemplify the typical overall result interpretation. The figures and plots for the entire case study are provided in Appendix A.

Figs-5.6 and Fig-5.7 show the results by damage index and matrix update methods respectively for Case-I which considers no error in frequency and mode shape measurements and complete mode shapes.

In Fig-5.6(a), verticals spikes in the ranges between element number 53-58 and 174-186 represent damage in the elements identified by damage index original method (section-3.5) within those ranges. The identification is consistent with the simulated damage. In Fig-5.7(b), it is apparent that damage is also indicated properly in the right locations by modified damage index method (Section-3.5).

Figs 5.7(a) and 5.7(b) correspond to matrix update method using the pseudo-inverse and optimized methods, respectively as discussed in Section 3.6. Both variants of matrix update method show appropriate diagnosis of the damage scenario with proper damage severity.

Figs 5.8 and Fig-5.9 show the graphical output result of damage index and matrix update methods respectively for case-II which considers no error in frequency and mode shape measurements and incomplete mode shapes.

Though incomplete mode shapes should bring down the accuracy of the results comparing to those shown in Figs. 5.6 and 5.7, it does not seem to happen in this case. The diagnosis is almost is as good as in the case-I which assume complete mode shapes for the analysis.

Figs 5.10 and 5.11 show the graphical output of the various methods for case-III which considers up to 1% random error in both frequency and mode shape measurements and incomplete mode shapes is assumed.

In Fig-5.10(a) corresponding to damage index original method, there are some vertical spikes visible in the range of element no. 30 to 75 with biggest ones lie between 53 through 58, which are actually numbers of some of the simulated damage elements. There are other regions having noticeable spikes with the highest one corresponding to element no 240. These are actually false positives. The spikes in the range between 174 through 186 are significantly smaller than others. Therefore this damaged zone is not distinctly identified.

Fig-5.10(b) corresponds to damage index modified method. The identification here is slightly better than previous one. The biggest of the spikes lie in the range between element numbers 53-58. So, these simulated damage elements are identified properly. There are a few false positives, but the identification of elements 174 through 186 is clearer than it is in Fig-10(a).

Fig-5.11(a) shows the result of matrix update pseudo-inverse method. It shows the highest positive vertical lines in between the element number 174 and 186. Therefore these simulated damage elements are diagnosed here properly, but the damage severity is 15% which is 50% larger than simulated value. There are some vertical lines on the

number of other simulated elements (53-58), but these lines are smaller than other false positives which also are present in the graph.

Fig-11 (b) presents the result of matrix update optimized method. It shows some vertical lines clearly with correct severity value in the ranges of 53-58 and 174-186 and there is no contrasting false positive. A few of the elements within the damaged zone are not identified here.

From graphs (Appendix-A) produced for various cases of damage states and errors as mentioned in previous section, it is apparent that the identification of the simulated elements by the process can be classified as three levels

- Level l, distinctly indemnified: The simulated damaged element(s) is/are clearly shown by output as damaged with proper damage severity and no prominent false identification.
- Level 2, partial identification: Some of the simulated damaged element(s) is/are identified with wrong/ correct damage severity, or there is some false identification of undamaged element(s).
- Level 3, no identification: No damaged element by simulation is identified or the output is totally obscure.

The Tables 5.2 and 5.3 show the identification status of each case by methods considering analytical and measured frequencies respectively. From the Table 5.2, it is

apparent that all methods are good at successfully identifying damage fairly in all cases, but Case-III, which involves errors in frequencies and modes and also incomplete mode shape. There is no significant difference in accuracy of identification within the range of simulated damage severity (10% to 30%), but it is expected that it should be prominent at significantly lower damage than 10% and higher damage than 30%.

In general modified damage index method shows better stability of the results than the original method. An explanation for this difference is that in original method, occurrence of numerical errors due to very small value of the denominator of some damage indices can produce incorrect result, as explained in Section-3.5. The modified method overcomes this limitation by adding 1 to both numerator and denominator of the indices (Eq. 3.18).

In the cases of applying measured frequencies only, the results of Case-I which assumes no error in frequencies and modes show good accuracy in detection. Accuracy of detection for other two cases shows some level of acceptability.

It has been observed by applying various methods that detection accuracy decreases with the increase of the random errors in frequencies and mode shapes. Also consideration of incomplete mode shapes affects the analytical outputs. It can be inferred that this would pose challenge to the feasibility of the algorithms for practical application.

Still these methods can be useful considering their limitations. It has been already exemplified in the discussion on the output of the VBDI methods of the Crowchild Bridge in Fig-5.6-5.11 that a hybrid analysis by combining different algorithms can improve the quality of the diagnosis. When one method fails to detect the damage correctly in some cases, the other methods may diagnose it correctly. By screening process it is possible to guess the probable candidates for damaged elements. Therefore, the application of multiple detection algorithms on a single structure is recommended to detect damage in practical fields.

Another advantage of VBDI methods is that, even in some cases, if they cannot pinpoint the damaged elements, they can narrow down the possible region of damage at a macro level, with greater success. This would help in selecting elements for manual damage detection methods such as traditional non-destructive evaluation, thereby saving some valuable labor and expenditure.

5.5 Damage simulation for the 3D-Space Frame

The second test article is a 3D-space eight-bay space frame. The full description of the structure is presented in Section 5.2.2. Damage simulation performed in this study is somewhat similar to the one performed by Amin (2002). However, the simulation process and the cases considered differ from that study. Amin (2002) used commercial FEM software, COSMOS for both modeling and damage detection simulation. Consequently, the damage detection algorithms needed to be applied separately using the modal analysis

results from the software. In this study, however, the damage detection methods are integrated to the FEM software, M-FEM (Bagchi et al., 2007) used in this study. Also the damage detection algorithms used by Amin (2002) differ from those used in this study. Here both damage index method and matrix update method are applied in their original and modified forms.

5.5.1 Finite element modeling of the structure

The nominal values of the physical properties of the components of the structures are used for FEM. The elements are modeled as 3d beam element. The joints are modeled as being rigid. To simulate the effect of payload, added lumped masses, each of having mass of 1.75kg are added to the nodes 4, 9, 25, 28 and 36, while masses of 2.75 kg are added to each of nodes 6, 17 and 30. The model has a total of 216 DOF's.

For the purpose of comparison and verification of the FEM, the measured values of the frequencies as obtained by Amin (2002) through laboratory experimentation of the structure are taken. Among those frequencies, the first three non-rigid frequencies were found to be the most effective for damage detection by Amin (2002). In this study those frequencies will be considered. The measured value of the first three non-rigid body frequencies corresponding to non-rigid body modes are 50.98, 51.15 and 57.51 Hz, and the corresponding computed frequencies in this study are 49.87, 53.61 and 55.86 Hz, respectively. It has been observed that the difference between computed to and measured frequencies is 3.28%, which is reasonably low considering practical uncertainties. The first three non-rigid body mode shapes of the frame are shown in Fig-5.12.

Amin (2002) conducted thorough computations for the determination of optimal response points of the structure. The purpose was to identify those degrees of freedom of which displacement measurements will give fairly accurate modes shapes. He found that 79 translation DOFs were required to formulate an adequate modal data base for identification of damage in any of the detectable elements. In this work, the same 79 DOFs are taken and they are presented in Table- 5.4

5.5.2 Damage simulation

To test the feasibility of the proposed damage identification algorithms explained in Chapter 3, different damage cases were considered. These cases are similar to the ones considered by Amin in his project. Table 5.4 shows the DOFs numbers corresponding to each node and Table 5.5 lists the simulated damage cases. Either 50% or 80% damage factor is considered in each case. Damage identification process is carried out for two cases:

- Case-A: Consideration of no error in measurement of frequencies and modes shapes with complete modal data
- Case-B: Consideration of up to 2% error in measurement of frequencies, up to 10% error in the measurement of mode shapes with incomplete modal data

The results of the analysis are explained below, and more results are presented in Appendix B.

5.5.3 Discussion on the results of case studies on 3D Space Frame

The same three levels of damage identification as defined in Section 5.4.3 are considered here for assessing the results of the diagnosis. In this section, the output graphs for the simulated damage cases of Element-29 are considered for illustration. Other output results of VBDI analysis on 3D space frame are shown in the Appendix B.

Fig-5.13 and Fig-5.14 show the graphical output of the damage identification by damage index and matrix update methods for the Element-29 in Case-A which considers no error and complete mode shapes and considered damage severity is 80%.

Fig-5.13(a) shows the graphical output of the damage identification by original damage index method for the Element-29. Though it is identified as damaged element, there is a false positive identification which is shown to have greater damage.

Fig-5.13(b) illustrates the output of the damage identification by modified damage index method. It identifies the Element-29 correctly as damaged element. Identification of the element is better by this method than by the original method. The reason for this false positive for certain elements is because of the numerical errors produced by a small magnitude of the denominator representing the negligible strain energy contribution by the corresponding elements. The modified method removes this error.

In Fig-5.14(a) and Fig-5.14(b) show the output results of matrix update pseudo-inverse and optimized respectively. The results show clear identification with correct severity.

Fig 5.15 and Fig-5.16 show the graphical output of the damage identification by damage index and matrix update methods respectively for the Element-29 on case-A which considers no error and complete mode shapes and considered damage severity is 50%.

Fig-5.15(a) shows the graphical output of the damage identification by original damage index method for the Element-29. It is identified as damaged element, but there is a false positive identification which is shown to have slightly greater damage severity.

Fig-5.15(b) illustrates the output of the damage identification by modified damage index method. It identifies the Element-29 correctly as damaged element. Identification of the element is better by this method than by the original method. A possible reason has been already explained.

In Fig-5.16(a) and Fig-5.16(b) show the output results of matrix update pseudo-inverse and optimized methods respectively. Both methods identify the Element-29 as damaged element. There are a few false identifications with greater damage severity.

Fig-5.17 and Fig-5.18 show the graphical output of the damage identification by damage index and matrix update methods respectively for Element-29 on case-B which considers up to 2% error in frequency and 10% error in mode shapes and incomplete mode shapes and considered damage severity is 50%.

Fig-5.17(a) shows the graphical output of the damage identification by original damage index method for the Element-29. It is not identified as clearly selectable damaged element, and there is some false positive identification.

Fig-5.17(b) illustrates the output of the damage identification by modified damage index version. It identifies the Element-29 correctly as damaged element. There is a false peak in graphs but its value is smaller, Identification of the element is better by this method than by original method. The reason has been already explained.

Fig-5.18(a) shows the output results of matrix update pseudo-inverse method. It identifies the element-29 as the most damaged element. Fig-5.18(b) shows the result by optimized method. It has produced obscured output. Most probably the solution could not converge. There are similar results occurred in other configurations applied on Case-B by pseudo-inverse method.

The Table 5.6 and 5.7 shows the identification status for all damage configurations listed in Table-5.5 of each case by proposed methods for damage severity 80% and 50% respectively. From the Table-5.6, it appears that either damage index (original or modified) or matrix update (pseudo inverse or optimized) or both methods are able to detect simulated 80% damage appropriately for case-A in all damage cases except D2. However for Case-B, mostly damage index method (modified) seems to be able to detect damage in some damage of 80% damage severity. Matrix update method is able to detect damage properly for a few damage cases of case-B of 80% severity.

Similar scenario of the results is observed for 50% damage severity by reviewing Table 5.7 and accuracy is some what reduced on a few cases in comparison to the corresponding 80% severity cases.

It has been already exemplified in the discussion on the output of the VBDI methods of the 3D Space Frame in Figs 5.13-5.18, the combined analysis by four types of variants of algorithms can be effective to identify simulated damage correctly even in error induced cases outputs of which are some times ambiguous. When damage index method fails to detect the damage correctly in some case, the matrix update method diagnoses it correctly and vice versa. By combined interpretation, it is possible to guess the most possible candidates for damaged elements. The advantage of combined analysis has already become obvious having analyzed the result of the Crowchild Bridge case study.

Even in error induced cases, if the simulated element is not diagnosed clearly, it is identified with a few false positives. This output can be of good practical use, since it narrows down the possible damaged locations greatly. It should help in initiating local damage detection techniques.

Bridge model	Mode	Frequency		
		Measured	Uncorrelated	correlated
CC-97	1	2.78	2.89	2.78
	2	3.13	3.41	3.13
	3	3.76	3.44	3.72
	4	4.05	3.89	4.03
CC-99	1	2.60	2.76	2.60
	2	2.90	3.23	2.90
	3	3.63	3.28	3.63
	4	3.85	3.71	3.85

Table 5.1: Natural frequencies of the Crowchild bridge model (Bagchi, 2005)

		Case type	Damage Index Method		Matrix Update method	
			Original	Modified	Pseudo-inverse	Optimized
Damage Severity	10%	I	1	1	1	1
		II	1	1	1	1
		III	3	2	3	2
	20%	I	1	1	1	1
		II	1	1	1	1
		III	3	2	3	2
	30%	I	1	1	1	1
		II	1	1	1	1
		III	3	2	3	3

Table-5.2: Crowchild Bridge Damage Identification:1- full identification, 2-partial and 3-no identification as defined in section 5.4.3, case type is defined section 5.4.2.

		Case type	Damage Index Method		Matrix Update method	
			Original	Modified	Pseudo-inverse	Optimized
Damage Severity	10%	I	1	2	1	1
		II	1	2	2	2
		III	3	2	3	2
	20%	I	1	2	1	1
		II	2	2	2	2
		III	3	2	3	2
	30%	I	1	2	1	1
		II	2	2	2	2
		III	3	2	3	2

Table-5.3: Crowchild Bridge Damage Identification for measured frequencies: 1- full identification, 2-partial and 3-no identification as defined in section 5.4.3, case type defined section 5.4.2

Measured X-DOF at nodes			**Measured Y-DOF at nodes**			**Measured Z-DOF at nodes**		
3	15	26	6	17	29	2	13	24
5	16	27	7	20	30	3	14	25
6	17	28	9	22	31	4	15	26
7	18	29	12	23	35	5	16	27
8	19	30	14	15		6	17	28
9	20	31	15	28		7	18	29
10	21	32				8	19	30
11	22	33				9	20	31
12	23					10	21	32
13	24					11	22	33
14	25					12	23	34

Table5-4: Proposed 79 DOF's by Amin (2002) for analysis of 3d space frame by VBDI (FEM)

Damage Case ID	Damaged Elements	Elements Connectivity	Damage Severity %
D1	102	6-8	80
D2	72	22-23	80
D3S	29	20-24	80
D3L	29	same as above	50
D4S	61	14-Dec	80
D4L	61	same as above	50
D5S	28	16-20	80
	79	13-18	80
D5L	28 &79	same as above	50
D6S	5	17-21	80
	13	19-23	80
	55	17-23	80
D6L	5, 13 &55	same as above	50
D7S	12	15-19	80
	28	16-20	80
D7L	12 &28	same as above	50
D8S	4	13-17	80
	20	14-18	80
	28	16-20	80
	5	17-21	80
D8L	4, 20, 28 &5	same as above	80

Table-5.5: Simulated damage cases for 3-D Space Frame

Damage case	Case type	Damage Index Method		Matrix Update method	
		Original	Modified	Pseudo-inverse	Optimized
D1	A	1	1	3	3
	B	2	3	3	3
D2	A	1	3	3	3
	B	3	3	3	3
D3S	A	2	1	1	1
	B	3	1	3	3
D4S	A	2	1	1	1
	B	3	3	3	3
D5S	A	2	1	2	2
	B	3	1	3	3
D6S	A	3	1	1	1
	B	3	2	3	3
D7S	A	2	1	1	1
	B	3	1	3	3
D8S	A	3	1	3	2
	B	3	2	3	3

Table-5.6: 3D space frame Damage Identification for 80% damage severity cases: 1- full identification, 2-partial &3-no identification as defined in section 5.4.3, and case type is defined in section 5.5.2

Damage case	Case type	Damage Index Method		Matrix Update method	
		Original	Modified	Pseudo-inverse	Optimized
D3L	A	2	1	3	3
	B	3	2	3	3
D4L	A	2	1	3	3
	B	3	3	3	3
D5L	A	2	1	3	2
	B	3	2	3	3
D6L	A	2	1	3	2
	B	3	2	3	3
D7L	A	2	1	1	1
	B	3	2	3	3
D8L	A	3	2	3	2
	B	3	1	3	3

Table-5.7: 3D space frame Damage Identification for 50% damage severity cases: 1- full identification, 2-partial &3-no identification as defined in section 5.4.3, and case type is defined in section 5.5.2

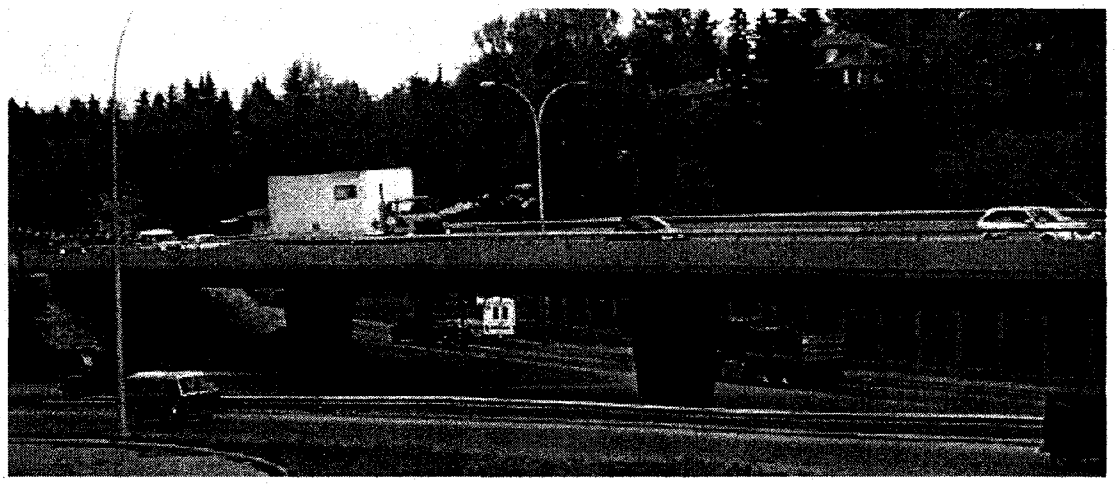

Fig 5.1: Crowchild Bridge of Calgary, Alberta, Canada

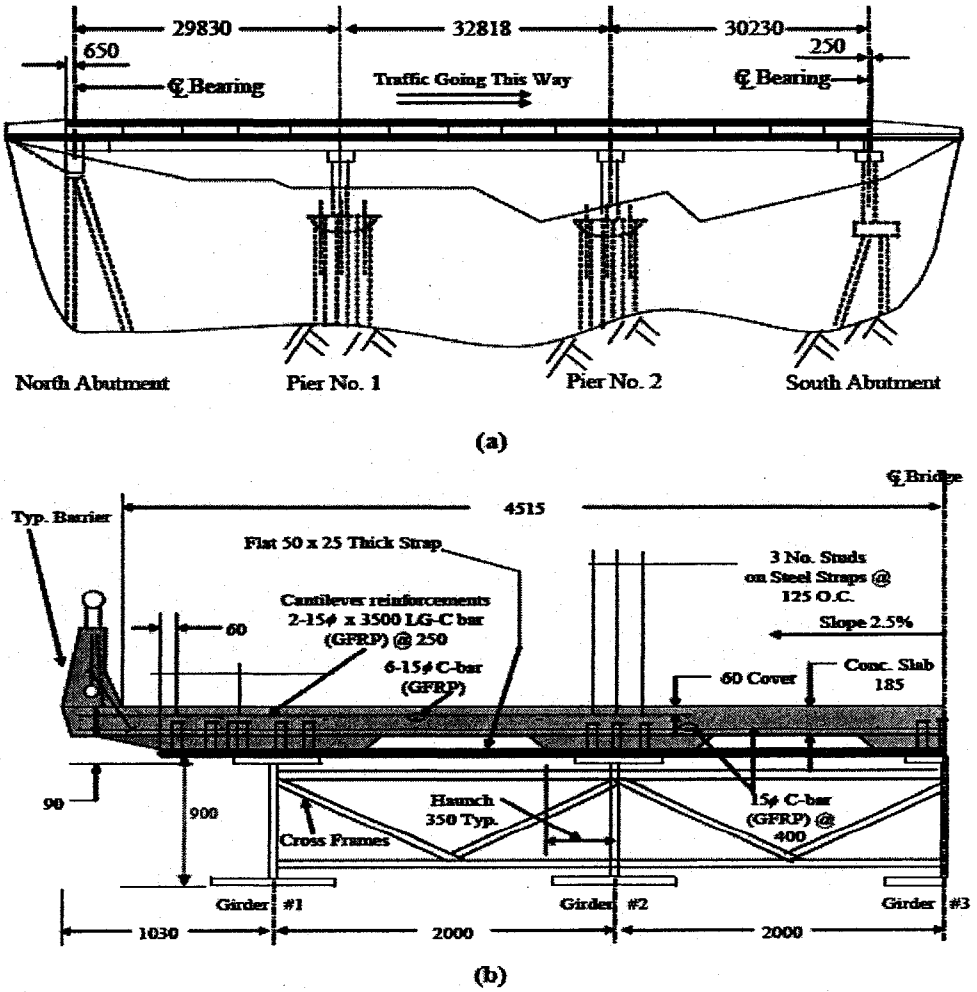

Fig 5.2: Details of the Crowchild Bridge – (a) west elevation, (b) Cross section (All dimensions are in mm) (Bagchi 2005)

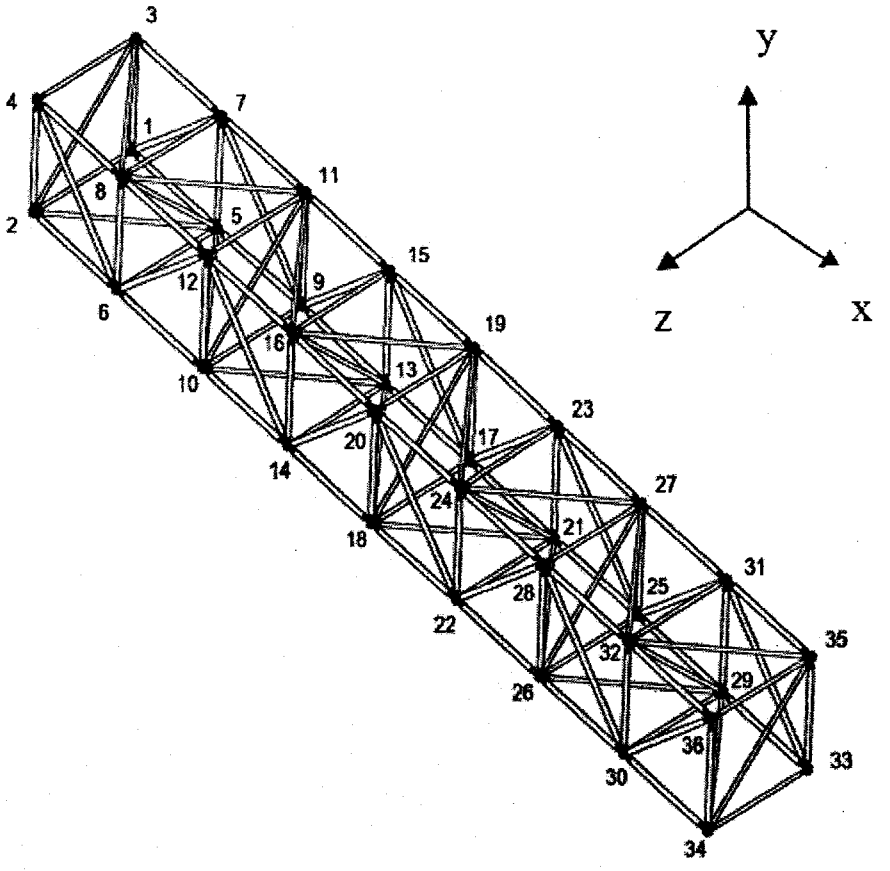

(a)

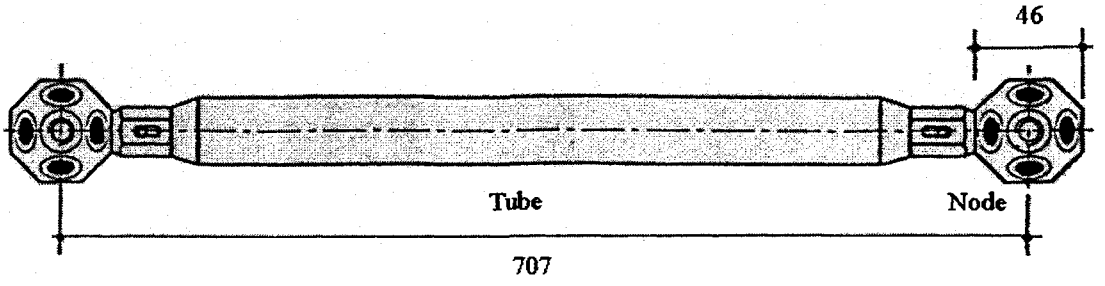

(b)

Fig 5.3: (a) Nodes and element connections of 3D Space Frame; (b) details of an element of 3D space frame.

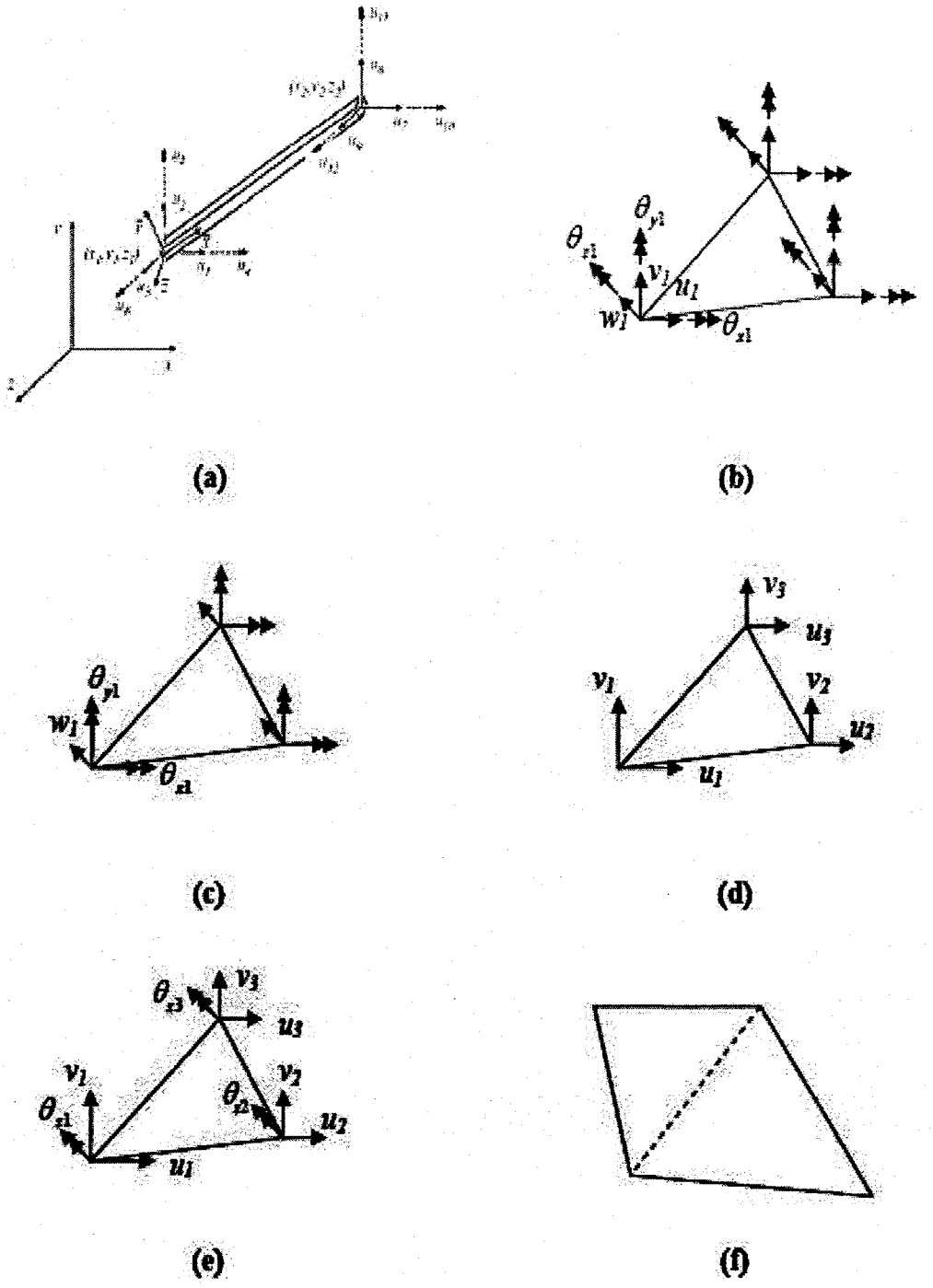

Fig 5.4: Three dimensional beam and plate-shell elements in M-FEM – (a) 3D beam element, (b) 3D plate-shell element, (c) DKT plate bending element, (d) CST plane stress element, (e) Allman's plane stress element, and (f) quadrilateral plate shell element constructed by combining two triangular elements. (Bagchi 2005)

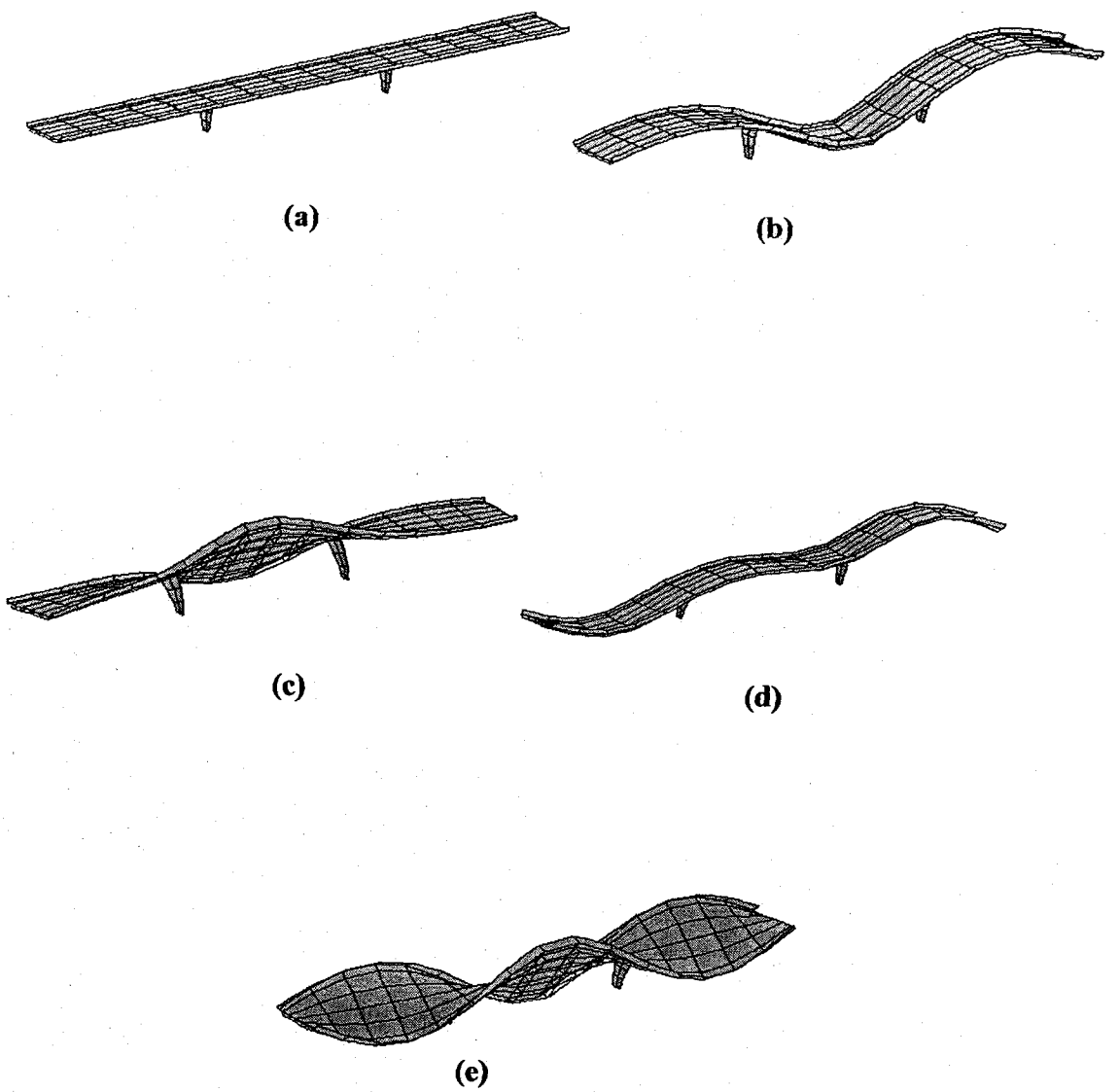

Fig 5.5: The mode shapes for CC-97 model – (a) The Finite Element Model, (b) Mode 1, (c) Mode 2, (d) Mode 4 and (e) Mode 5

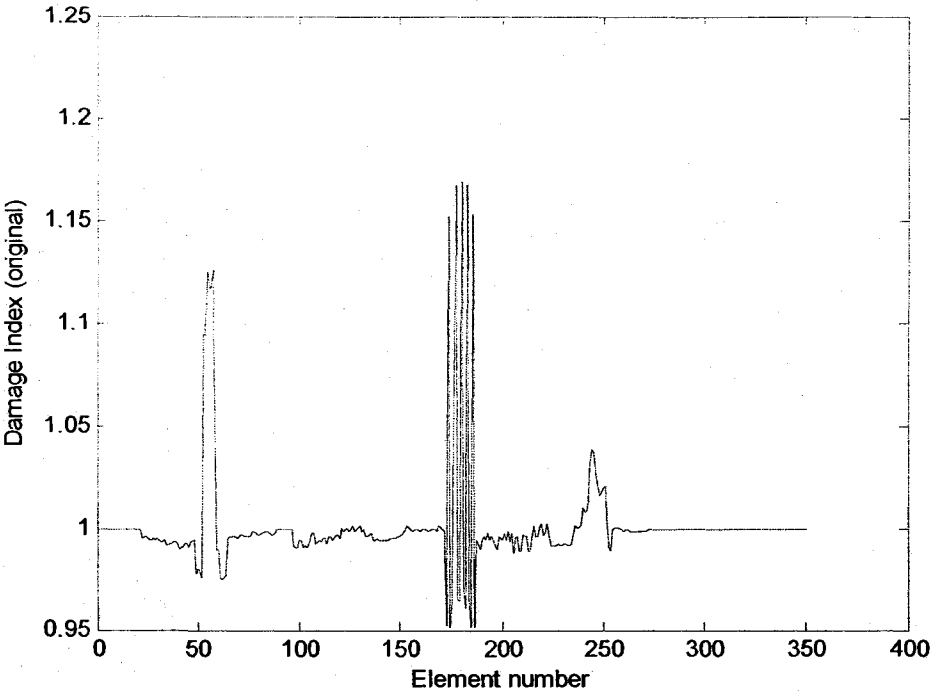

(a)

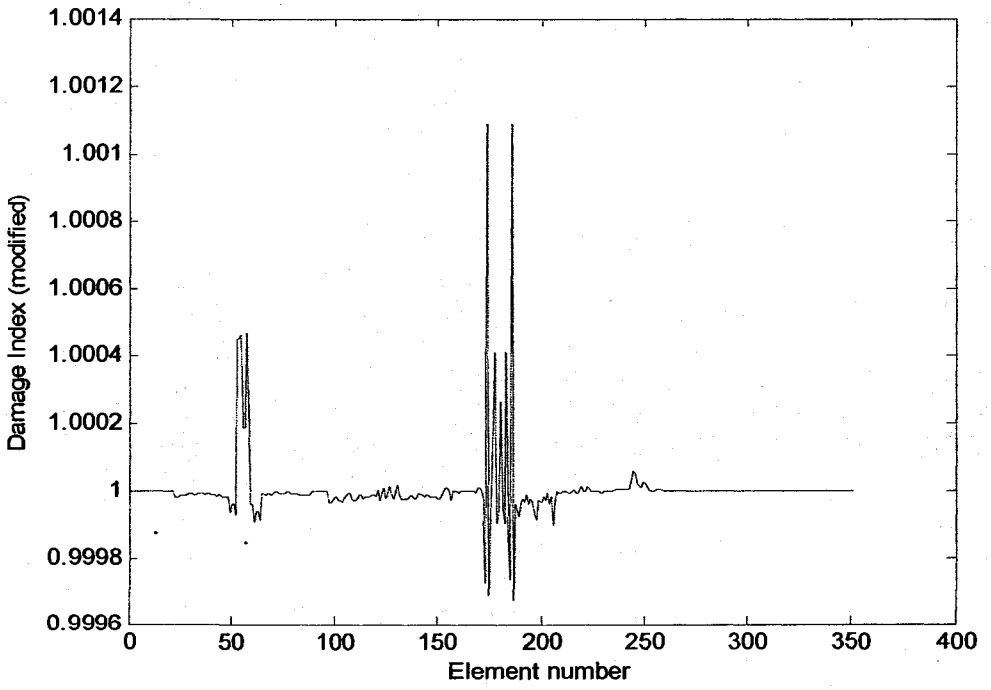

(b)

Fig 5.6: The Crowchild bridge case study. Graphs showing damage with element numbers for no error and complete modes with 10% damage severity by Damage Index Method **(a)** original and **(b)** modified.

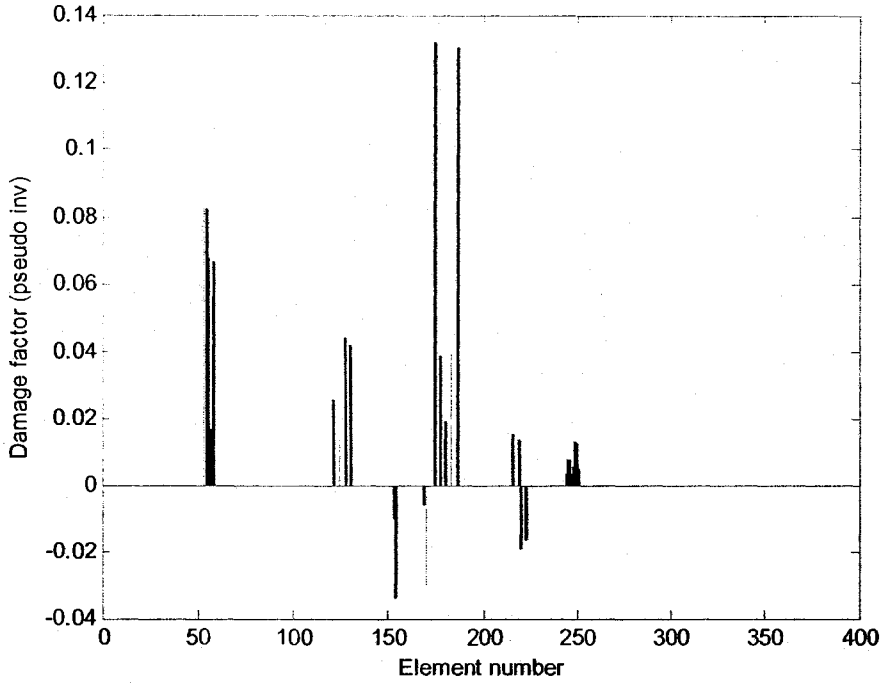

(a)

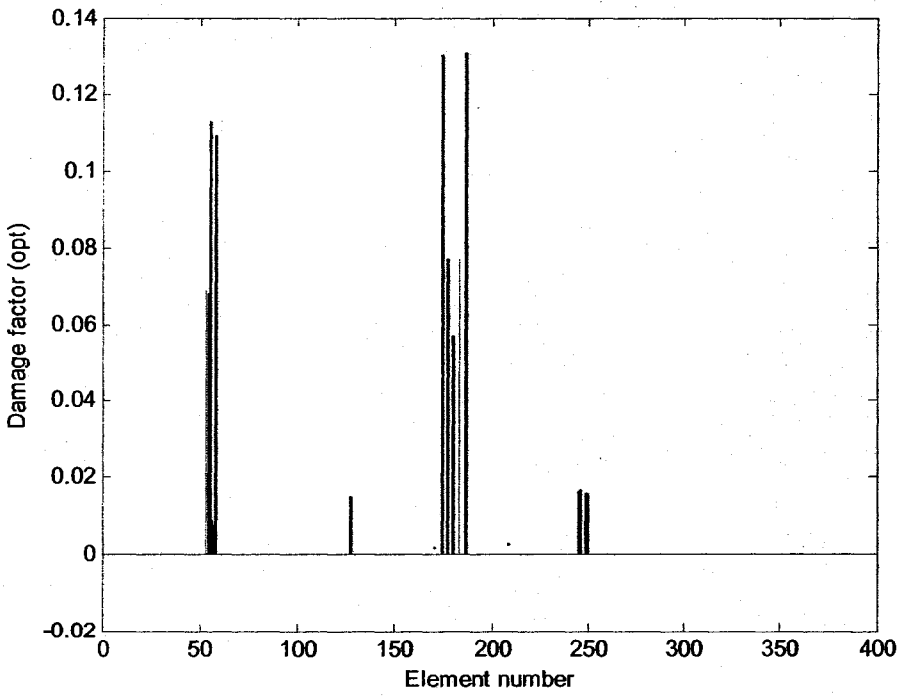

(b)

Fig 5.7: The Crowchild bridge case study. Graphs showing damage with element numbers for no error and complete modes with 10% damage severity by Matrix Update Method **(a)** Pseudo Inverse **(b)** Optimized

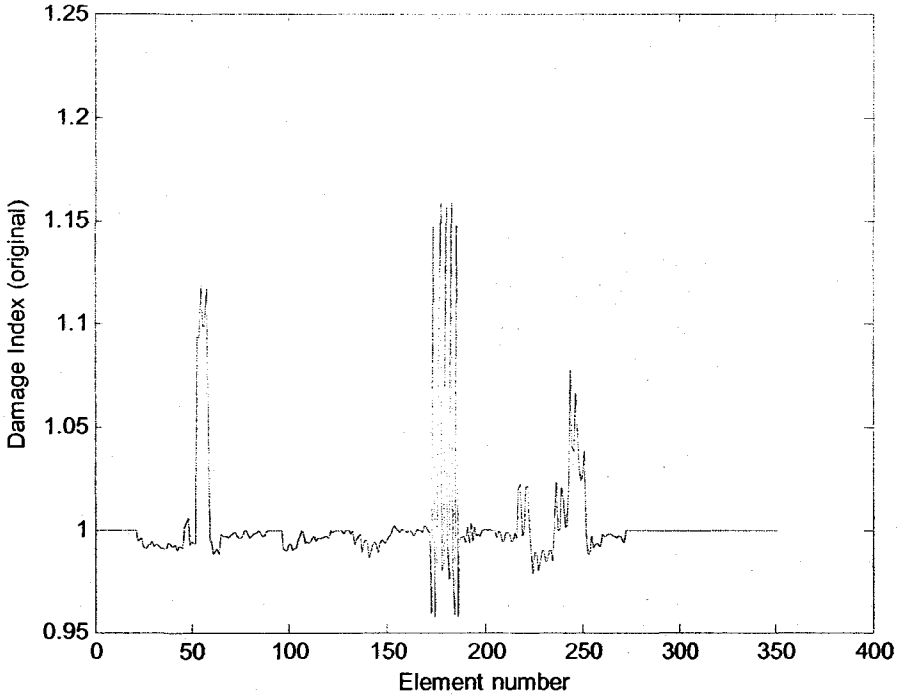

(a)

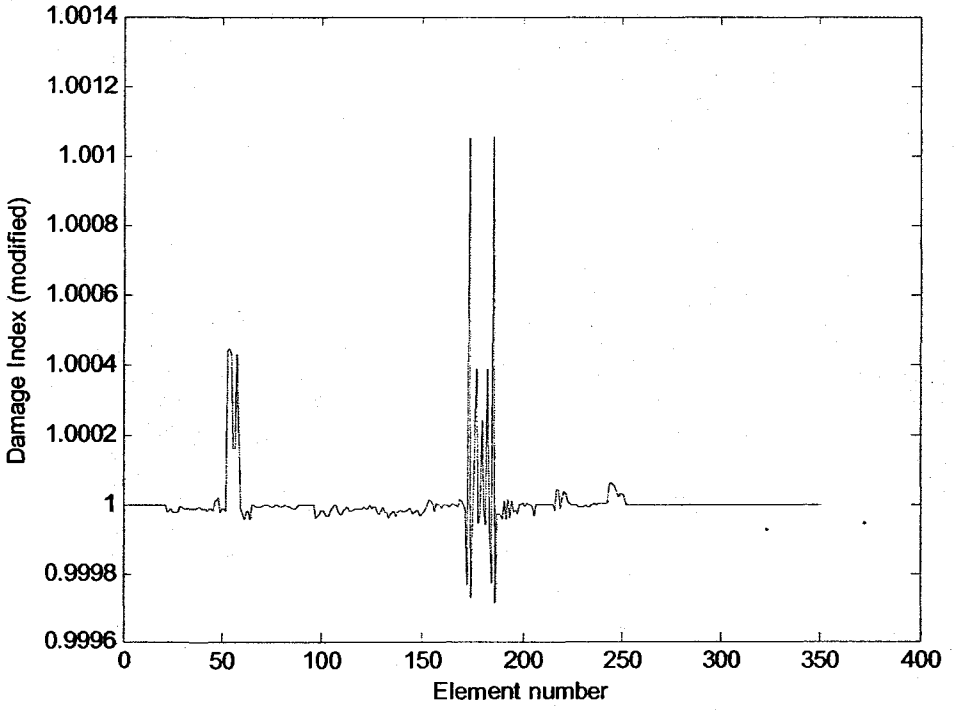

(b)

Fig 5.8: The Crowchild bridge case study. Graphs showing damage with element numbers for no error and incomplete modes with 10% damage severity by Damage Index Method **(a)** original and **(b)** modified.

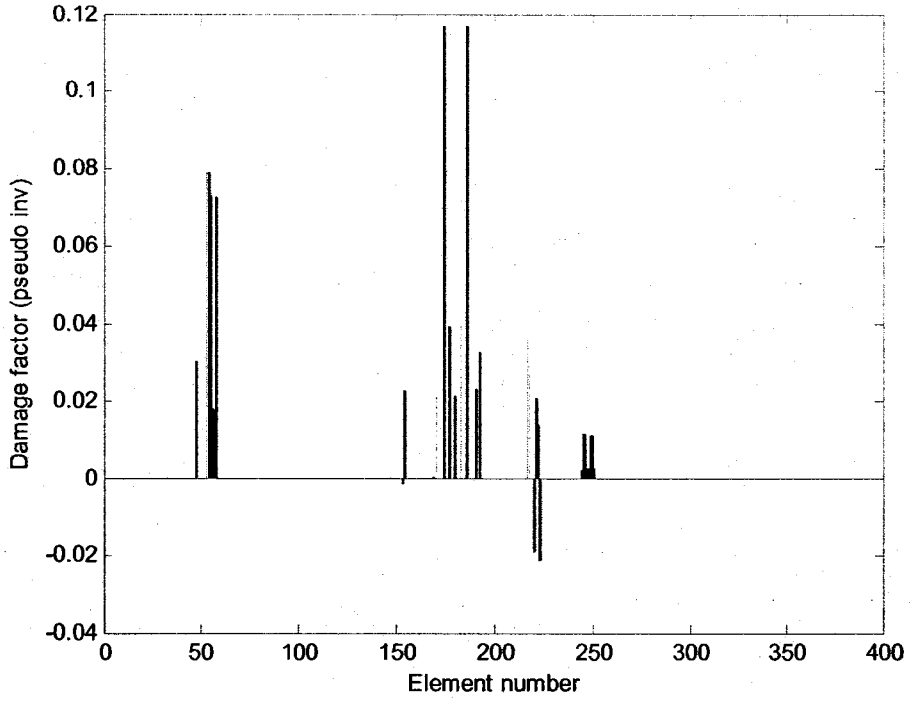

(a)

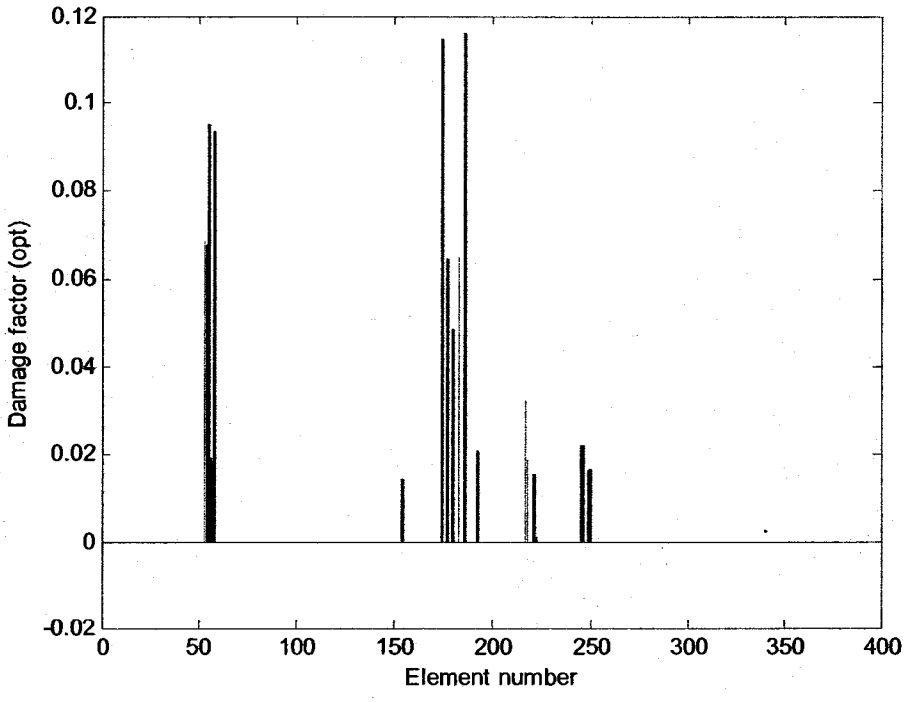

(b)

Fig 5.9: The Crowchild bridge case study. Graphs showing damage with element numbers for no error and incomplete modes with 10% damage severity by Matrix Update Method **(a)** Pseudo Inverse **(b)** Optimized

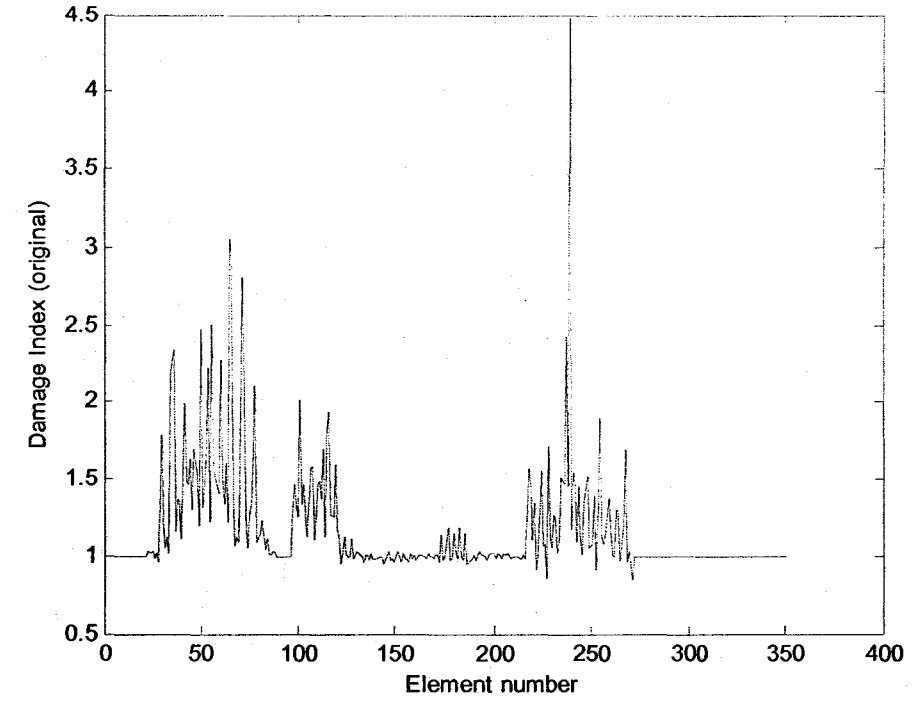

(a)

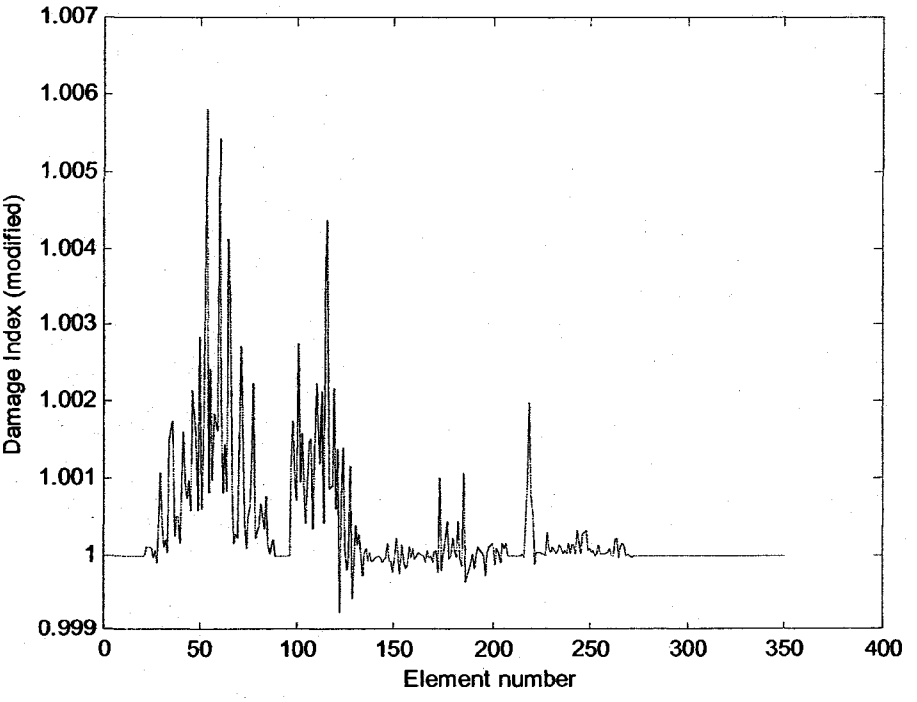

(b)

Fig 5.10: The Crowchild bridge case study. Graphs showing damage with element numbers for random error up to 1% and incomplete modes with 10% damage severity by Damage Index Method **(a)** original and **(b)** modified.

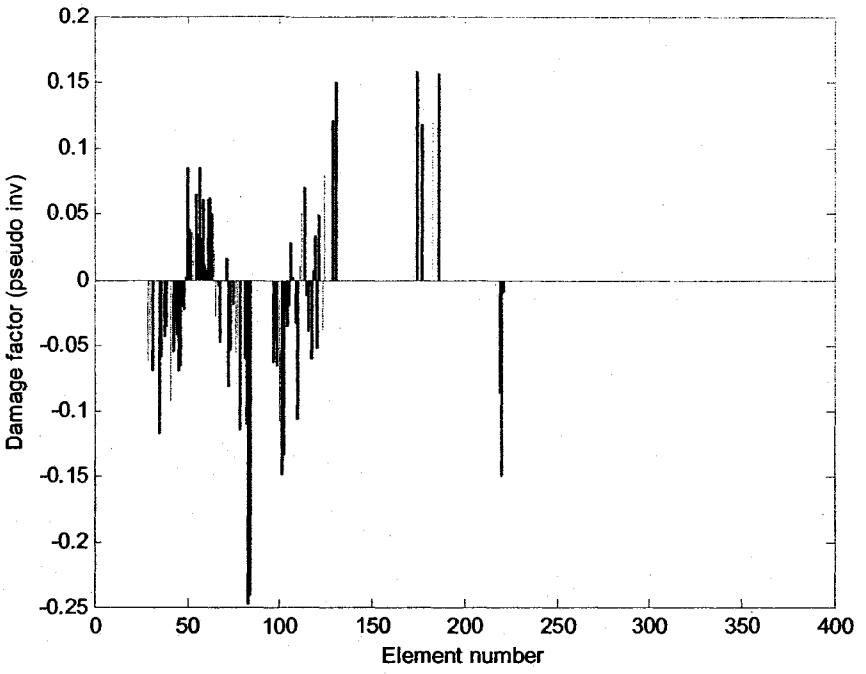

(a)

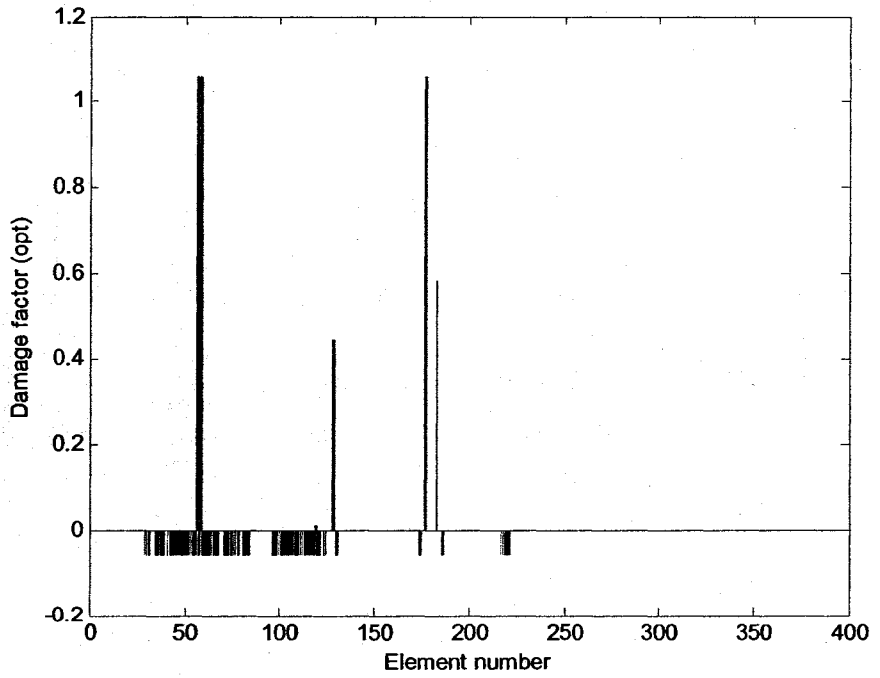

(b)

Fig 5.11: Graphs showing damage with element numbers for random error up to 1% and incomplete modes with 10% damage severity by Matrix Update Method **(a)** Pseudo Inverse **(b)** Optimized

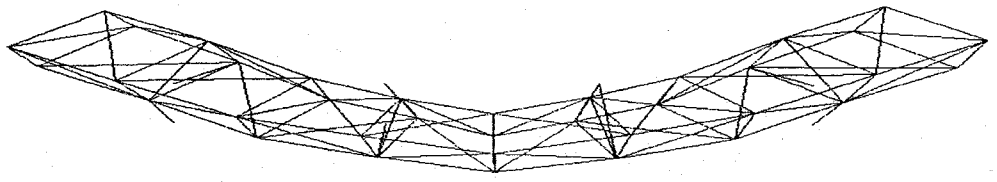

(a)

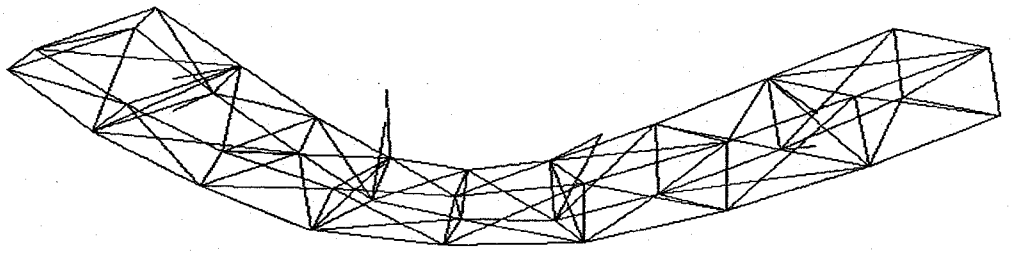

(b)

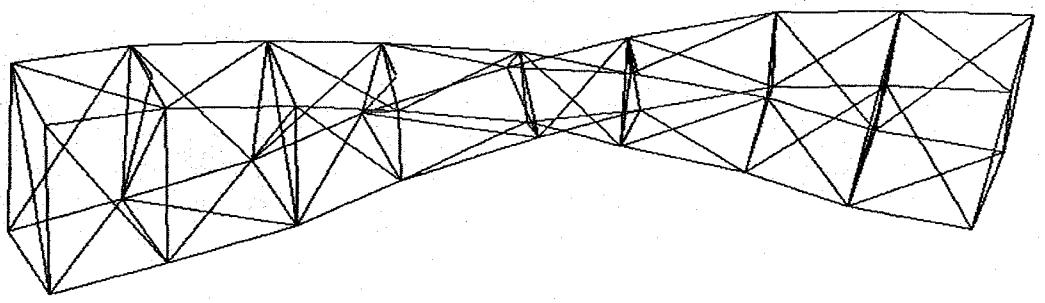

(c)

Fig-5.12: Mode shapes of 3D Space Frame: **(a)** Mode-1, (b) Mode-2, and (c) Mode-3

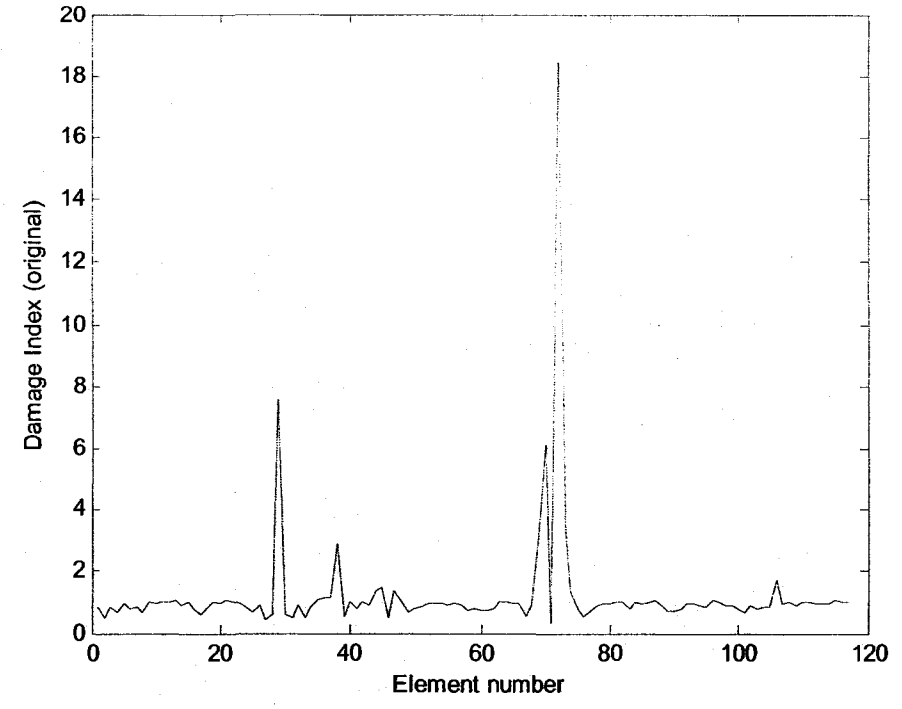

(a)

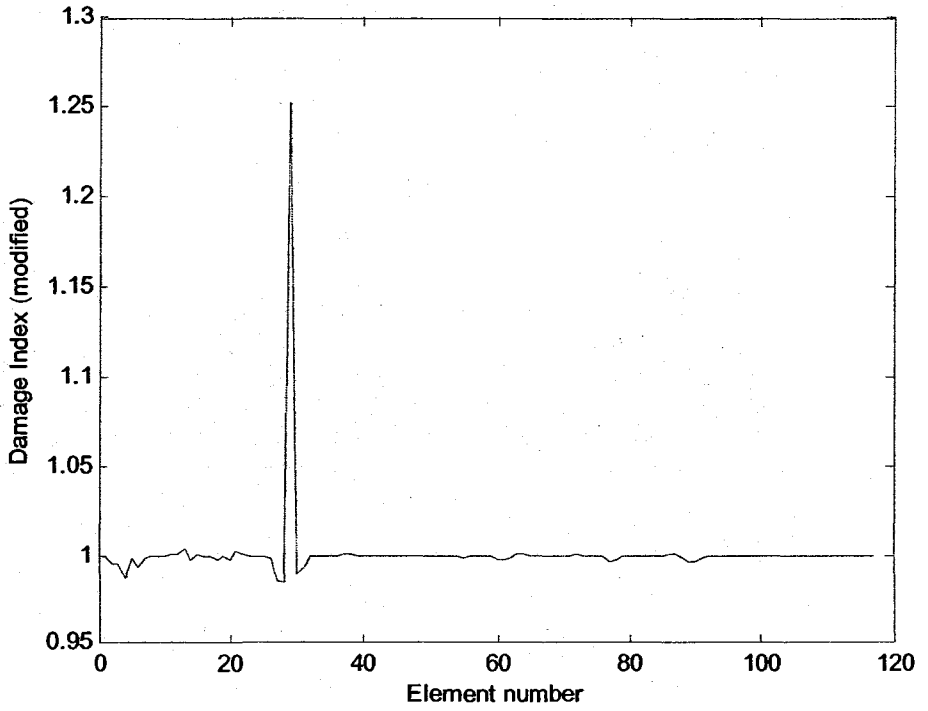

(b)

Fig 5.13: 3D Space Frame case study. Graphs showing damage with no error in frequencies and complete modes assumed for Damage Index Method **(a)** original and **(b)** modified. (for element-29, 80% damage severity)

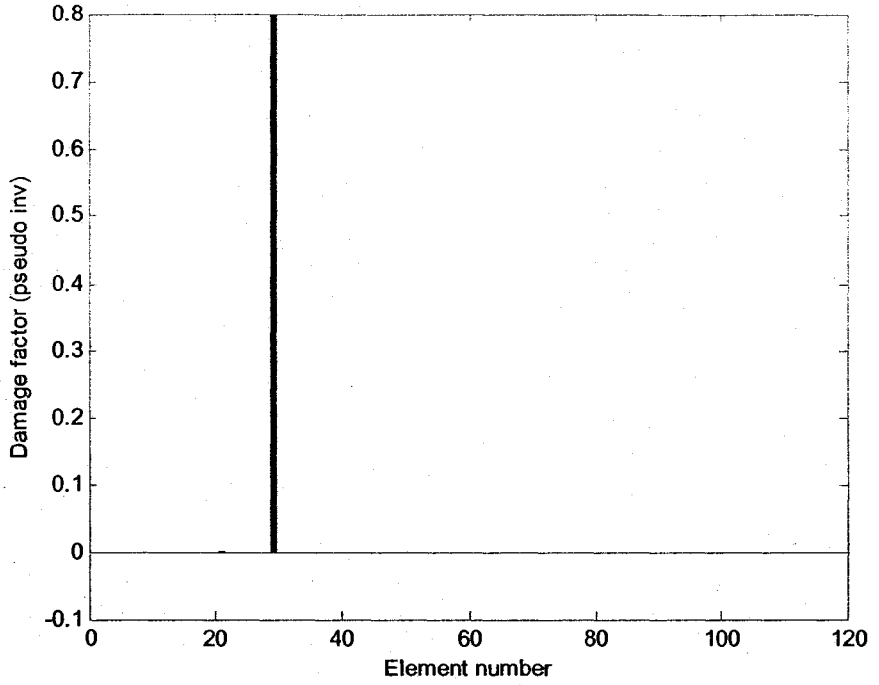

(a)

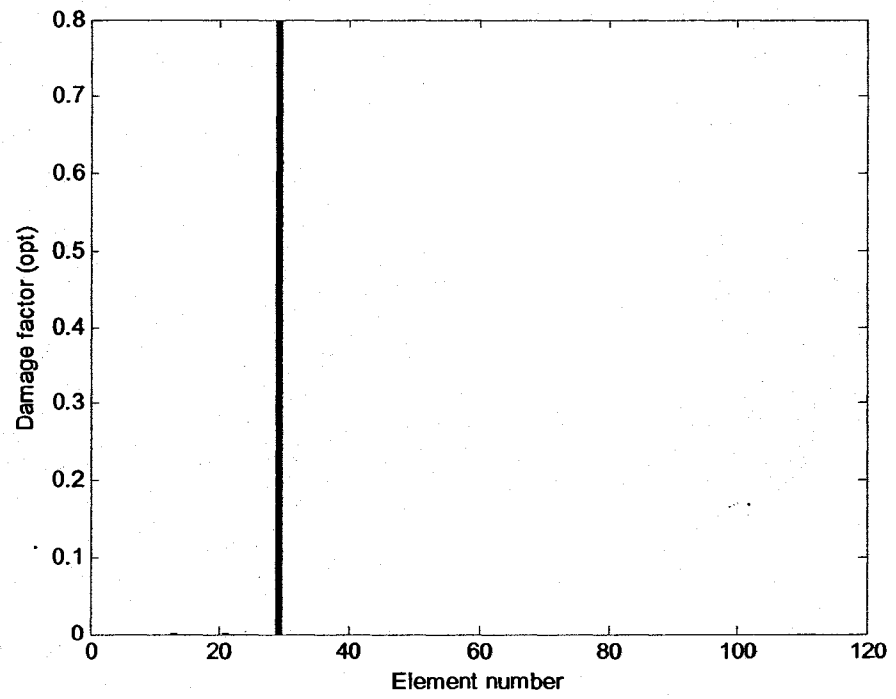

(b)

Fig 5.14: 3D Space Frame case study. Graphs showing damage with no error in frequencies and complete modes assumed. Matrix Update **(a)** pseudo-inverse **(b)** optimized. (For element-29, 80% damage severity)

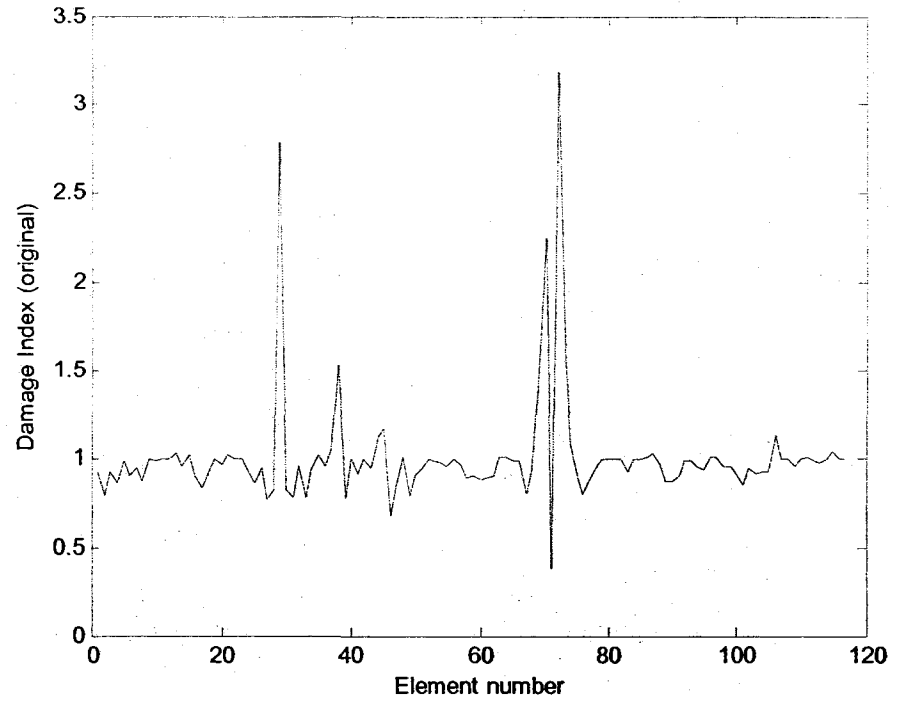

(a)

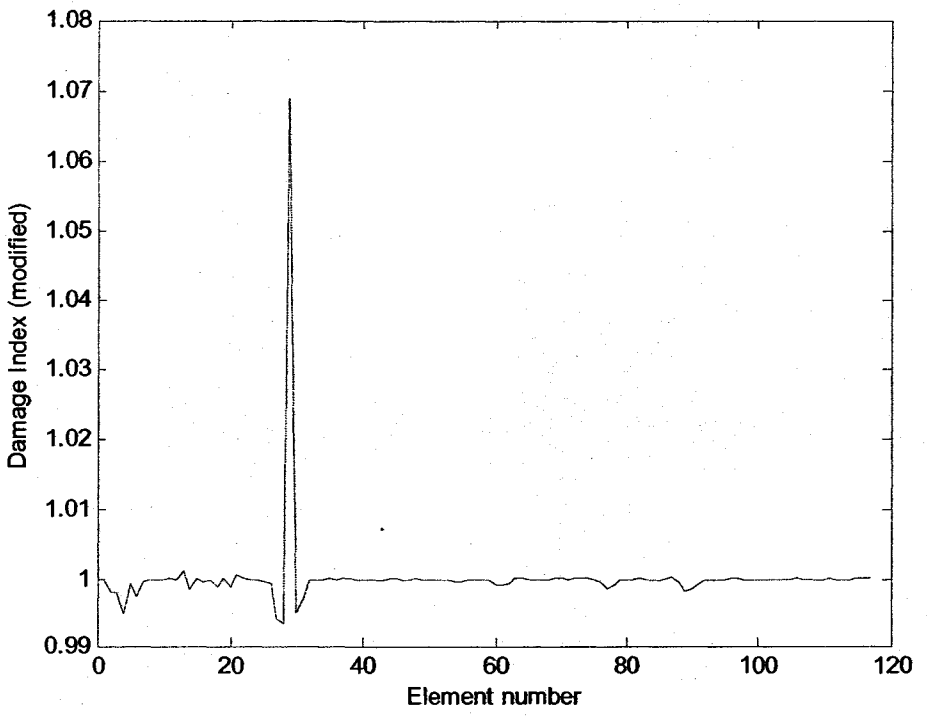

(b)

Fig 5.15: 3D Space Frame case study. Graphs showing damage with no error in frequencies and complete modes assumed. Damage Index Method **(a)** original and **(b)** modified. (for element-29, 50% damage severity)

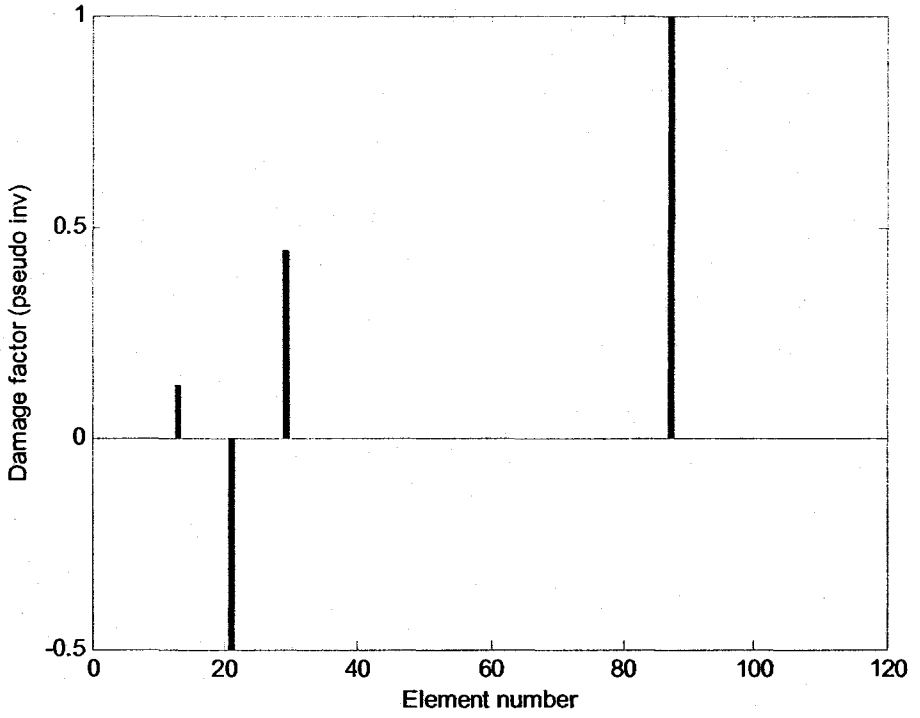

(a)

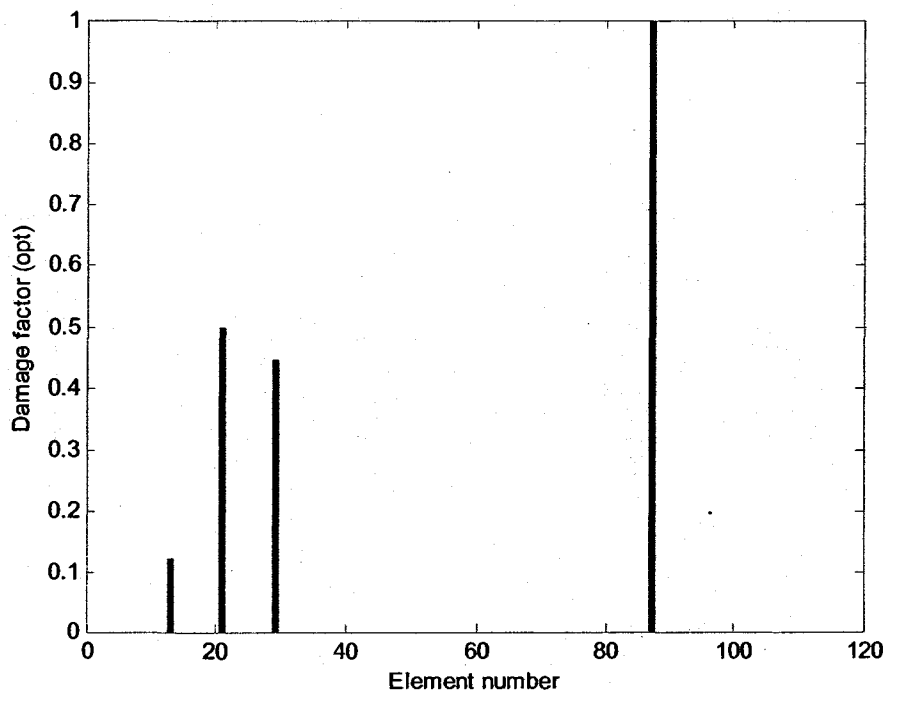

(b)

Fig 5.16: 3D Space Frame case study. Graphs showing damage with no error in frequencies and complete modes assumed. Matrix Update **(a)** pseudo-inverse **(b)** optimized. (Elemenent-29, 50% damage severity)

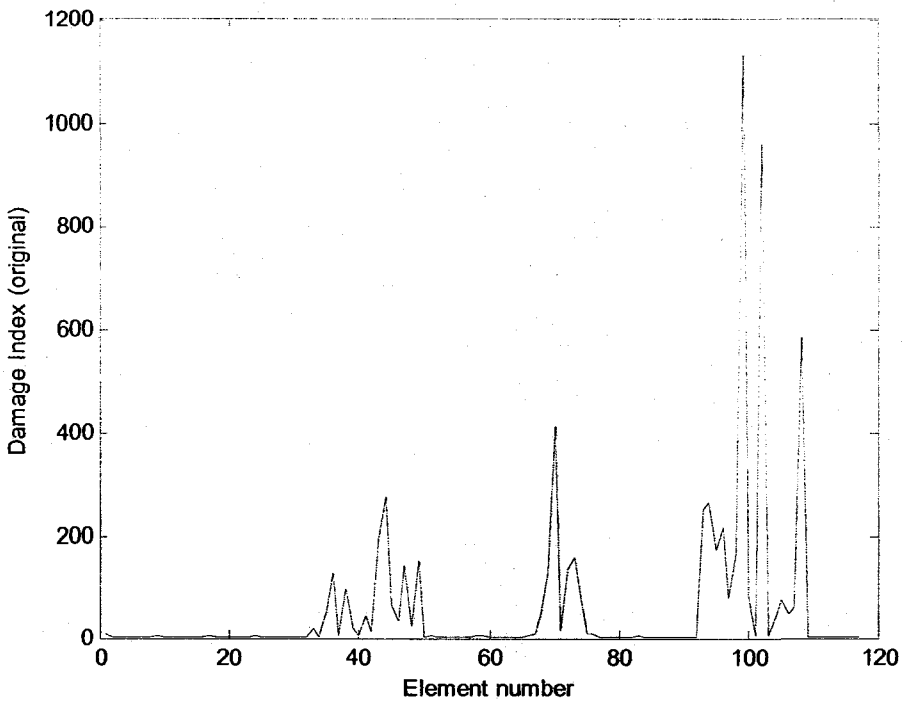

(a)

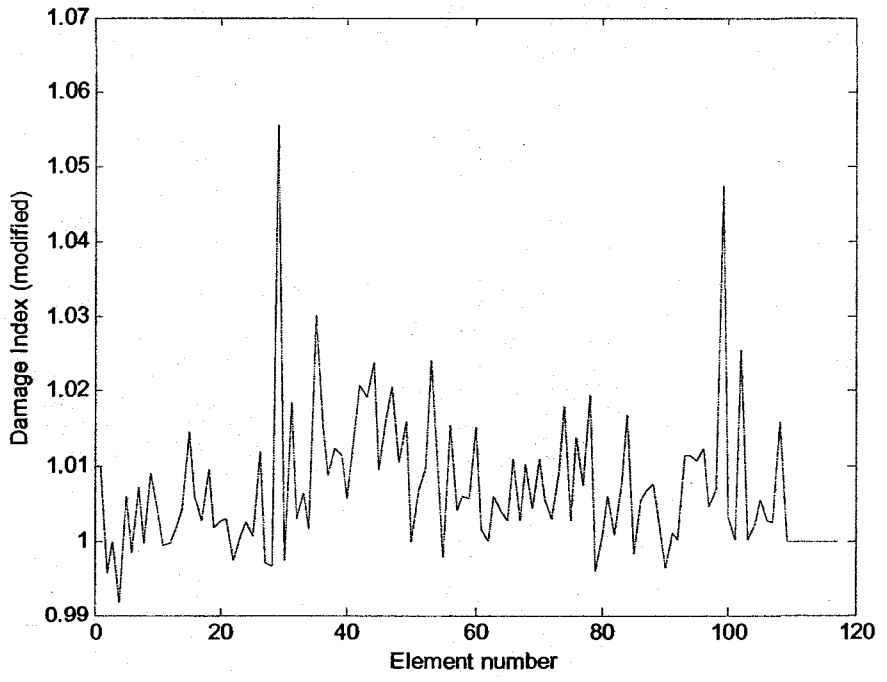

(b)

Fig 5.17: 3D Space Frame case study. Graphs showing damage with element numbers for random error up to 2% on frequencies and 10% on modes and assuming incomplete mode shapes. Damage Index Method **(a)** original and **(b)** modified. (element-29, 50% damage severity)

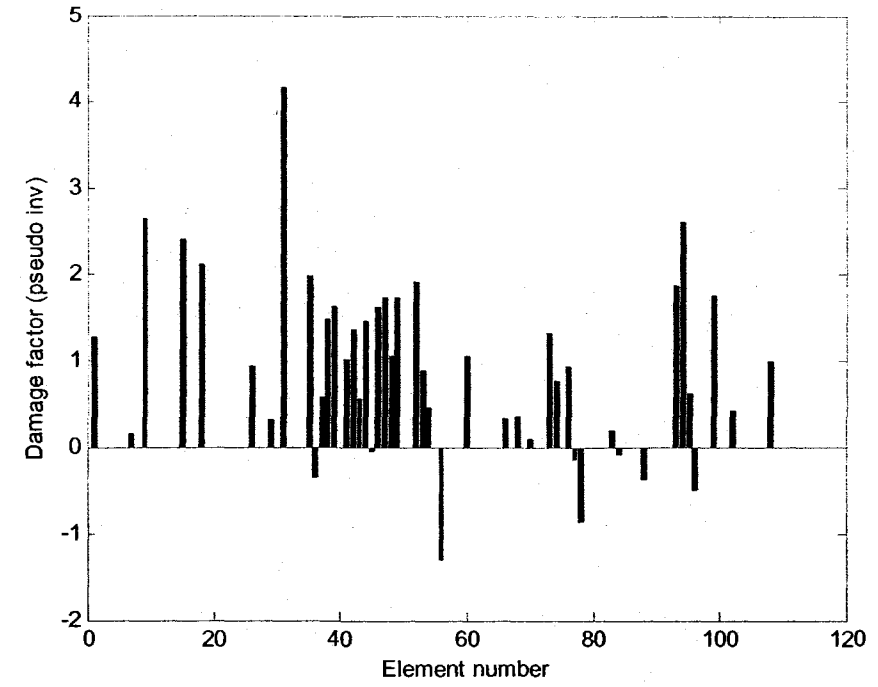

(a)

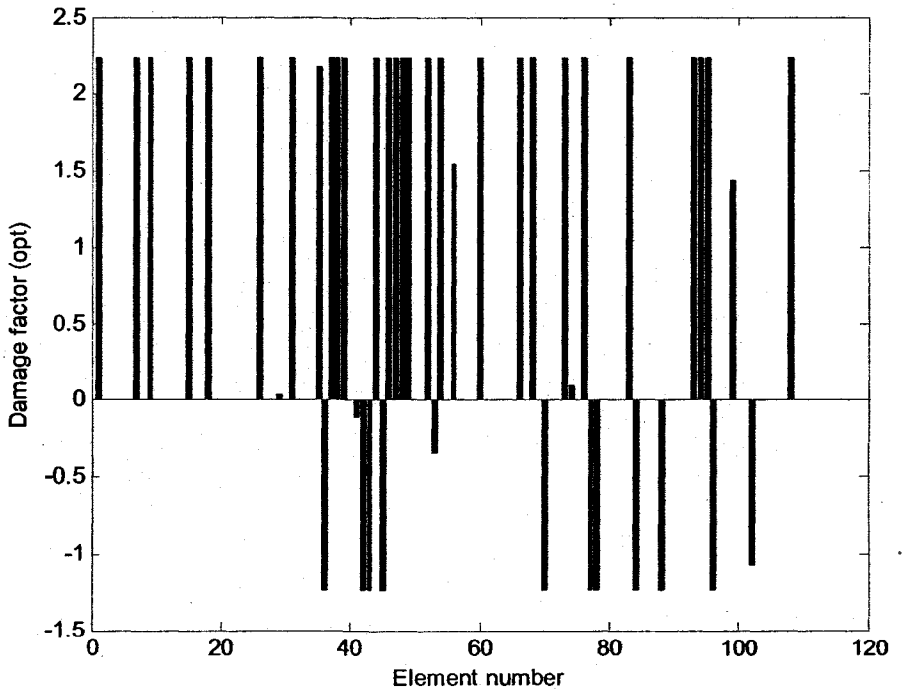

(b)

Fig 5.18: 3D Space Frame case study. Graphs showing damage with element numbers for random error up to 2% on frequencies and 10% on modes and assuming incomplete mode shapes. Matrix Update Method **(a)** pseudo inverse and **(b)** optimized. (element-29, 50% damage severity)

Chapter 6

Application of Statistical Pattern Recognition to Damage Detection

6.1 General

In this chapter, the damage detection method using statistical pattern recognition approach as described in Chapter 4 has been applied to experimental vibration and strain data of a real structure. The goal here is to evaluate the feasibility of the proposed approach to structural damage detection and determination of structural degradation over time.

6.2 Description of the monitored structure

Here, an approach of damage detection by statistical pattern recognition technique is tested on Portage Creek Bridge (Fig-6.1), located in Victoria in British Columbia in Canada. The information on the sensing system and also some other research work is available in a research paper by Huffman et al. (2006). The Portage Creek Bridge is a 124m long, three-span structure with a reinforced concrete deck supported on two reinforced concrete piers, and abutments on H piles.

The bridge was designed prior to the introduction of current bridge seismic design codes and construction practices. Therefore, it was not designed to resist the earthquake forces as required by today's standards. Later dynamic analysis done on the two piers showed that strength of the columns of Pier-2 was insufficient.

The innovative solution of Fiber Reinforced Polymer wraps (FRPs) was chosen to strengthen the short columns The FRP wraps and the bridge were instrumented as one of 36 demonstration projects across Canada sponsored by ISIS (Intelligent Sensing for Innovative Structures) Canada, a federally funded Network of Centers of Excellence, to assess the performance of FRP and the use of FOS (Fiber Optic Sensors) for Structural Health Monitoring (SHM). The two columns of the bridge pier were strengthened with GFRP (Glass Fiber Reinforced Polymer) wraps with eight bi-directional rosette type strain gauges, and four long gauge fiber optic sensors attached to the outer layer of the wraps (Fig-6.2.) In addition, two 3-D Crossbow accelerometers are installed on the pier cap above the columns, and a traffic web-cam mounted above the deck at the pier location.

6.3 Data collection and preprocessing

The data is collected through high speed internet line from an interactive web page at ISIS Canada's web site (ISIS, 2008). The bridge data can now be monitored from anywhere. The earliest and the last time of data available for downloading from the database are 2003-04-23 13:54:33 and 2006-08-26 17:58:57 respectively. However there

are some times where data are not available from the source. These down-times have occurred at all the range of the monitoring. The duration of down times varies from a few hours to a few months. A number of sensors including 16 2D-strain gauges, 2 3D-accelometers, 1 thermocouple, and 16 long gauge fibre optic strain/displacement sensors are installed in the structure. Some of the data are archived in ISIS database and the query sampling rates available in the database lookup are 1/32s, 1s, 10s and 1min. Number of data points available in a single download varies from 32 to 30,000. Data can be obtained both graphically and numerically.

The data was made available for retrieval from the ISIS database in the text, graphical or comma separated values (CSV) format. A data file in CSV format containing the retrieved data starting from a certain point time of all strain, accelometer and temperature readings at the rate of 32 Hz and length 30,000 points (highest frequency and length available) is typically around 9.2 Mb. To download the entire database in hard disk, the space required as per approximate calculation is 950 GB. The amount is too big for a normal PC and time consuming as there is no automated downloading tool available for this in ISIS website. However, downloading the whole database is not required for our current work as it will be explained in this section later.

In the beginning, the data were viewed graphically using various sample rates and length at random starting times to visually identify the overall nature and trends of the data. For example, Fig -6.3 (a) shows the data plotted for S_1_1_C1 (strain gauge reading 1 along strain direction 1 of column 1) taken at 1 reading per second of 30,000 points starting at

time 17:48:57 on 2006-04-14. This data time duration is 8 hours 20 minutes. Careful inspection shows there are some slopes with continuous oscillation about x–axis. There are also some random vertical straight lines. It seems that those random lines were resulted from some sudden impacts. Four of them are long enough to be distinctive. Later analysis revealed that slopes are mostly the effect of temperature changes and those random vertical lines are the results of some moving loads, most possibly the vehicles.

If we gradually zoom in by increasing the sample rate, narrowing the data range, and picking the starting time very close to the left of the rightmost vertical line, we can get a clearer picture. By gradual inspection of the location of the line and changing starting point accordingly we finally arrive at a start time of 00:02:42 on 2006-04-15, we get the graph shown in Fig-6.3(b). The rightmost and longest vertical straight line in Fig-6.3(a) now looks like a spike. Sample rate of the signal block is 1 s and length is 256 points. The time duration of this block is 256 seconds. If we increase the rate to 32Hz, data plotted graph is shown in Fig 6.3(c). The time duration of this block is 8 seconds. It shows clearly that the change of strain over a short period of time is the result a gradually (not an impact as appeared in Fig 6.3(a)) changing load. This is the characteristic of a load applied on a pier by a heavy vehicle moving on the bridge.

Based on the observations similar to the one mentioned above, it is apparent that in order to study the structural behavior of the bridge we need to analyze it under two conditions, 1) steady state condition when only small oscillations are observed, and 2) the agitated condition as shown in the Fig-6.3(c) in addition to small oscillations.

6.3.1 Data block Sampling Scheme

The data, or in other words signal blocks, are collected for 4 types of analysis.

1) Steady state strain
2) Live load strain
3) Accelometer reading under live load.
4) Temperature effect on strain

How data was collected for all cases is briefly described below.

1) Steady state strain: Fig-6.3 (d) shows a plot of strain in a typical steady state condition. It represents the condition when there is no live load such as a heavy vehicle on the bridge. Steady state strain at direction 1 of strain gauge 1 of column 1 was taken for the study in this case. The data blocks are taken for the starting time of 00:00 of the 1st day of every month. The sampling rate is 32 Hz and length is 256 points. Total number of data blocks is 27. Time duration of all blocks- steady or live- were taken 8 seconds as passing of a vehicle was never found taking more that this time.

2) Live load strain: Fig-6.3(c) is typical live loaded conditioned time series of strain readings. These data block are selected by inspection as explained earlier, and shown in Figs-6.3(a), 6.3(b) and 6.3(c). These data block are selected such that the peak values are more approximately 6 times more than those at steady state conditions as shown in 6.3(c) in S_1_1_C2. Correspondingly, nine random data blocks which include heavy vehicle loads for each of 7 selected strain readings of

C1 and 8 of C2 have been taken. Each block has sampling rate of 32 Hz and duration of 8 seconds. These strain gauges are: S_1_1_C1, S_1_2_C1, S_2_1_C1, S_3_1_C1, S_3_2_C1, S_1_1_C2, S_1_2_C2, S_2_1_C1, S_2_2_C2, S_3_1_C2, and S_3_2_C2. In addition, for the purpose of statistical modeling, more data has been taken (Table-6.1). These data are also used in the pattern comparison method. Analysis of these signal blocks can be used in the study of structural behavior of the bridge over time under the live loads, as well as to determine if all the sensors are working properly, and identify the faulty one, if there is any. The magnitude and signs (+/-) may vary among the gauges, but the relative values with a reference block of data from a particular channel should not vary significantly.

3) Accelometer reading under live load: The data blocks of accelometer were taken at the same time, frequency of sampling and duration of the blocks of live load condition. The sampling process is shown in Table-6.1. An example of time series is shown in Fig-6.4

4) Temperature effect on strain: The stain values and temperature at time 00:00 of the first day of each month is taken for the analysis. The care was taken that data thereby obtained is of strictly steady state conditions. Then linear regression is performed on the data of several months to determine the temperature strain relation over those months and also over entire period of the observation.

6.4 Feature extraction

The concept of feature extraction is explained in Section 4.2.3. As any data block in this study is essentially a time series, time series analysis as explained in Chapter-4 is adopted for the purpose of feature extraction, and also residual error determination for the use in pattern comparison technique. All data are analyzed as AR(p) process as described in Chapter-4. The Variation of AR process is mainly dependent on AR coefficients ϕ_{xj}. Hence, ϕ_{xj} is considered as structural degradation feature or damage sensitive feature. For the calculation of the AR coefficients, Yule-Walker method has been applied.

Statistical analysis software, ITSM2000 (B&D Enterprises Inc., 2002) was used for the time series analysis. Since the AR process is a zero mean method, in order to attain this property of the series, the mean value of a data series is subtracted from the data points. Every observation is mean corrected before applying the AR process. For the determination of the degree of AR, guideline presented in section 4.3.5 is used. For example, from plotting of PACF of a typical time series of a strain (in live loaded condition) is shown in Fig-6.5. It can be seen that after a lag of 17, no PACF value falls out side the critical boundaries as defined in section 4.3.5. Therefore p = 17 can be feasible order for the AR process. It is observed that the tentative order of all time series for live loaded state falls below 22. For the general consideration a common order of 20 is used in all analysis. In the case of accelometer, a higher order is needed for the analysis. A degree of 27 is in general used here for all accelometer AR processes.

6.5 Damage Identification by Statistical Model Development

Statistical model development has been implemented through appropriate algorithm to analyze the distribution of extracted features to determine the damage state of the structure. Preference of algorithm used is discussed in the section 4.2.4.

As no damaged case is known, algorithm for unsupervised technique is used. In this study control chart analysis, which is the most commonly used in Statistical Process Control technique for Outlier Analysis is used. It is applied to the calculated and selected damage sensitive feature as explained in the previous section. When the structure undergoes damage or it is weakened, the mean and/or variance of the extracted features should change accordingly.

The signal blocks in Table 6.1 of strains S_1_2_C1 &S_3_1_C1 and accelometer A_x_1, A_y_1 and A_z_1 are used for creating the pools of features, which are given by the AR coefficients. The selected data block include 132 signal blocks for strain, 124 signal blocks for horizontal accelerations A_x_1 and A_y_1, and 108 blocks for vertical acceleration A_1_z. These data blocks are arranged chronologically. According to Nair and Kiremidjian (2006), in the process control analysis, the first three AR coefficients give most robust damage indication. In this work, the first four coefficients for the AR analysis are considered. The mean and standard deviation of the first quarter of the arranged features are taken as basic mean and standard. Here X-bar control charts are employed to monitor the changes of the selected feature over time. Subgroup of 4

features is considered here. The subgroup size is taken as 4 according to the suggestion of Montgomery (1997). The results are presented in Fig-6.6 through Fig-6.21.

6.6 Damage Identification Approach by Pattern Comparison

To apply this method several sample data blocks for selected strain and accelometer readings are collected. The first block of each series of a particular strain or accelometer is considered to be the reference blocks and the remaining blocks are considered to be the test data blocks to be used for comparison. The sampling scheme is outlined in the section 6.3.1. The output of the analysis is presented the Figs 6.22 through 6.30.

6.7 Discussion on the results on damage identification

The following two methods are utilized for structural health monitoring by statistical pattern recognition: 1) statistical modeling, and 2) pattern comparison. In this section results of both methods are discussed, and relevant explanations are presented.

6.7.1 Results of Identification by Statistical modeling

Examining the control charts in Figs 6.6 through 6.9, only 1 outlier of total 132 (0.75%) subgroups of the first four AR coefficients of Strain S_1_1_C1 is detected. However slight downward tendency of towards of the features is noticeable. From Figs 6.10 through 6.17 no outlier of total 124 of subgroups of the first four AR coefficients of each

of Accelometer A_1_x and A_1_y is noticed. From Figs 6.18 through 6.21, 3 outliers of total 108 (2.78%) subgroups of the first four AR coefficients of Accelerometer A_1_z have been found.

In the control charts of accelometer data, there are tendency towards limits is more visible towards the end of the period. In a study by Sohn et al (2000) on a concrete column in a laboratory environment, at very mild damaged state, statistical modeling showed 6.25% and at significant damage 29.17% outliers of total subgroups. Comparing their results, we can consider our structure still in a safe condition which is expected for a bridge of this age. However the increased tendency of features getting closer to the limits at the third or fourth quarters of the chart indicates that the structure is undergoing some small degradation towards the end of the monitoring period.

6.7.2 Results of Identification by pattern comparison method

The *R*-value which indicates the goodness of fit of AR model of reference data block to others can be also a good indicator of structural health over time. It is logical that *R*-values over time, a particular strain or accelometer should be steady and they should stay close to baseline of 1. Upward trend over time indicates degradation.

From Fig-6.22, graph of *R*-values for 27 monthly blocks of S_1_1_C1 at steady state shows no trend. Same characteristic is noticed in the graphs of 55 successive occurrences, 31 blocks (1 per day), 39 blocks (1 per 5 days) and 23 blocks (1 per month) of live loaded condition of S_1_1_C1 in Figs 6-23 through 6.26.

There is a noticeable peak value corresponding to the block sequence 30 in Fig-6.23. There are 2 possible causes for this:

1) A heavy vehicle passed over C1 such that it produced higher strains in S_1_1_C1 as compared to the rest of the strain gauges, and its pattern deviated from the normal state.
2) There was another vehicle nearby and the combined effect produced a non-regular pattern

Fig 6.27 and 6.28 show the graph of *R*-values of 9 blocks of 7 stains of C1 and 8 blocks of 8 stains of C2 at 1 block per 4 month over the total monitored time. All 15 strain gauge data were taken at same times. No clear trend is present here to. This also indicates that all strain gauge meters are working properly.

For S_4_1_C2, a high value at 7-th point is observed. The first cause of anomaly stated above may be applicable for this occurrence. Fig-6.29 and 6.30 showing results for Accelometer A_1_x, A_1_y and A_1_z do not indicate any visible trend. According to the analysis by pattern comparison method, there is no indication that the structure is damaged or undergoing abnormal strength degradation.

6.8 Temperature effect on Strains

Temperature has significant on the values of strains. Data blocks taken at different temperature with similar working conditions should show different values.

6.8.1 Need for relation of temperature to strain values

The AR Process as applied in the previous section to analyze all time blocks of series is a zero mean process. Occurrence of such events in real life condition is very rare. Subtraction of means from original values not only normalizes the data but also reduces the sample mean. As temperature is almost constant for duration of 8 seconds for data blocks considered here in the time series analysis, the temperature component in the strain or accelerometer readings are canceled out by reduction of the mean from all observations and the transformed values represent mostly the structural component. However, for other type of analytical processes on the strain data where zero mean process or any kind of normalization is not applied, temperature correction is needed often to get the actual values of structural components of the data.

For research enquiry on temperature effect on strain, Strain S1_1_C1 is selected. Fig-6.34 shows the graph of time vs. strain values of S_1_1_C1 at 1 second interval for 8 hours and 20 minutes, starting from time 0:0 on 2006-03-01. The big spikes in the graph are effects of live loads due to heavy vehicles passing over the prier to which the strain-gauge meter of S_1_1_C1 are attached. The continuous small oscillations represent the steady state. The general upward trend of the graph towards the right is accounted for temperature effect.

6.8.2 Temperature vs. Strain relationship and comments

Twenty seven (27) monthly readings of temperature nearest to S_1_1_C1 are taken at time 0:0:0 on the first available day in each month. Linear relationships have been

established by considering 1) all 27, 2) the first 10, 3) The next 10 and 4) the last 7 monthly readings. Fig 6.35 through 6.38 presents the results. It should be noted every strain gauge has its unique temperature-strain relationship.

Though a linear relationship is ideally expected between temperature and strain, the graphs produced in Figures 6.35 through 6.37 show that linear regression does not represent the accurate trend of the data. However Figures 6.36 and 6.38 show better linearity in trend.

There are some uncertainties involving the structure such as humidity, internal stress distribution, etc. These factors may account for deviation from linear relationship, though still it is possible to extract temperature strains with moderate accuracy.

Another reason for scattered behavior of the data is perhaps due to the fact that the incidence of sunlight may vary between the column and the sensor, which may cause uneven distribution of temperature.

Type	Interval	Number of data
1	Continuous	54
2	1 day	25
3	5 days	38
4	1 month	23

Table-6.1: Sample collection for data of strains S_1_2_C1, S_3_1_C1, Accelometers, A_1_x, A_1_y and A_1_z.

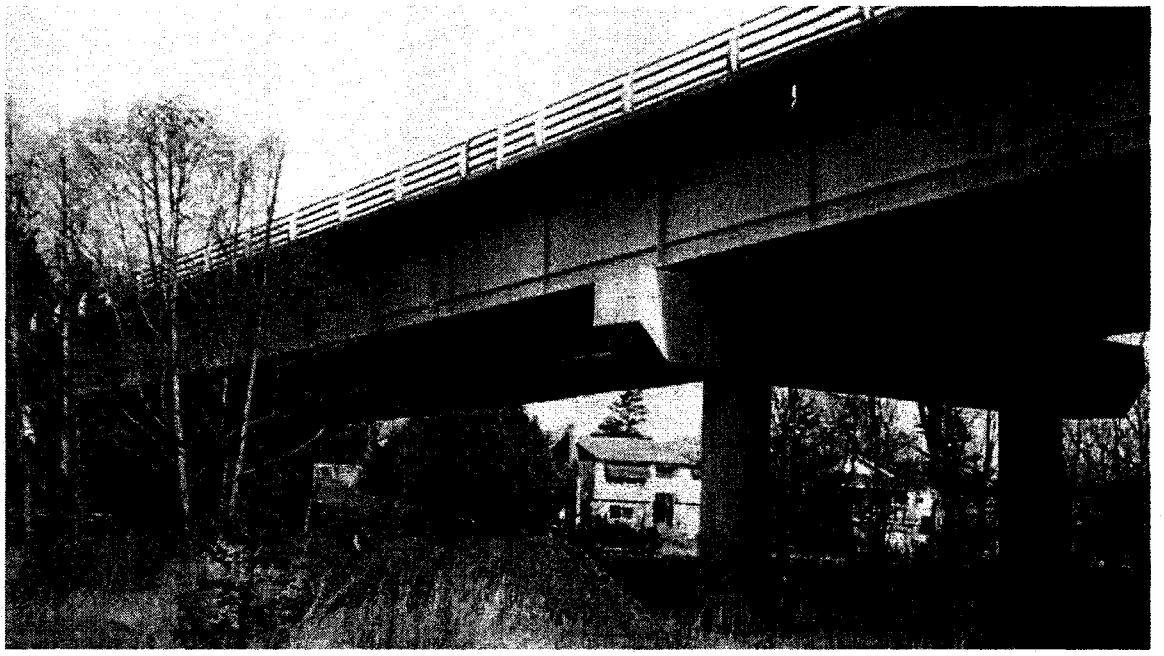

Fig 6.1: Portage Creek Bridge, Victoria, British Columbia, Canada

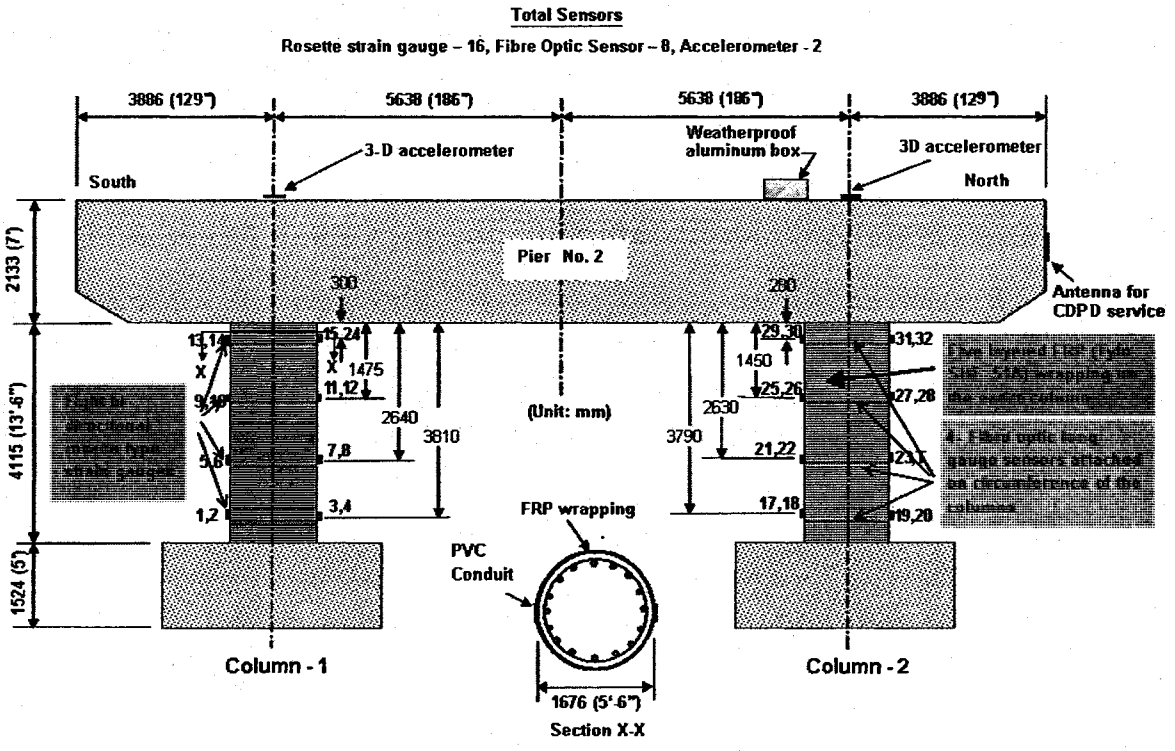

Fig-6.2: Portage Creek Bridge Elevation of pier-2 (short columns) with sensor locations. (Huffman et al, 2006)

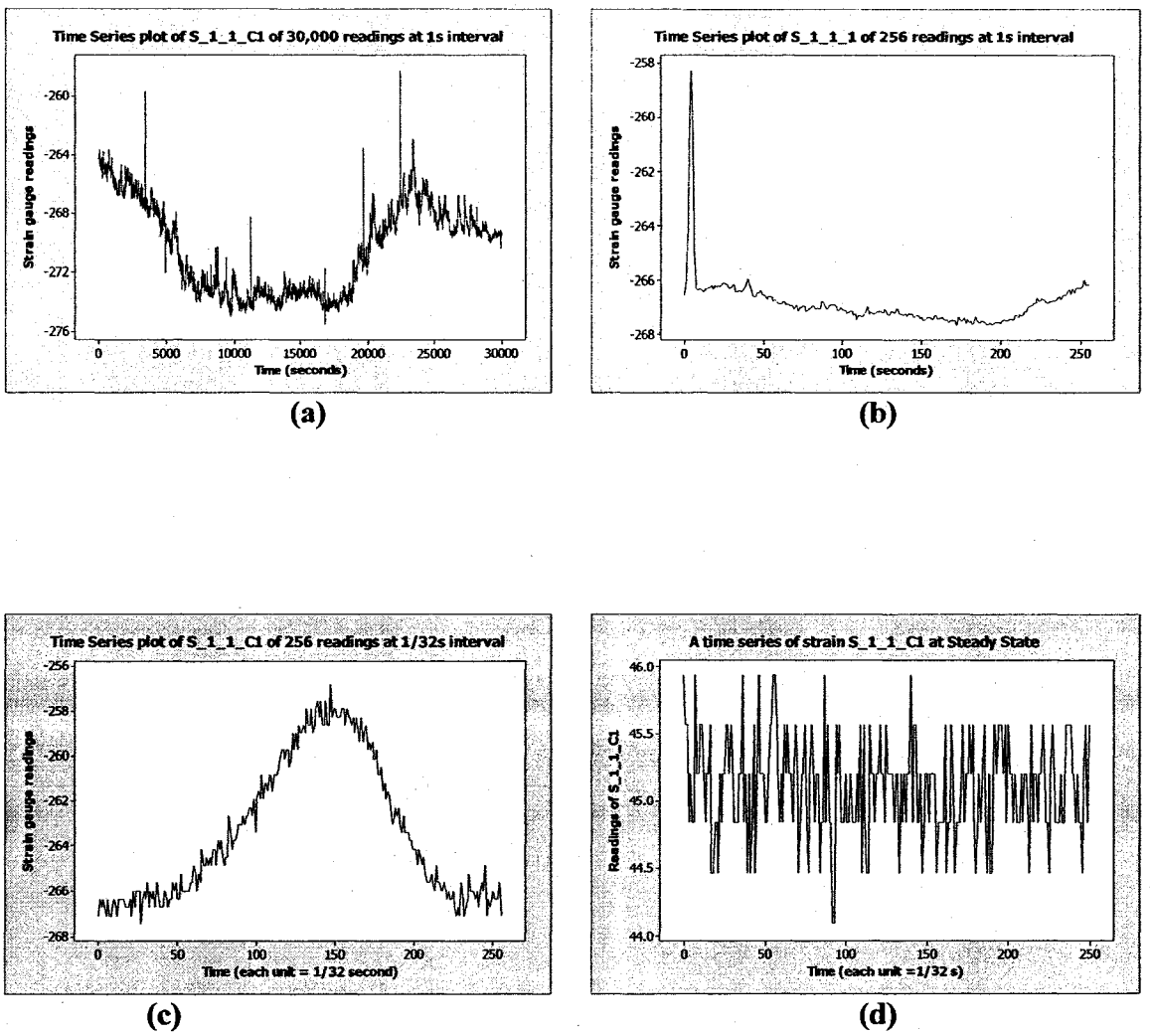

Figure 6.3: Time series of strain S_1_1_C1: **(a)** starting at 07:48:57 on 2006-4-14, No. of observations =30,000 at 1 second interval; **(b):** starting at 00:02:42 on 2006-4-15, No. of observations =256 at 1 second interval; **(c):** starting at 00:02:42 on 2006-4-15, No. of observations =256 at 1/32 second interval; **(d):** a steady state time series of strain S_1_1_C1

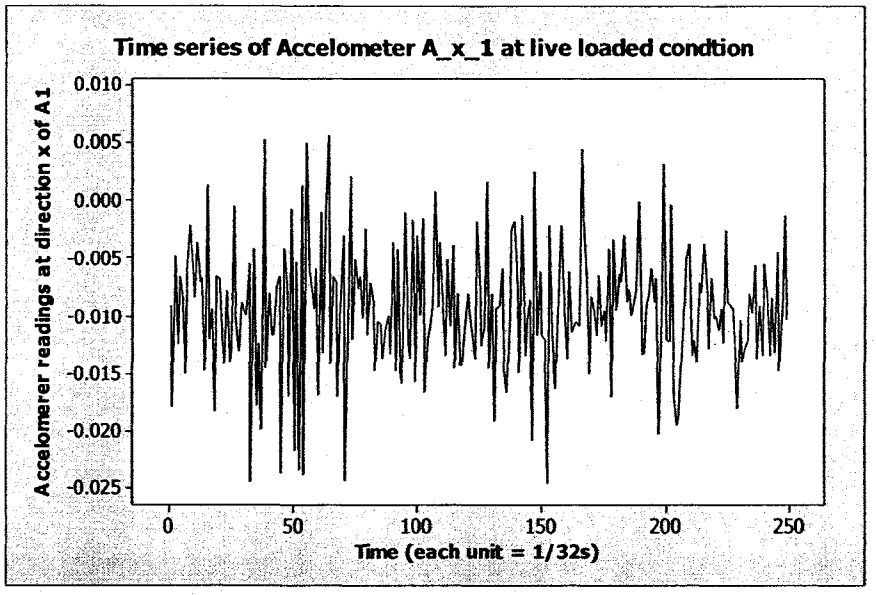

Fig 6.4: An accelometer time series at live loaded condition

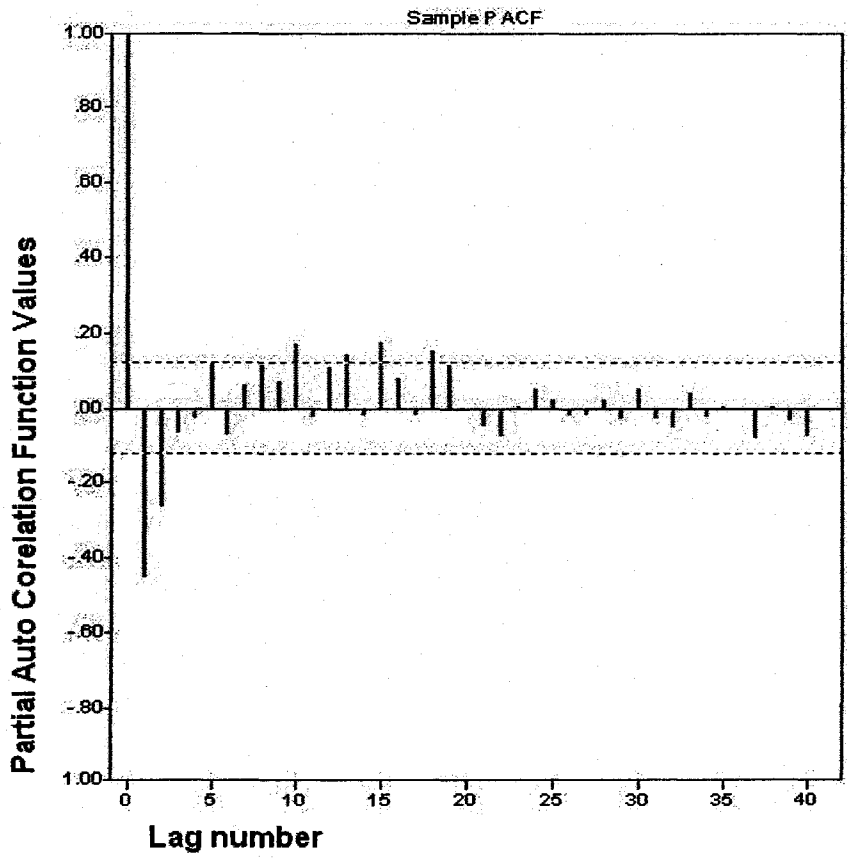

Fig-6.5: Example of plotting of PACF by ITSM. The figure corresponds to a series of S_1_1_C1, live loaded condition after differencing by 1

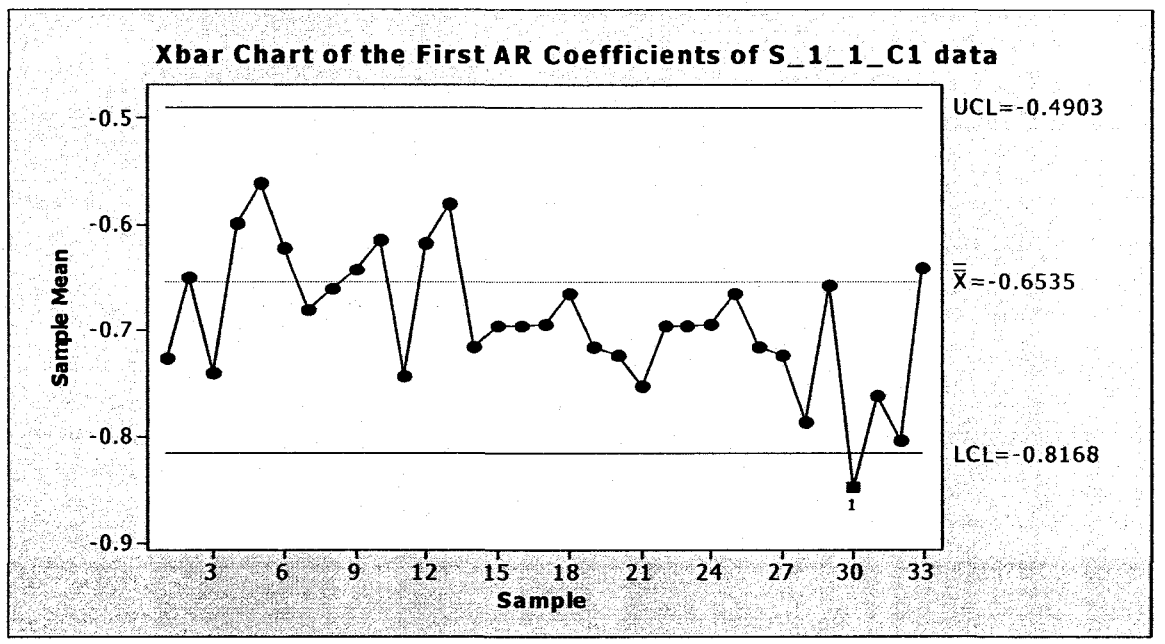

Fig 6.6: Outlier analysis of the first AR Coefficients of Strain readings of S_1_1_C1. Pool size=132, Subgroup size = 4.

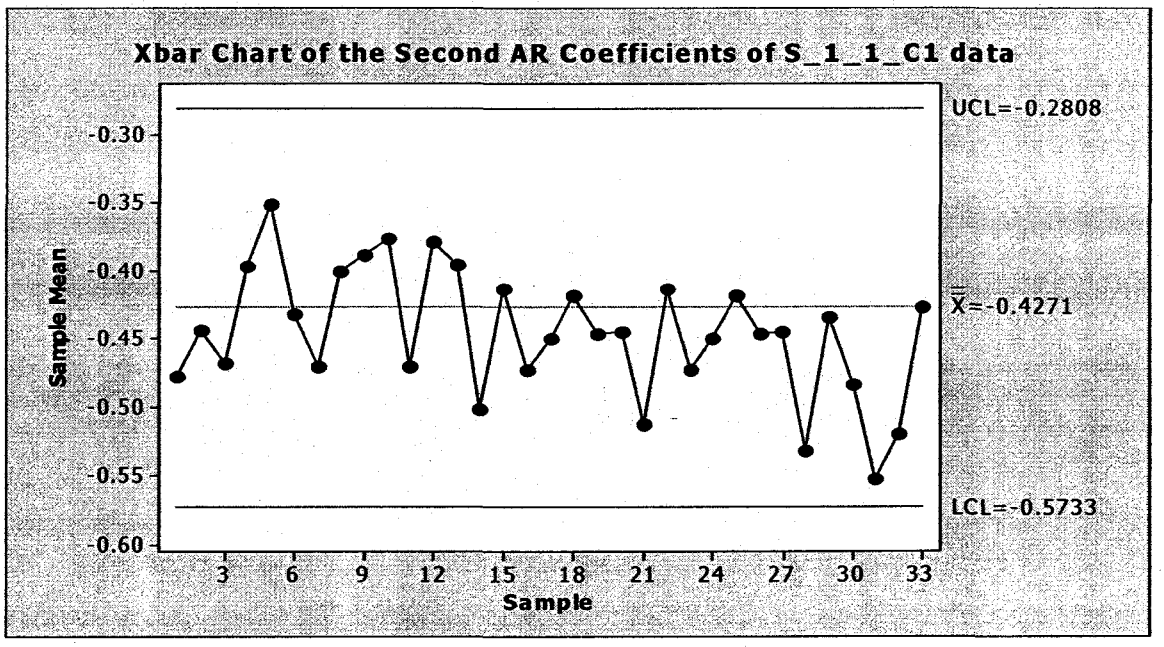

Fig 6.7: Outlier analysis of the second AR Coefficients of Strain readings of S_1_1_C1. Pool size=132, Subgroup size = 4.

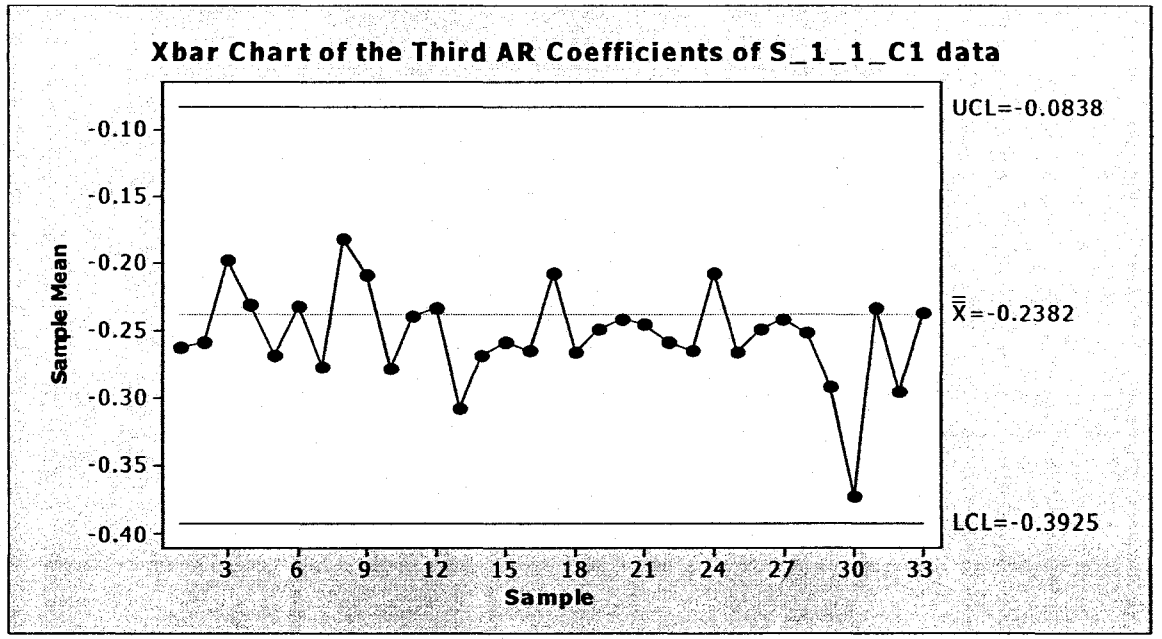

Fig 6.8: Outlier analysis of the third AR Coefficients of Strain readings of S_1_1_C1. Pool size=132, Subgroup size = 4.

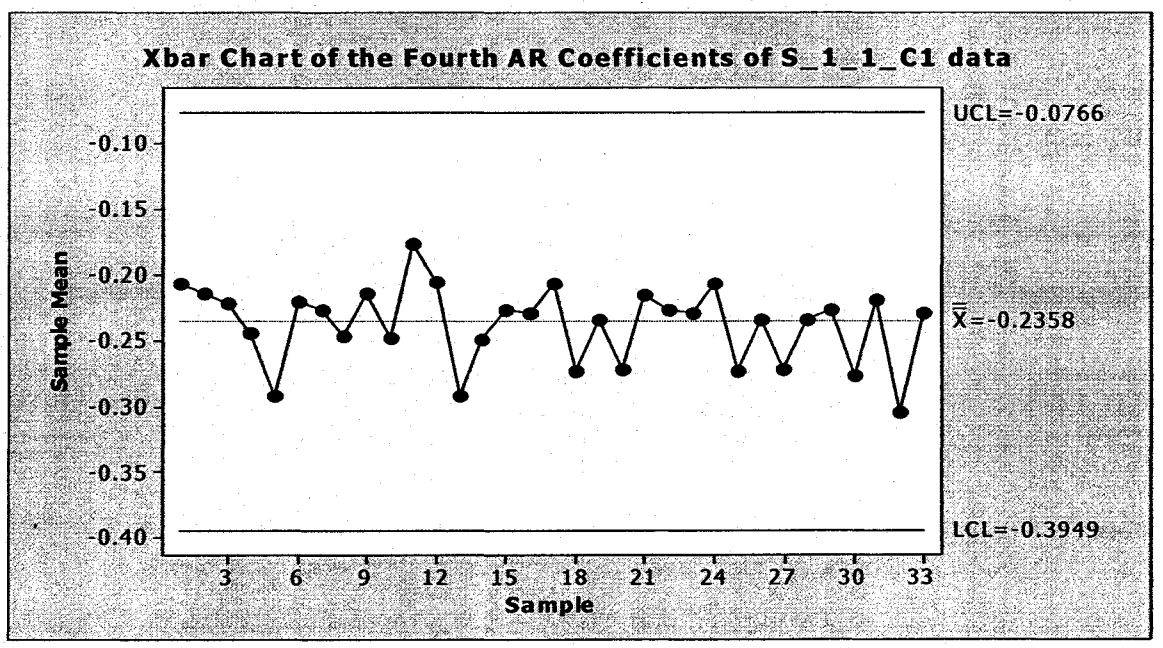

Fig 6.9: Outlier analysis of the Fourth AR Coefficients of Strain readings of S_1_1_C1. Pool size=132, Subgroup size = 4.

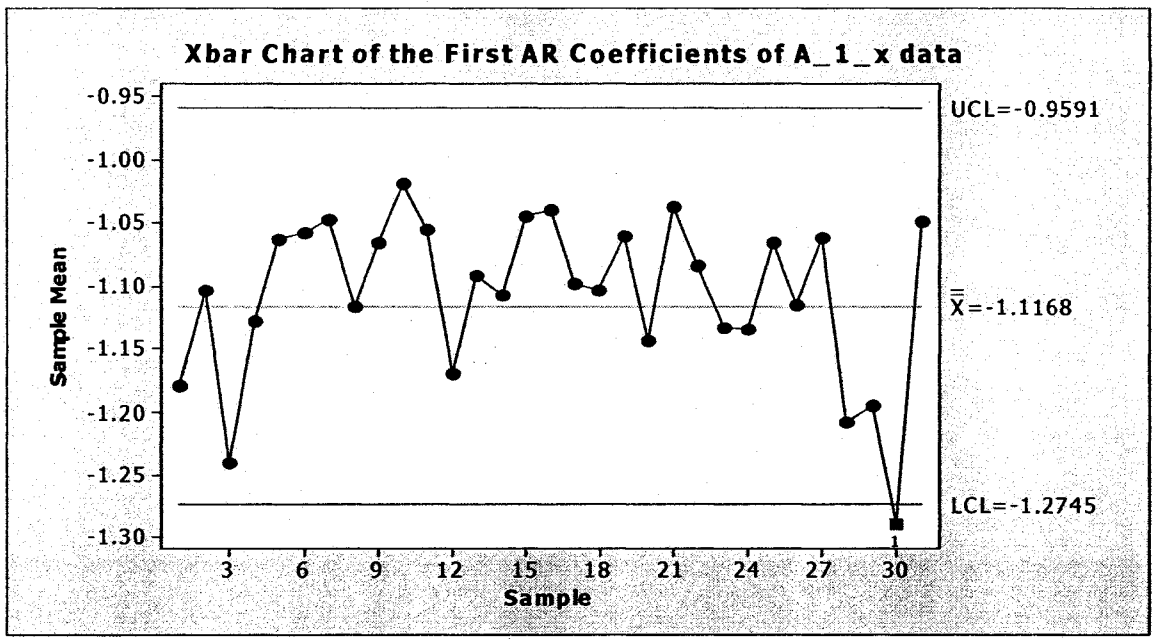

Fig 6.10: Outlier analysis of the First AR Coefficients of Accelometer readings of A_1_x. Pool size=124, Subgroup size = 4.

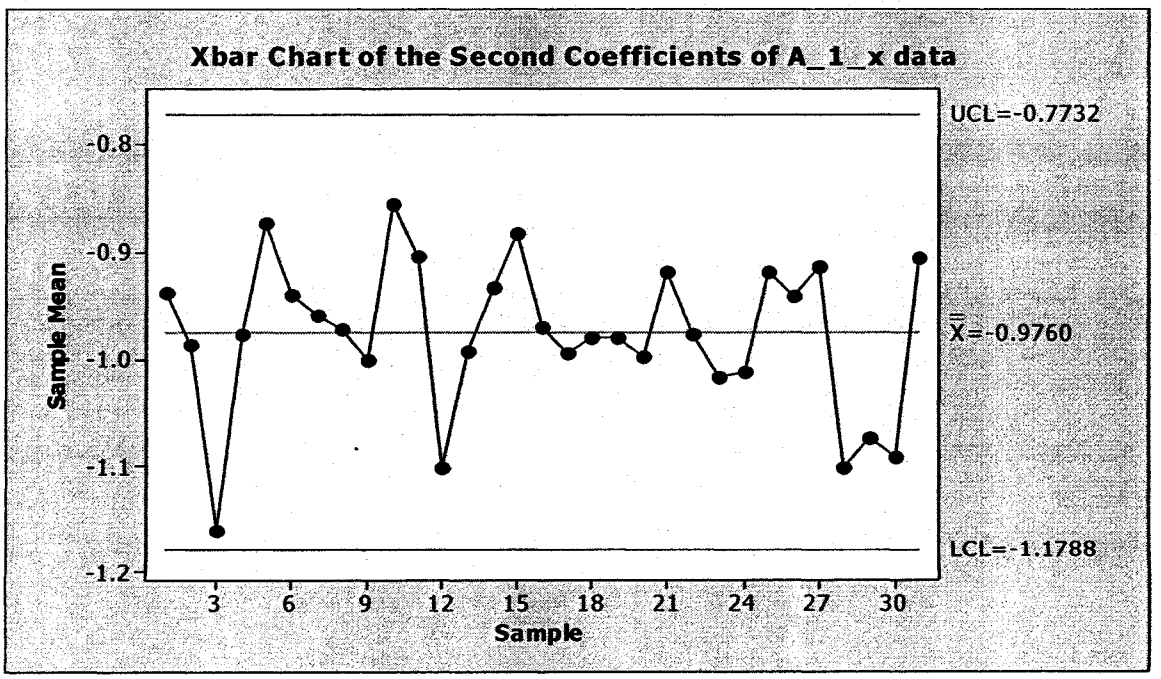

Fig 6.11: X-bar Control Chart of the Second AR Coefficients of Accelometer readings of A_1_x. Pool size=124, Subgroup size = 4.

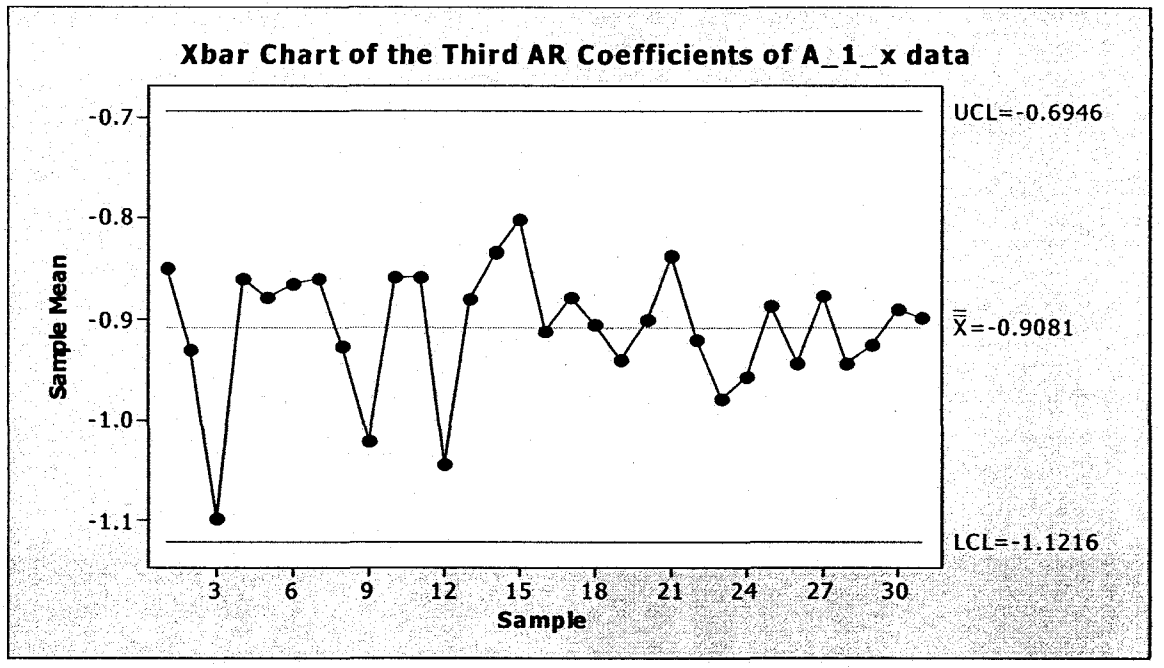

Fig 6.12: Outlier analysis of the third AR Coefficients of Accelometer readings of A_1_x. Pool size=124, Subgroup size = 4.

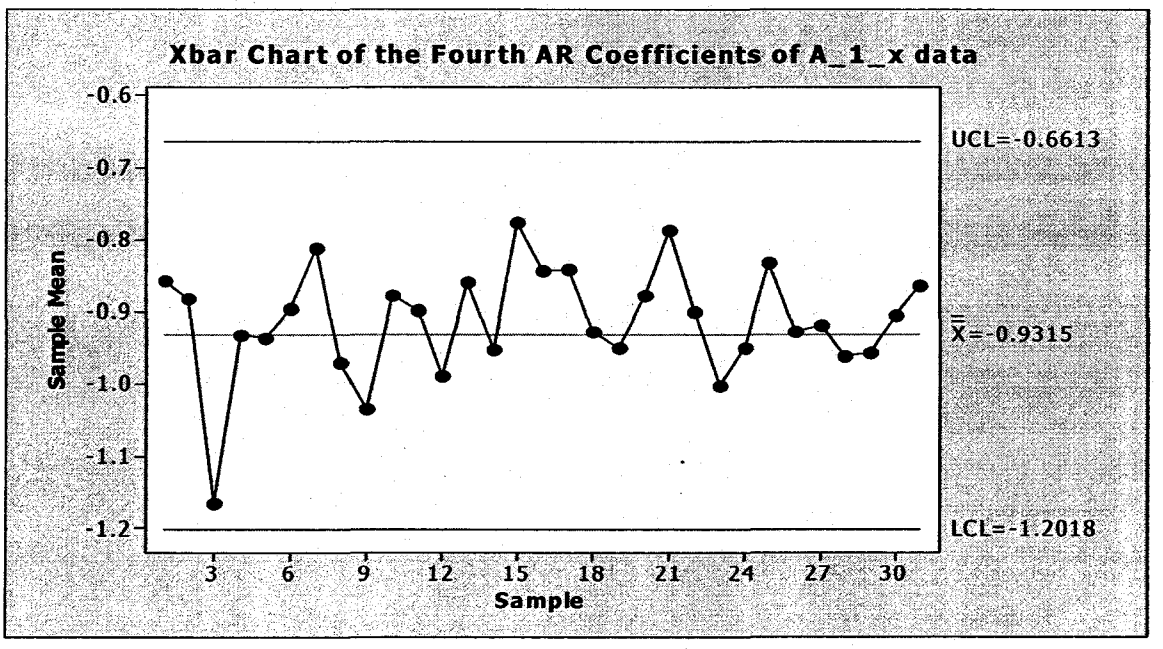

Fig 6.13: Outlier analysis of the Fourth AR Coefficients of Accelometer readings of A_1_x. Pool size=124, Subgroup size = 4.

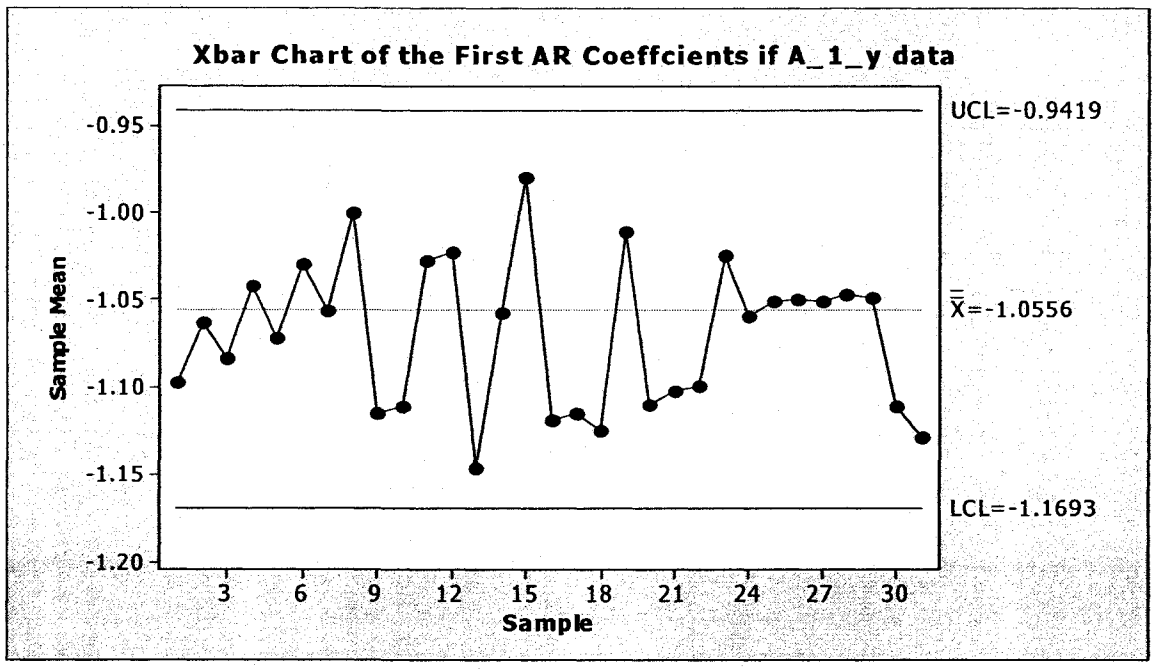

Fig 6.14: Outlier analysis of the First AR Coefficients of Accelometer readings of A_1_y. Pool size=124, Subgroup size = 4.

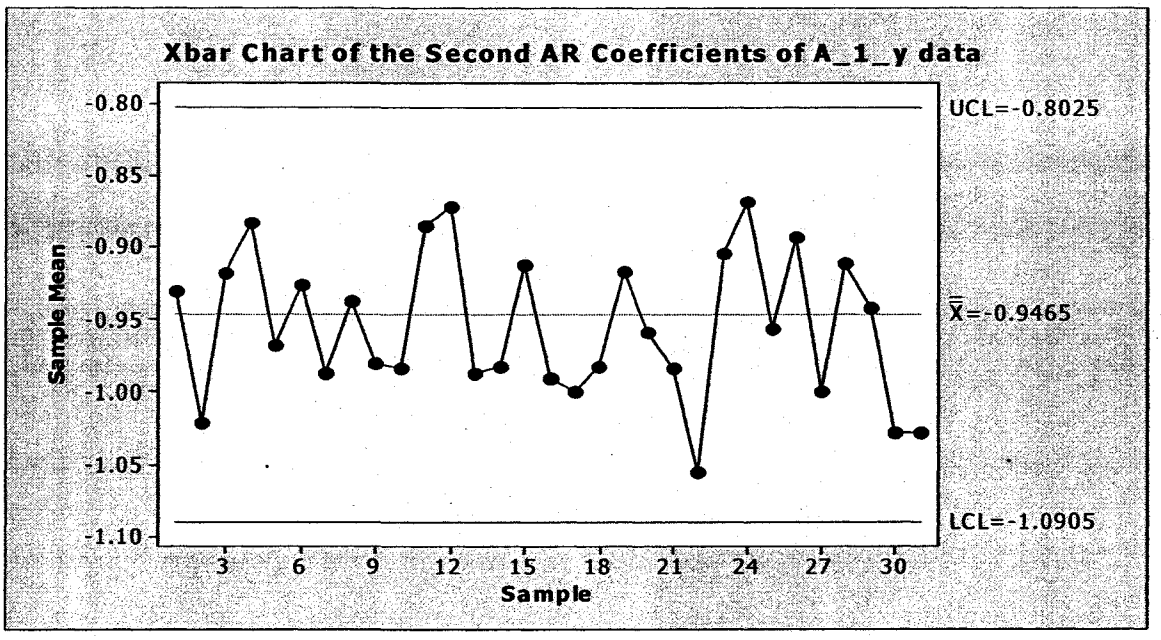

Fig 6.15: Outlier analysis of the Second AR Coefficients of Accelometer readings of A_1_y. Pool size=124, Subgroup size = 4.

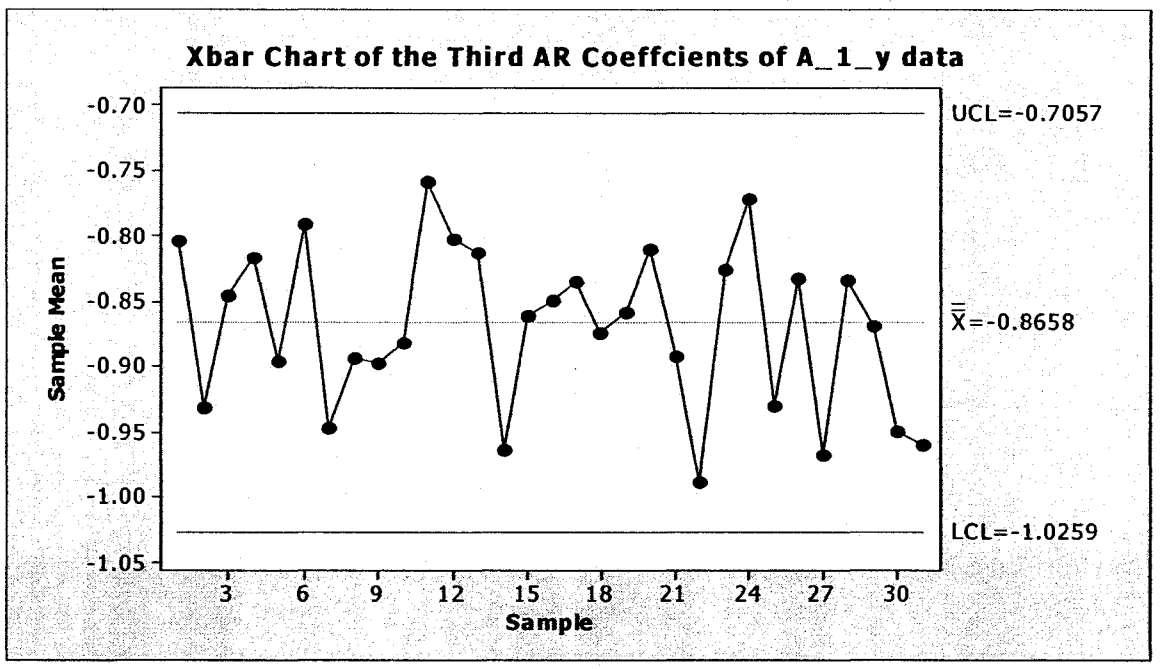

Fig 6.16: Outlier analysis of the third AR Coefficients of Accelometer readings of A_1_y. Pool size=124, Subgroup size = 4.

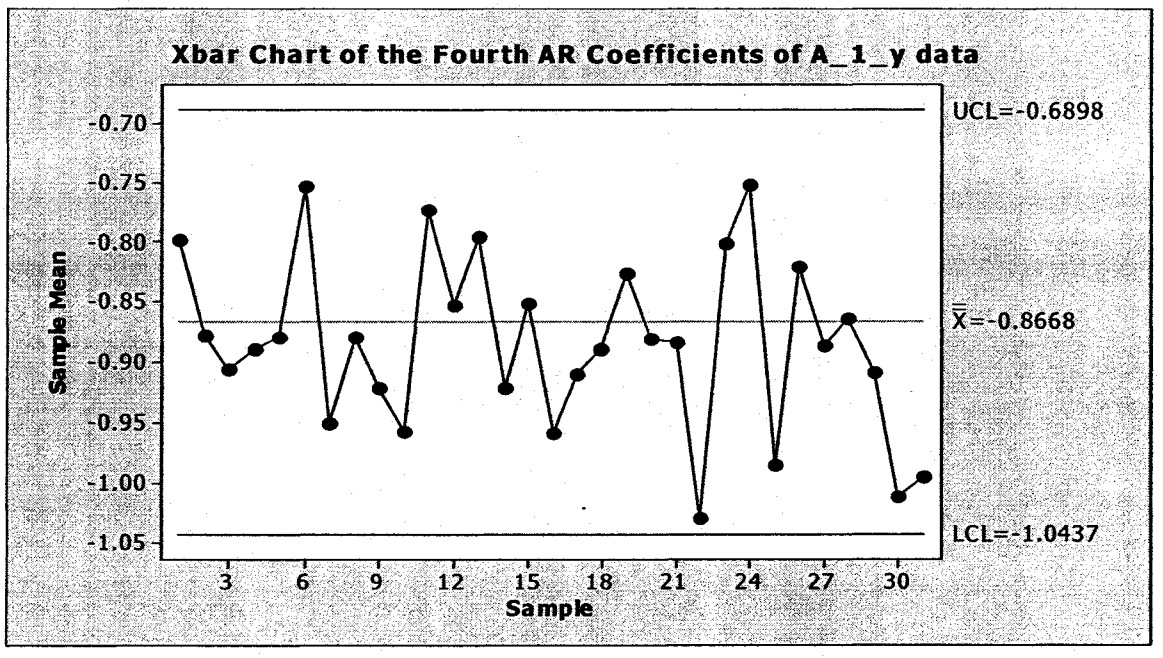

Fig 6.17: Outlier analysis of the Fourth AR Coefficients of Accelometer readings of A_1_y. Pool size=124, Subgroup size = 4

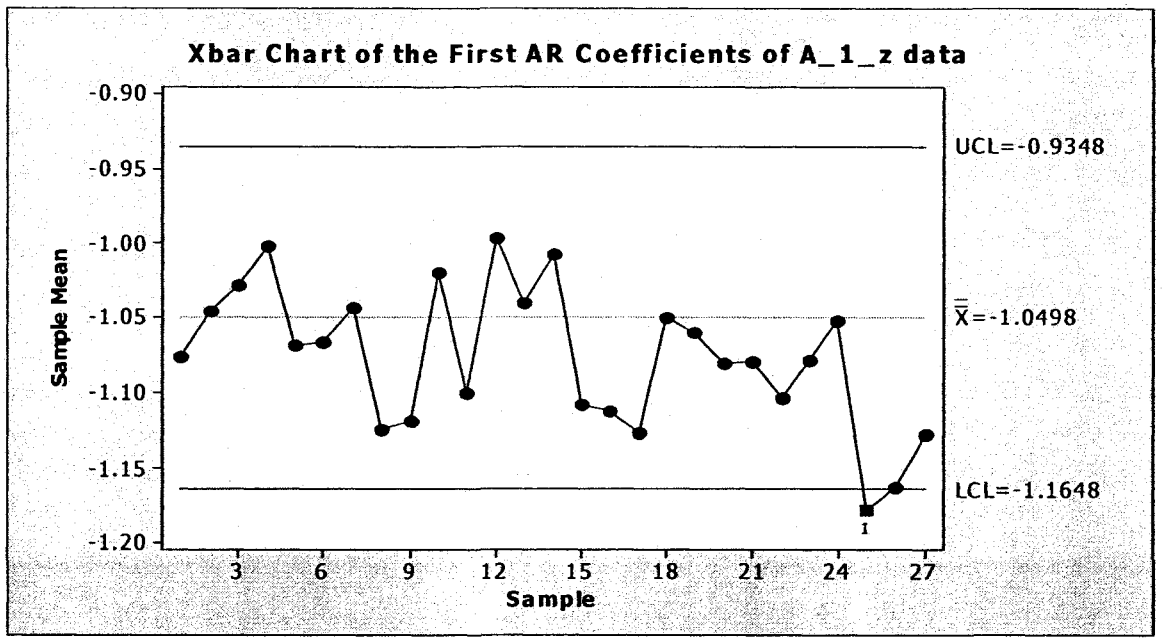

Fig 6.18: Outlier analysis of the First AR Coefficients of Accelometer readings of A_1_z. Pool size=108, Subgroup size = 4

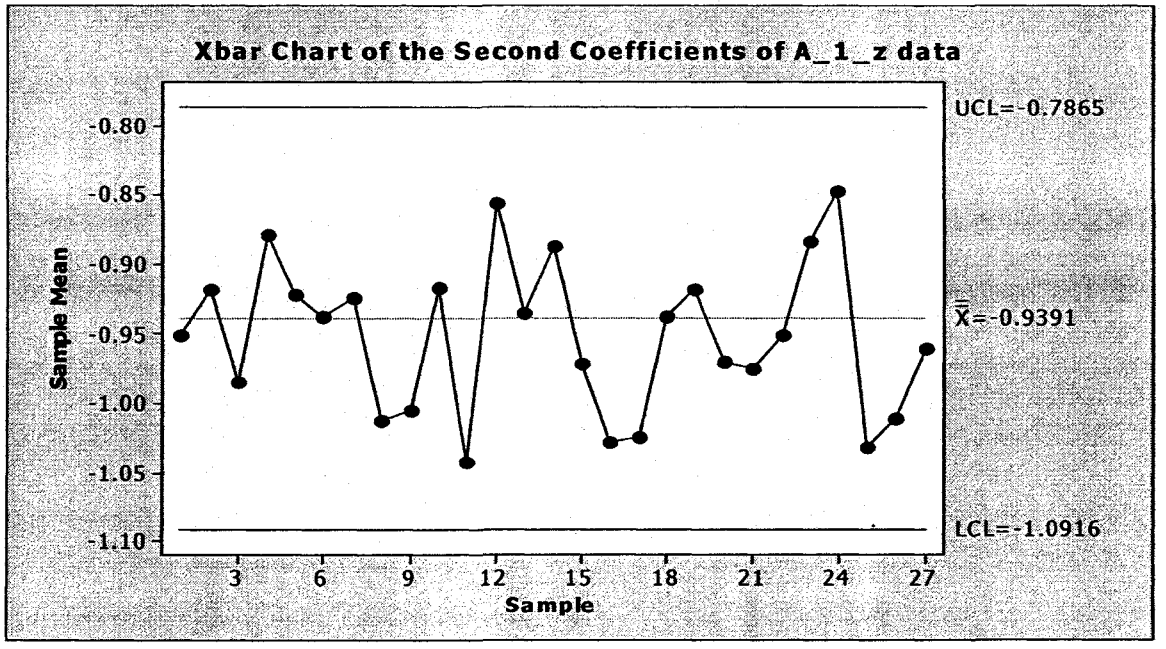

Fig 6.19: Outlier analysis of the Second AR Coefficients of Accelometer readings of A_1_z. Pool size=108, Subgroup size = 4

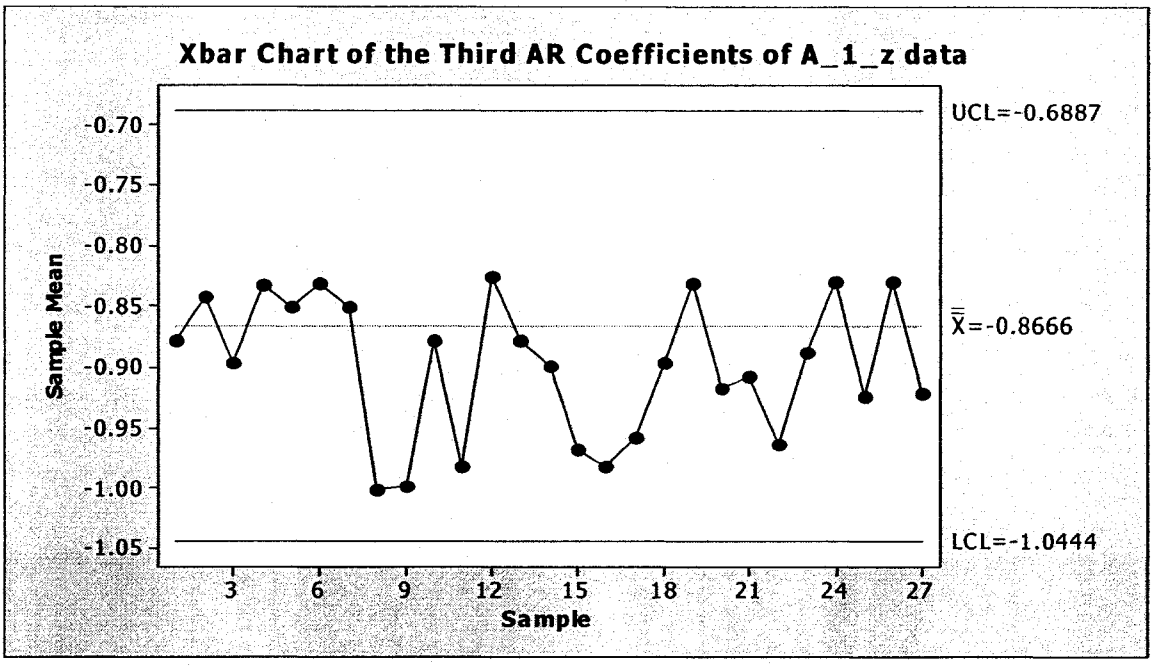

Fig 6.20: Outlier analysis of the third AR Coefficients of Accelometer readings of A_1_z. Pool size=108, Subgroup size = 4

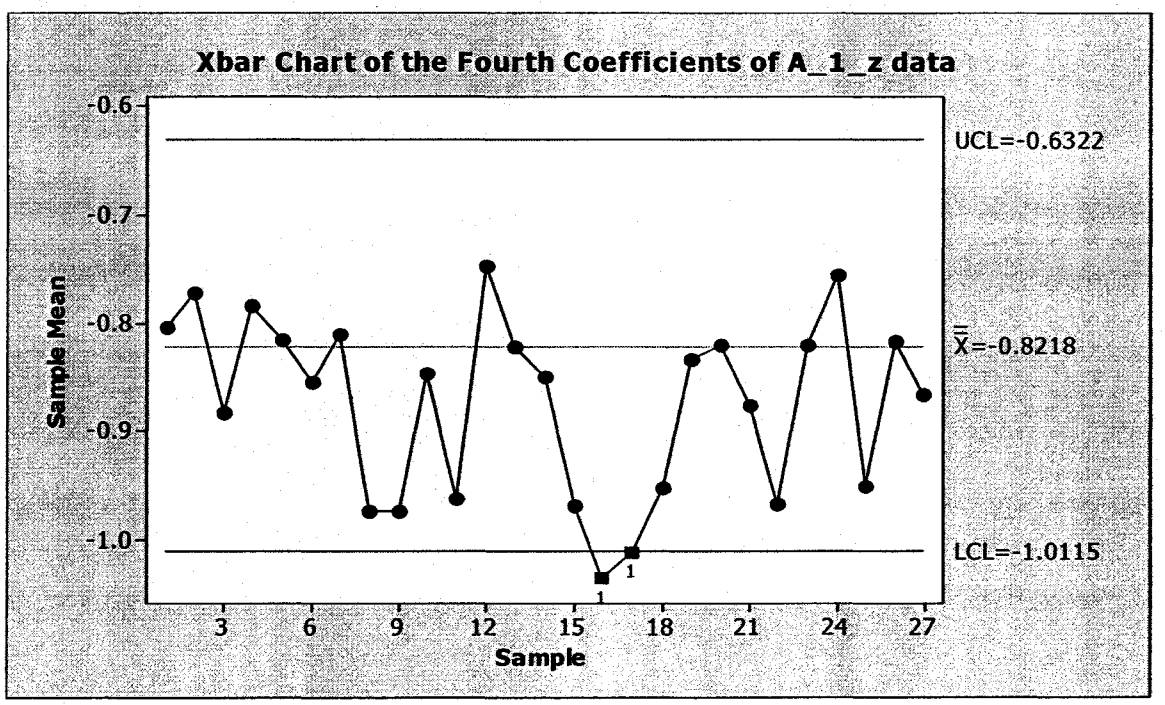

Fig 6.21: Outlier analysis of the fourth AR Coefficients of Accelometer readings of A_1_z. Pool size=108, Subgroup size = 4

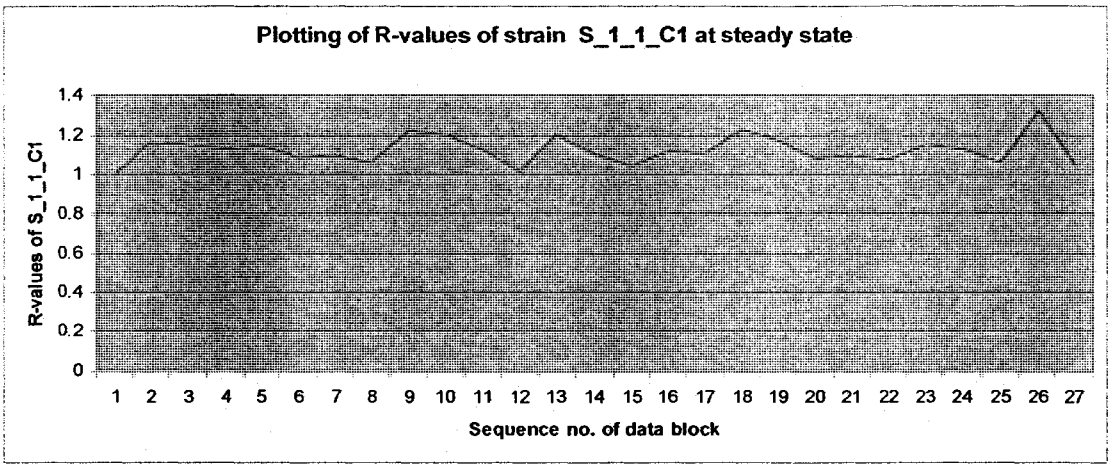

Fig 6.22: *R*-values of 27 data blocks of Strain S_1_1_C1 at Steady State Condition

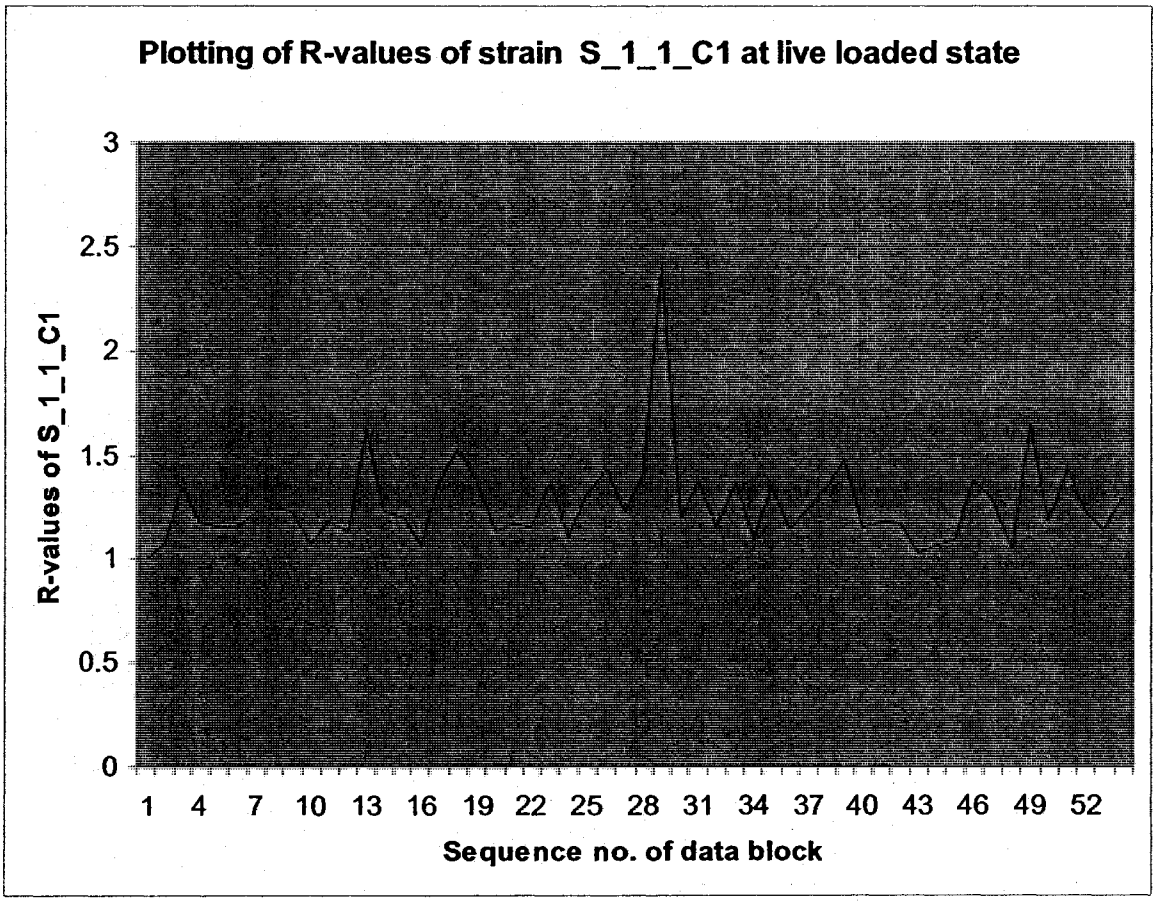

Fig-6.23: Plotting of *R*-values of Strain S_1_1_C1 for 55 live loaded occurrences on continuous scanning.

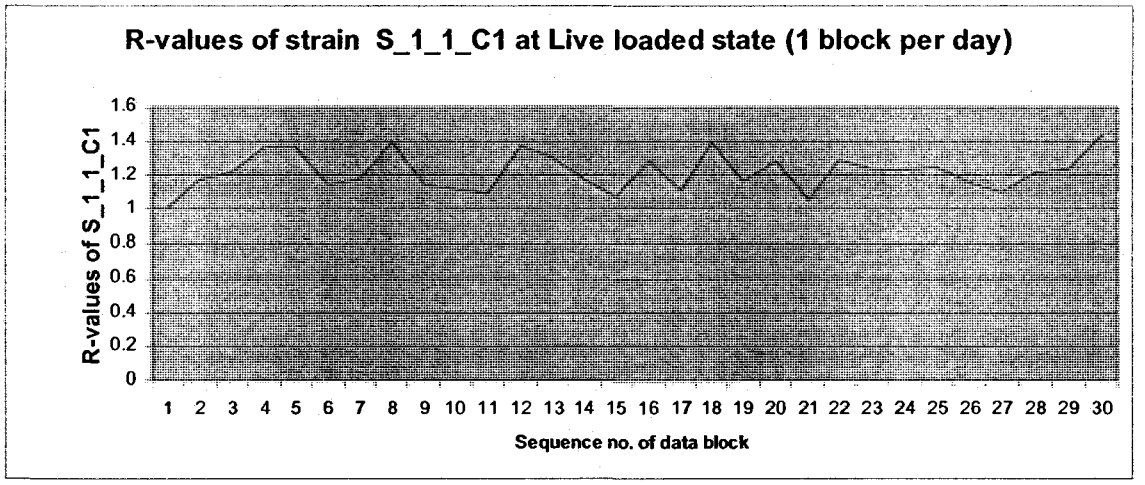

Fig-6.24: Plotting of *R*-values of 31 daily live loaded condition of Strain S_1_1_C1 at 1 data block per day.

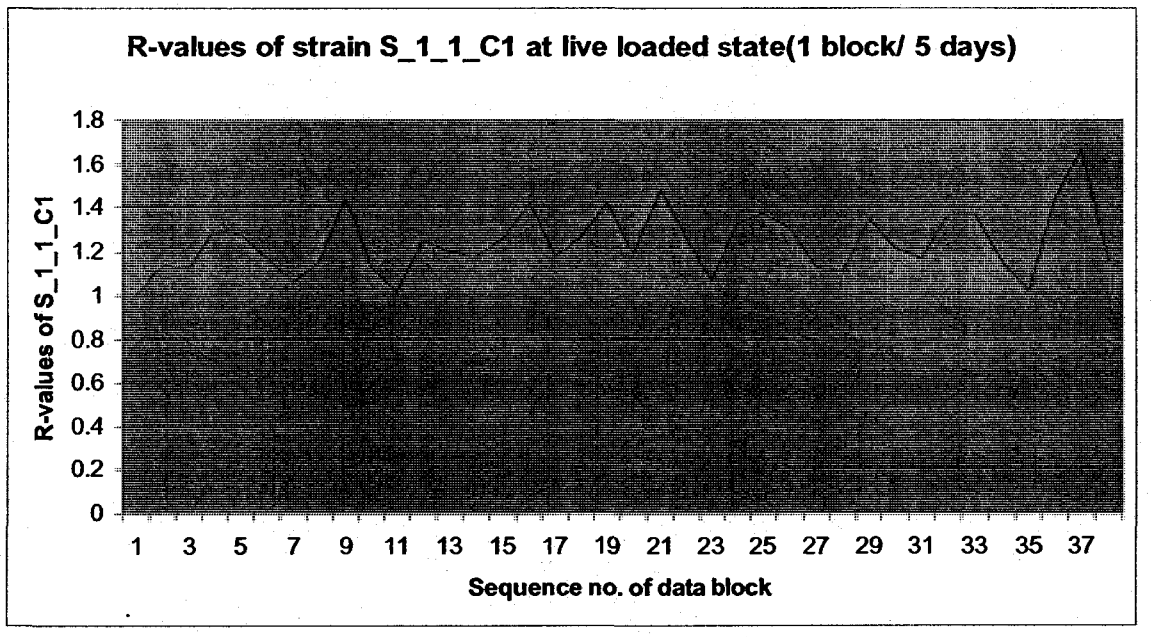

Fig-6.25: Plotting of *R*-values of 39 live loaded condition of Strain S_1_1_C1 on 5 days interval

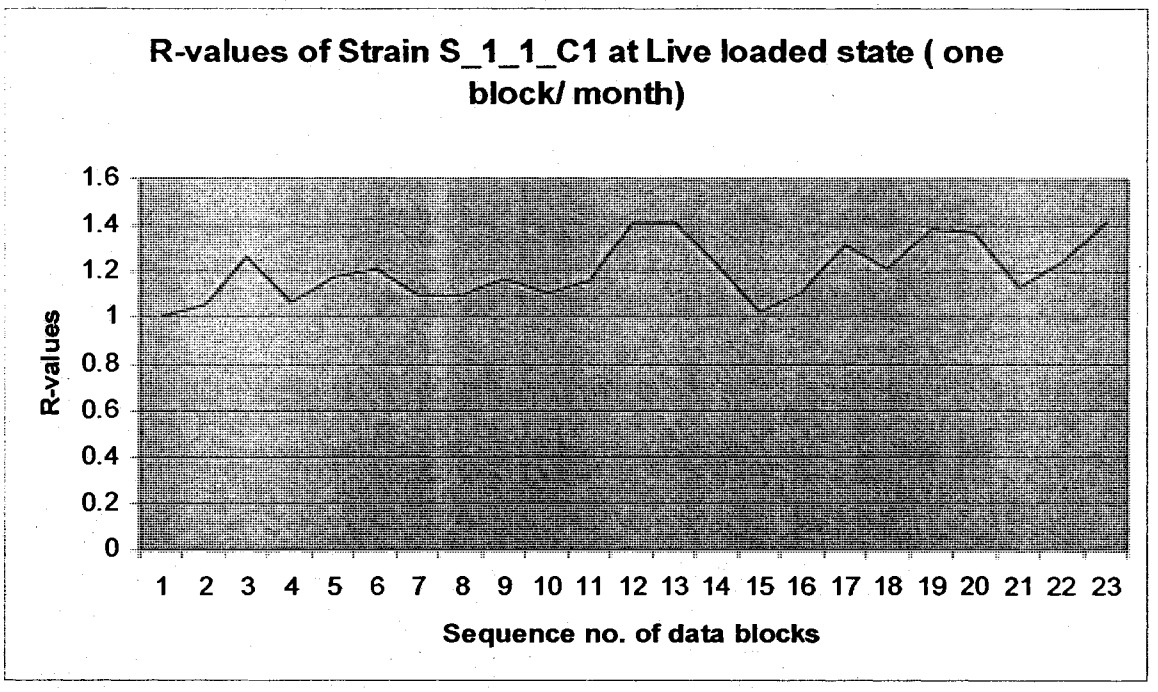

Fig-6.26: Plotting of R-values of 23 live loaded conditions of Strain S_1_1_C1 by monthly basis.

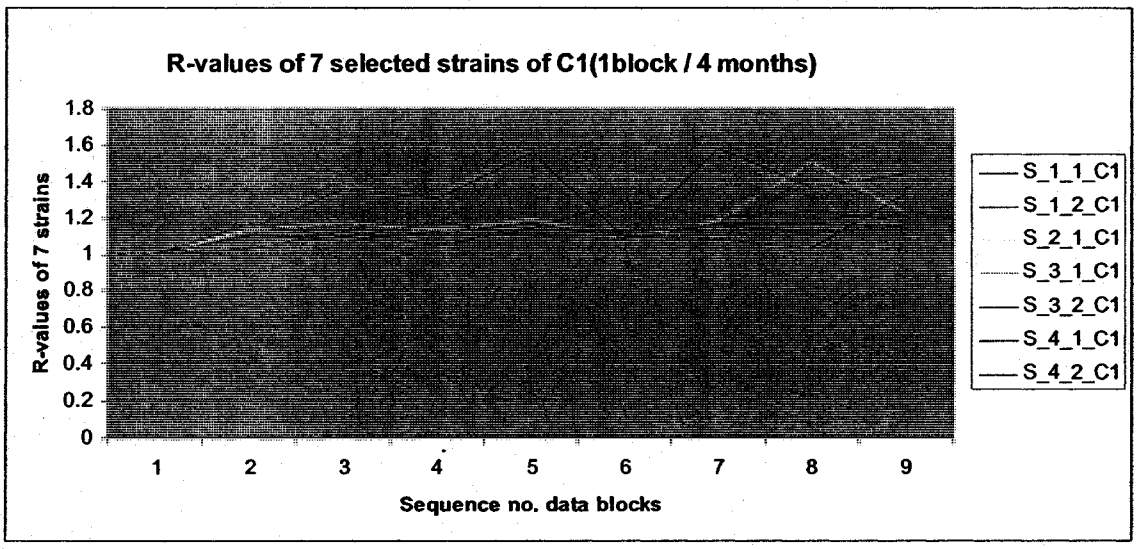

Fig-6.27: Plotting of R-values 7 selected strains of C1 at 9 live loaded conditions taken over the monitoring of the bridge

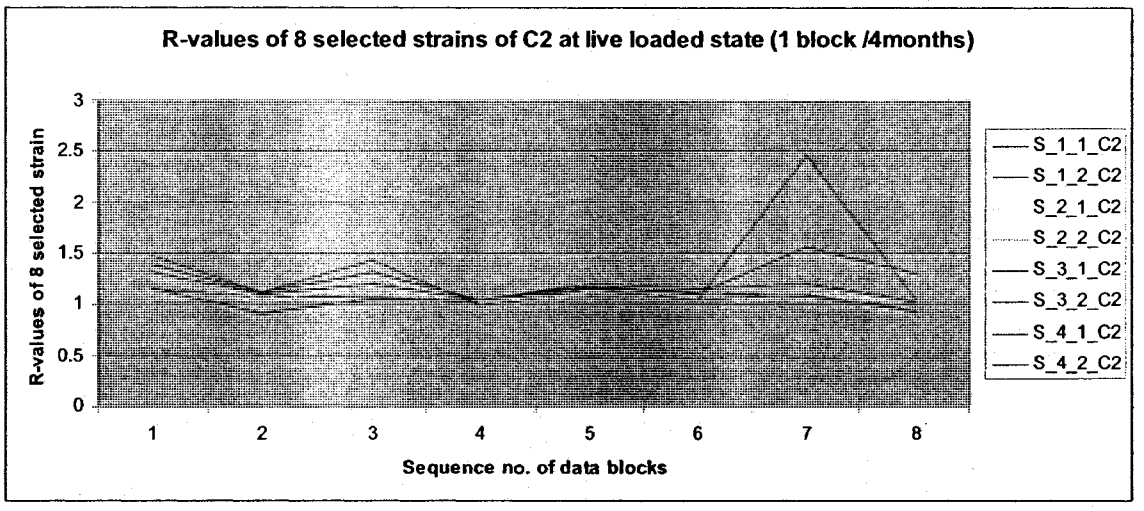

Fig-6.28: Plotting of R-values 8 selected strains of C2 at 9 live loaded conditions taken over the monitoring of the bridge

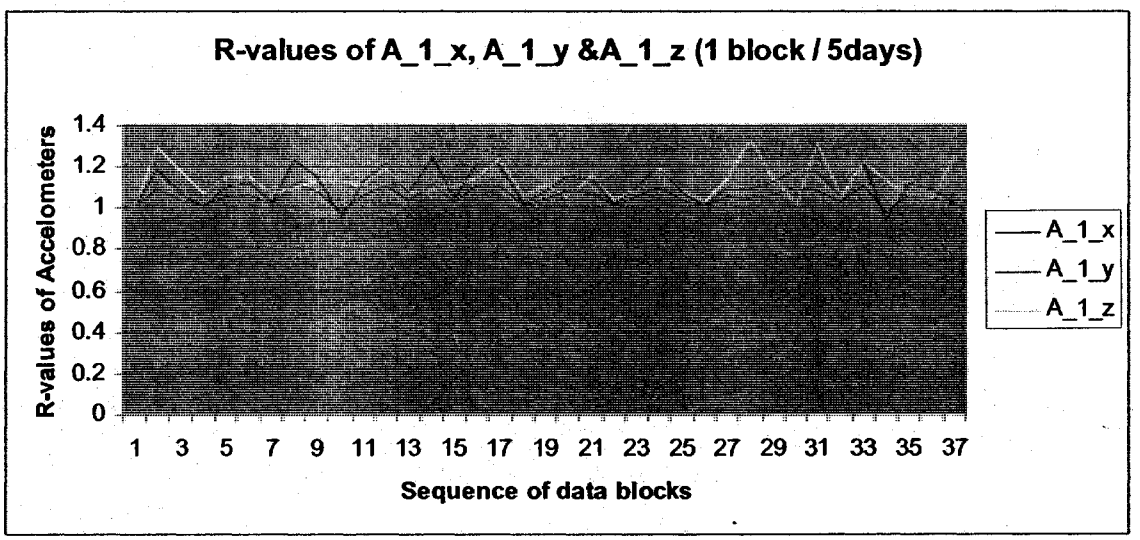

Fig-6.29: Plotting of *R*-values of 37 live loaded conditions of accelometer A_1_x, A_1_y and A_1_z (1 data block per 5days)

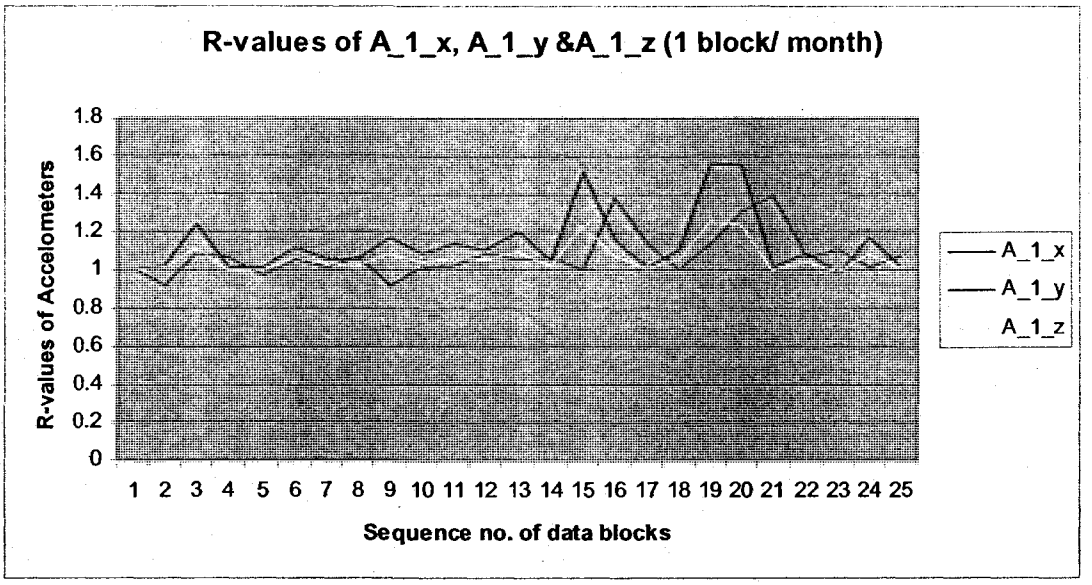

Fig 6.30: Plotting of *R*-values of 24 live loaded conditions of accelometer A_1_x, A_1_y and A_1_z (1 data block per month)

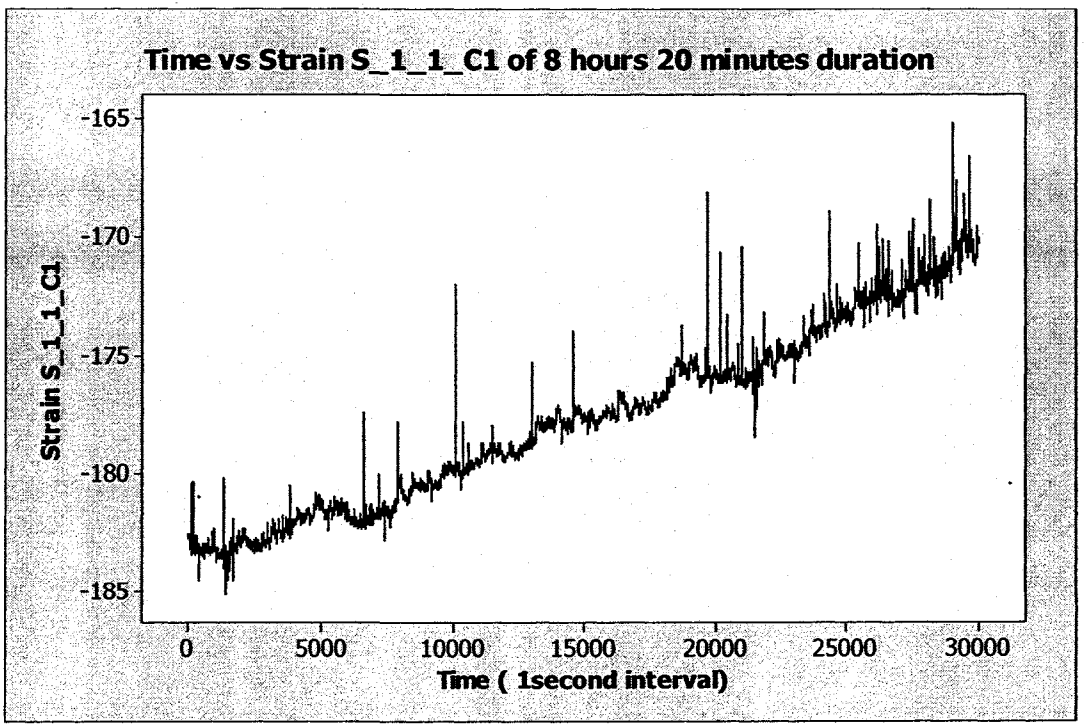

Fig-6.31: Graph of strain values of Strain S_1_1_C1 at 1second interval for 8 hours and 20 minutes at 0:0:0 time on 2006-03-01.

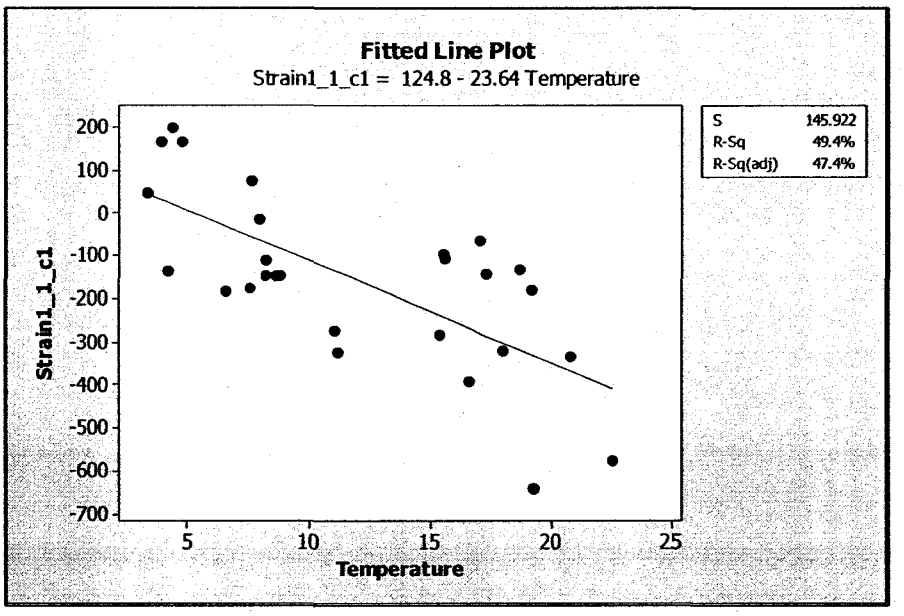

Fig-6.32: Overall Strain vs. Temperature relationship of Strain S_1_1_C1 taking 27 monthly readings

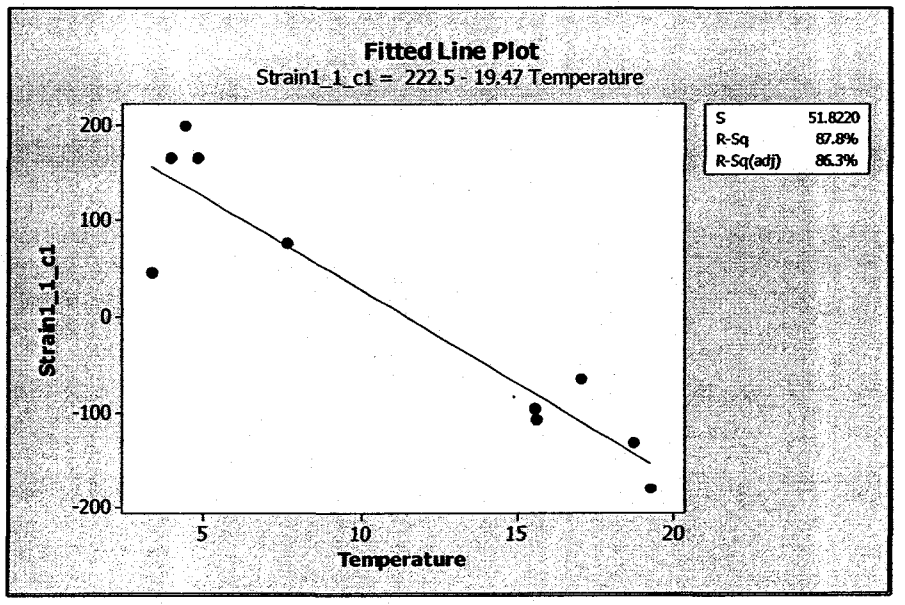

Fig-6.33: Strain vs. Temperature relationship of S_1_1_C1 taking first 10 monthly

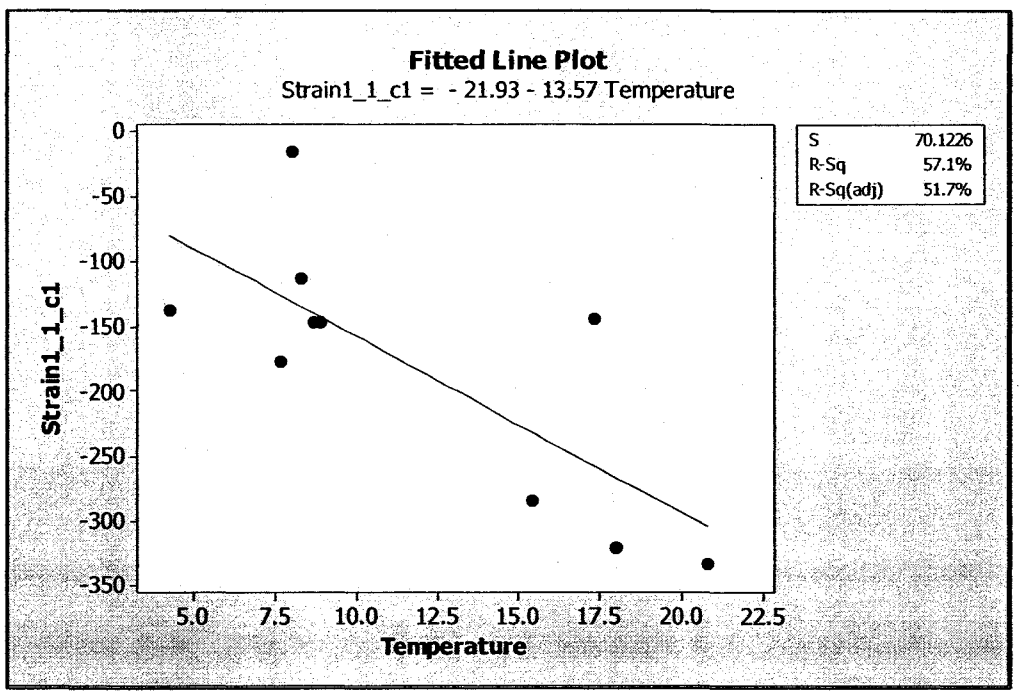

Fig 6.34: Strain vs. Temperature relationship of Strain S_1_1_C1, taking 11th to 20th monthly readings.

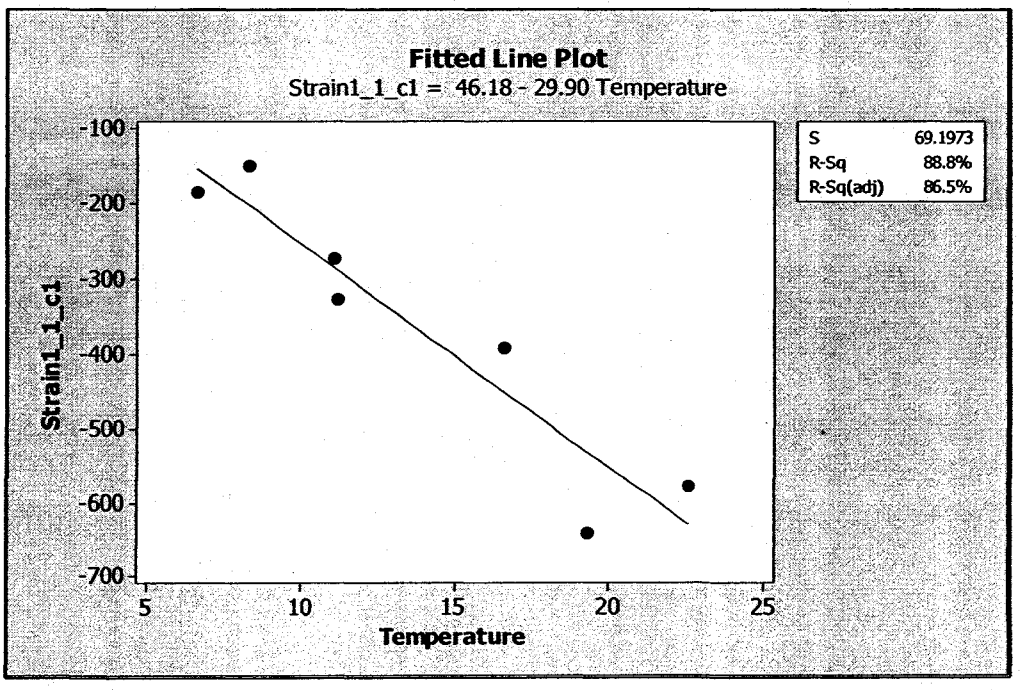

Fig-6.35: Strain vs Temperature relationship of S_1_1_C1 taking last 7 monthly readings

Chapter 7

Summary and Conclusions

7.1 Summary

The thesis has been organized in two parts: the first part deals with Vibration Based Damage Identification (VBDI) techniques by analyzing the dynamic characteristics of structures, and the other part is related to damage detection by statistical pattern recognition techniques. The work has been summarized in the following sections.

7.1.1 Vibration based damage identification by modal analysis

In the first part two structures, the Crowchild Bridge, and a 3D- Space Frame have been considered as the test articles. For generating FEM model of the structures and implementing the VBDI algorithms, the M-FEM software developed by Bagchi et al. (2007) has been used.

The bridge has been analyzed using its FEM model for different damage levels in the central elements of the deck for different damage scenario. Analysis has been performed in three conditions: the first, assuming no error in frequency and mode shapes and complete mode shapes; the second, assuming no error in frequencies and modes and incomplete mode shapes; and the third, assuming 1% error in frequencies and mode shapes and incomplete mode shapes. The entire process has been also repeated using

measured frequencies. Damage Index Method and Matrix Update Method have been utilized as damage detection algorithms.

The FEM model of the other test article, 3D Space Frame has been developed so that analytical frequencies are as close as possible to the measured frequencies. Then this model has been applied to detect damage by computer application. Various elements of the structure were tested at 50% and 80% simulated damage severity. Scenario includes both single and multiple element damage. Analysis was performed in two conditions: the first, assuming no error in frequency and mode shapes and complete mode shapes; and the second, assuming 2% error in frequencies and 10% error in modes shapes and incomplete mode shapes.

7.1.2 Structural damage detection by statistical method

The second part of the project involved the application of statistical process to damage detection of structure. Portage Creek Bridge in Victoria, BC, Canada has been selected as test article. The bridge has been monitored continuously by ISIS Canada Research Network (ISIS, 2008) for strain, vibration and temperature of the columns of its two piers for last four years.

Data have been collected following a particular sampling scheme as described in chapter 6. Strain S_1_1_C1 and Accelometer A_1_x, A_1_y and A_1_z were given the most attention.

Data blocks have been chosen for mainly two states: steady and live loaded state. Live loaded conditions have been scanned by visual inspection of the plotting of raw data. Also 6 more strains of C1 and 8 strains from C2 have been selected at large time intervals for testing the reliability of data S_1_1_C1. First the sampling approach for live loaded condition has been continuous, then gradually the interval has been increased to 1 day to 5 days for 8 months then 1 data block per month was taken until the end of the available data period for S_1_1_C1 and selected accelometer reading types.

All data blocks have been processed for the features that are sensitive to damage of the structures. For this purpose Auto Regressive model has been adopted for all blocks and the coefficients of AR models have been considered the damage sensitive features. Then the first four features of all data blocks of a particular measurement type, (for example, A_1_x) have been arranged in order of time to make feature pools. Each pool has been then analyzed for statistical modeling to classify damage. In this case outlier detection, which is appropriate form unsupervised condition, has been unitized. X-bar charts have been generated for every feature pool of a measurement type. From the result of X-bars, decision has been made of damage condition of the structure.

Statistical pattern recognition paradigm by pattern comparison: alternative method has been applied for damage detection. For comparison purpose, the first block of the series has been assigned as reference block for a particular measurement type. Then AR model of the reference model has been considered as the reference model. This model has been

tested on remaining testing blocks gradually. *R* (Residual Error Ratio) is considered the goodness of the fit of the reference block model to a test block.

Finally all the *R*-values of a particular measurement type have been plotted to see the trend and consistency of the structural condition. It is assumed for a healthy structure the trend should be horizontal and for damaged one, consistently upward. The slope of the curve should indicate the degradation rate.

7.2 Conclusions

- The results of the application of Damage Index Method and Matrix Update Method on the Crowchild Bridge indicate that both methods are fairly accurate in identification of the simulated damage when there is no or negligible amount of measurement noise in the frequencies and mode shapes. However, small amount of error in frequency and mode shape measurement may affect the accuracy of the damage detection.

- Damage detection scenario is a bit different in the case of the 3D Space Frame. Considering the error free modes, in most damage cases the process is able to identify the damage. However, in some cases only Damage Index Method is successful, whereas in other cases where it fails, the matrix update method seems to be successful. Therefore it is apparent that the combined result of two or more methods is useful for structural damage detection in practical cases.

- When error has been introduced to both frequencies and mode shape vectors, and incomplete mode shapes have been used, accuracy of the Matrix Update Method reduces. On the other hand, the damage index method produces somewhat better results in several damage cases.

- Apparently, the accuracy of the structural diagnosis by vibration-based damage detection algorithms such as Matrix Update Method and Damage Index Method seems to depend greatly on the following two factors: 1) accuracy of determination of frequencies and modal parameters, and 2) closeness of the numerical or FEM model to the real structure. The process demands fairly accurate measurement of modal parameters and determination of geometric and material properties of the structural members and their connectivity and support conditions as closely as possible.

- There are small discrepancies of measured and analytical frequencies in the finite elements models developed. Given the change of frequencies are not so sensitive to damage unless it is severe, these models still work fairly in error induced modes and incomplete mode shapes in the diagnosis of the structures, especially the Crowchild Bridge.

- Despite some lack of accuracy in of proposed VBDI methods in the cases of measurement error in frequency and mode shapes, they can still be very useful in detection of damage. In error induced cases, they can still indicate the possible

damage region if they cannot identify the exact elements. This information can be useful for other NDE methods. The results from various methods can be taken together to remove false positive results and improve the accuracy of VBDI methods. Also hybrid methods by combining VBDI and other methods such as statistical methods can provide promising improvement in diagnosis.

- Structural damage detection by statistical pattern recognition methods has been applied on the Portage Creek Bridge, Canada. From the source database, some measurement types have been selected for the experimentation. The AR process has been applied from derived data blocks to extract the AR coefficients which are then statistically modeled for damage classification by X-bars. From the X-bars of strain and vibration readings, percentages of outliers found are not so high to indicate any damage in the structure or prominent structural degradation, if any. However, a few cases suggest that the structure may be getting slightly degraded towards the end of the period considered, though it is still adequately safe.

- As an alternative approach, the pattern comparison method, based on fitting of the reference models to test blocks has been performed. Computed *R*-values that represent the goodness of fit do not show any trend or consistent discrepancies to indicate any damage in the structure. The sensors are also found to function properly by this method. Considering the age of the bridge there should not be any degradation too. The results of this method and the previous one have confirmed the structural health of the bridge to be at good state.

7.3 Recommendations on future research work

1) Since very low measurement error in modes shapes and frequencies can be allowed for the VBDI methods to work well, high accuracy is required in determining the modal parameters, which may not always be achievable. The other damage detection methods listed in Section- 3.4 should be tested. It is possible that fairly accurate diagnosis can be obtained even assuming higher percentages of error if combined results of several methods are considered together. By developing some screening process it can be possible to narrow down the number of possible candidates of damaged elements in the case of obscured diagnosis outputs.

2) The statistical pattern recognition method proposed here is found to be a good technique for classification of patterns of any sort. The recognition paradigms can be used on the output result by damage index or matrix update method as well. This technique should be useful in identifying structural damage more accurately from obscured outputs as compared to other algorithms.

3) The process of damage detection by statistical methods can be performed by entirely automated system without intermediate manual intervention. It can greatly save time, money and increase accuracy. This can be done by developing and integrating software tools for data acquisition and cleansing, scanning the entire data for relevant and interesting features, then performing feature extraction and modeling for damage classification and finally making the decision. Entire

system can be integrated through a computer network with the implementation of the applications on it. A research on integrated automated statistical pattern recognition system is a possible scope for future research.

4) In this work only unsupervised damage classification has been used since patterns of known damaged state are not available. By developing and applying a realistic FEM of the structure and appropriate programs, it is possible to generate patterns of strain and vibration data for various damage cases by computer simulation. These patters can be used as defined classes which can be used to develop supervised pattern recognition for the actual structure.

References

Aktan, A. E., C.J., Tsikos, C. J.,Cathbas, F.N., Grimmelsman, K. and British, R. 1999, Challenges and Opportunities in Bridge Health Monitoring, Proceedings of the 2nd International Workshop on Structural Health Monitoring, Stanford University, Stanford, CA September 8-10.

Aktan, A.E., Lee, K.L., Chuntavan, C., and Aksel, T. 1994. Modal testing for Structural identification and condition assessment of constructed facilities. Proceedings of the 12th International Modal Analysis Conference, Honolulu, H.I., pp. 462-468..

Allemang, R.J. 2002. The modal assurance criterion (MAC): twenty years of use and abuse. Proceedings of the 20th International Modal Analysis Conference, Los Angeles, Calif., pp. 397-405.

Allman D. J., 1984,A compatible triangular element including vertex rotations for plane elasticity analysis, Computers & Structures, 19(1-2):1-8.

Amin M., S., A., Z., 2002, An Integrated Vibration-Based Structural Health Monitoring System, Ph, D thesis submitted to Department of Civil and Environmental Engineering, Carleton University, Ottawa, Canada, March

Anderson, J., Pellionisz, A., and Rosenfeld, E., 1990, Neurocomputing 2: Directions for Research. Cambridge Mass.: MIT Press.

B&D Enterprises Inc., 2002, Brockwell, P., J. and Davis, R., A., Software *ITSM 2000, the Student Version 7.1,* http://www.stat.colostate.edu/~pjbrock

Bagchi, A., 2005, Updating the mathematical model of a structure using vibration data, *Journal of Vibration and Control,* 11(12): 1469-1486.

Bagchi, A., Humar, J. and Noman, A. 2007, Development of a Finite Element System for Vibration Based Damage Identification in Structures, *Journal of Applied Sciences,* 7(17): 2404-2413.

Batoz, J. L., 1982, an explicit formulation for an efficient triangular plate bending element, Int. J of Numerical Methods in Engineering,,18: 1077-1089.

Brockwell, P. J., and Davis, R. A., 2002 Introduction to Time Series and Forecasting. 2nd edition, Springer.

Casas, J.R. and Aparicio, A.C. 1994. Structural damage identification from dynamic-test data. Journal of Structural Engineering, ASCE, **120**(8): 2437-2450.

Catbas, F.N. and Aktan, A.E. 2002. Condition and damage assessment: issues and some promising indices. Journal of Structural Engineering, ASCE, 128(8): 1026-1036.

Cawaley, P. and Adams, R. D., 1979; The location of defects in structures from measurements natural frequencies, Journal of Strain Analysis 14(2): 49-57.

Chance, J., Tomlinson, G.R. and Worden, K. 1994. A simplified approach to the numerical and experimental modeling of the dynamics of a cracked beam. Proceedings of the 12th International Modal Analysis Conference, pp. 778-785.

Chang, F.K., ed. 1997. Structural Health Monitoring: Current Status and Perspectives. Proceedings of the 1st International Workshop on Structural Health Monitoring, Stanford, CA, Technomic Publishing Co., Lancaster, PA.

Chang, F.K., ed. 1999. Structural Health Monitoring 2000. Proceedings of the 2nd International Workshop on Structural Health Monitoring, Stanford, CA, Technomic Publishing Co., Lancaster, PA.

Chase, S.B. and Washer G. 1997. Non-destructive evaluation for bridge management in the next century. Public Road, 61 (1), Available from http://www.tfhrc.gov/pubrds/july97/ndejuly.htm.

Chen, S.E., Venkatappa, S., Petro, S. and GangaRao, H. 1999. Damage detection using 2-D strain energy distribution and scanning laser. Proceedings of the 17th International Modal Analysis Conference, pp. 869-875.

Cheng, J.J.R., and Afhami, S., 1999; Field Instrumentation and Monitoring of Crowchild Bridge in Calgary, Alberta, University of Alberta Report for ISIS Canada. Nov. 1999.

CINDE 2008, Canadian Institute for Non Destruction Evaluation http://www.cinde.ca/ndt.shtml.

COSMOS / M: User Guide Version 1.75 1995, Structural Research and Analysis Corporation

Doebling, S.W., Farrar, C.R., and Prime, M.B. 1998. A summary review of vibration based damage identification methods. Shock Vibration Digest, 30(2): 91-105.

Doebling, S.W., Farrar, C.R., Prime, M.B., and Shevitz, D.W. 1996. Damage identification and health monitoring of structural and mechanical systems from changes in their vibration characteristics: a literature review. Reprot No. LA 13070- MS, Los Alamos National Laboratory, Los Alamos, NM.

Ewins, D.J. 2000. Model Testing: Theory, Practice and Applications. 2nd Edition, Research Studies Press Ltd., Hertfordshire, England.

Fares, N. and Maloof, R. 1997. A probabilistic framework for detecting and identifying anomalies. Probability Engineering Mechcanics, **12**(2):63-73.

Farrar, A. R., Sohn, H, Fugate, M. L., Czarnecki, J. J., 2001; Integrated structural health monitoring, SPIE's 8th Annual International Symposium on Smart Structures and Materials, Newport Beach, CA, March 4-8..

Farrar, C. R., Duffey, T. A., Doebling, S. W., and Nix D. A., 1999; A Statistical Pattern Recognition Paradigm for Vibration-Based Structural Health Monitoring, the 2nd International Workshop on Structural Health Monitoring Stanford, CA Sept 8-10,

Farrar, C.R, Baker, W.E., Bell, T.M., Cone, K.M., Darling, T.W., Duffey, T.A., Eklund A., and Migliori, A. 1994. Dynamic Characterization and Damage Detection in the I-40 Bridge Over the Rio Grande. Report No. LA 12767-MS, Los Alamos National Laboratory, Los Alamos, NM.

Farrar, C.R. and Duffey, T.A. 1999. Vibration-based damage detection in rotating machinery. Key Engineering Materials, 167-168: 224-235.

Federal Highway Administration (FHWA). 2001. Reliability of visual inspection. Report Nos. FHWA-RD-01-020 and FHWA-RD-01-021, Washington, DC

Fox, C.H.J. 1992. The location of defects in structures: a comparison of the use of natural frequency and mode shape data. Proceedings of the10th international Modal Analysis Conference, San Diego, California, pp. 522-528.

Friswell, M.I. and Mottershead, J.E., 1995; Finite Element Model Updating in Structural Dynamics, Kluwer Academic Publishers, Norwell,, MA,

Fugate, M. L., Sohn, H., and Farrar, C. R., 2000, Vibration-Based Damage Detection using Statistical Process Control, *accepted for publication of Mechanical Systems and Signal Processing*, Academic Press, London, UK.

Guyan, R.J., 1965; Reduction of Stiffness and Mass Matrices, AIAA Journal,3(2): 380.

Hajela, P. and Soeiro, F.J. 1990. Recent developments in damage detection based on system identification methods. Structural Optimization, 2(1): 1-10.

Hu, N., Wang, X., Fukunaga, H., Yao, Z.H., Zhang, H.X., and Wu, Z.S. 2001. Damage assessment of structures using modal test data. International Journal of Solid Structure, **38**(18): 3111-3126.

Huffman S., Bagchi, A., Mufti, A., Neale, K., Sargent, D., and Rivera, E., 2006, GFRP Seismic strengthening and structural health monitoring of Portage Creek Bridge Concrete Columsn, *The Arabian Journal for Science and Engineering, Volume 31, Number 1C.*

Humar. J., Bagchi, A., and Xu, H., 2006, Performance of vibration based techniques for the Identification of Structural Damage, *Structural Health Monitoring – An International Journal,* 5(3): 215-227.

Hunt, D.L., Weiss, S.P., West, W.M., Dunlap, T.A., and Freemeyer, S.R. 1990. Development and implementation of a shuttle modal inspection system. Sound and Vibration, 24(8): 34-42.

Hurvich C. M., and Tsai C. I., 1999, Regression and time series model selection in wall samples, Biometrika, 76: 297-307.

ISIS, 2008, Intelligent Sensing for Innovative Structures, A Network of Centres of Excellence, www.isiscanada.com, University of Manitoba, Winnipeg, Canada.

Jain, A. K., Duin, R. P. W., and Mao, J., 2000; Statistical Pattern Recognition: A Review, 4 IEEE Transactions on pattern analysis and machine Intelligence, vol. 22, no.1, Jan 2000.

Jain, A.K., Mao, J., and Mohiuddin, 1996; K. M., Artificial Neural Networks: A Tutorial, Computer, pp. 31-44, Mar. 1996.

Jauregui, D.V. and Farrar, C.R. 1996. Comparison of damage identification algorithms on experimental modal data from a bridge. Proceedings of the 14th International Modal Analysis Conference, Dearborn, MI, pp. 1423-1429.

Kabe, A. M., 1985; Stiffness Matirx Adjustment Using Mode Data, ALAA Journal, vol. 23No. 9, 1985.

Kaouk, Mohamed, and Zimmerman, D.C. 1994, Structural Damage Assessment using a Generalized Minimum Rank Perturbation Theory, *AIAA Journal*, 32(4), 836-842.

Kim, J.T. and Stubbs, N. 1995. Model uncertainty impact and damage-detection accuracy in plate girder. Journal of Structural Engineering, ASCE, **121**(10): 1409-1417.

Kim, J.T. and Stubbs, N. 2003. Non-destructive crack detection algorithm for full-scale bridges. Journal of Structural Engineering, ASCE, 129(10): 1358-1366.

Kohonen, T., 1995; Self-Organizing Maps. Springer Series in Information Sciences, vol. 30, Berlin.

Leung, Y. –T., 1978; An accurate method of dynamic condensation in structural analysis, International Journal of Numerical Methods in Engineering, 12: 1705- 1715.

Loland, O. and Dodds, J.C. 1976. Experience in developing and operating integrity monitoring system in North Sea. Proceedings of the 8th Annual Offshore Technology Conference, pp. 313-319.

Masri, S.F., Smyth, A.W., Chassiakos, A.G., Caughey, T.K., and Hunter, N.F,.2000.Application of neural networks for detection of changes in nonlinear systems. Journal of Engineering Mechanics, ASCE, **126**(7): 666-676.

MATLAB 1999, User Guide, Mathworks Inc., Natick, MA,

Miller C.A., 1980; Dynamic reduction in structural models, Journal of Structural Engineering, ASCE, 106(ST10): 2097-2108.

Mita A., and Qian Y., Y., 2006; Qualitative and quantitative damage detection algorithm for structures using pattern classification and sensitivity anlysis, Structural Health Monitoring and Intelligent Infrastructure-Qu, Li &Duan, Taylor &Francis Group, London.

Montgomery, D. C., 1997, Introduction *to Statistical Quality Control*, John Wiley & Sons Inc, New York, NY.

Montgomery D. C., Jennings C. L., and Kulahci M., 2008, *Introduction to Time Series Analysis and Forecasting* John Wiley & Sons Inc, New York, NY.

Mufti, A.A. 2001. Guidelines for Structural Health Monitoring. ISIS Canada (The Canadian Network of Centres on Intelligent Sensing for Innovative Structures), Design Manual No.2, Sept. 2001.

Nair, K., K., and Kiremidjian A., S., 2006, A comparison of local damage detection algorithms based on statistical processinh of vibration based measurements, Structural Health Monitoring and Intelligent Infrastructure-Qu, Li &Duan, Taylor &Francis Group, London.

Nasser, H., Mevel, L. and Chapelle, D. 2005. Damage detection under environmental perturbation. Proceedings of the 23rd International Modal Analysis Conference, Orlando, Florida, Paper No. 114, (CD-ROM).

O'Callahan, J., Avitabile, P., Riemer, R., 1989. System Equivalent Reduction Expansion Process (SEREP). *7th International Modal Analysis Conference*, Las Vegas, Nevada, 29-37.

Pandey, A.K., Biswas, M., and Samman, M.M. 1991. Damage detection from changes in curvature mode shapes. Journal of Sound Vibration, 145(2): 321-332.

Peeters, B. 2000. System identification and damage detection in civil engineering. Ph.D thesis, Dept. of Civ. Engrg., Katholieke Universiteit Leuven, Belgium.

Ripley, B., 1993; Statistical Aspects of Neural Networks, Networks on Chaos: Statistical and Probabilistic Aspects. U. Bornndorff-Nielsen, J. Jensen, and W. Kendal, eds., Chapman and Hall.

Rytter, A. 1993. Vibration-based inspection of civil engineering structures. Doctoral Dissertation, Department of Building Technology and Structural Engineering, University of Aalborg, Aalborg, Denmark.

Salawu, O.S. 1997. Detection of structural damage through changes in frequency: a review. Engineering Structures, 19(9): 718-723.

Salawu, O.S. and Williams, C. 1995. Bridge assessment using forced-vibration testing.Journal of structural engineering, **121**(2): 161-173.

Shives, T.R. and Mertaugh, L.J. eds. 1986. Detection, diagnosis and prognosis of rotating machinery to improve reliability, maintainability, and readiness through the application of new and innovative techniques. Cambridge University Press, Cambridge, UK.

Sohn, H., Czarneck, J. J., and Farrar, C. R., 2000; Structural Health Monitoring using Statistical Process Control, *Journal of Structural Engineering, ASCE*, 126(11):1356-1363.

Sohn, H., Farrar, C. R., Hunter N. F., and Worden, K., 2001; Structural Health Monitoring Using Statistical Pattern Recognition Techniques, Transactions of the ASME, Vol. 123.

Srinivasan, M.G. and Kot, C.A. 1992. Effects of damage on the modal parameters of a cylindrical shell. Proceedings of the 10th International Modal Analysis Conference, San Diego, Calif., pp. 529-535.

Stubbs, N. and Kim, J. T., 1994; Field verification of a non-destructive damage localization and severity estimation algorithm, Texas A&M University Report prepared for New Mexico State University.

Stubbs, N., Kim, J.-T., and Farrar, C.R., 1995; Field Verification of a Non-destructive Int. J of Numerical Methods in Engineering,18:1077-1089, 1982.

Stubbs, N., Kim, J.T., and Topple, K. 1992. An effect and robust algorithm for damage localization I offshore platforms. Proceedings of ASCE 10th Structural Congress, San Antonio, Texas, pp. 543-546.

Taha, M., M., R., and Lucero, J., 2005; Damage identification for structural health monitoring using fuzzy pattern recognition, Engineering Structures, 27(12): 1774-1783

Toksoy, T. and Aktan, A.E. 1994. Bridge-condition assessment by modal flexibility Experimental Mechanics, 34(3): 271-278.

Ventura, C.E., Brincker, R., Andersen, P., and Cantieni, R. 2002. Identification and damage detection studies of the Z24 highway bridge in Switzerland. Proceedings of the 6th International Conference on Short and Medium-span Bridges, Vancouver, Canada, pp 851-858.

Ventura, C.E., Onur, T., and Tsai, R.C., 2000; Dynamic characteristics of the Crowchild Trail Bridge, Can J of Civil Eng., 27:.1046-1056.

West, W.M. Jr. 1984. Single point random model test technology application to failure detection. Shock and Vibration Bulletin, May, pp. 25-31.

Wu, X., Ghaboussi, J. and Garrett, J.H. Jr. 1992. Use of neural networks in detection of structural damage. Computation Structure, **42**(4): 649-659. Zhang, Z. and Aktan, A.E. 1995. The damage indices for constructed facilities. Proceedings of the 13th International Modal Analysis Conference, Nashville, TN, pp. 1520-1529.

Zhang, Z. and Aktan, A.E. 1998. Application of modal flexibility and its derivatives in structural identification. Research of Non-destructive Evaluation, 10(1): 43-61.

Zhou, Z., 2006; Vibration-Based Damage Detection of Simple Bridge Superstructures, Ph. D, Thesis, Department of Civil and Geological Engineering University of Saskatchewan, Saskatoon.

Zienkiewicz, O.C. and Taylor, R.L., 1989; The Finite Element Method, Vol 1 and 2, Fourth Edition, McGraw Hill, UK.

Zimmerman, D.C. and Kaouk, M. 1992. Structural damage detection using a Subspace rotation algorithm. Proceedings of the AIAA/ASME/ASCE/AHS/ASC, 33rd structures structural dynamics and materials conference, Dallas, Texas, pp. 2341-2350.

Zimmerman, D.C. and Smith, S.W. 1992. Model refinement and damage location for intelligent structures. Intelligent structural systems. H.S. Tzou and G.L. Anderson, eds., Boston: Kluwer Academic Publishers. pp. 403-452.

Appendix A

A.1 Graphical output of VBDI case study on the Crowchild Bridge

In Appendix A, figures showing the graphical output by Damage Index and Matrix Update methods applied on the Crowchild Bridge are presented. The cases are defined in section 5.4.2.

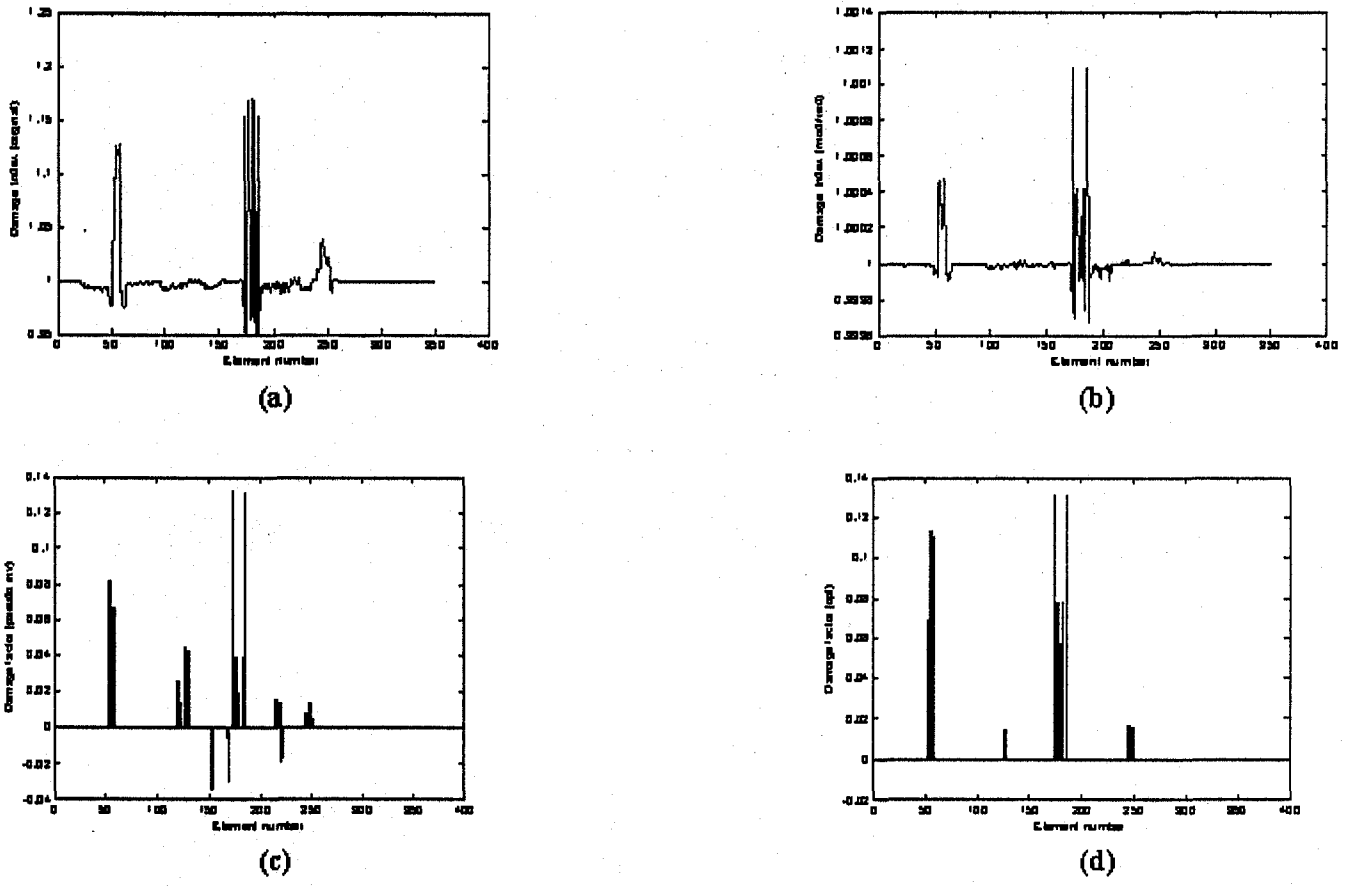

Fig A.1: Graphs showing damage with element numbers for no error and complete modes with 10% damage severity by Damage Index Method **(a)** original and **(b)** modified; by Matrix Update Method **(c)** Pseudo Inverse **(d)** Optimized

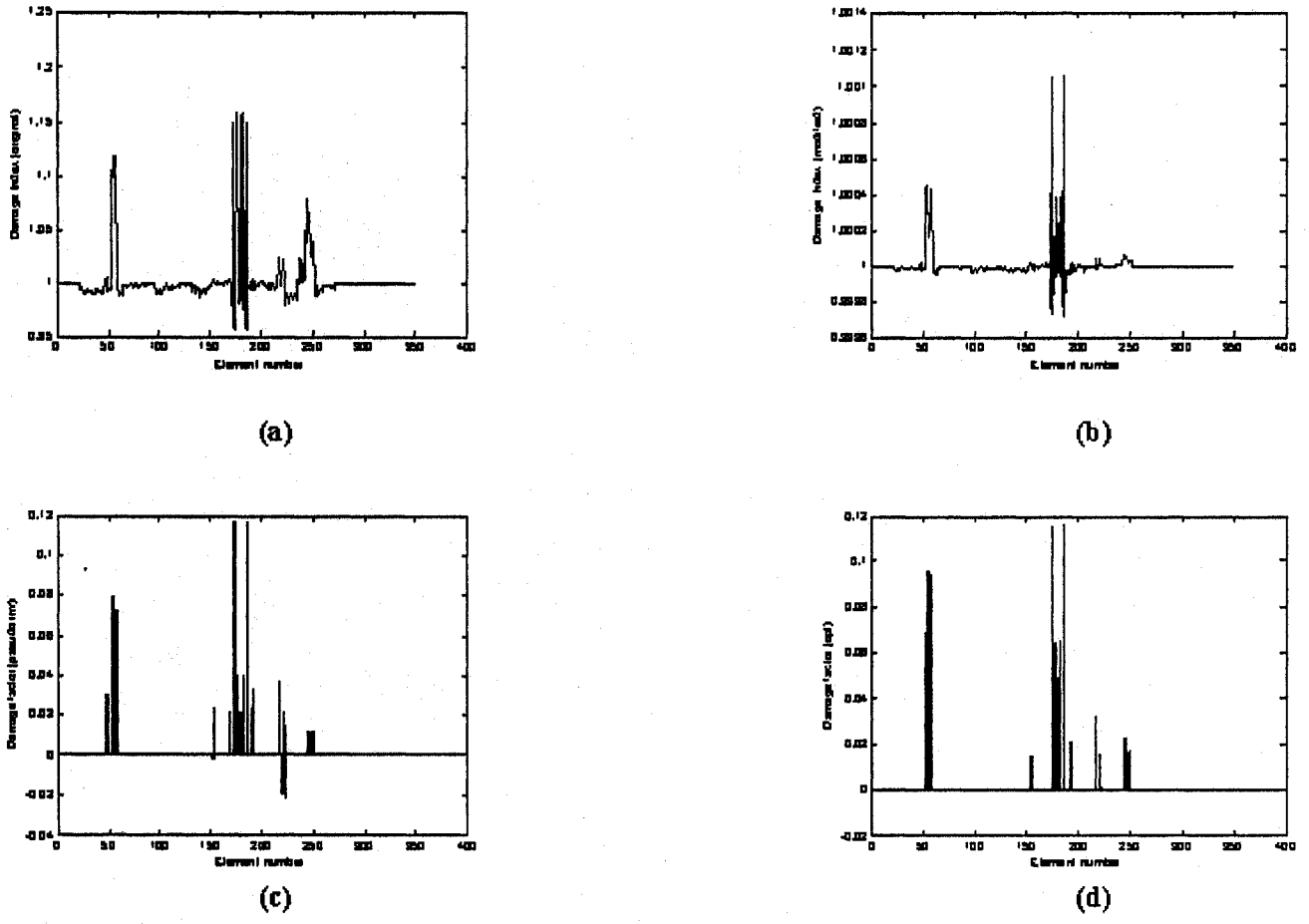

Fig A.2: Graphs showing damage with element numbers for no error and incomplete modes with 10% damage severity by Damage Index Method **(a)** original and **(b)** modified; by Matrix Update Method **(c)** Pseudo Inverse **(d)** Optimized

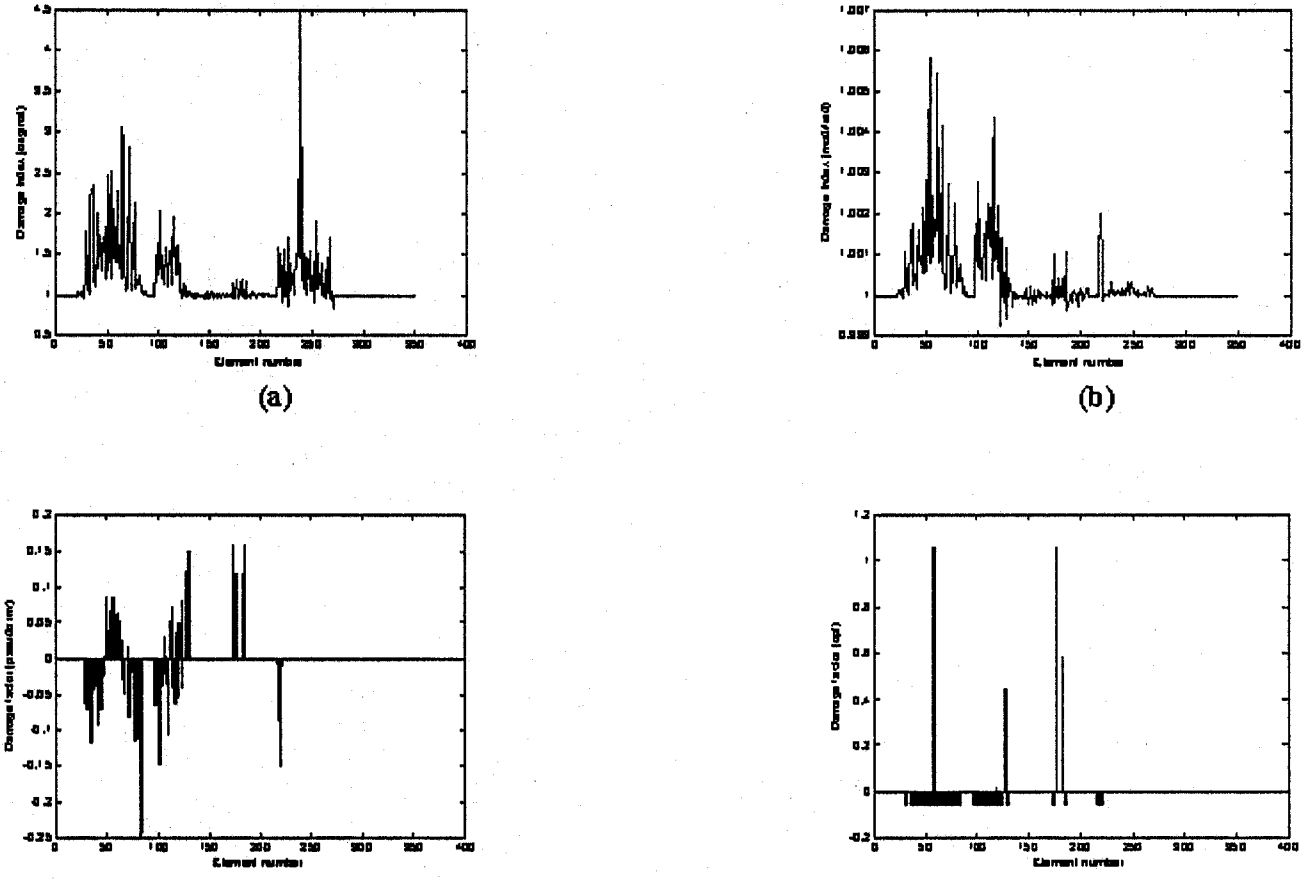

Fig A.3: Graphs showing damage with element numbers for random error up to 1% and incomplete modes with 10% damage severity by Damage Index Method **(a)** original and **(b)** modified.; by Matrix Update Method **(a)** Pseudo Inverse **(b)** Optimized

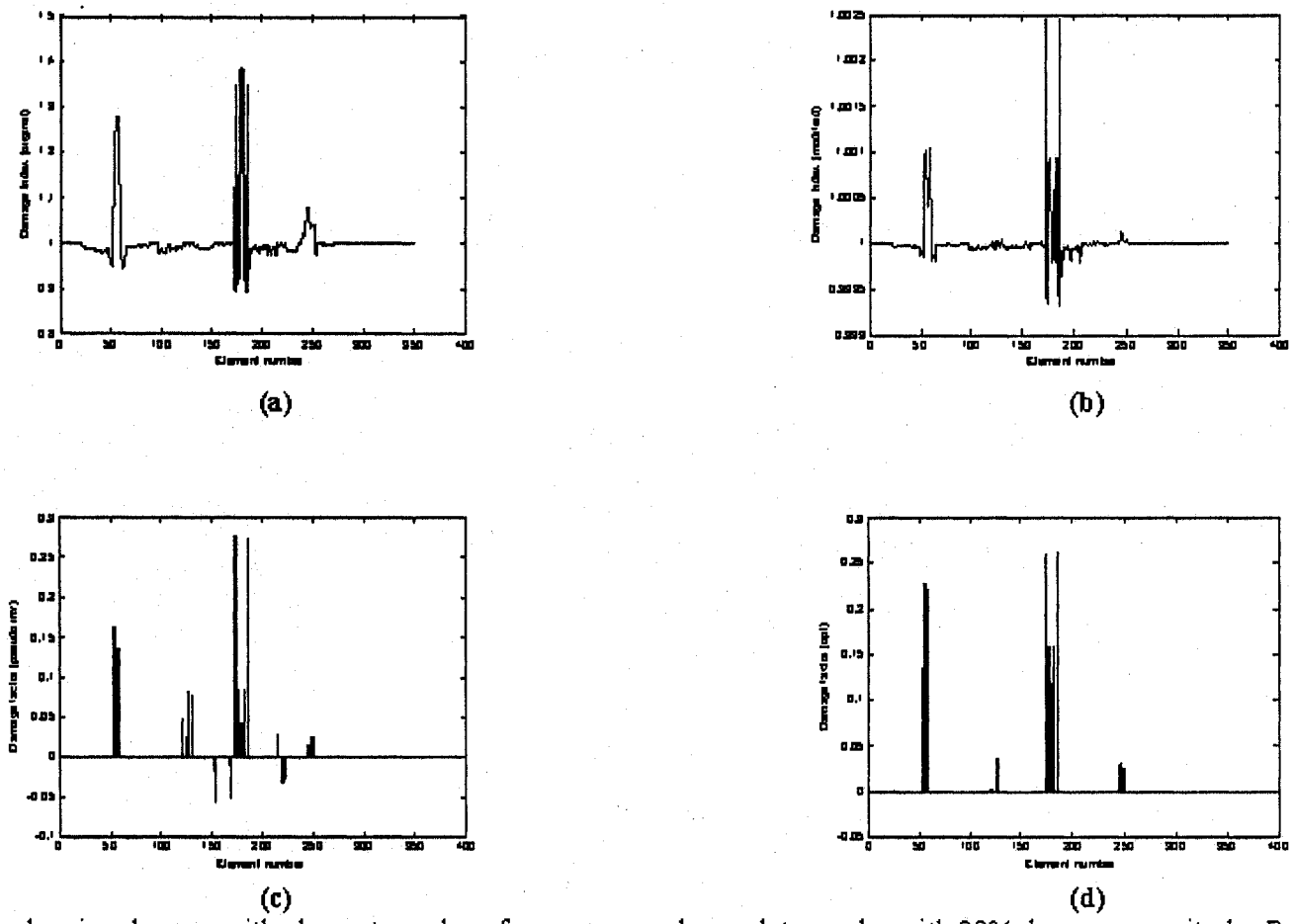

Fig A.4: Graphs showing damage with element numbers for no error and complete modes with 20% damage severity by Damage Index Method **(a)** original and **(b)** modified; by Matrix Update Method **(c)** Pseudo Inverse **(d)** Optimized

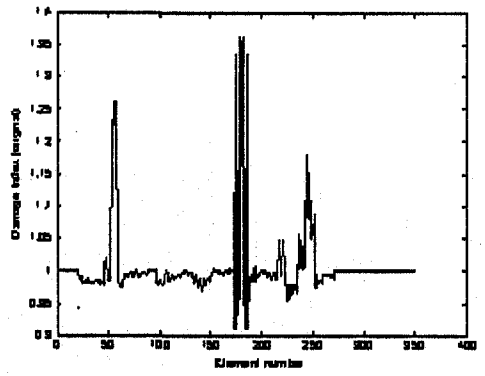

(a)

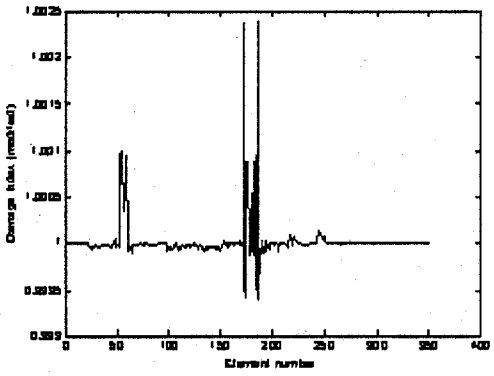

(b)

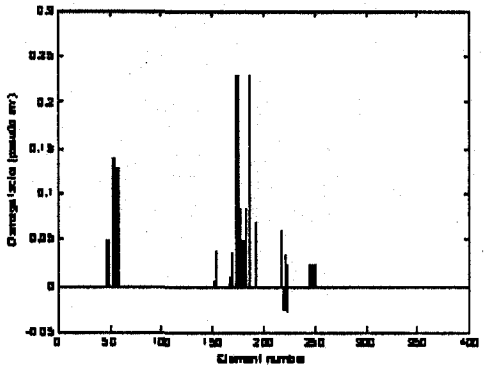

(c)

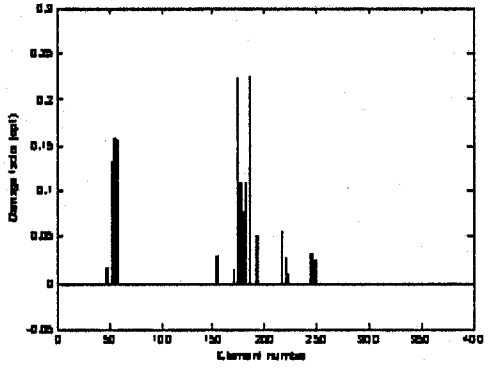

(d)

Fig A.5: Graphs showing damage with element numbers for no error and incomplete modes with 20% damage severity by Damage Index Method **(a)** original and **(b)** modified; by Matrix Update Method **(c)** Pseudo Inverse **(d)** Optimized

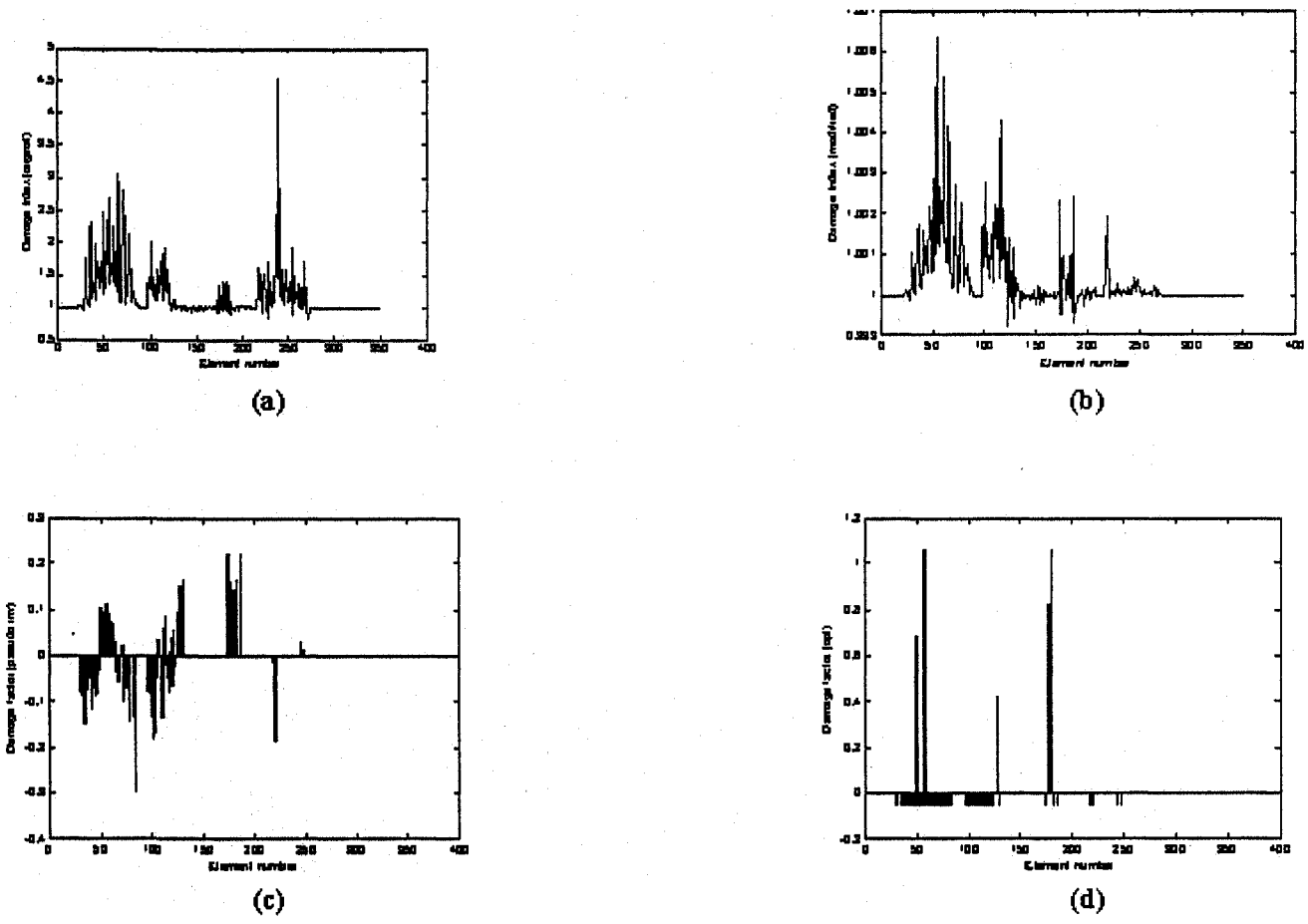

Fig A.6: Graphs showing damage with element numbers for random error up to 1% and incomplete modes with 20% damage severity by Damage Index Method **(a)** original and **(b)** modified; by Matrix Update Method **(c)** Pseudo Inverse **(d)** Optimized

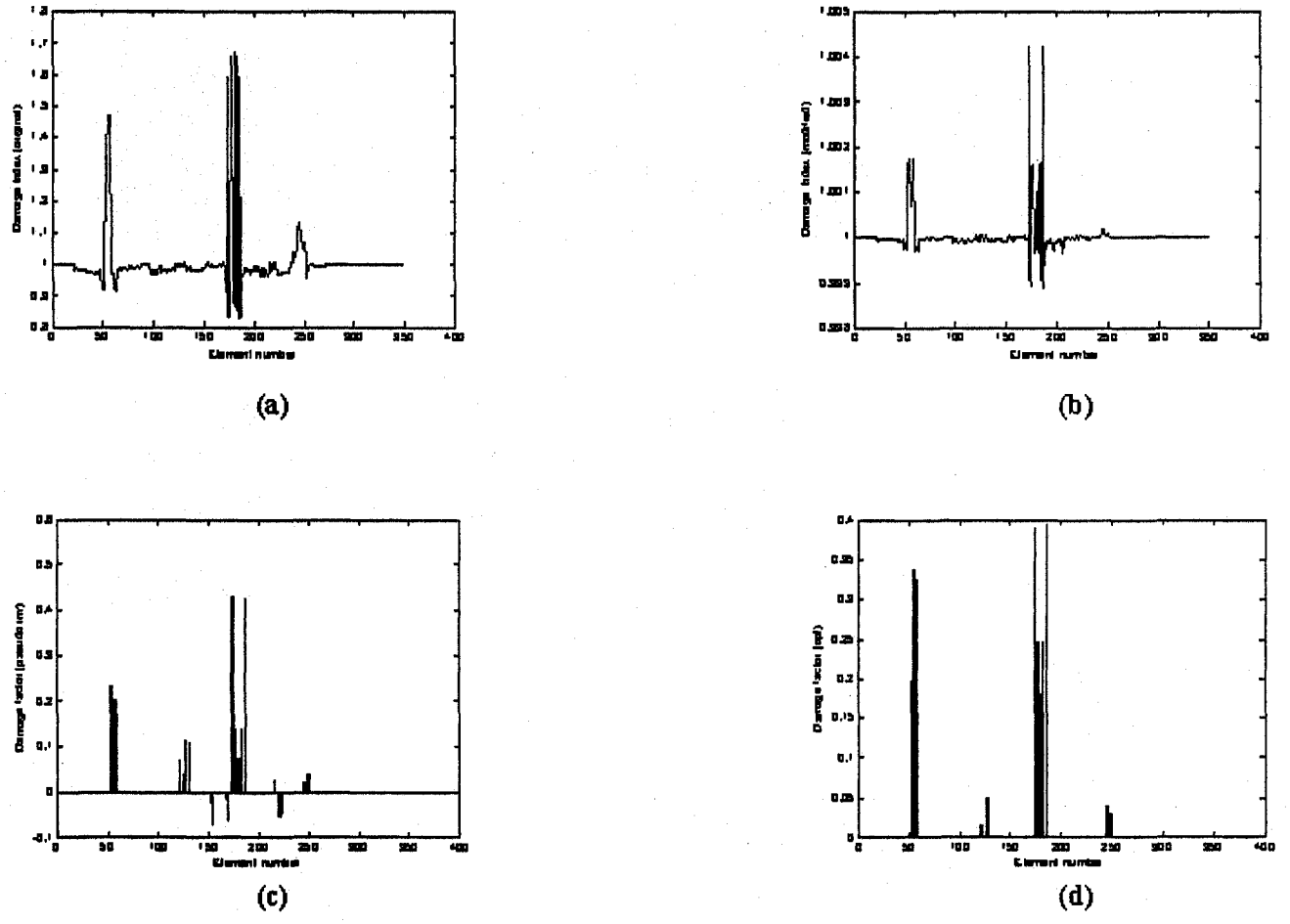

Fig A.7: Graphs showing damage with element numbers for no error and complete modes with 30% damage severity by Damage Index Method **(a)** original and **(b)** modified; by Matrix Update Method **(c)** Pseudo Inverse **(d)** Optimized

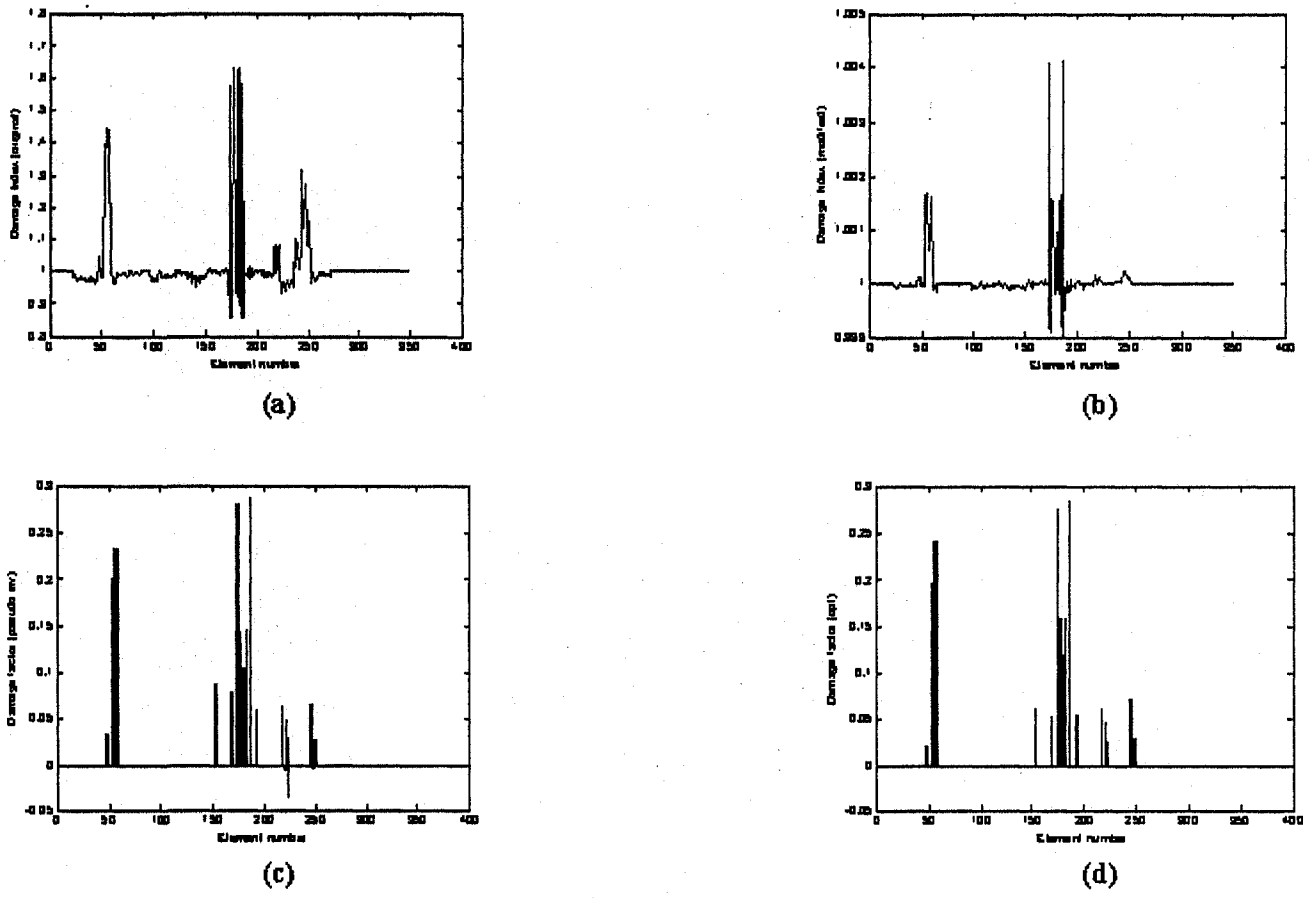

Fig A.8: Graphs showing damage with element numbers for no error and incomplete modes with 30% damage severity by Damage Index Method **(a)** original and **(b)** modified; by Matrix Update Method **(c)** Pseudo Inverse **(d)** Optimized

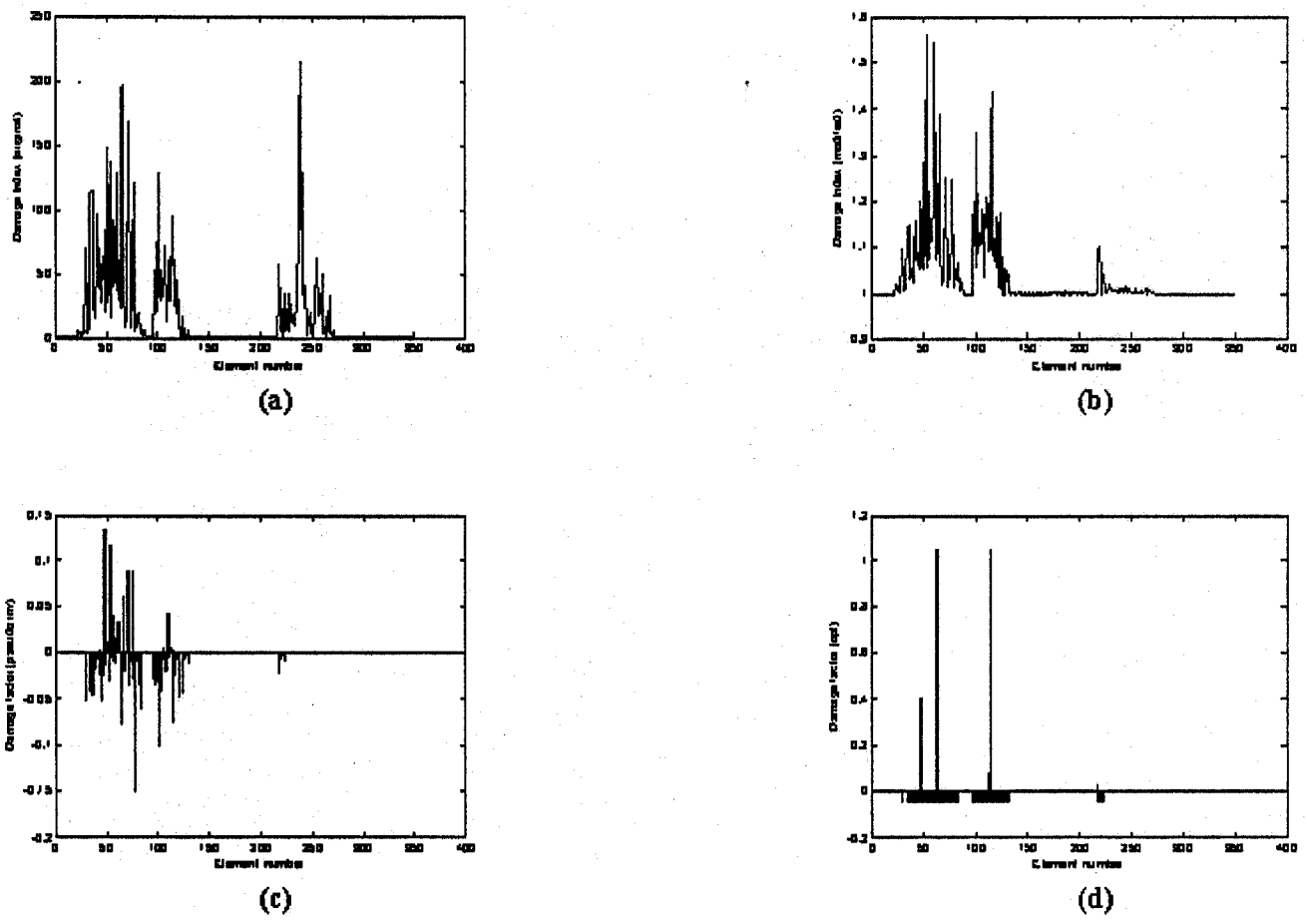

Fig A.9: Graphs showing damage with element numbers for random error up to 1% and incomplete modes with 30% damage severity by Damage Index Method **(a)** original and **(b)** modified; by Matrix Update Method **(c)** Pseudo Inverse **(d)** Optimized

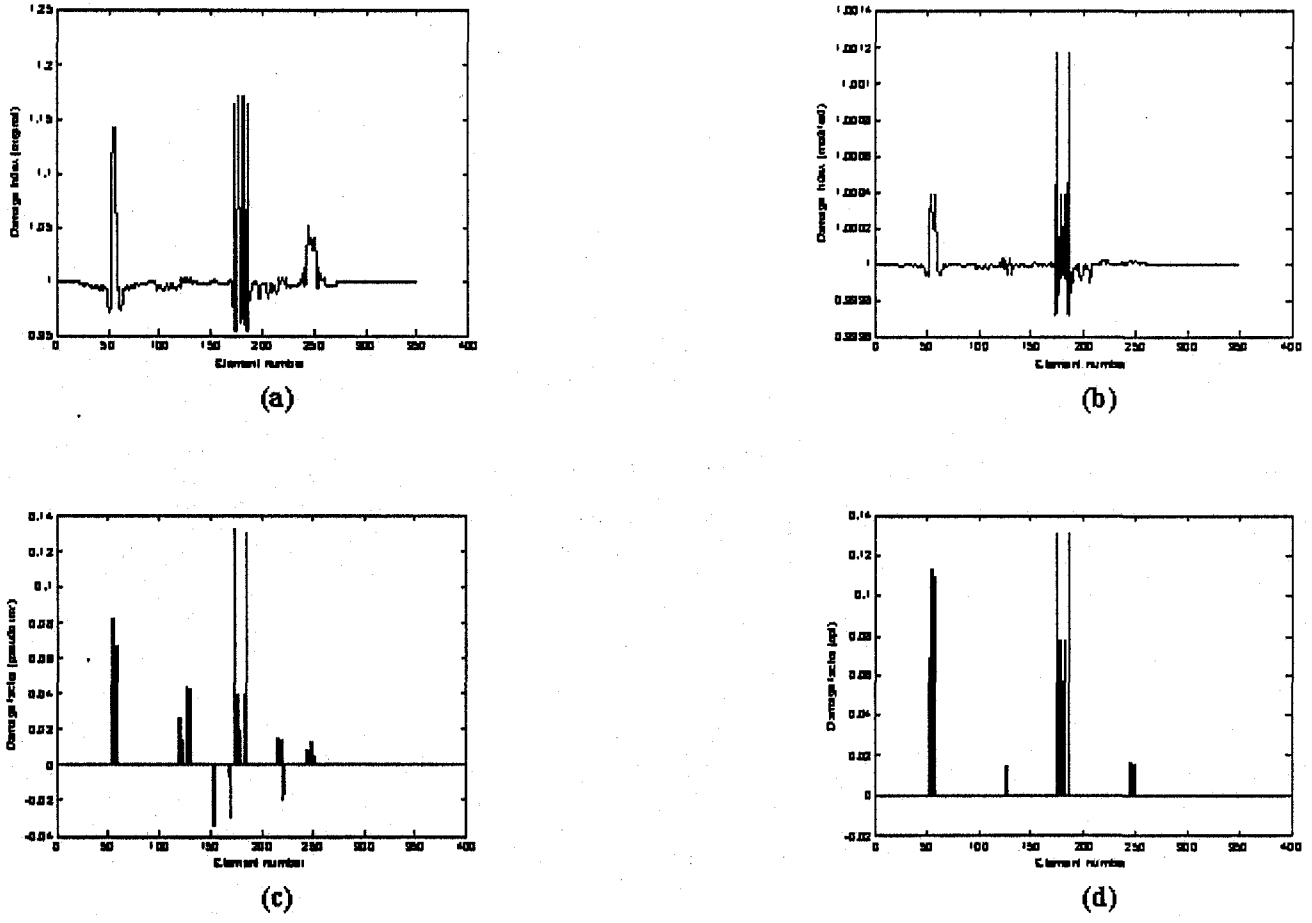

Fig A.10: Graphs showing damage with element numbers for no error using measured frequencies and complete modes with 10% damage severity by Damage Index Method **(a)** original and **(b)** modified; Matrix Update Method **(c)** Pseudo Inverse **(d)** Optimized

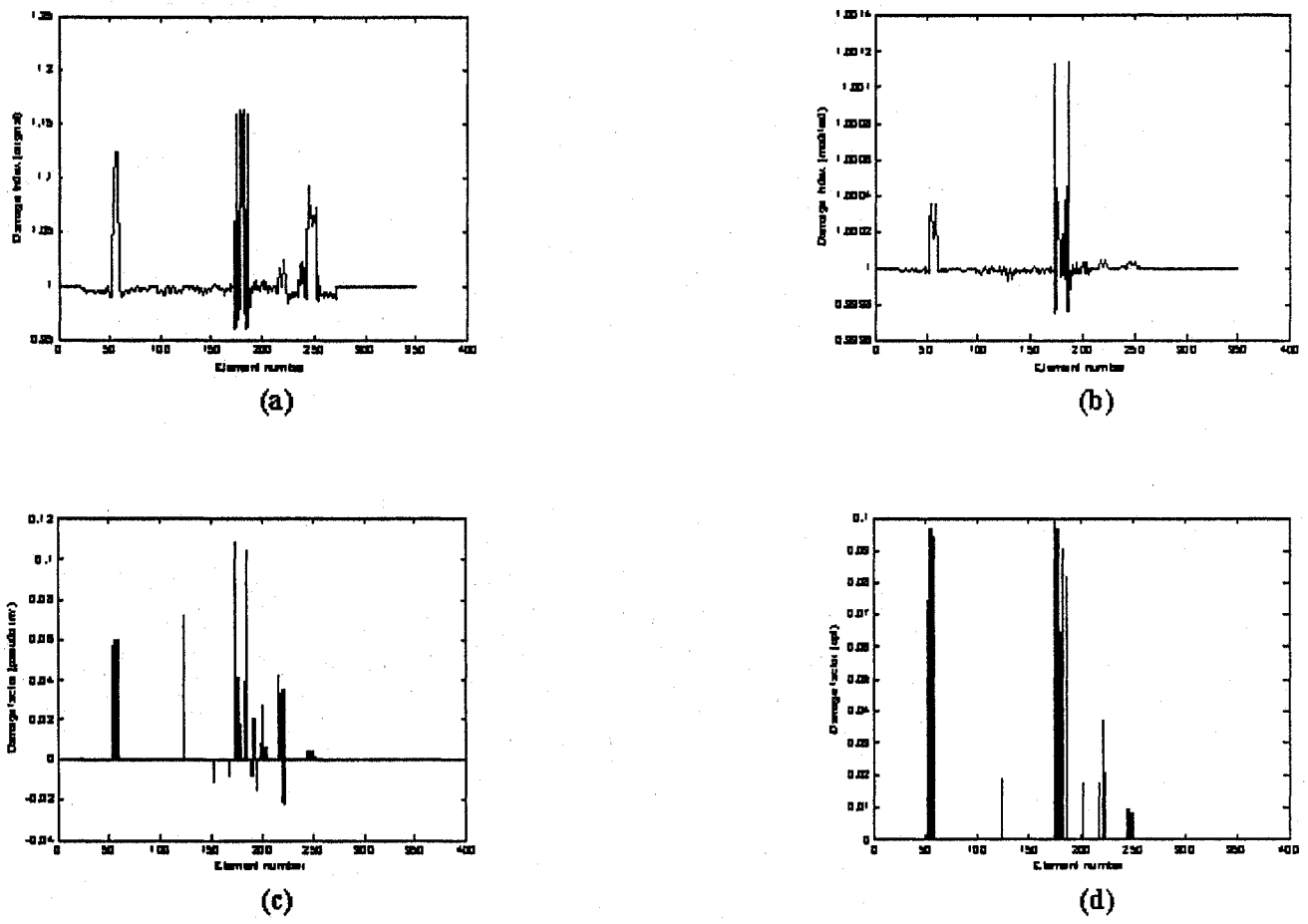

A.11: Graphs showing damage with element numbers for no error using measured frequencies and incomplete modes with 10% damage severity by Damage Index Method **(a)** original and **(b)** modified; by Matrix Update Method **(c)** Pseudo Inverse **(d)** Optimized.

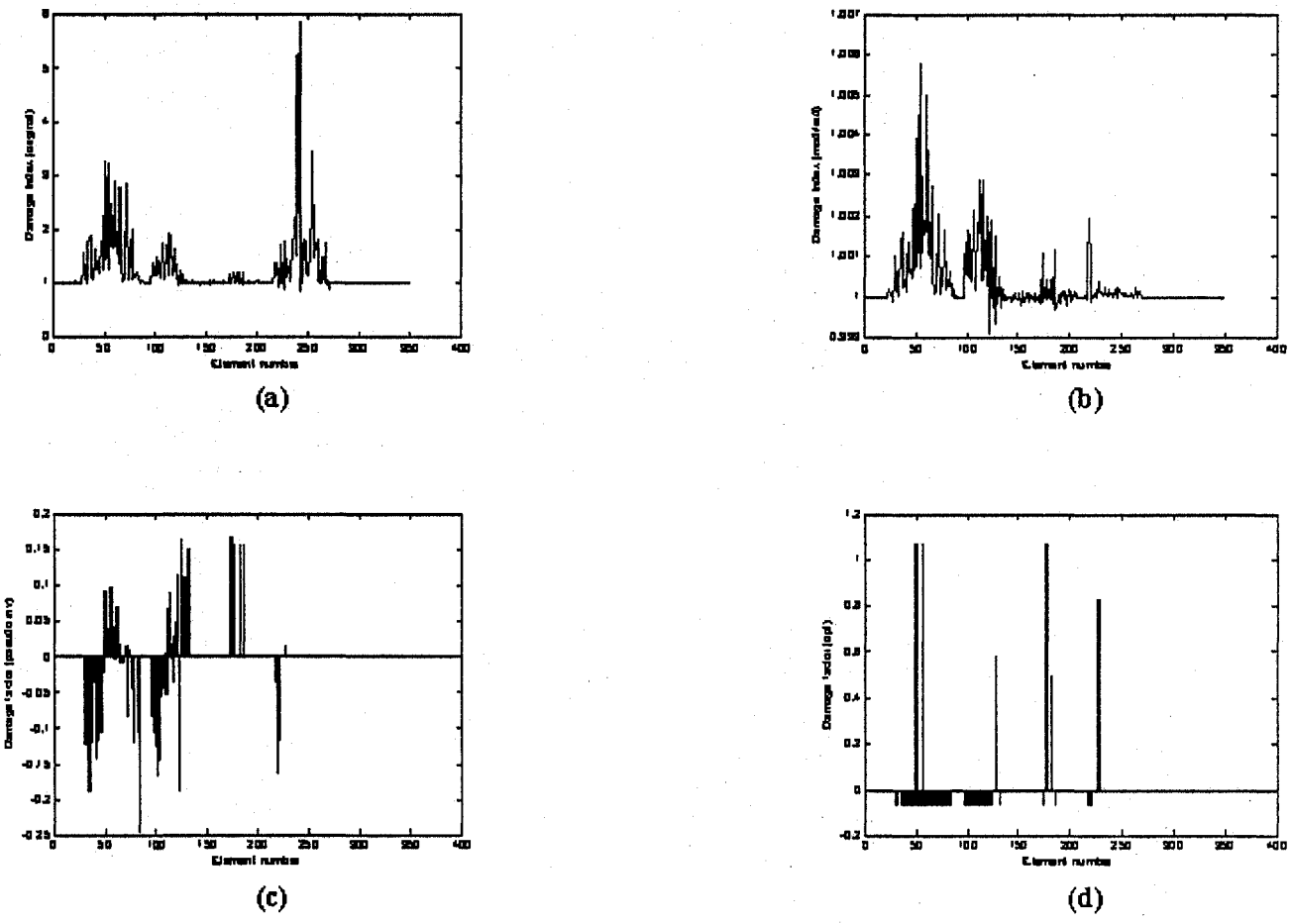

Fig A.12: Graphs showing damage with element numbers for random error up to 1% using measured frequencies and incomplete modes with 10% damage severity by Damage Index Method **(a)** original and **(b)** modified; by Matrix Update Method **(c)** Pseudo Inverse **(d)** Optimized

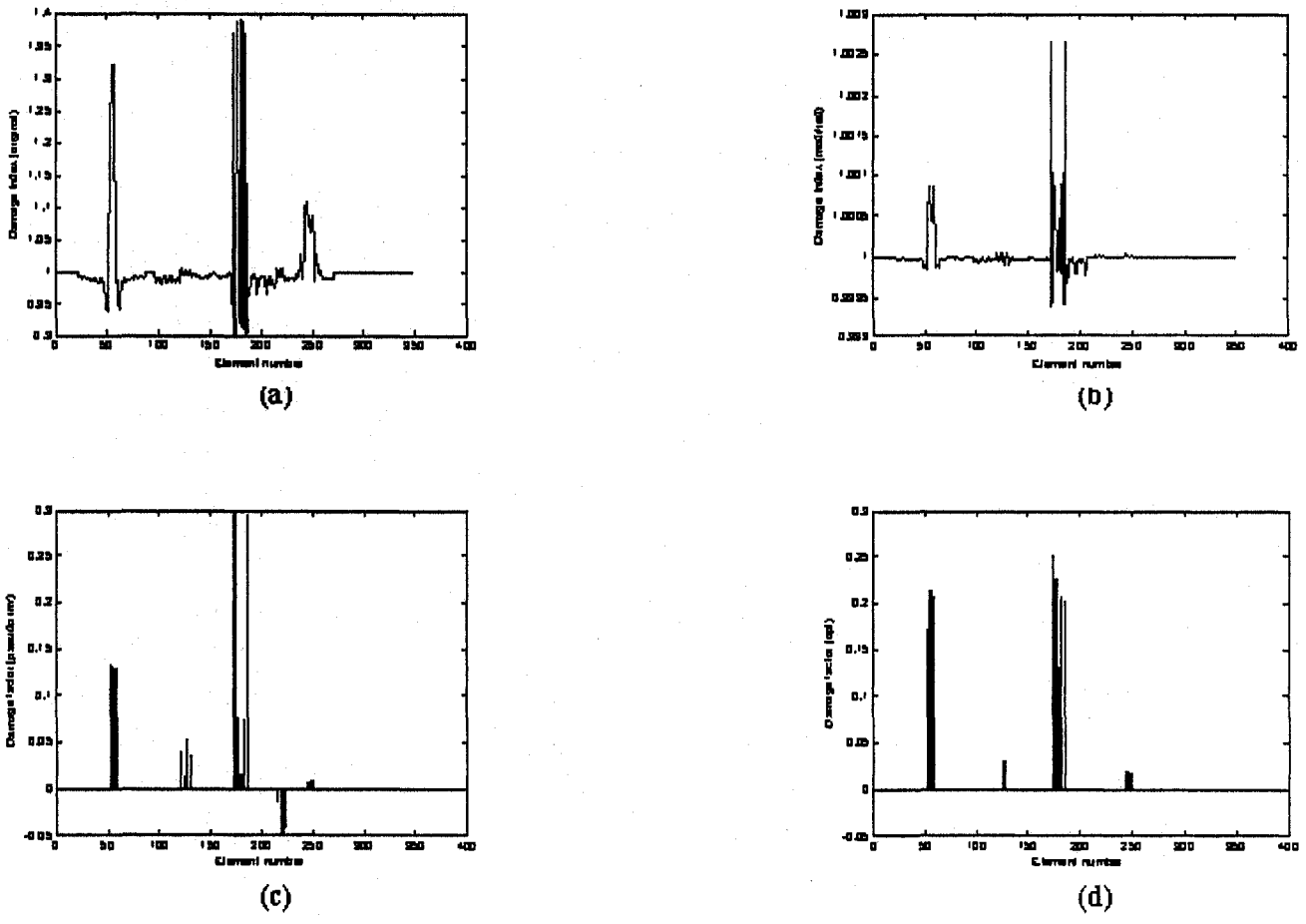

Fig A.13: Graphs showing damage with element numbers for no error using measured frequencies and complete modes with 20% damage severity by Damage Index Method **(a)** original and **(b)** modified; by Matrix Update Method **(c)** Pseudo Inverse **(d)** Optimized

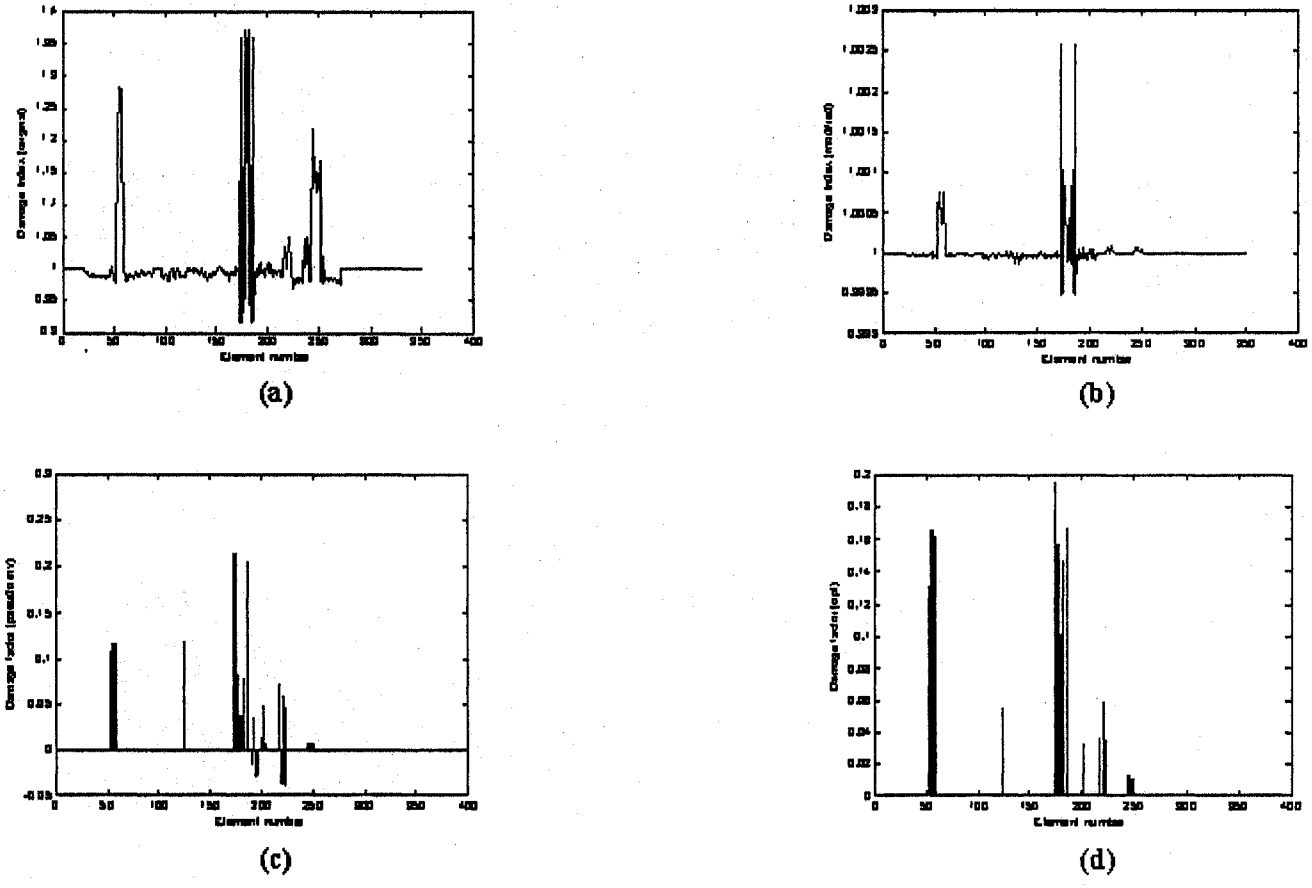

Fig A.14: Graphs showing damage with element numbers for no error using measured frequencies and incomplete modes with 20% damage severity by Damage Index Method **(a)** original and **(b)** modified; by Matrix Update Method **(c)** Pseudo Inverse **(d)** Optimized

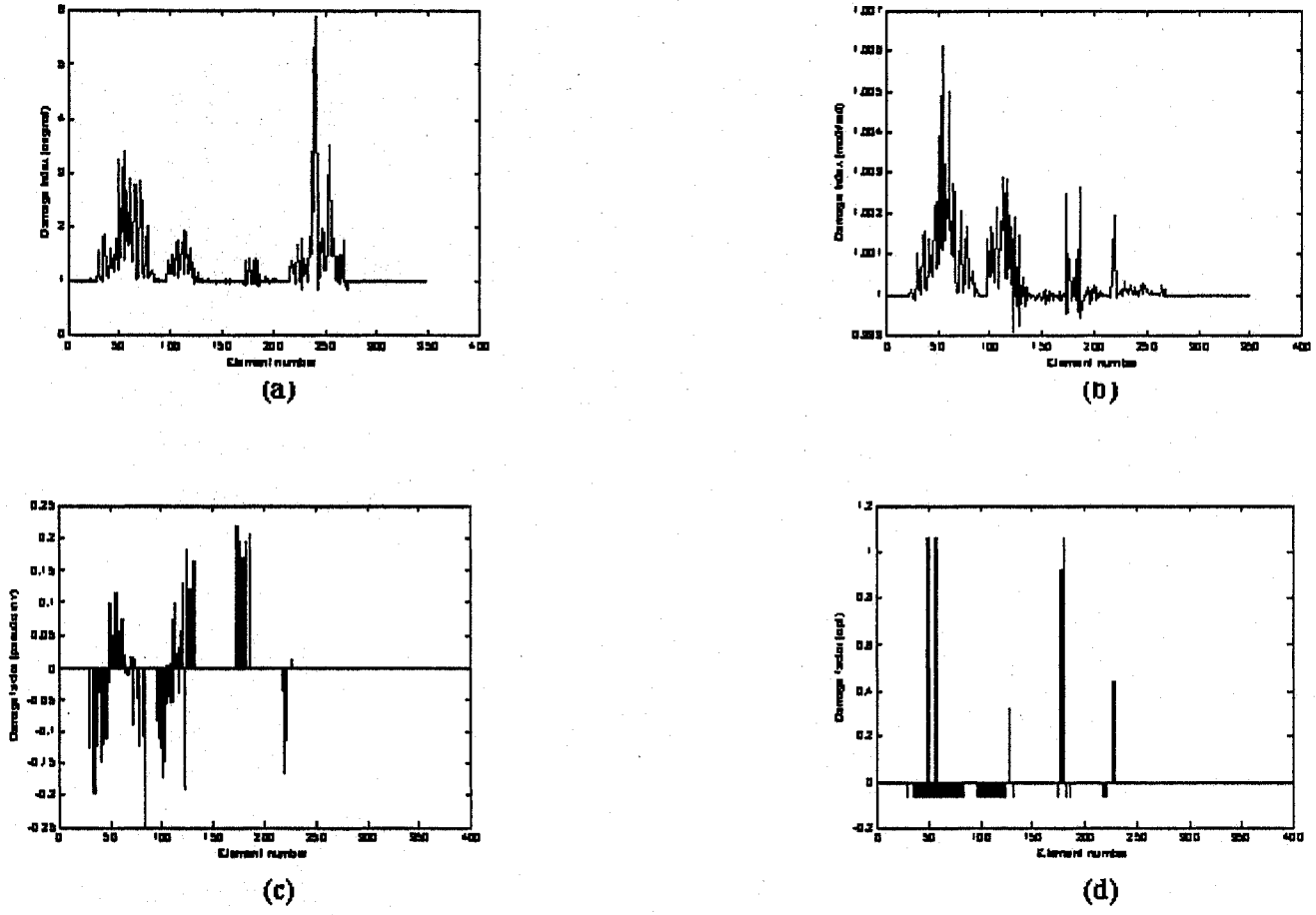

Fig A.15: Graphs showing damage with element numbers for random error up to 1% using measured frequencies and incomplete modes with 20% damage severity by Damage Index Method **(a)** original and **(b)** modified; by Matrix Update Method **(c)** Pseudo Inverse **(d)** Optimized

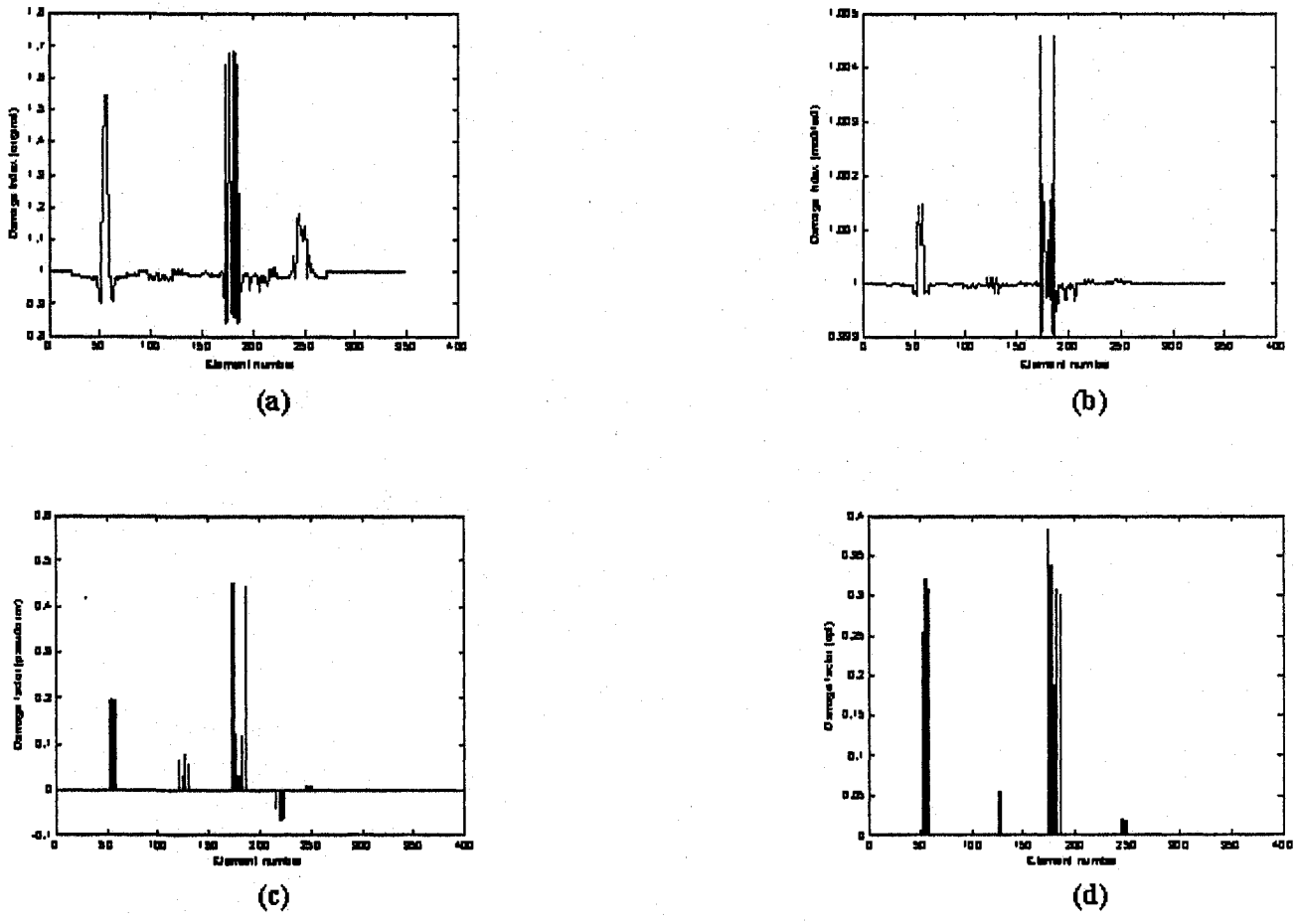

Fig A.16: Graphs showing damage with element numbers for no error using measured frequencies and complete modes with 30% damage severity by Damage Index Method **(a)** original and **(b)** modified; by Matrix Update Method **(c)** Pseudo Inverse **(d)** Optimized

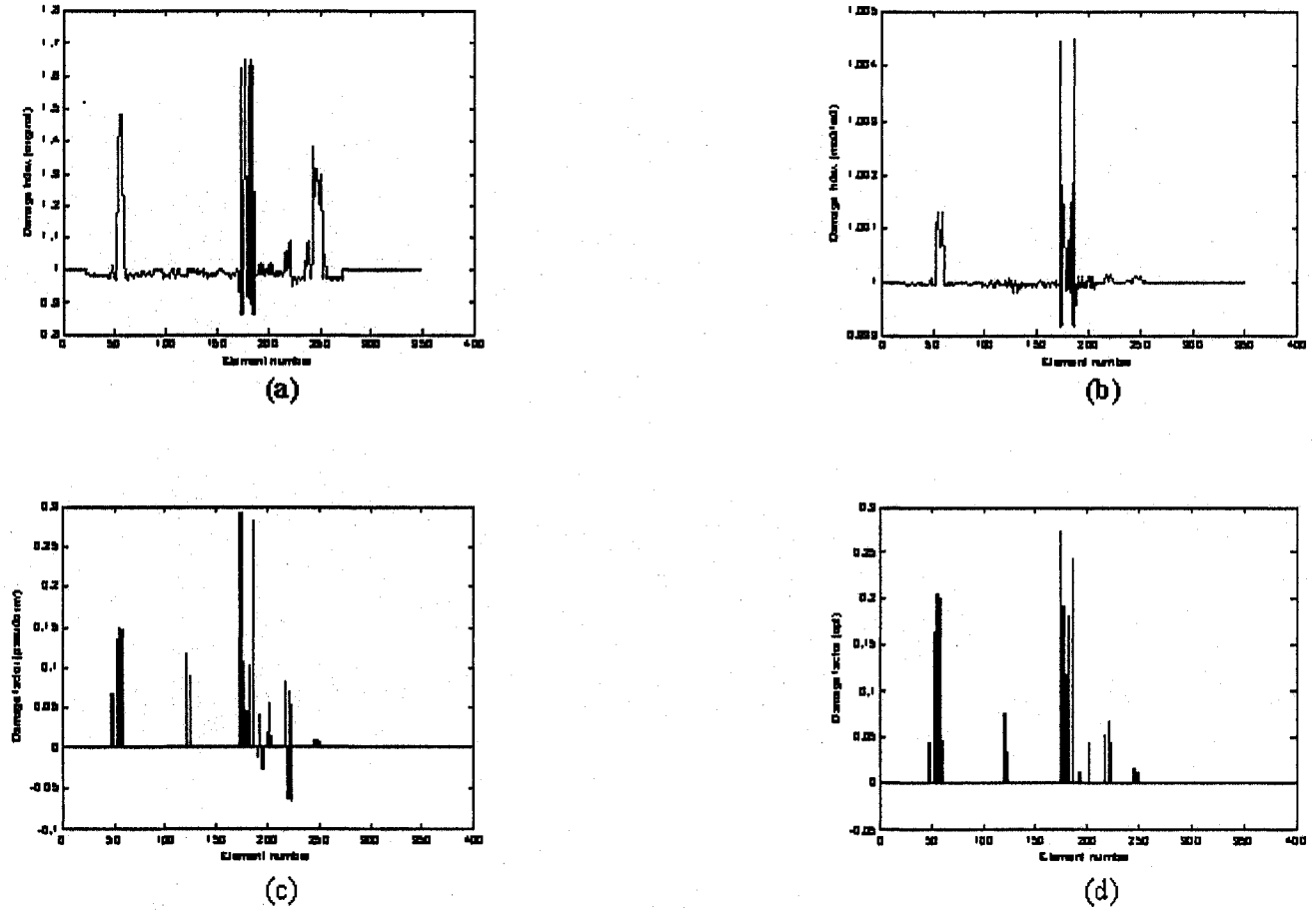

Fig A.17: Graphs showing damage with element numbers for no error using measured frequencies and incomplete modes with 30% damage severity by Damage Index Method **(a)** original and **(b)** modified; by Matrix Update Method **(c)** Pseudo Inverse **(d)** Optimized

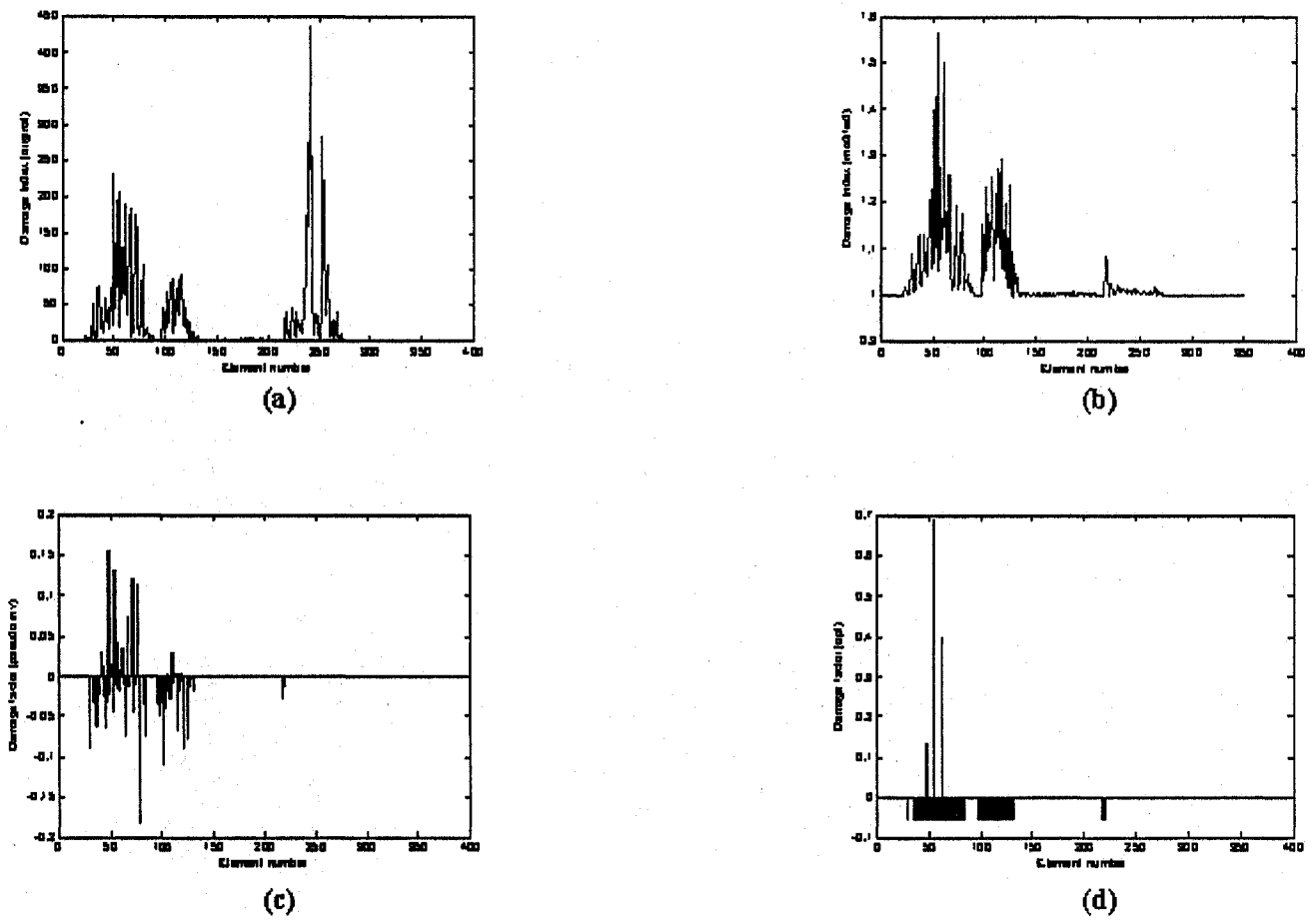

Fig A.18: Graphs showing damage with element numbers for random error up to 1% using measured frequencies and incomplete modes with 30% damage severity by Damage Index Method **(a)** original and **(b)** modified; by Matrix Update Method **(c)** Pseudo Inverse **(d)** Optimized

Appendix B

B.1 Graphical output of VBDI case study on the 3D Space Frame

In Appendix B, figures showing the graphical output by Damage Index and Matrix Update methods applied on the 3D Space Frame are presented. The cases are defined in the section 5.5.2 and damage cases with element connectivity are shown in Table 5.5.

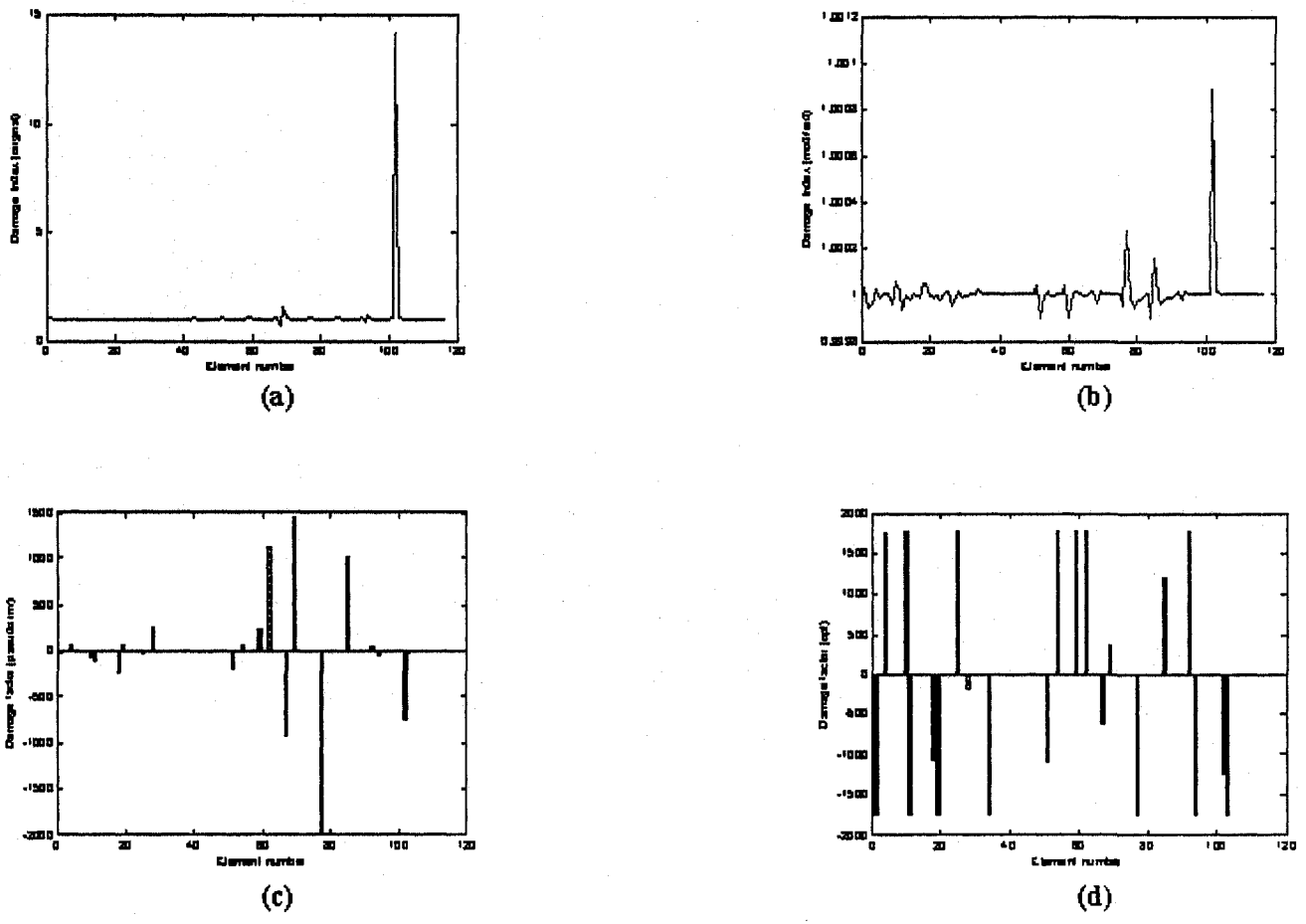

Fig B.1: Graphs showing damage with no error in frequencies and complete modes assumed for case-D1 by Damage Index Method **(a)** original and **(b)** modified; by Matrix Update **(c)** pseudo-inverse **(d)** optimized.

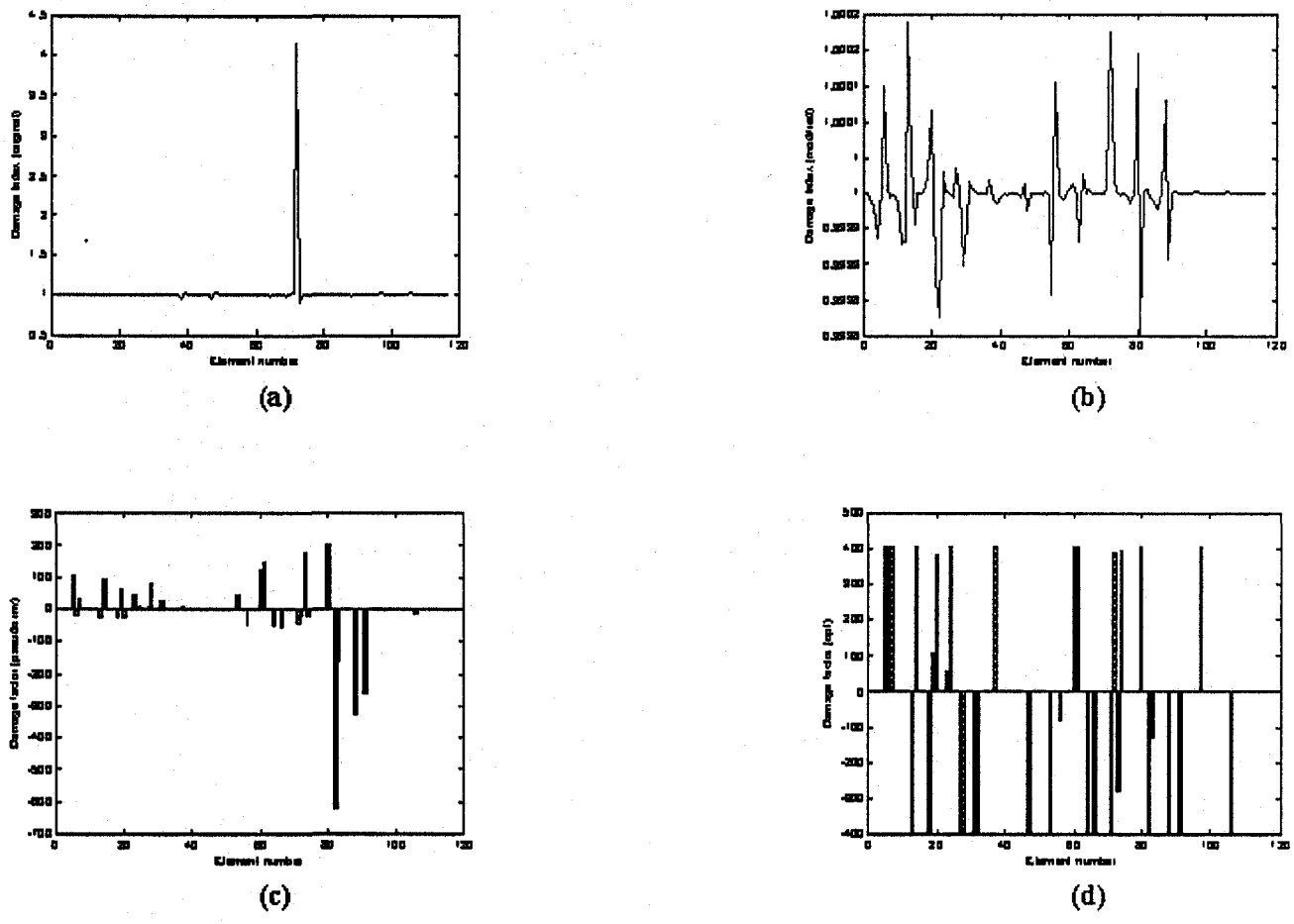

Fig B.2: Graphs showing damage with no error in frequencies and complete modes assumed for case-D2 by Damage Index Method **(a)** original and **(b)** modified; by Matrix Update **(c)** pseudo-inverse **(d)** optimized.

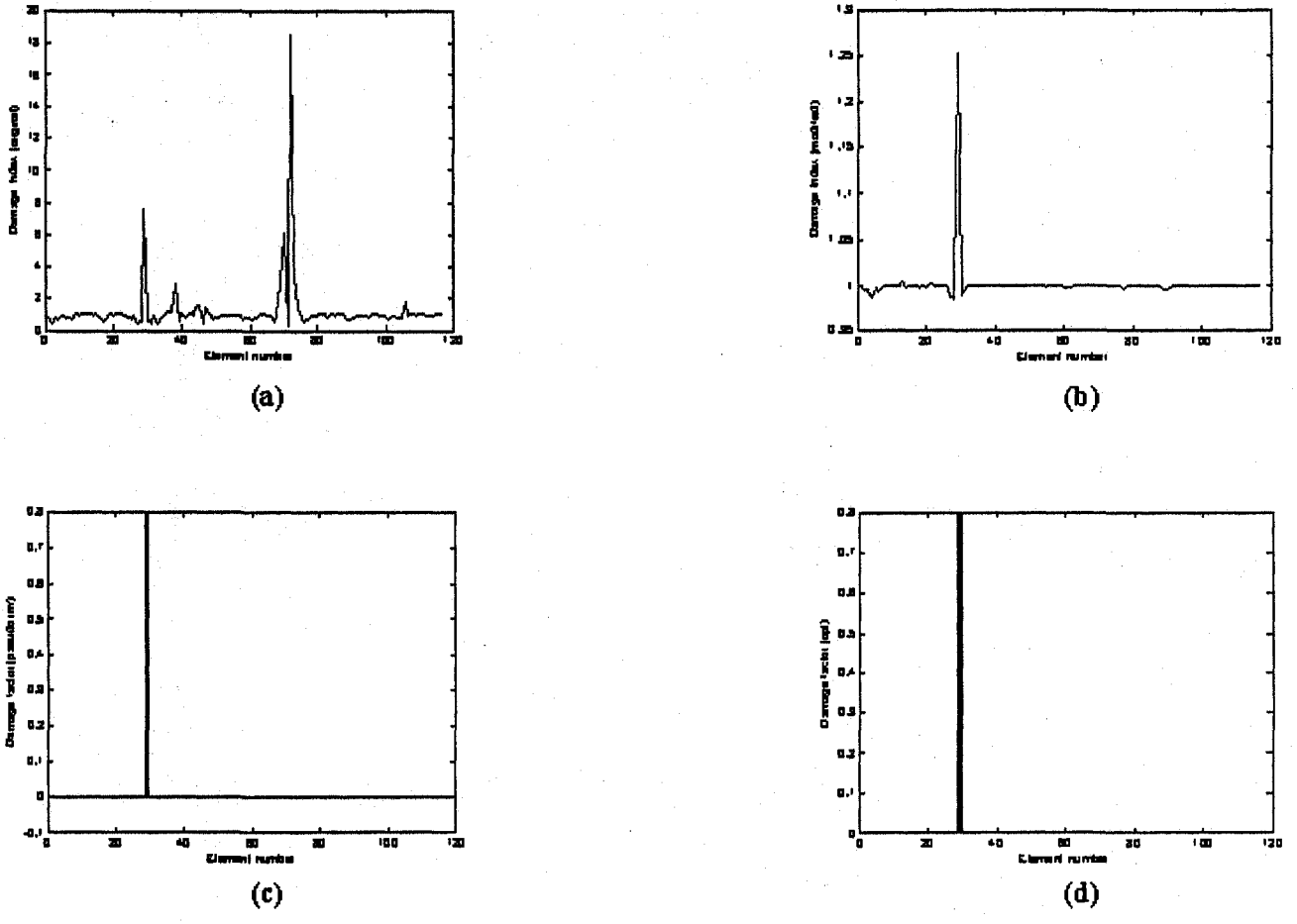

Fig B.3: Graphs showing damage with no error in frequencies and complete modes assumed for case-D3S by Damage Index Method **(a)** original and **(b)** modified; by Matrix Update **(c)** pseudo-inverse **(d)** optimized

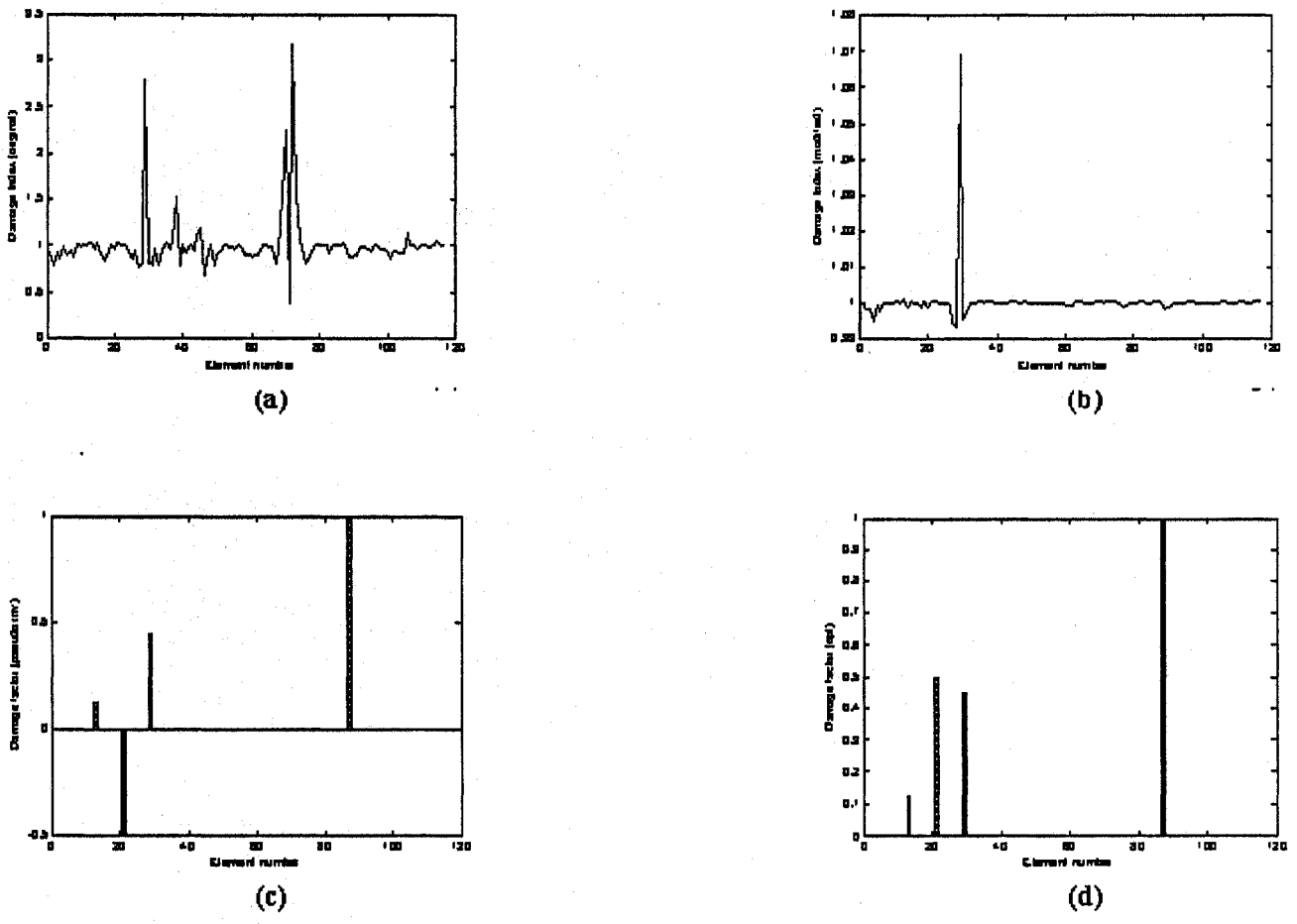

Fig-B.4: Graphs showing damage with no error in frequencies and complete modes assumed for case-D3L by Damage Index Method **(a)** original and **(b)** modified; by Matrix Update **(c)** pseudo-inverse **(d)** optimized.

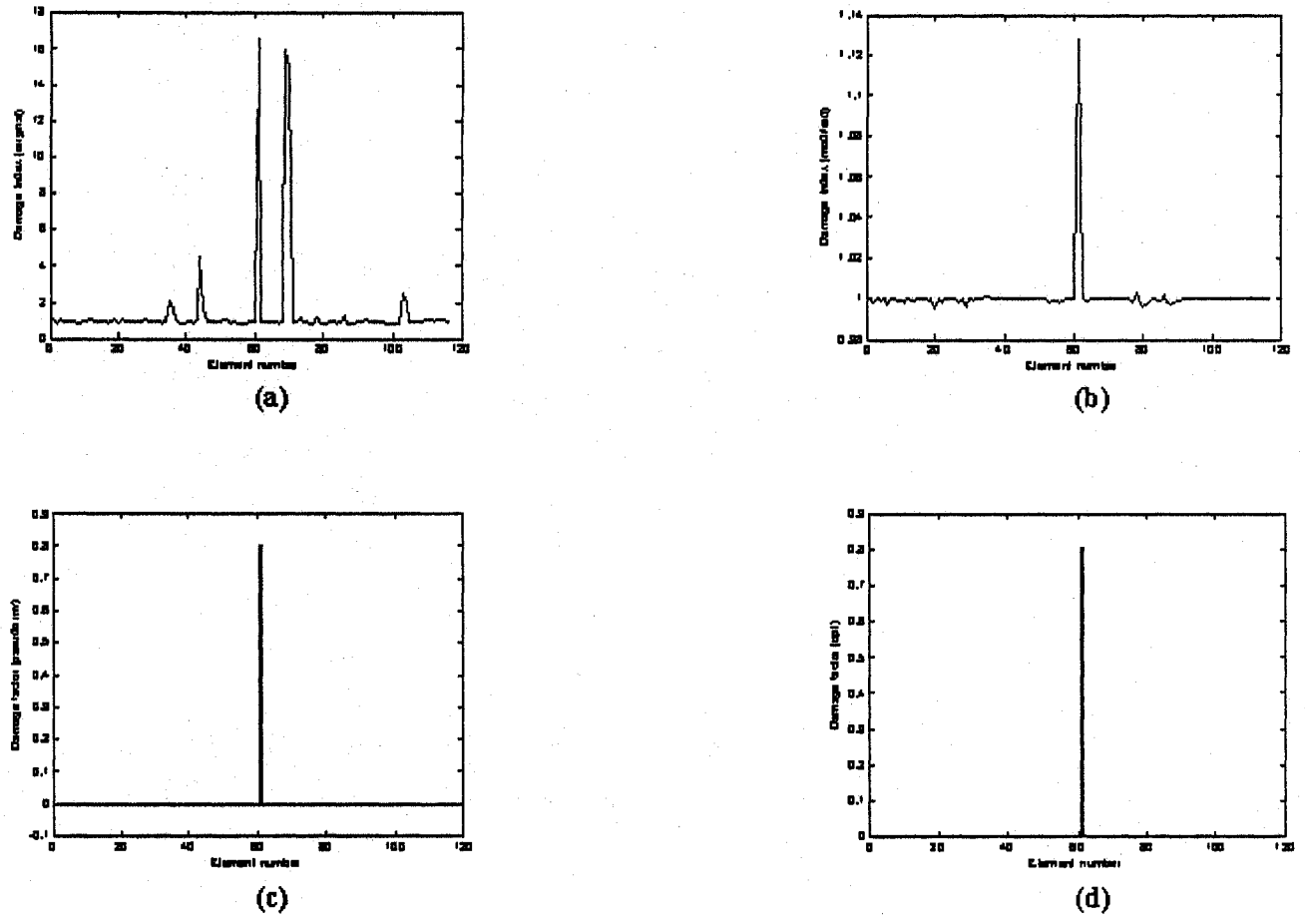

Fig B.5: Graphs showing damage with no error in frequencies and complete modes assumed for case-D4S by Damage Index Method **(a)** original and **(b)** modified; by Matrix Update **(c)** pseudo-inverse **(d)** optimized.

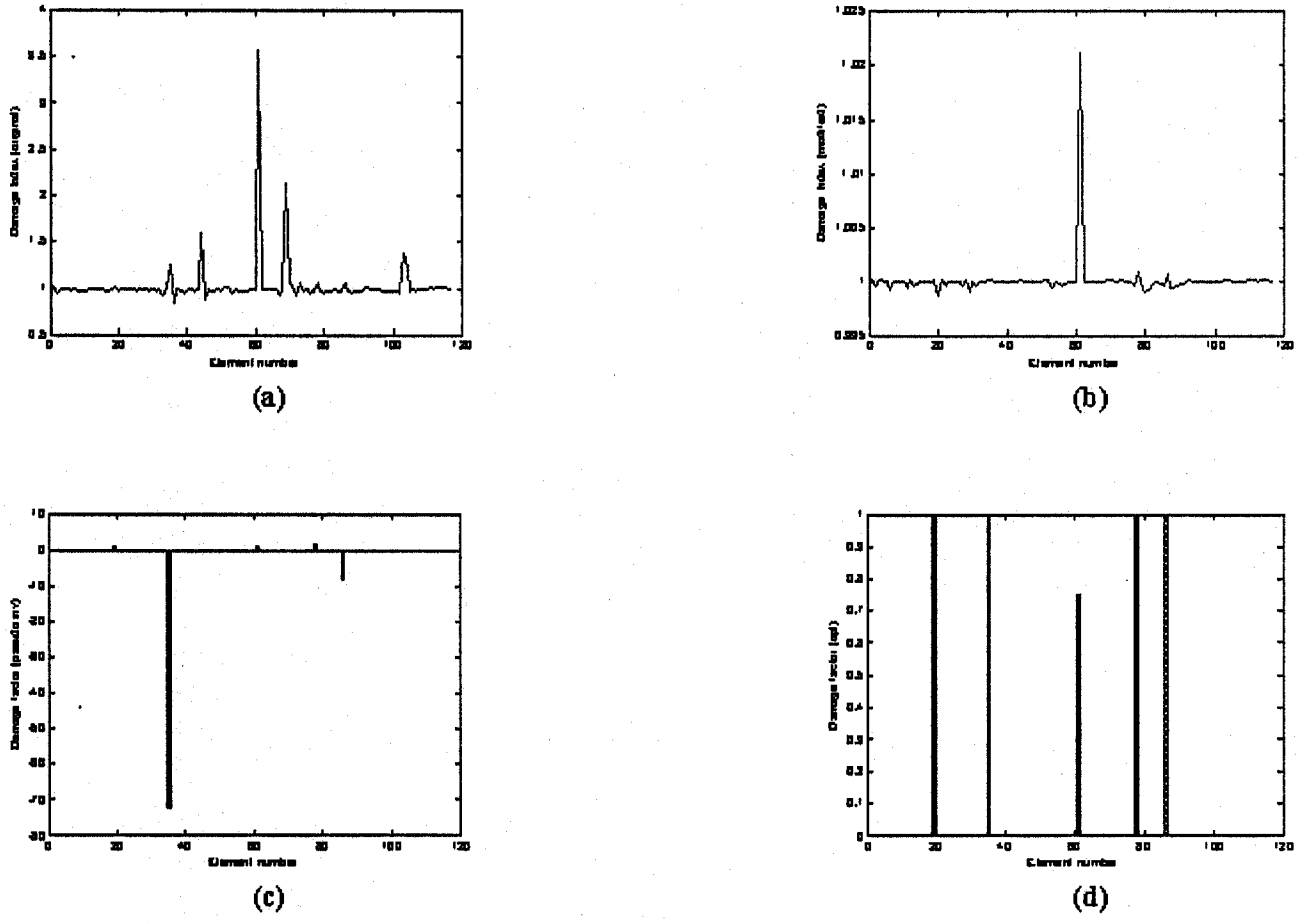

Fig B.6: Graphs showing damage with no error in frequencies and complete modes assumed for case-D4L by Damage Index Method **(a)** original and **(b)** modified; by Matrix Update **(c)** pseudo-inverse **(d)** optimized

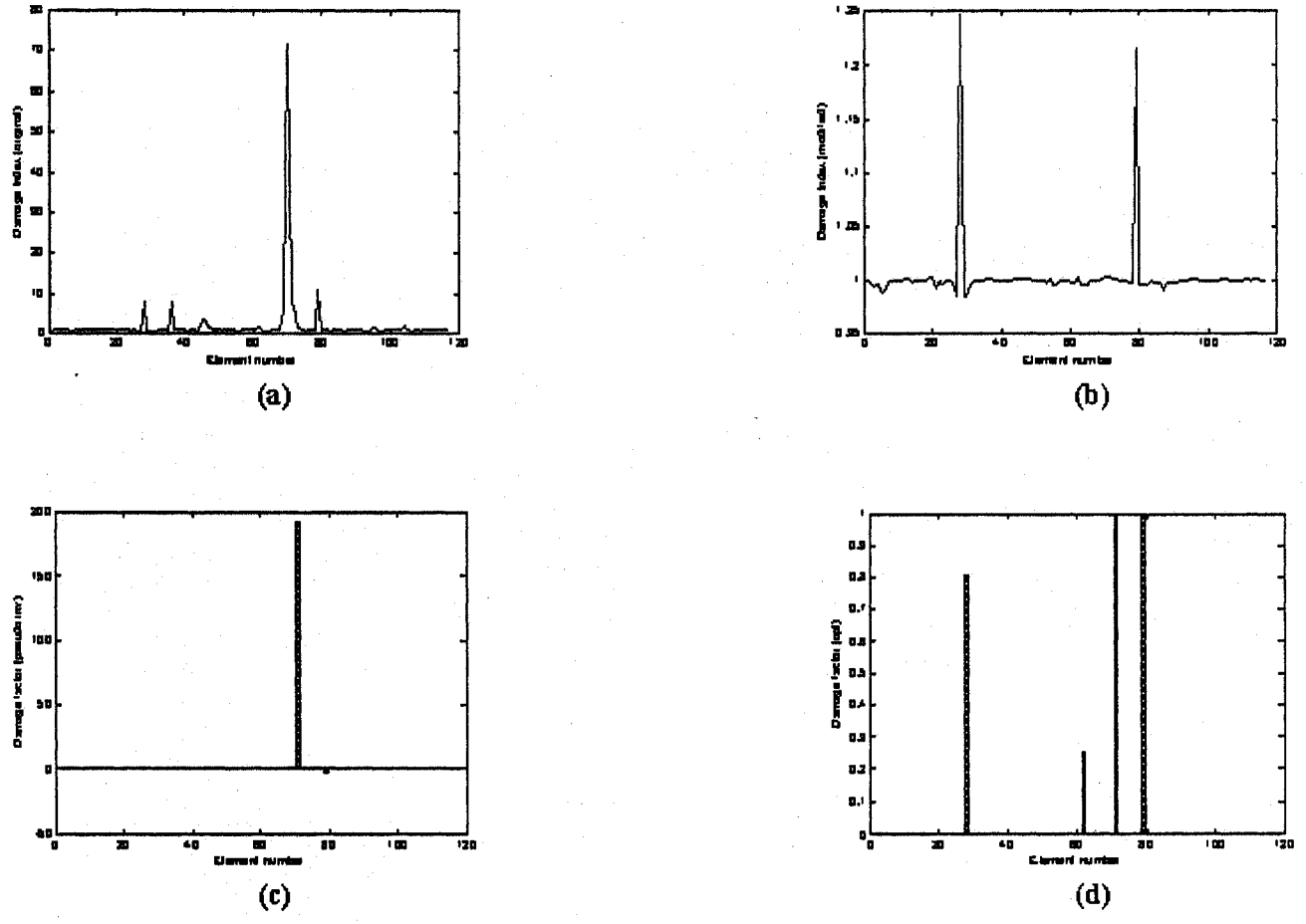

Fig B.7: Graphs showing damage with no error in frequencies and complete modes assumed for case-D5S by Damage Index Method **(a)** original and **(b)** modified; by Matrix Update **(c)** pseudo-inverse **(d)** optimized

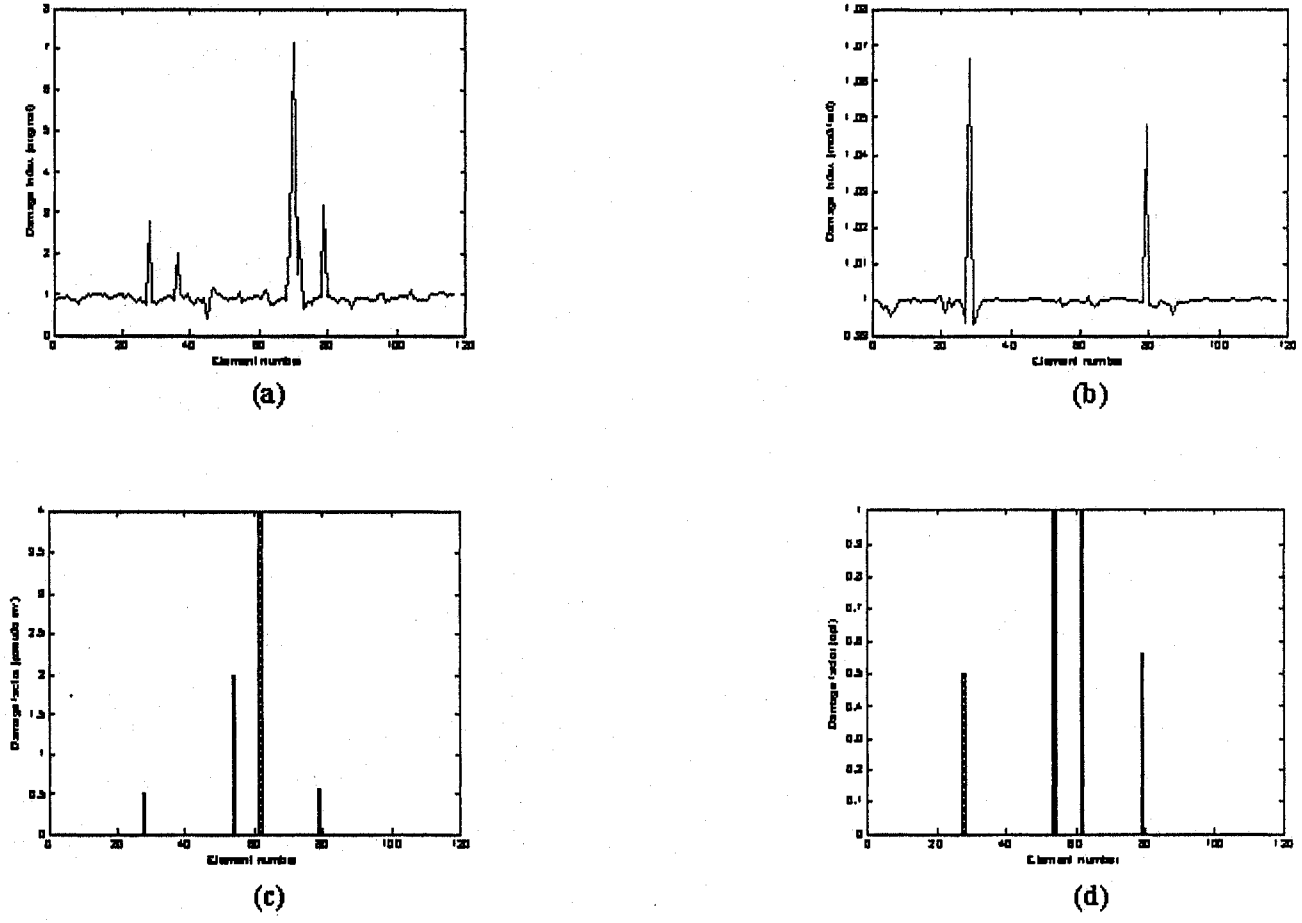

Fig B.8: Graphs showing damage with no error in frequencies and complete modes assumed for case-D5L by Damage Index Method **(a)** original and **(b)** modified; by Matrix Update **(c)** pseudo-inverse **(d)** optimized.

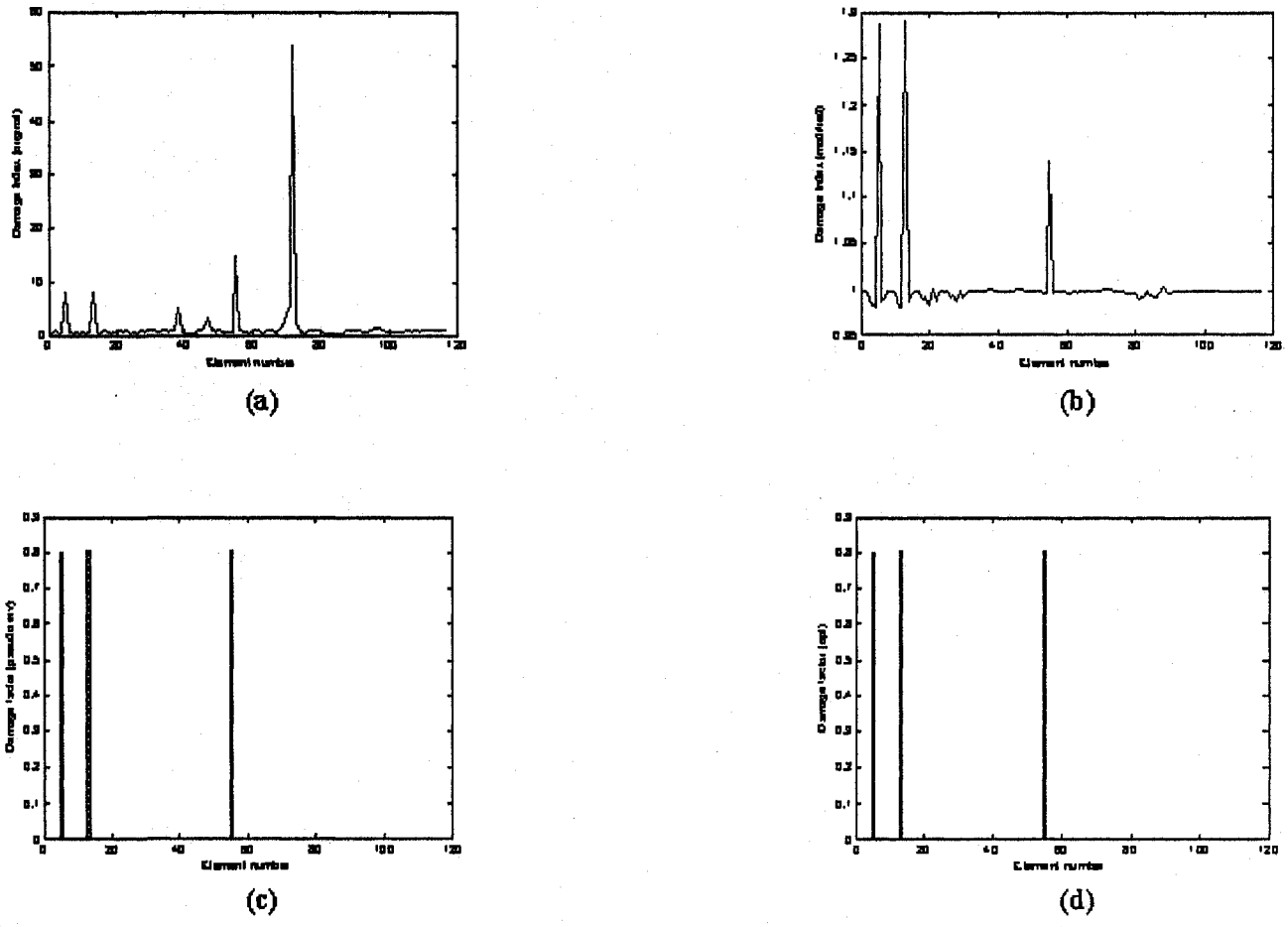

Fig B.9 Graphs showing damage with no error in frequencies and complete modes assumed for case-D6S by Damage Index Method **(a)** original and **(b)** modified; by Matrix Update **(c)** pseudo-inverse **(d)** optimized.

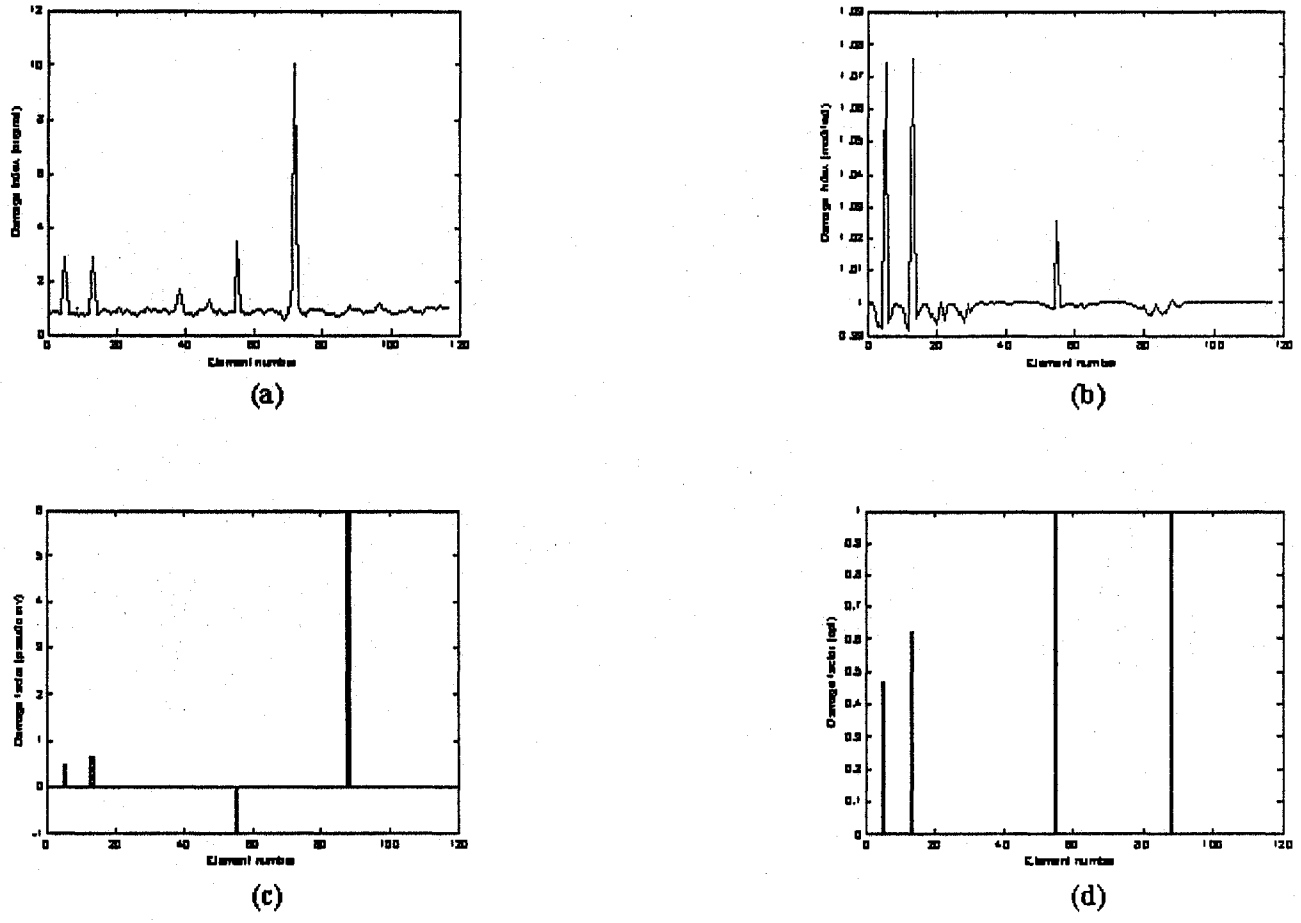

Fig B.10: Graphs showing damage with no error in frequencies and complete modes assumed for case-D6L by Damage Index Method **(a)** original and **(b)** modified; D6Lby Matrix Update **(c)** pseudo-inverse **(d)** optimized

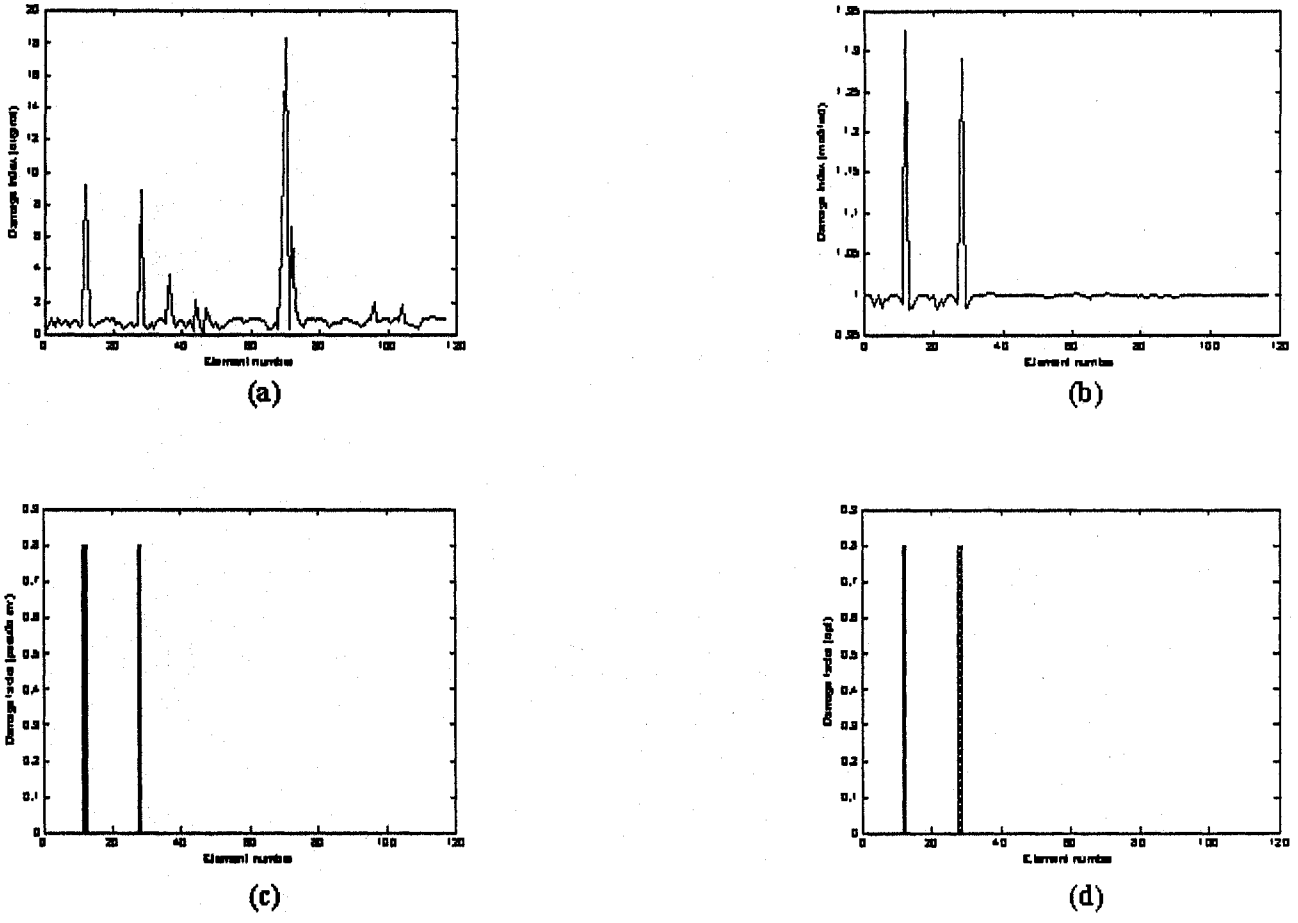

Fig B.11: Graphs showing damage with no error in frequencies and complete modes assumed for case-D7S by Damage Index Method **(a)** original and **(b)** modified; by Matrix Update **(c)** pseudo-inverse **(d)** optimized

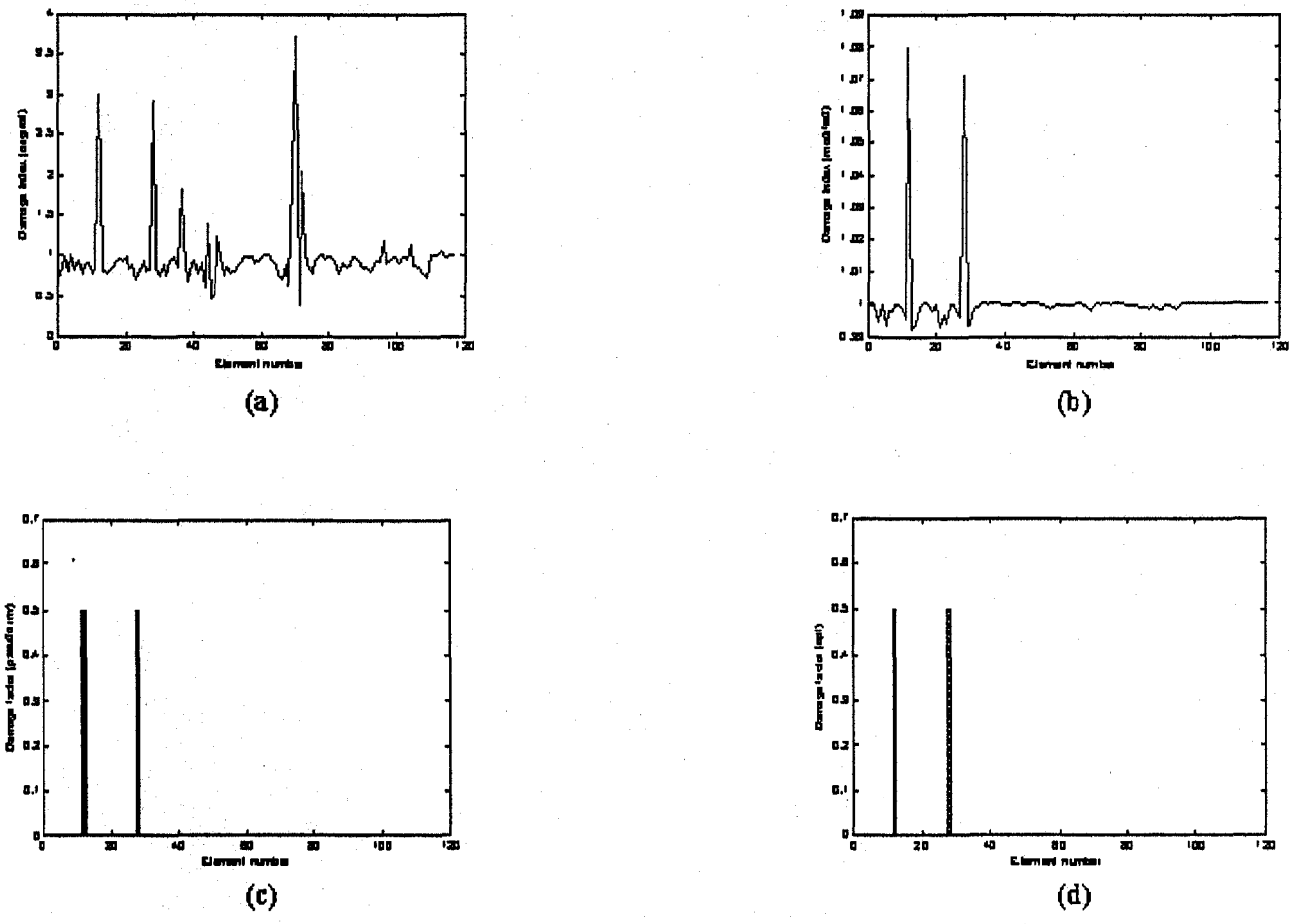

Fig B.12: Graphs showing damage with no error in frequencies and complete modes assumed for case-D7L by Damage Index Method **(a)** original and **(b)** modified; by Matrix Update **(c)** pseudo-inverse **(d)** optimized

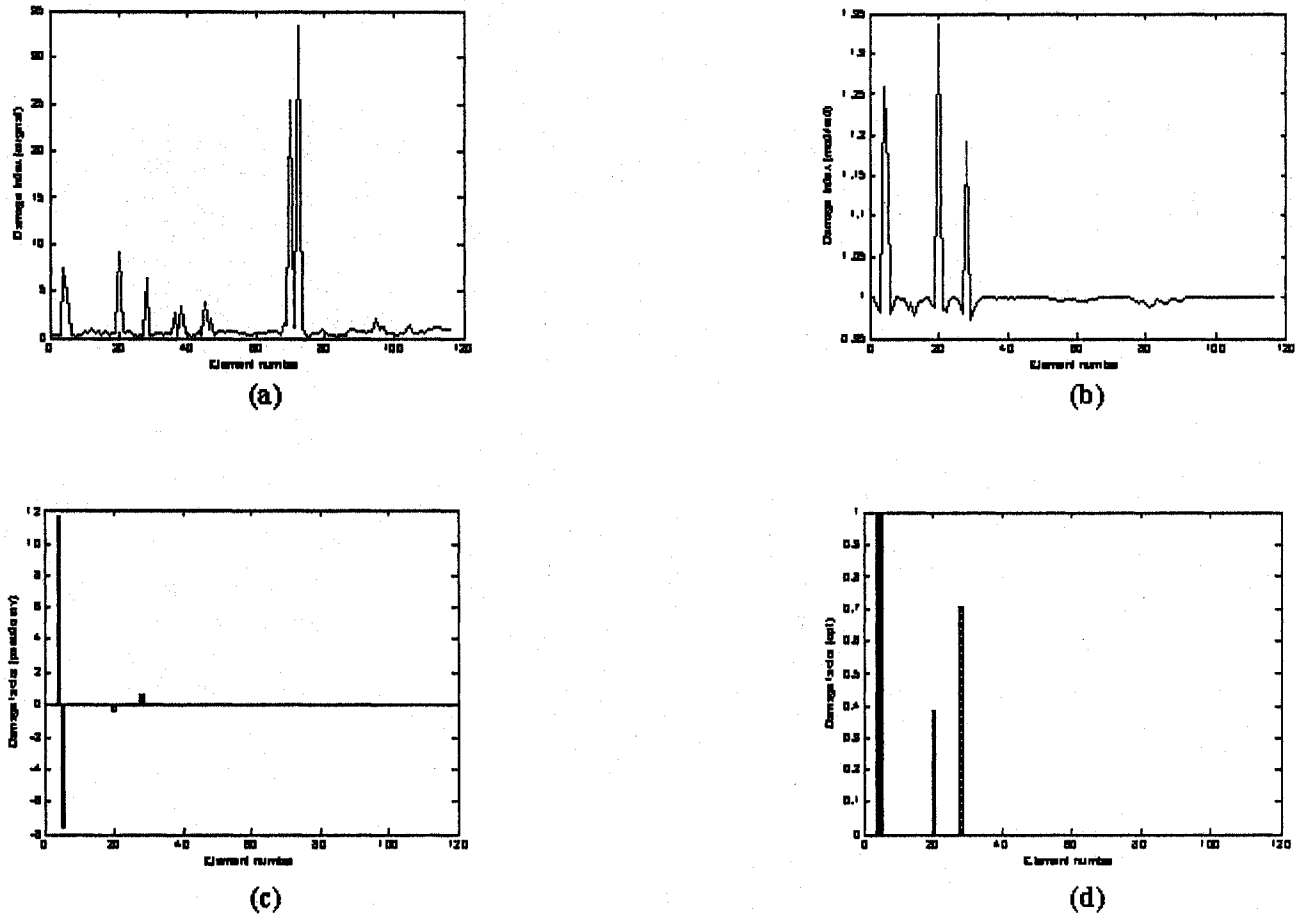

Fig B.13: Graphs showing damage with no error in frequencies and complete modes assumed for case-D8S by Damage Index Method **(a)** original and **(b)** modified; by Matrix Update **(c)** pseudo-inverse **(d)** optimized

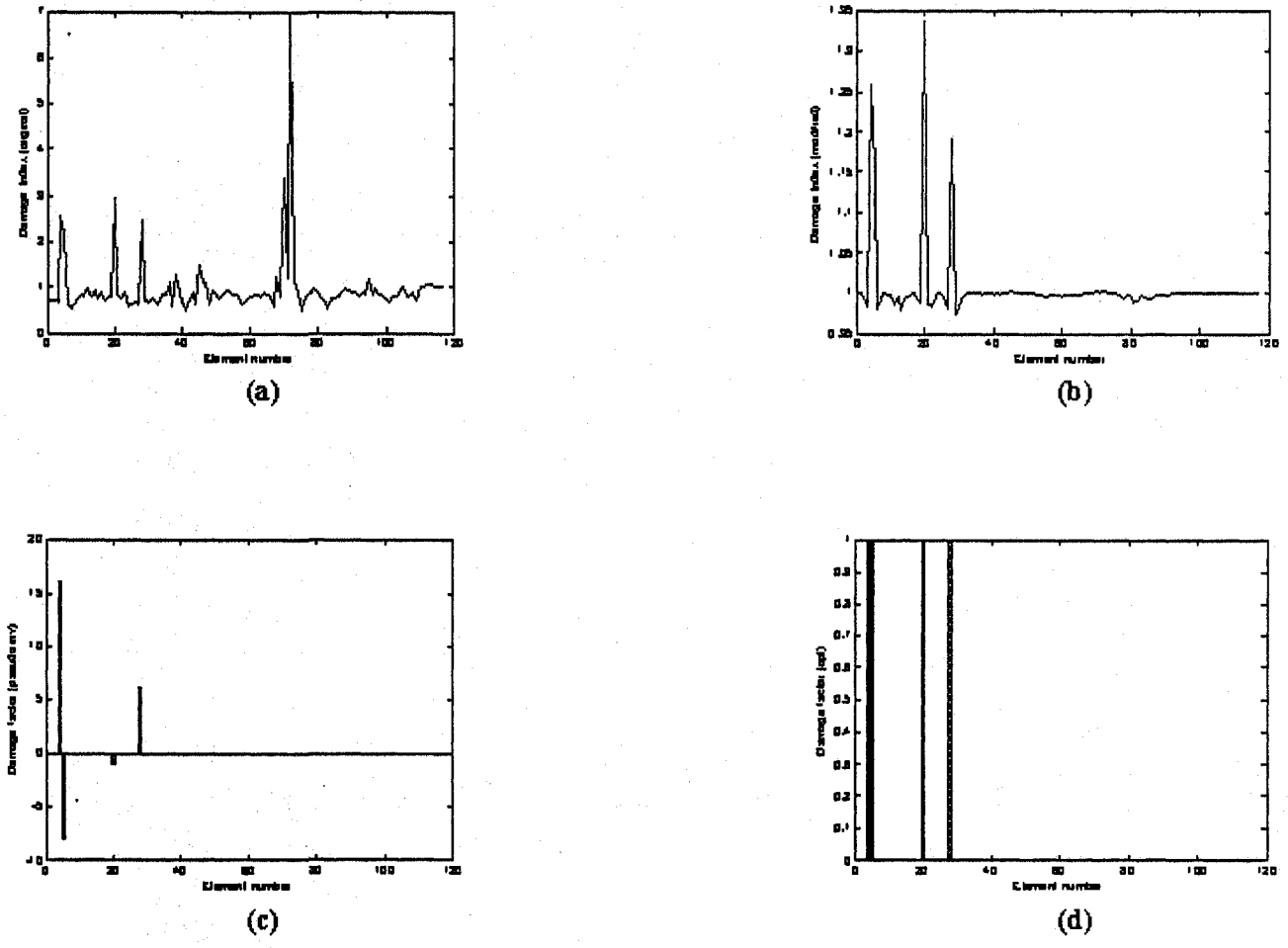

Fig B.14: Graphs showing damage with no error in frequencies and complete modes assumed for case-D8L by Damage Index Method **(a)** original and **(b)** modified; by Matrix Update **(c)** pseudo-inverse **(d)** optimized

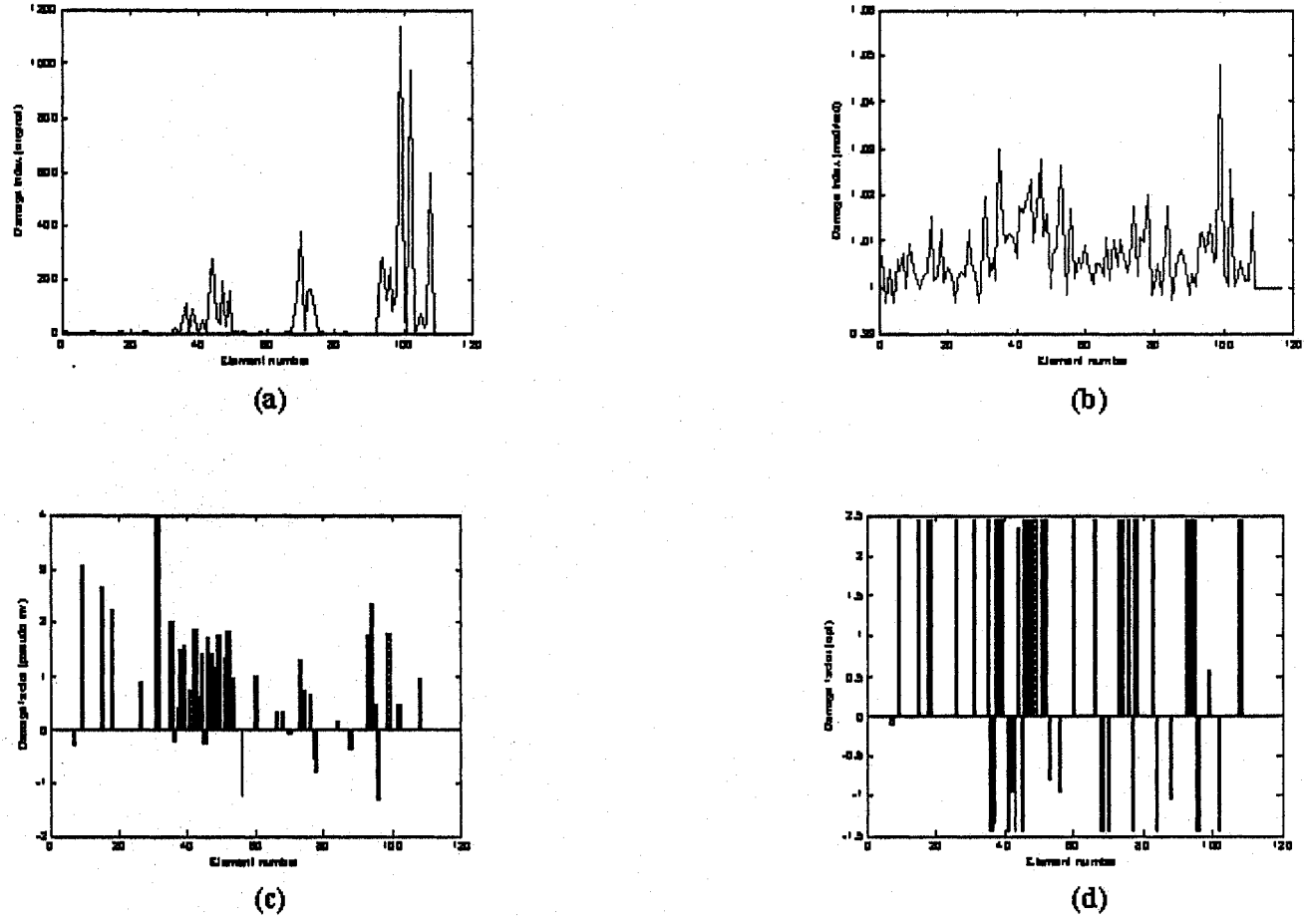

Fig B.15: Graphs showing damage with element numbers for random error up to 2% on frequencies and 10% on modes and assuming incomplete mode shapes for case-D1 by Damage Index Method **(a)** original and **(b)** modified; by Matrix Update Method **(c)** pseudo inverse and **(d)** optimized.

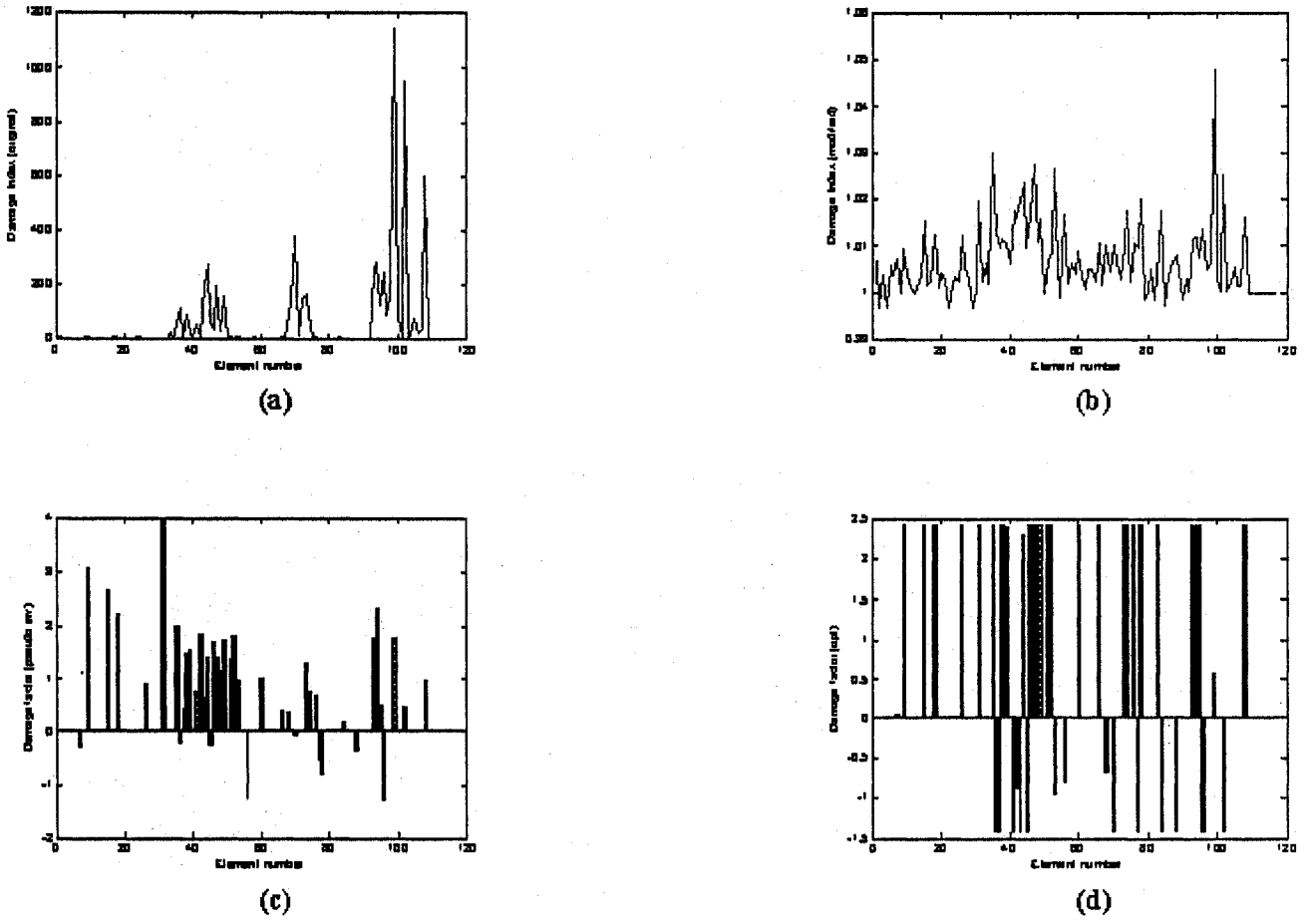

Fig B.16: Graphs showing damage with element numbers for random error up to 2% on frequencies and 10% on modes and assuming incomplete mode shapes for case-D2 by Damage Index Method **(a)** original and **(b)** modified; by Matrix Update Method **(c)** pseudo inverse and **(d)** optimized.

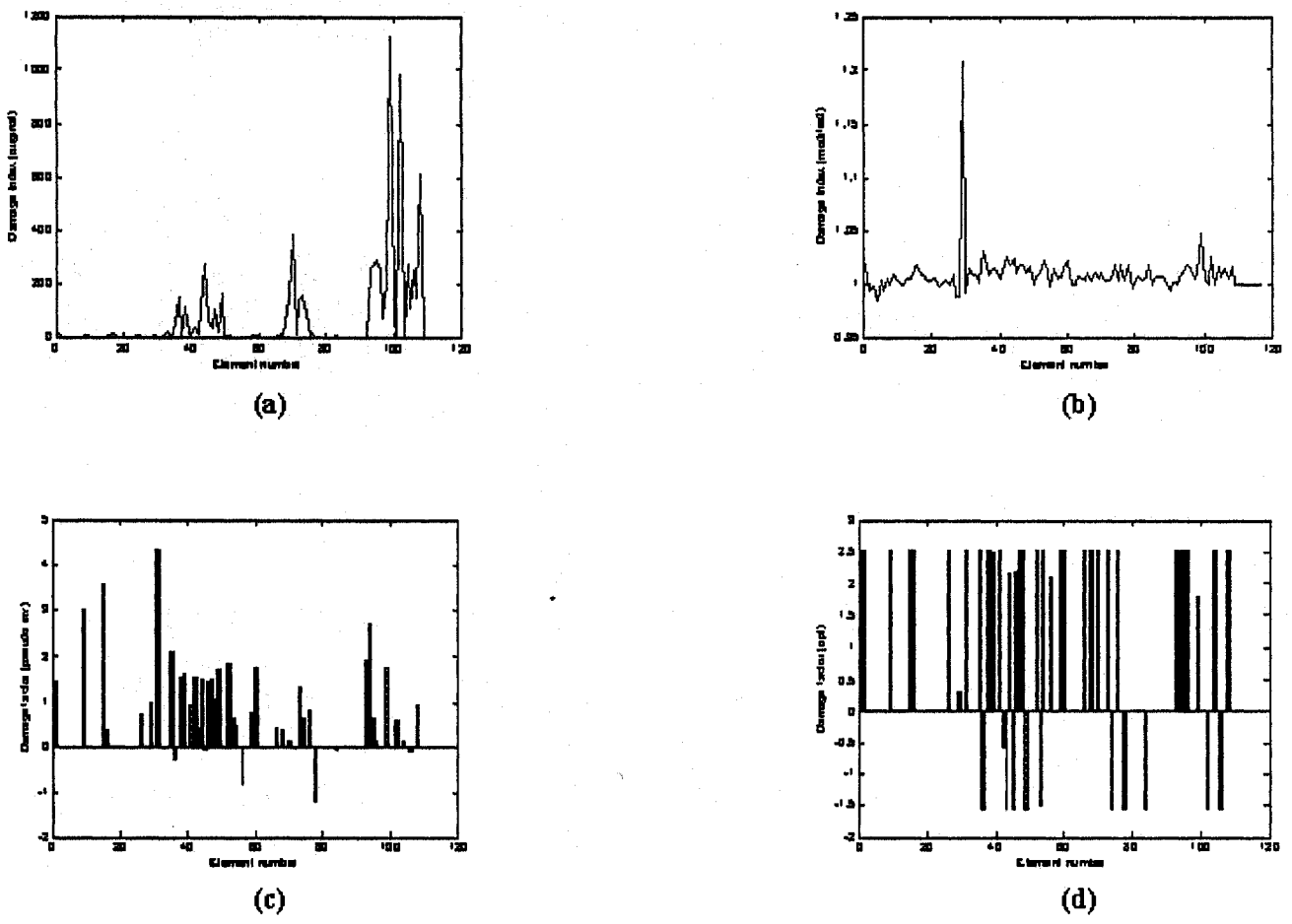

Fig B.17: Graphs showing damage with element numbers for random error up to 2% on frequencies and 10% on modes and assuming incomplete mode shapes for case-D3S by Damage Index Method **(a)** original and **(b)** modified; by Matrix Update Method **(c)** pseudo inverse and **(d)** optimized.

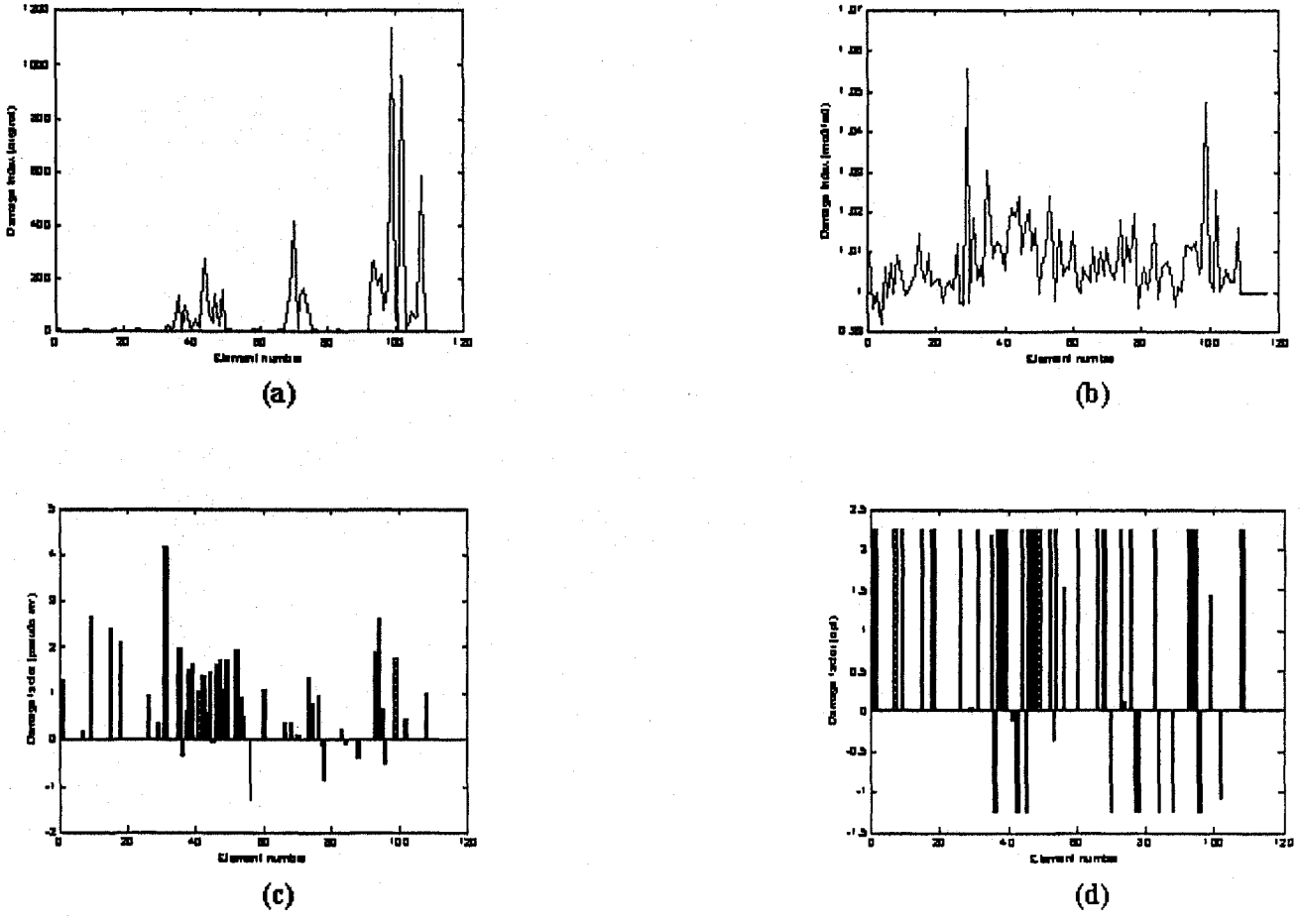

Fig B.18: Graphs showing damage with element numbers for random error up to 2% on frequencies and 10% on modes and assuming incomplete mode shapes for case-D3L by Damage Index Method **(a)** original and **(b)** modified; by Matrix Update Method **(c)** pseudo inverse and **(d)** optimized

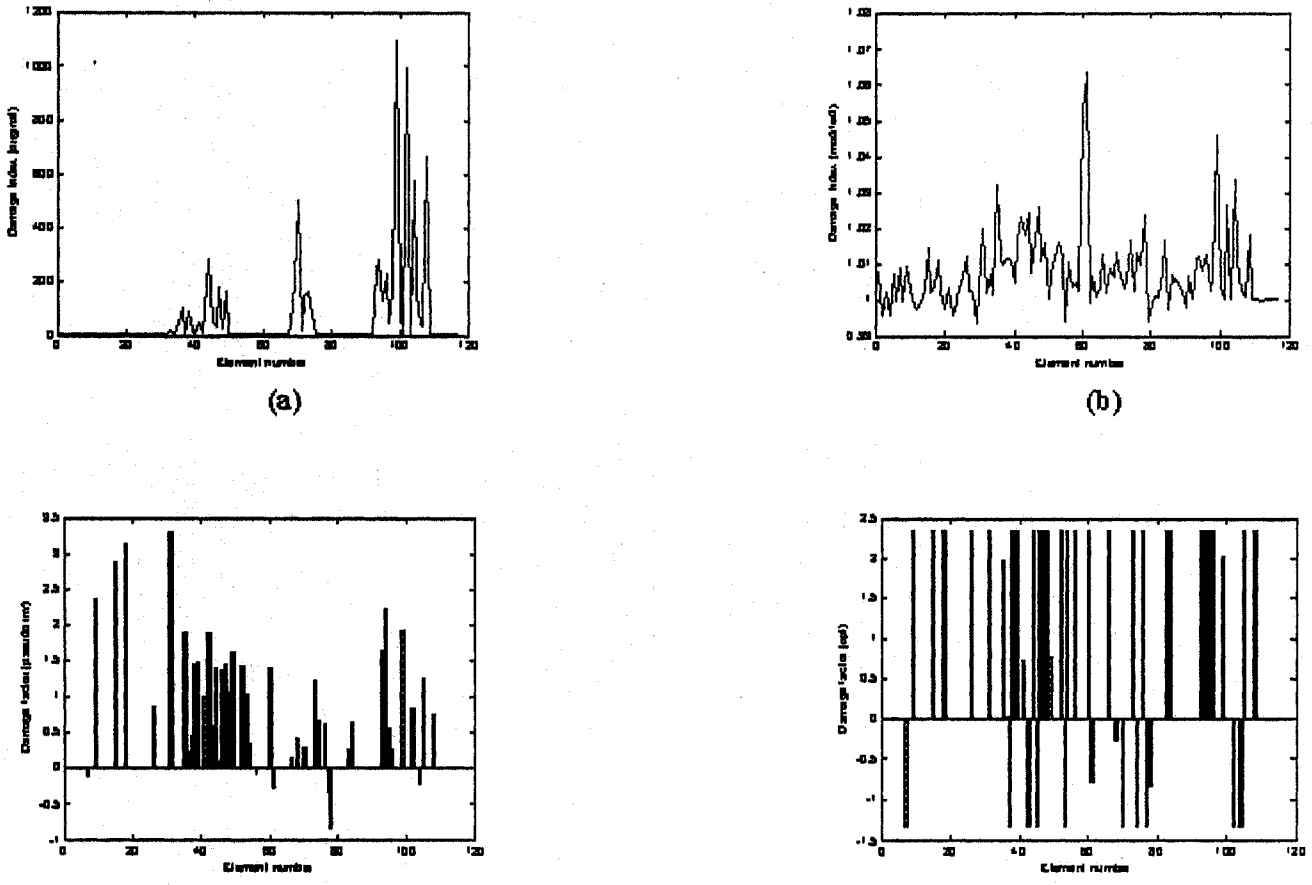

(a) (b)

(c) (d)

Fig B.19: Graphs showing damage with element numbers for random error up to 2% on frequencies and 10% on modes and assuming incomplete mode shapes for case-D4S by Damage Index Method **(a)** original and **(b)** modified; by Matrix Update Method **(c)** pseudo inverse and **(d)** optimized

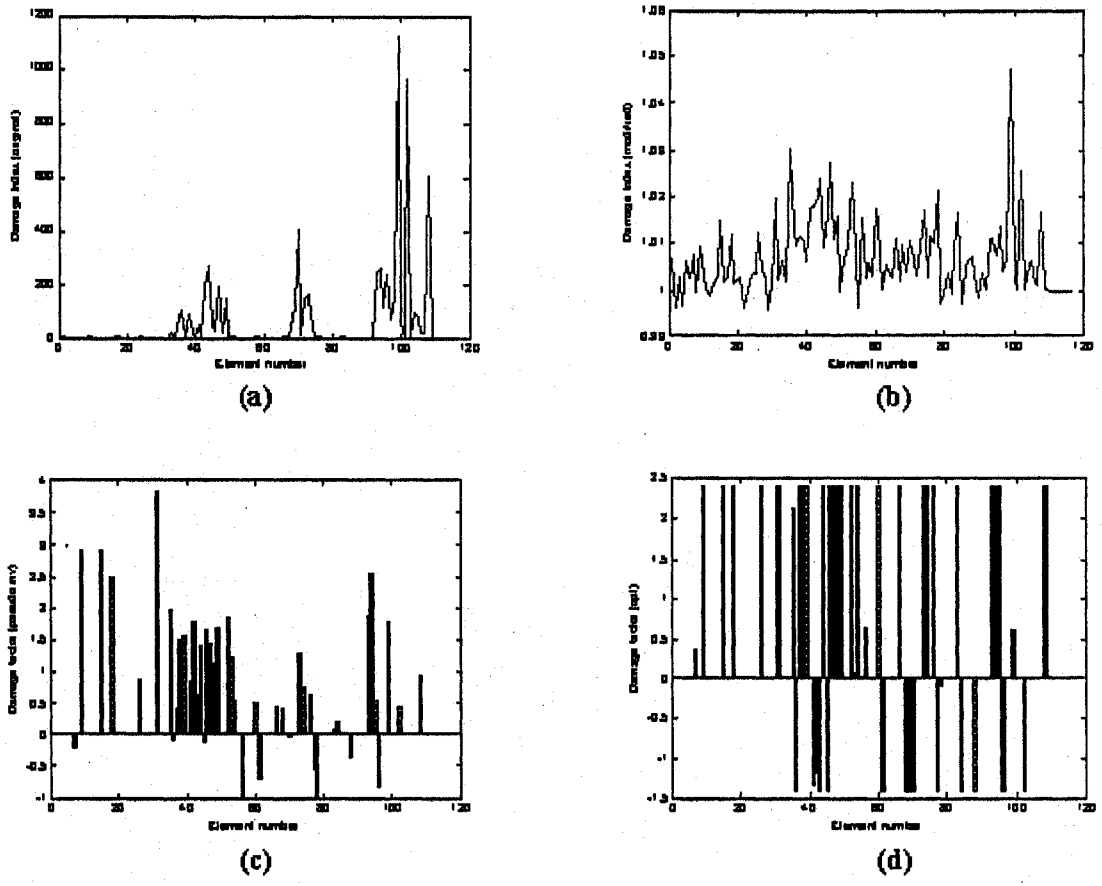

Fig B.20: Graphs showing damage with element numbers for random error up to 2% on frequencies and 10% on modes and assuming incomplete mode shapes for case-D4L by Damage Index Method **(a)** original and **(b)** modified; by Matrix Update Method **(c)** pseudo inverse and **(d)** optimized

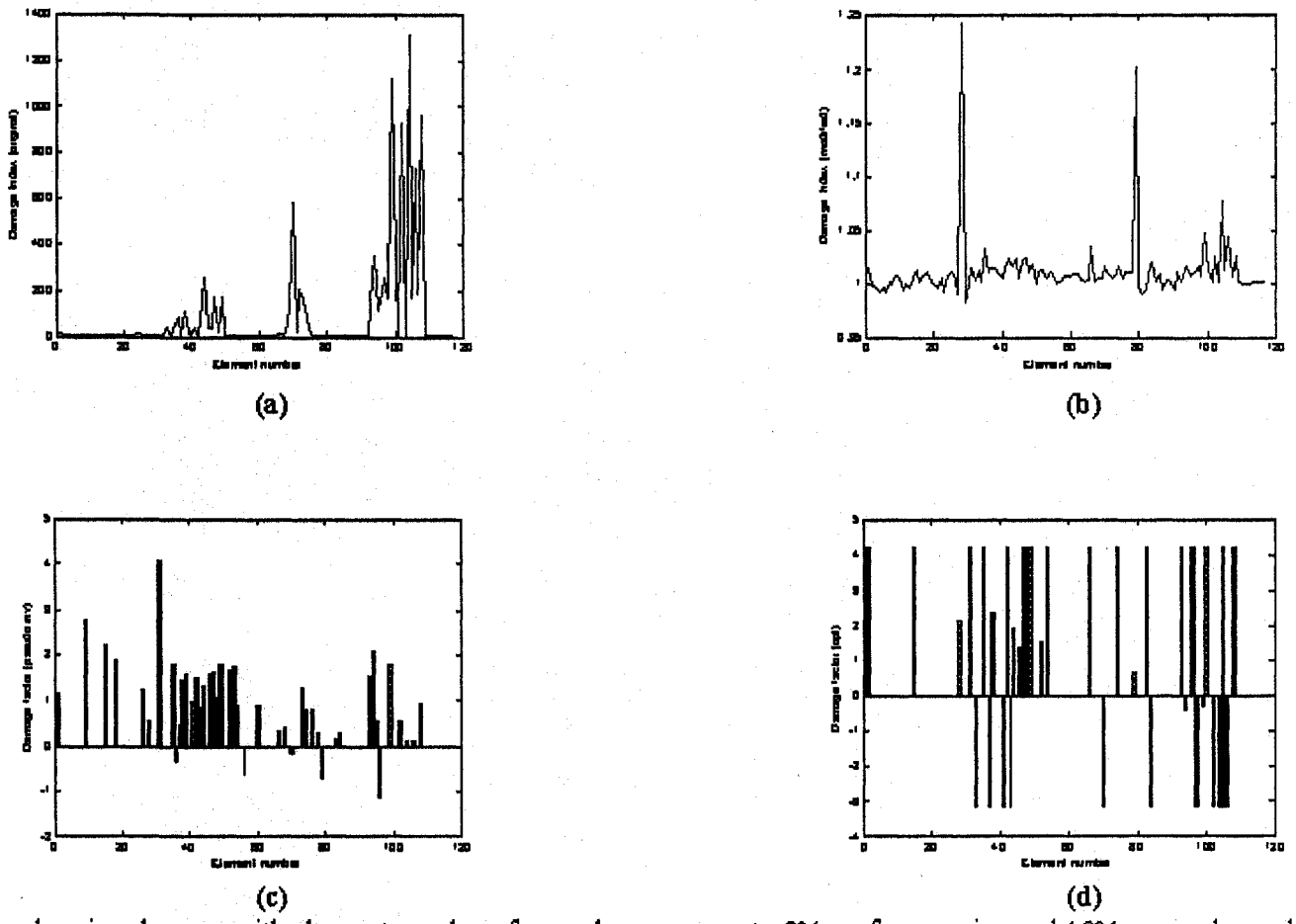

Fig B.21: Graphs showing damage with element numbers for random error up to 2% on frequencies and 10% on modes and assuming incomplete mode shapes for case-D5S by Damage Index Method **(a)** original and **(b)** modified; Matrix Update Method **(c)** pseudo inverse and **(d)** optimized

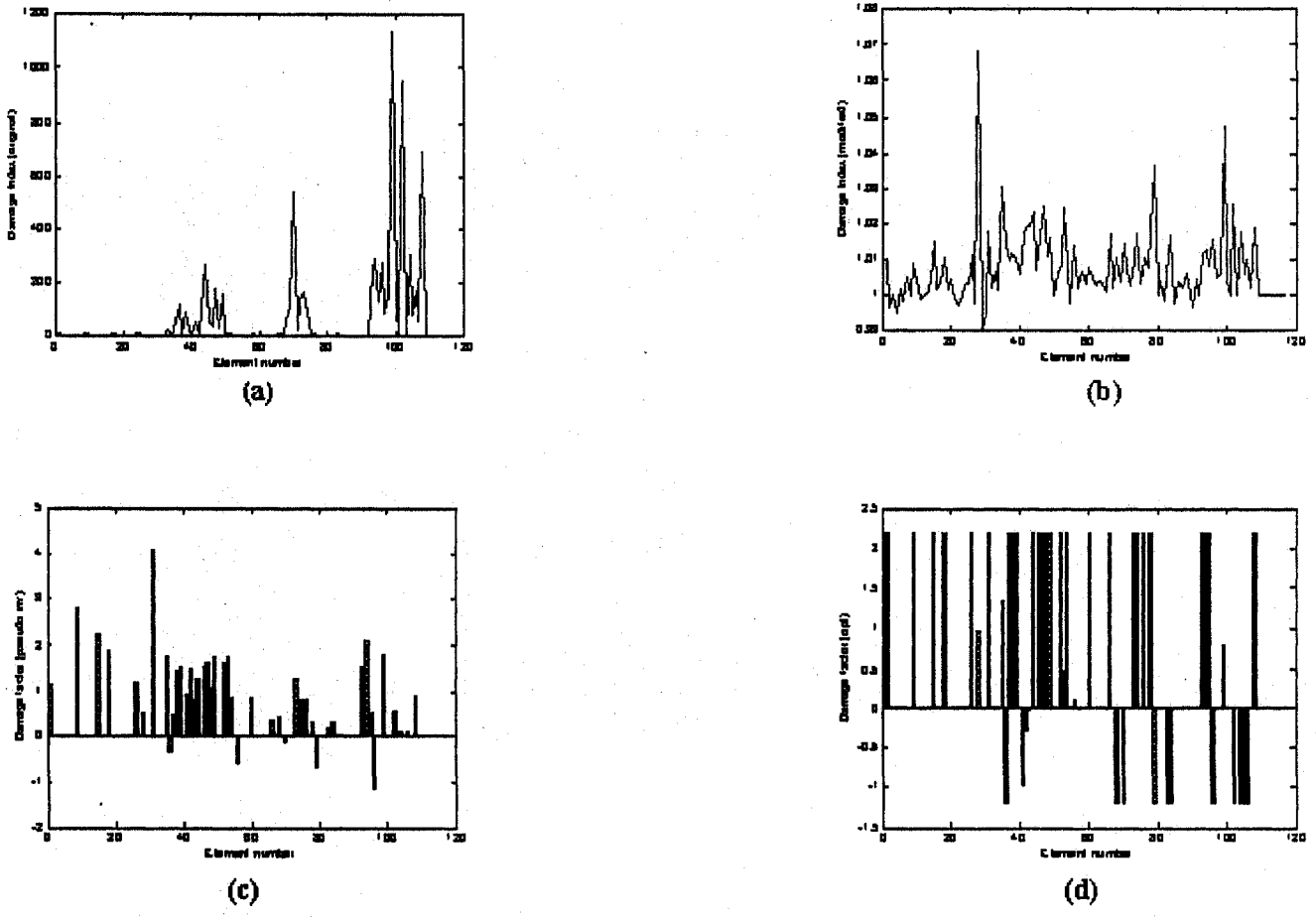

Fig B.22: Graphs showing damage with element numbers for random error up to 2% on frequencies and 10% on modes and assuming incomplete mode shapes for case-D5L by Damage Index Method **(a)** original and **(b)** modified; by Matrix Update Method **(c)** pseudo inverse and **(d)** optimized

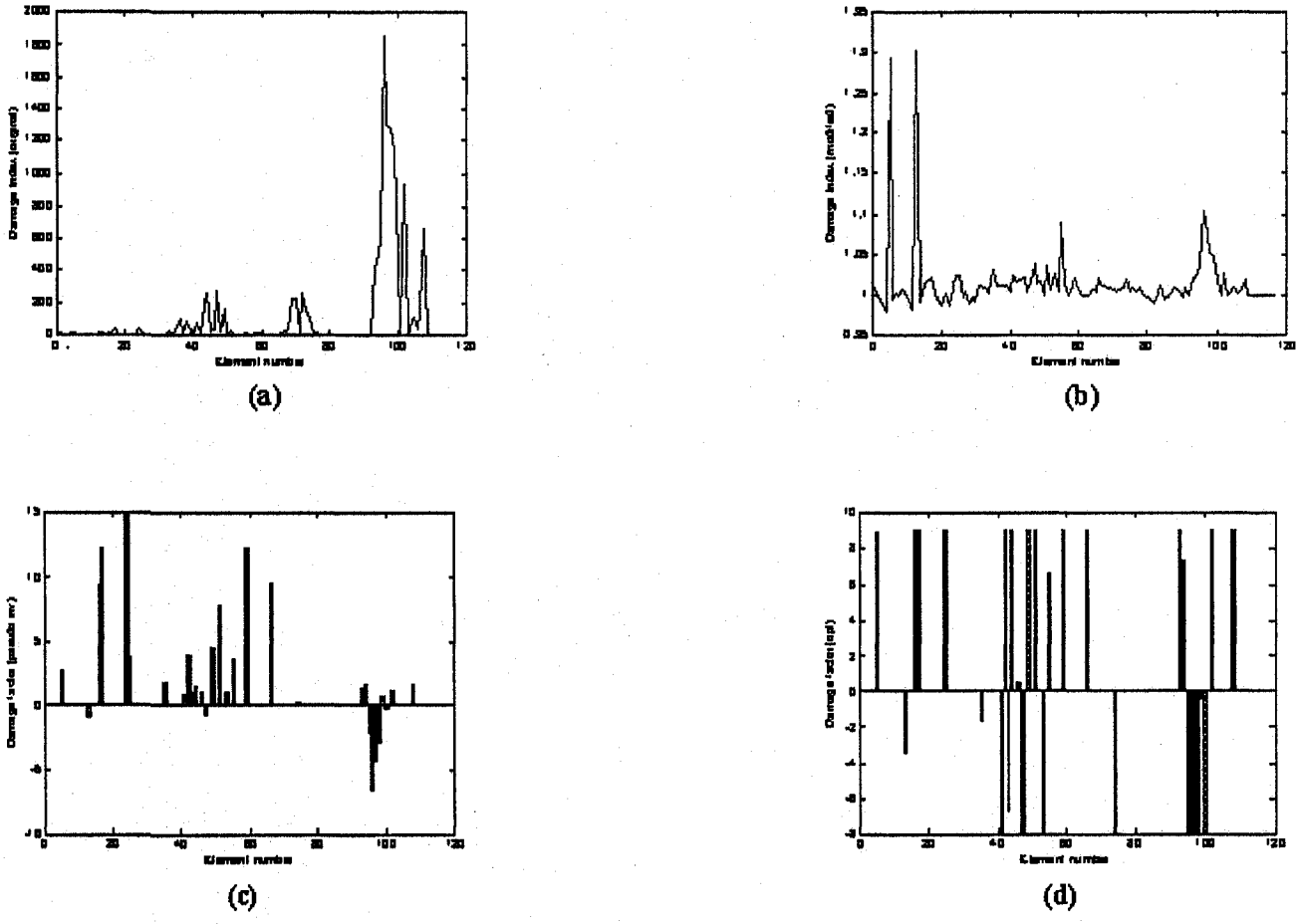

Fig B.23: Graphs showing damage with element numbers for random error up to 2% on frequencies and 10% on modes and assuming incomplete mode shapes for case-D6S by Damage Index Method **(a)** original and **(b)** modified; by Matrix Update Method **(a)** pseudo inverse and **(b)** optimized

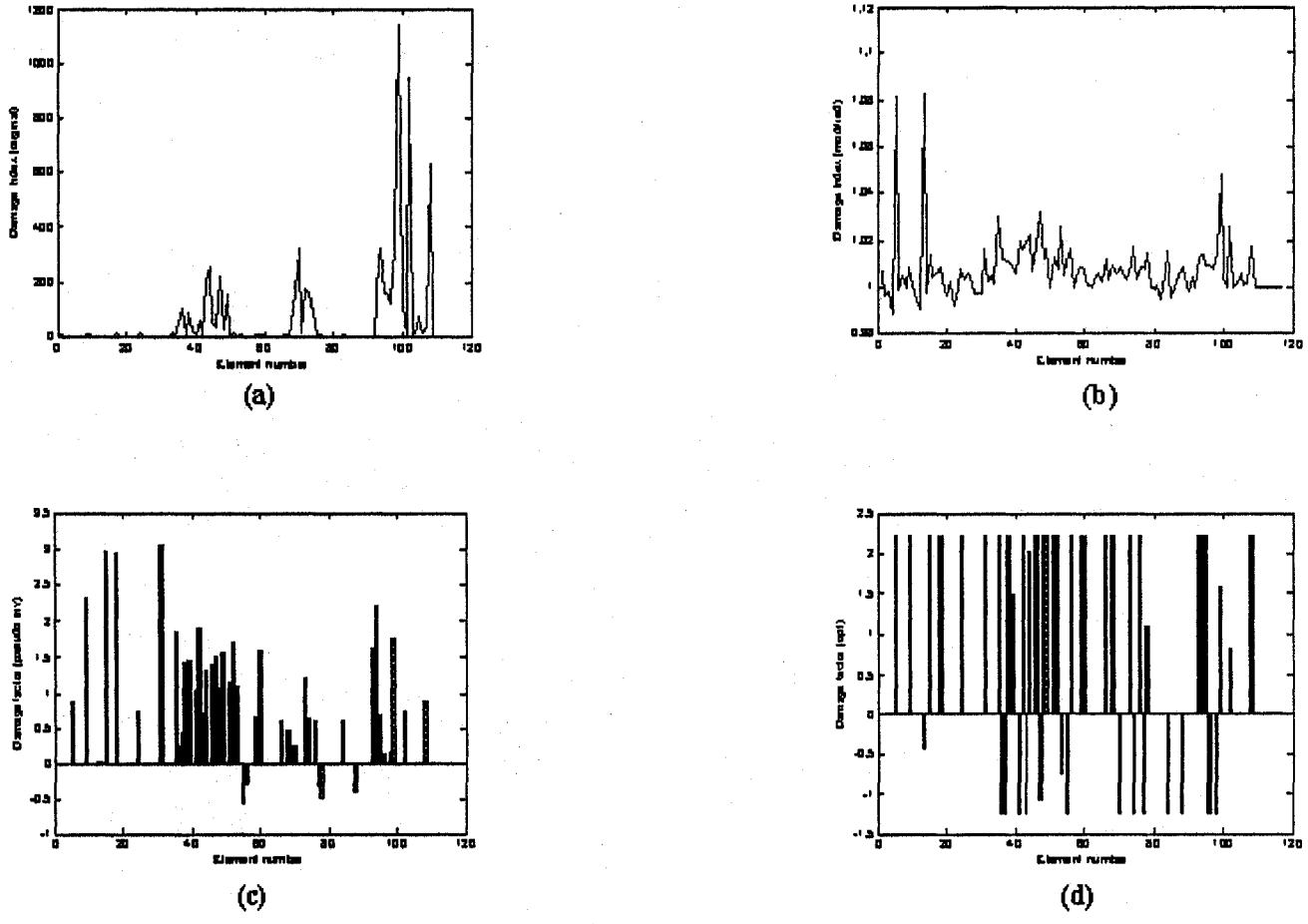

Fig B.24: Graphs showing damage with element numbers for random error up to 2% on frequencies and 10% on modes and assuming incomplete mode shapes for case-D6L by Damage Index Method **(a)** original and **(b)** modified; by Matrix Update Method **(c)** pseudo inverse and **(d)** optimized

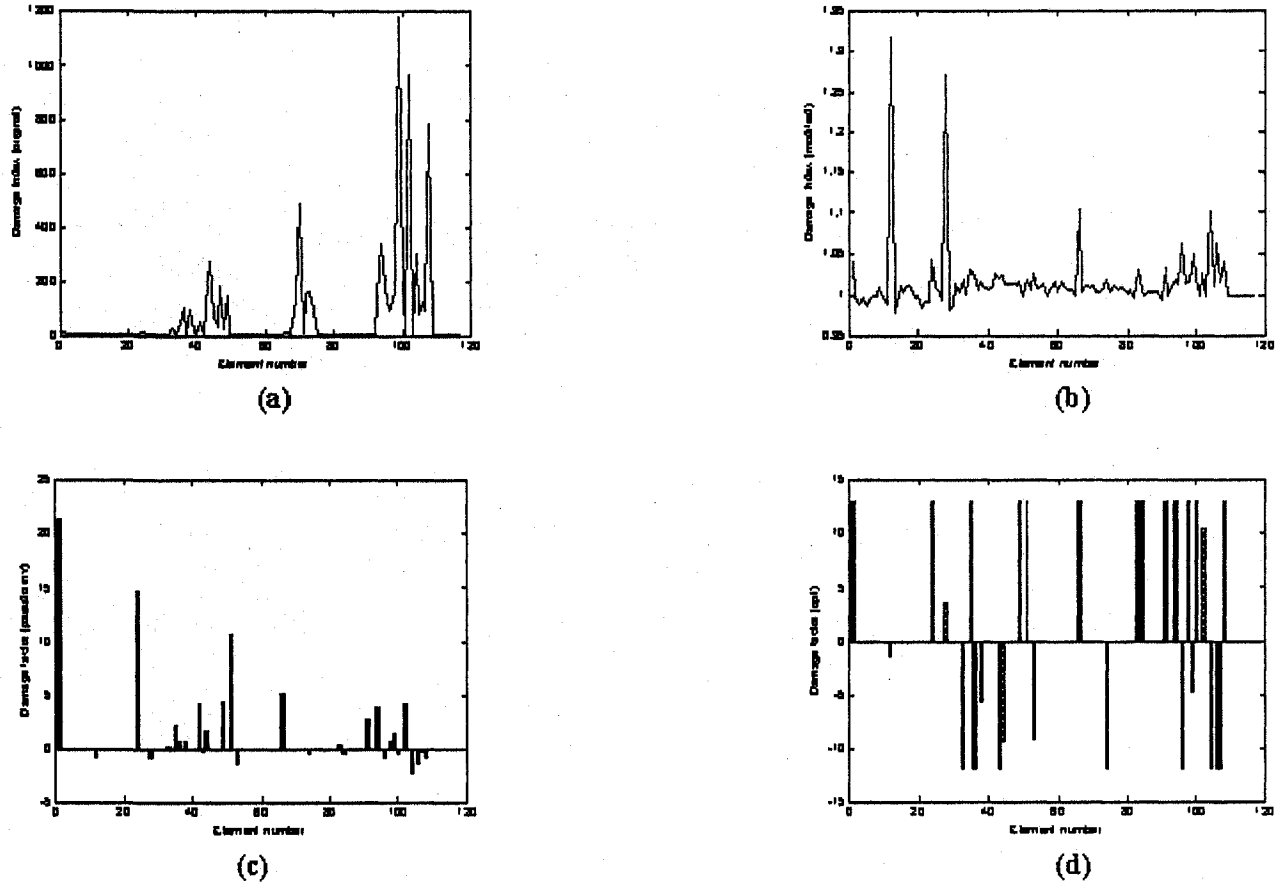

Fig B.25: Graphs showing damage with element numbers for random error up to 2% on frequencies and 10% on modes and assuming incomplete mode shapes for case-D7S by Damage Index Method **(a)** original and **(b)** modified; by Matrix Update Method **(c)** pseudo inverse and **(d)** optimized

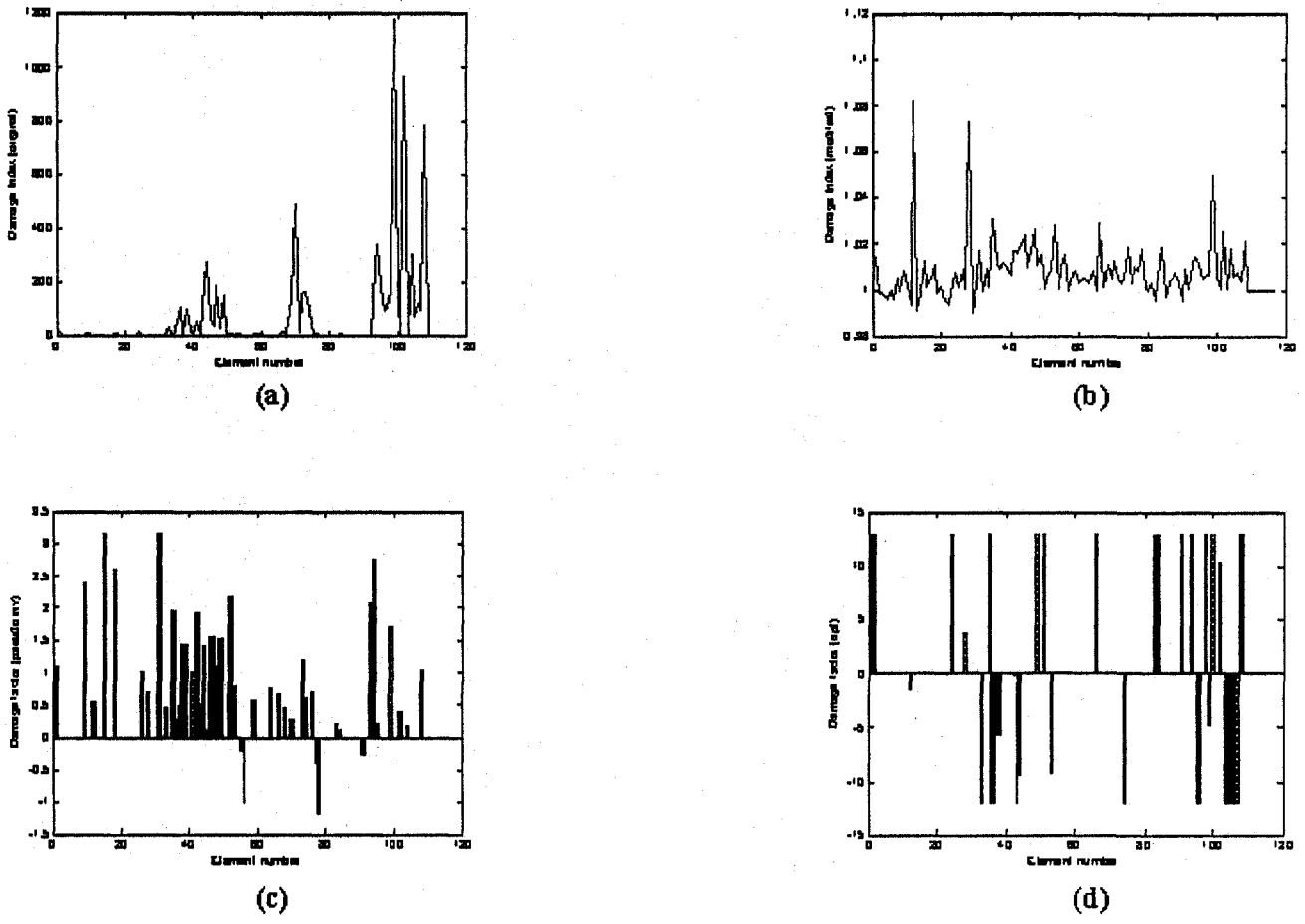

Fig B.26: Graphs showing damage with element numbers for random error up to 2% on frequencies and 10% on modes and assuming incomplete mode shapes for case-D7L by Damage Index Method **(a)** original and **(b)** modified; by Matrix Update Method **(c)** pseudo inverse and **(d)** optimized

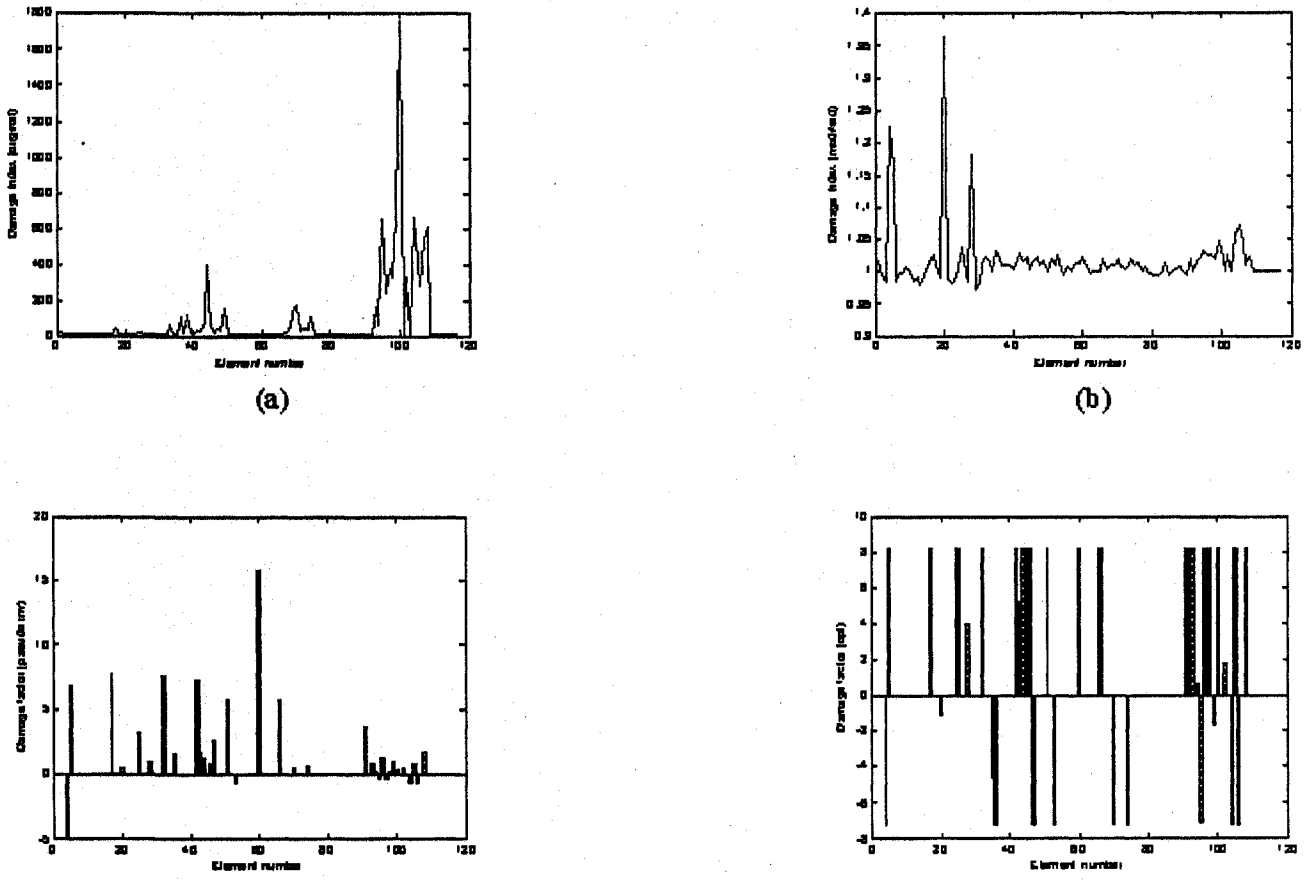

Fig B.27: Graphs showing damage with element numbers for random error up to 2% on frequencies and 10% on modes and assuming incomplete mode shapes for case-D8S by Matrix Update Method **(a)** pseudo inverse and **(b)** optimized; by Matrix Update Method **(c)** pseudo inverse and **(d)** optimized

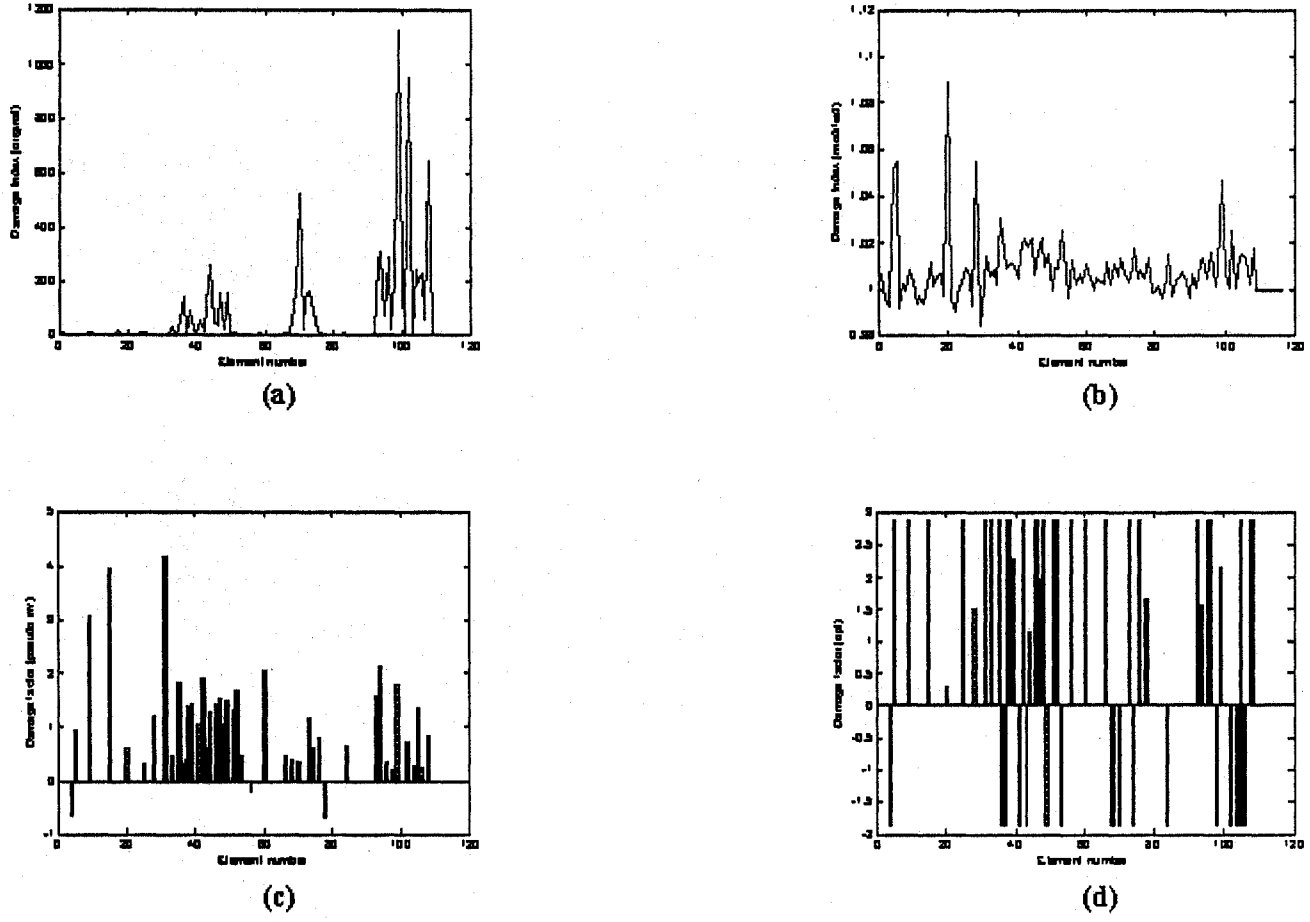

Fig B.28: Graphs showing damage with element numbers for random error up to 2% on frequencies and 10% on modes and assuming incomplete mode shapes for case-D8L by Damage Index Method **(a)** original and **(b)** modified; by Matrix Update Method **(c)** pseudo inverse and **(d)** optimized